

2016

Assessment, Prevention And Remediation Of Corrosion In Weathering Steel Transmission Line Poles

Matthew Bruce Barragan
University of South Carolina

Follow this and additional works at: <http://scholarcommons.sc.edu/etd>

 Part of the [Civil and Environmental Engineering Commons](#)

Recommended Citation

Barragan, M. B. (2016). *Assessment, Prevention And Remediation Of Corrosion In Weathering Steel Transmission Line Poles*. (Master's thesis). Retrieved from <http://scholarcommons.sc.edu/etd/3826>

This Open Access Thesis is brought to you for free and open access by Scholar Commons. It has been accepted for inclusion in Theses and Dissertations by an authorized administrator of Scholar Commons. For more information, please contact SCHOLARC@mailbox.sc.edu.

**ASSESSMENT, PREVENTION AND REMEDIATION OF CORROSION IN
WEATHERING STEEL TRANSMISSION LINE POLES**

by

Matthew Bruce Barragan

Bachelor of Science
University of South Carolina, 2014

Submitted in Partial Fulfillment of the Requirements

For the Degree of Master of Science in

Civil Engineering

College of Engineering and Computing

University of South Carolina

2016

Accepted by:

Fabio Matta, Director of Thesis

Branko Popov, Reader

Paul Ziehl, Reader

Lacy Ford, Senior Vice Provost and Dean of Graduate Studies

© Copyright by Matthew Bruce Barragan, 2016
All Rights Reserved.

DEDICATION

For my mother.

ACKNOWLEDGEMENTS

This report was prepared under the sponsorship of CEATI International and participant utilities in CEATI's Overhead Line Design & Extreme Event Mitigation Interest Group (TODEM). I am grateful to CEATI for the opportunity to work on this remarkable issue. The constant support and guidance by the CEATI Technical Advisors, Asim Haldar and George Juhn, and the CEATI Project Monitors, Aleksandra Modelewska, Alex Mogilevsky, and Anand Goel, was greatly appreciated. Thanks must also be given to Project Monitors Darren Wiebe of SaskPower, Melanie Bragdon of Florida Power and Light Company, Rendall Farley and Damon Fisher of Avista Utilities, and Jude Awiylika of San Diego Gas & Electric Company. Special recognition is extended to Mr. Kevin Niles of Osmose Utilities Services, Inc., who aided in field inspections, as well as Dr. Sebastian Stoian of the National High Magnetic Field Laboratory and Dr. Soumitra Ghoshroy of the University of South Carolina Electron Microscopy Center, who assisted the completion of laboratory trials. Lastly, this work could not have been completed without the tutelage of Dr. Fabio Matta, a brilliant mind and benevolent man.

ABSTRACT

Electric utilities routinely use weathering steel (WS) in transmission line structures, capitalizing on corrosion resistance and associated cost savings. The formation of a protective iron-oxide patina on uncoated above-ground WS surfaces depends on the operating environment and exposure conditions. In fact, exposure to common aggressive environments, such as those found in sulfate-contaminated industrial areas and chloride-laden coastal areas, may dramatically hinder the corrosion resistance of WS transmission line structures.

To assess the corrosion behavior of WS transmission line poles, field inspections were conducted at five test sites comprising diverse operating environments and pole designs. These sites included three locations in Saskatchewan, Canada, and two sites in Florida, USA. The exposure environments include rural, industrial and marine (i.e., chloride-laden) atmospheres. For each WS pole structure inspected, assessment based on visual inspection was paired with a quantitative assessment of atmospheric and soil corrosivity, corrosion rates based on thickness measurements, and corrosion potential measurements. In addition, the microstructure and chemical composition of oxide samples collected from the WS poles inspected were studied by means of scanning electron microscopy and energy-dispersive X-ray spectroscopy, X-ray diffraction (XRD), and Mössbauer spectroscopy analysis. The resulting information, data and evidence offer the means to practically understand the combined impact of the environmental corrosivity parameters examined, together with other factors influencing corrosion behavior (e.g.,

design and detailing). In particular, it is demonstrated how the results of field inspections and measurements, and laboratory characterization tests, can be used to understand present and future susceptibility to corrosion damage, for example as a result of the formation of unstable and non-adherent surface oxides. Therefore, this information can be leveraged for diagnosis and prognosis purposes, thereby enabling owners to make informed decisions on allocating and prioritizing prevention and remediation resources. To this end, best practices for corrosion assessment, prevention and remediation for WS transmission line poles are discussed, and case-specific recommendations are made for WS poles located in operating environments that feature a representative range of atmospheric corrosivity characteristics.

TABLE OF CONTENTS

DEDICATION.....	iii
ACKNOWLEDGEMENTS	iv
ABSTRACT.....	v
LIST OF TABLES	x
LIST OF FIGURES	xii
CHAPTER 1.0 INTRODUCTION.....	1
CHAPTER 2.0 WEATHERING STEEL TRANSMISSION LINE POLES	4
2.1 Historical Development	4
2.2 Alloy Composition.....	8
2.3 Corrosion Resistance	13
2.4 Representative Corrosion Forms.....	17
CHAPTER 3.0 TEST SITES AND VISUAL ASSESSMENT OF POLE STRUCTURES.....	23
3.1 Site 1 – Directly Embedded Pole in Rural/Urban Environment	24
3.2 Site 2 – Directly Embedded Poles in Industrial Environment	29
3.3 Site 3 – Directly Embedded Poles in Rural/Industrial Environment.....	34
3.4 Site 4 – Directly Embedded Pole in Marine Environment	40
3.5 Site 5 – WS Poles on Caisson Foundations in Rural Environment	49
3.6 Damage Assessment based on Visual Inspection	60
3.7 Concluding Remarks	63

CHAPTER 4.0	ASSESSMENT OF ENVIRONMENTAL CORROSIVITY	65
4.1	Atmospheric Corrosivity	65
4.2	Soil Corrosivity.....	100
4.3	Concluding Remarks	118
CHAPTER 5.0	ASSESSMENT OF CORROSION RATE AND POTENTIAL	122
5.1	Corrosion Rate	122
5.2	Corrosion Potential.....	142
5.3	Concluding Remarks	155
CHAPTER 6.0	ASSESSMENT OF OXIDE MICROSTRUCTURE AND COMPOSITION	160
6.1	Literature Review of Microstructure and Composition of Surface Oxides.....	161
6.2	Oxide Sampling from WS Pole Structures	168
6.3	Microstructure Characterization via SEM and EDX Analysis	172
6.4	Quantification of Oxide Composition via XRD and MS Analysis....	182
6.5	Modified Protective Ability Index	204
6.6	Concluding Remarks	211
CHAPTER 7.0	CORROSION PREVENTION AND REMEDIATION	213
7.1	Design and Detailing	213
7.2	Protective Measures.....	214
7.3	Remediation.....	224
CHAPTER 8.0	CONCLUSIONS AND RECOMMENDATIONS.....	228
8.1	Literature Review of Corrosion Behavior of Weathering Steel Poles.....	228
8.2	Test Sites and Visual Assessment	229
8.3	Assessment of Environmental Corrosivity	231

8.4	Assessment of Corrosion Rate and Corrosion Potential	234
8.5	Assessment of Oxide Microstructure and Composition	238
8.6	Corrosion Prevention and Remediation	239
8.7	Research Needs.....	242
REFERENCES.....		245
APPENDIX A: SUPPLEMENTARY RESULTS FROM LABORATORY		
ANALYSIS		256
A.1	Scanning Electron Microscopy (SEM).....	257
A.2	X-Ray Diffraction (XRD)	265
A.3	Mössbauer Spectroscopy (MS)	277

LIST OF TABLES

<i>Table 2.1 Chemical composition of modern WS alloys.</i>	<i>6</i>
<i>Table 3.1 Pertinent identification details on field testing sites and structures.....</i>	<i>61</i>
<i>Table 3.2 Assessment of visible corrosion damage in inspected poles.....</i>	<i>62</i>
<i>Table 4.1 Time of wetness categories per ISO 9223 (ISO 2012b).....</i>	<i>79</i>
<i>Table 4.2 Sulfur dioxide deposition rate categories per ISO 9223 (ISO 2012b).....</i>	<i>79</i>
<i>Table 4.3 Chloride deposition rate categories per ISO 9223 (ISO 2012b).....</i>	<i>79</i>
<i>Table 4.4 Categorization of atmospheric corrosivity per ISO 9223 (ISO 2012b).....</i>	<i>81</i>
<i>Table 4.5 TOW values and categories for each test site.....</i>	<i>97</i>
<i>Table 4.6 Contaminant concentrations and estimated deposition rate for WS poles.....</i>	<i>97</i>
<i>Table 4.7 Atmospheric corrosivity categories based on ISO 9223 (ISO 2012b).....</i>	<i>99</i>
<i>Table 4.8 Soil corrosivity classification based on soil resistivity (Roberge 2008).....</i>	<i>103</i>
<i>Table 4.9 Soil corrosivity parametric criteria per AWWA (2010).....</i>	<i>105</i>
<i>Table 4.10 Soil corrosivity classification per AWWA (2010).....</i>	<i>105</i>
<i>Table 4.11 Soil corrosivity parametric criteria per DVGW (2011).....</i>	<i>106</i>
<i>Table 4.12 Soil corrosivity classification per DVGW (2011).....</i>	<i>107</i>
<i>Table 4.13 Soil corrosion parameter measurements.</i>	<i>111</i>
<i>Table 4.14 Concentrations of soluble soil contaminants from field tests.</i>	<i>113</i>
<i>Table 4.15 Soil corrosivity classification of Sites 1, 2 and 3 (Saskatchewan, Canada) according to Roberge (2008), AWWA (2010) and DVGW (2011).....</i>	<i>115</i>
<i>Table 4.16 Soil corrosivity classification of Sites 4 and 5 (Florida, USA) according to Roberge (2008), AWWA (2010) and DVGW (2011).....</i>	<i>116</i>
<i>Table 5.1 Atmospheric corrosivity and corrosion rates for carbon steel (ISO 2012b)..</i>	<i>123</i>

<i>Table 5.2 Thickness measurements on circular WS poles at Sites 1, 2 and 3 (Saskatchewan, Canada).....</i>	<i>130</i>
<i>Table 5.3 Thickness measurements on paneled WS poles at Sites 4 and 5 (Florida, USA).</i>	<i>131</i>
<i>Table 5.4 Thickness measurements on circular poles at Sites 4 and 5 (Florida, USA).</i>	<i>132</i>
<i>Table 5.5 Structure-to-soil corrosion potential (SSP) for WS poles inspected.....</i>	<i>146</i>
<i>Table 6.1 Iron oxides and hydroxides typically found in WS surface patina.</i>	<i>161</i>
<i>Table 6.2 Surface oxide samples collected from WS poles inspected.....</i>	<i>170</i>
<i>Table 6.3 Elemental compositions of iron oxides and hydroxides.....</i>	<i>173</i>
<i>Table 6.4 EDX data for solid rust specimens collected from WS poles, including pack-rust samples from Site 2, pack-out samples from Site 4, and loose rust samples from Site 5.....</i>	<i>178</i>
<i>Table 6.5 Quantity of iron oxide and hydroxide species determined via XRD analysis.</i>	<i>186</i>
<i>Table 6.6 Mass ratio of iron oxide species determined through MS and XRD analysis.</i>	<i>201</i>
<i>Table 6.7 Values of α/γ^+ and α/γ^* based on data from XRD analysis (Table 6 5).</i>	<i>209</i>
<i>Table 6.8 Proposed PAI rating criteria.</i>	<i>210</i>
<i>Table A.1 Parameters obtained from simulations of spectra for pack-rust sample from reflective tape region of Pole CIF-20 at Site 1.</i>	<i>277</i>
<i>Table A.2 Parameters obtained from simulations of spectra for pack-rust sample from coating line region of Pole Q3C-2L at Site 2.</i>	<i>279</i>
<i>Table A.3 Parameters obtained from simulations of spectra for pole wall sample from Pole S3B-2L at Site 3.</i>	<i>281</i>
<i>Table A.4 Parameters obtained from simulations of spectra for inner pack-out sample from Pole TL-1 at Site 4.....</i>	<i>283</i>
<i>Table A.5 Parameters obtained from simulations of spectra for loose rust sample from GS fastener region of Pole 8Z-2L at Site 5.</i>	<i>285</i>

LIST OF FIGURES

<i>Figure 2.1 Effect of Cu content on corrosion-induced thickness loss of steel exposed to different aggressive environments for 15.5 years (Larrabee and Coburn 1962).</i>	9
<i>Figure 2.2 Effect of Cr content for different Cu contents on corrosion-induced thickness loss of steel exposed to industrial atmosphere for 18 years (Copson 1960).</i>	10
<i>Figure 2.3 Effect of P content for different Cu contents on corrosion-induced thickness loss of steel exposed to industrial atmosphere for 15.5 years (Larrabee and Coburn 1962).</i>	11
<i>Figure 2.4 Effect of Ni content on corrosion-induced mass loss of steel exposed to marine atmosphere for 15.5 years (Copson 1960).</i>	12
<i>Figure 2.5 Atmospheric corrosion tests of steel specimens (Larrabee and Coburn 1962).</i>	14
<i>Figure 2.6 Corrosion thickness loss trend for CS, Cu-bearing and Cor-Ten B steel samples exposed to industrial atmosphere in Kearny, NJ (Larrabee and Coburn 1962).</i>	16
<i>Figure 2.7 Examples of pack-rust damage near ground line of WS poles: (a) multiple layers stacking on one another; and (b) more severe thickness loss.</i>	18
<i>Figure 2.8 Pack-out damage at connection in WS transmission line lattice structure. Note bent steel member.</i>	19
<i>Figure 2.9 Widespread pitting over surface of WS pole wall.</i>	20
<i>Figure 2.10 Rating chart from ASTM G46 (ASTM 2013c) for pitting corrosion assessment.</i>	21
<i>Figure 3.1 Locations of test sites: (a) Saskatchewan, Canada; and (b) Florida, USA.</i> ...	23
<i>Figure 3.2 Site 1: (a) map indicating site and pole location; and (b) photographic view.</i>	25
<i>Figure 3.3 Ground-level view of Pole C1F-20 at Site 1.</i>	26
<i>Figure 3.4 Corrosion prevention measures for Pole C1F-20: (a) polyurethane coating and rock backfill; and (b) GEC link to grounding rod and magnesium anode connection.</i>	27

<i>Figure 3.5 Corrosion damage under reflective tape on Pole CIF-20: (a) pitting; and (b) non-uniform pack rust.</i>	28
<i>Figure 3.6 Site 2: (a) map indicating site and pole locations; and (b) photographic view.</i>	29
<i>Figure 3.7 Site 2 poles: (a) Q3C-1L; (b) Q3C-1R; (c) Q3C-2L; and (d) Q3C-2R.</i>	31
<i>Figure 3.8 Corrosion prevention measures seen on Site 2 poles, including GEC link to grounding rod and magnesium anode connection.</i>	31
<i>Figure 3.9 Severely delaminated coating line accompanied by widespread pack rust and pack out on ladder clip.</i>	32
<i>Figure 3.10 Pack-out corrosion damage: (a) rust removed from coating line; and (b) easily removed rust layer, with pack rust still visible along coating line.</i>	33
<i>Figure 3.11 Non-adherent patina sloughing off with light rubbing of pole wall surface.</i>	34
<i>Figure 3.12 Site 3: (a) map indicating site and pole locations; and (b) photographic view.</i>	35
<i>Figure 3.13 Site 3 poles: (a) S3B-2L; (b) S3B-3L; (c) S3B-7L; and (d) S3B-7R.</i>	37
<i>Figure 3.14 Site 3 pole bases showing corrosion prevention measures and: (a) coating barely extending above ground line; and (b) steady delamination of coating due to pack rust</i>	37
<i>Figure 3.15 Dense pitting sites on pole wall surfaces: (a) Pole S3B-2L facing power station; and (b) Pole S3B-7R facing coal company.</i>	38
<i>Figure 3.16 Pole S3B-3L showing minor coating delamination but overall dense and adherent patina.</i>	39
<i>Figure 3.17 Site 4: (a) map indicating site and pole location; and (b) wide photographic view.</i>	40
<i>Figure 3.18 Ground-level view of Site 4 poles: (a) TL-1 and (b) TL-2.</i>	41
<i>Figure 3.19 Ground-line coating on poles at Site 4: (a) Pole TL-1; and (b) Pole TL-2.</i> ..	42
<i>Figure 3.20 Damage around coating region in WS Pole TL-1 and GS Pole TL-2 near ocean: (a) deterioration of Pole TL-1 coating with visible pits; (b) pitting and pack-rust corrosion damage at Pole TL-1 coating lip; (c) coating delamination around bolted sleeve on Pole TL-2; and (d) crevice corrosion on Pole TL-2.</i>	43
<i>Figure 3.21 Corrosion behind junction boxes: (a) thick pack-out rust on Pole TL-1; (b) hole in WS pole wall exposed after removing pack-out rust; (c) pack-out damage from other side stretching length of junction box; and (d) no damage on Pole TL-2.</i>	45

<i>Figure 3.22 Condition of overhead slip joints near saltwater: (a) pack-rust damage on WS Pole TL-1 sections; (b) apparently sound, corrosion-free GS Pole TL-2.</i>	<i>46</i>
<i>Figure 3.23 IPLEX LX borescope camera (Olympus Corp.).....</i>	<i>47</i>
<i>Figure 3.24 Interior inspection of Pole TL-1 at Site 4 via borescope: (a) grinding pole wall; (b) drilling; (c) cleaning surface; (d) threading hole; (e) close-up image of hole; (f) inserting borescope camera; (g) examining pole interior; and (h) plugging hole after inspection.</i>	<i>48</i>
<i>Figure 3.25 Borecope images of interior of Pole TL-1: (a) uneven patina due to lack of wet/dry cycles; and (b) view of pole interior.</i>	<i>49</i>
<i>Figure 3.26 Site 5: (a) map indicating site and pole locations; and (b) wide photographic view.</i>	<i>50</i>
<i>Figure 3.27 Ground-level view of poles: (a) 8Z-2L and (b) 8Z-2R.</i>	<i>51</i>
<i>Figure 3.28 Ground-level view of Site 5 poles of Line 11Z: (a) Pole 11Z-2L; (b) Pole 11Z-2R; (c) Pole 11Z-6L; and (d) Pole 11Z-6R.</i>	<i>51</i>
<i>Figure 3.29 Visual assessment of poles at Site 5: (a) discolored patina, corroding fasteners, and vegetation build-up around Pole 8Z-2R; (b) uniform patina but corroding fasteners on Pole 11Z-6R; and (c) uniform patina and GS fasteners on Pole 11Z-2L.....</i>	<i>53</i>
<i>Figure 3.30 Close-up view of patinas on Site 5 poles: (a-b) rough and non-adherent patina with areas of discolored rust and pitting on wall and repair sleeves of Poles 11Z-2L and 11Z-6L; (c-d) smoother and more adherent patina than Line 11Z on wall of Pole 8Z-2L and Pole 8Z-2R, in addition to pitting.</i>	<i>55</i>
<i>Figure 3.31 Corrosion of GS fasteners connecting WS pole to GS caisson for Line 11Z poles at Site 5: (a) depletion of protective zinc layer on GS nuts of Pole 11Z-6L; and (b) pack-rust damage on bottom GS nuts of Pole 11Z-6R.....</i>	<i>56</i>
<i>Figure 3.32 Corrosion of GS fasteners connecting GS caissons to WS poles of Line 8Z at Site 5: (a) Pitting on top nuts and pack-rust damage on bottom GS nuts of Pole 8Z-2R; and (b) pack-rust damage on bottom GS nuts of Pole 8Z-2L.</i>	<i>57</i>
<i>Figure 3.33 Water pooling in GS caisson foundations leading to: (a) sludge build-up; and (b) pack-rust damage on GS nuts.....</i>	<i>58</i>
<i>Figure 3.34 Corrosion damage on interior of unsealed WS poles at Site 5: (a) dense pitting on Pole 8Z-2L; (b) pitting and pack rust on Pole 11Z-6R; (c) pitting and pack rust on Pole 11Z-6L; and (d) severe pack rust on Pole 11Z-2R.</i>	<i>59</i>
<i>Figure 3.35 Recent remediation of Poles 11Z-2L and 11Z-2R at Site 5: (a) new GS fasteners and cathodic protection for GS caisson; and (b) concrete filling for hollow GS caisson.....</i>	<i>59</i>

<i>Figure 3.36 Overhead corrosion damage on WS poles at Site 5: (a) failure of ladder-wall connection on Pole 11Z-6L; and (b) crack at cross-arm connection of Poles 8Z-2L and 8Z-2R.....</i>	<i>60</i>
<i>Figure 4.1 Photographs illustrating atmospheric exposure of WS pole structures in: (a) Site 1; (b) Site 2; (c) Site 3; (d) Site 4; and (e) Site 5.</i>	<i>66</i>
<i>Figure 4.2 Corrosion-induced thickness loss in atmospheres with different SO₂ content for WS and plain CS (Knotkova et al. 1982).....</i>	<i>72</i>
<i>Figure 4.3 Corrosion of WS as function of SO₂ concentration (Knotkova et al. 1982)....</i>	<i>73</i>
<i>Figure 4.4 Impact of airborne salinity on corrosion rate of WS (Morcillo et al. 2013)...</i>	<i>75</i>
<i>Figure 4.5 Corrosion-induced thickness loss history for ASTM A242 (Cor-Ten A) WS under different exposure conditions (Schmitt and Gallagher 1969).</i>	<i>77</i>
<i>Figure 4.6 Corrosion-induced thickness loss history for ASTM A588 (Cor-Ten B) WS under different exposure conditions (Townsend and Zoccola 1982).....</i>	<i>78</i>
<i>Figure 4.7 Steel panel specimens mounted on inclined rack for corrosion testing in chloride-laden atmosphere (Roberge 2008).....</i>	<i>83</i>
<i>Figure 4.8 Weather data collected for Site 1 from Regina International Airport (Regina, SK) weather station: (a) high and low temperature averages; and (b) high and low RH averages (WeatherSpark 2015d).....</i>	<i>88</i>
<i>Figure 4.9 Weather data collected for Site 2 from Saskatoon John G. Diefenbaker International Airport (Saskatoon, SK) weather station: (a) high and low temperature averages; and (b) high and low RH averages (WeatherSpark 2015e).</i>	<i>89</i>
<i>Figure 4.10 Weather data collected for Site 3 from Estevan Regional Aerodrome (Estevan, SK) weather station: (a) high and low temperature averages; and (b) high and low RH averages (WeatherSpark 2015b).</i>	<i>90</i>
<i>Figure 4.11 Weather data collected for Site 4 from Melbourne International Airport (Melbourne, FL) weather station: (a) high and low temperature averages; and (b) high and low RH averages (WeatherSpark 2015c).....</i>	<i>91</i>
<i>Figure 4.12 Weather data collected for Site 5 from Patrick Air Force Base (Cocoa Beach, FL) weather station: (a) high and low temperature averages; and (b) high and low RH averages (WeatherSpark 2015a).</i>	<i>92</i>
<i>Figure 4.13 Surface-swab testing for chloride and sulfate deposition: (a) test kit by MSES Consultants, Inc.; (b) pole swabbing; and (c) on-site analysis of swab samples.</i>	<i>94</i>
<i>Figure 4.14 Color-coded criteria for indicator strips in swab test kit: (a) sulfates and (b) chlorides. Results expressed in contaminant mass per liter of aqueous solution.</i>	<i>94</i>

<i>Figure 4.15 Areas of soil corrosivity concern: (a) coating deterioration near ground line of Pole Q3C-2L; and (b) pack rust at uncoated ground line of Pole S3B-2L.</i>	<i>101</i>
<i>Figure 4.16 Digital potential meter with CCSRE (M.C. Miller Co., Inc.).</i>	<i>108</i>
<i>Figure 4.17 Soil pH and resistivity meter (SRM-100, MSES Consultants, Inc.).</i>	<i>109</i>
<i>Figure 4.18 Color-coded criteria for carbonate indicator strip in swab test kit.</i>	<i>109</i>
<i>Figure 4.19 Field testing of soil corrosivity.</i>	<i>110</i>
<i>Figure 5.1 Ultrasonic thickness gage measurements: (a) instrument used (model 45MG, Olympus Corp.); and (b) measurement being performed on Pole S3B-3L.</i>	<i>127</i>
<i>Figure 5.2 Deep pit measurement: (a) pit gage (W.R. Thorpe & Co.); and (b) measurement being performed on Pole TL-1.</i>	<i>128</i>
<i>Figure 5.3 Coating thickness measurement: (a) thickness gage (model PenTest, ElektroPhysik); and (b) measurement being performed on Pole S3B-7R.</i>	<i>128</i>
<i>Figure 5.4 Comparison of average and maximum corrosion rate for all WS poles.</i>	<i>136</i>
<i>Figure 5.5 Maximum corrosion rates as a function of age for all WS poles.</i>	<i>139</i>
<i>Figure 5.6 Average corrosion rates as a function of age for all WS poles.</i>	<i>139</i>
<i>Figure 5.7 Measurement of structure-to-soil potential on WS pole at Site 2.</i>	<i>145</i>
<i>Figure 5.8 Pourbaix diagram of Fe with NACE (2013) cathodic protection threshold and corrosion potential-soil pH markers for WS poles at Sites 1 through 5.</i>	<i>152</i>
<i>Figure 6.1 Schematic of structure of protective oxide film in WS steel (Morcillo et al. 2014).</i>	<i>162</i>
<i>Figure 6.2 SEM micrographs of iron oxides and hydroxides in WS patina: (a) goethite (Zic et al. 2007); (b) lepidocrocite (Antony et al. 2004); (c) magnetite (Topal and Aksan 2016); (d) maghemite (Mozaffari et al. 2015); and (e) akaganeite (Roque-Malherbe et al. 2015).</i>	<i>164</i>
<i>Figure 6.3 Corrosion rates in WS for different atmospheric chloride concentrations (in mg/dm²-day or mdd) as function of α/γ^* (Kamimura et al. 2006).</i>	<i>166</i>
<i>Figure 6.4 Collection of surface oxide samples: (a) scraping of patina to obtain powder sample; and (b) pack-out rust sample removed by hand from junction box area of Pole TL-1.</i>	<i>169</i>
<i>Figure 6.5 SEM micrographs of pack-rust samples collected from coating line region of WS poles at Site 2: (a) Pole Q3C-1L; (b) Pole Q3C-2L; and (c) Pole Q3C-2R.</i>	<i>176</i>

<i>Figure 6.6 SEM micrographs of samples collected from Pole TL-1 at Site 4: (a) outer pack out; and (b) inner pack out.</i>	177
<i>Figure 6.7 SEM micrographs of loose rust samples collected from GS fastener region of WS poles at Site 5: (a) Pole 8Z-2L; (b) Pole 8Z-2R; and (c) Pole 11Z-6R.</i>	177
<i>Figure 6.8 XRD spectra for: (a) Pole C1F-20 wall sample; and (b) Pole TL-1 outer pack-out rust sample.</i>	185
<i>Figure 6.9 ⁵⁷Fe Mössbauer spectra for pack-rust sample from reflective tape of Pole C1F-20 at Site 1.</i>	196
<i>Figure 6.10 ⁵⁷Fe Mössbauer spectra for WS oxide samples from: (a) Pole S3B-2L; (b) Pole C1F-20; (c) Pole Q3C-2L; (d) Pole 8Z-2L; and (e) Pole TL-1.</i>	198
<i>Figure 6.11 ⁵⁷Fe Mössbauer spectra for pole wall sample from Pole S3B-2L at 4.2 K and 180 K, and difference between spectra at 4.2 K and 180 K.</i>	200
<i>Figure 7.1 Metallizing of steel pole.</i>	218
<i>Figure 7.2 Sacrificial WS sleeve installed at base of WS pole.</i>	220
<i>Figure A.1 Pack-rust sample from coating line region of Pole Q3C-1L at Site 2.</i>	257
<i>Figure A.2 SEM micrographs for pack-rust sample from coating line region of Pole Q3C-1L at Site 2: (a) full view; (b) magnified 100x; (c) magnified 1000x; and (d) magnified 5000x.</i>	257
<i>Figure A.3 Pack-rust sample from coating line region of Pole Q3C-2L at Site 2.</i>	258
<i>Figure A.4 SEM micrographs for pack-rust sample from coating line region of Pole Q3C-2L at Site 2: (a) full view; (b) magnified 100x; (c) magnified 1000x; and (d) magnified 5000x.</i>	258
<i>Figure A.5 Pack-rust sample from coating line region of Pole Q3C-2R at Site 2.</i>	259
<i>Figure A.6 SEM micrographs for pack-rust sample from coating line region of Pole Q3C-2R at Site 2: (a) full view; (b) magnified 100x; (c) magnified 1000x; and (d) magnified 5000x.</i>	259
<i>Figure A.7 Outer pack-out sample from Pole TL-1 at Site 4.</i>	260
<i>Figure A.8 SEM micrographs for outer pack-out sample from Pole TL-1 at Site 4: (a) full view; (b) magnified 100x; (c) magnified 1000x; and (d) magnified 5000x.</i>	260
<i>Figure A.9 Inner pack-out sample from Pole TL-1 at Site 4.</i>	261
<i>Figure A.10 SEM micrographs for inner pack-out sample from Pole TL-1 at Site 4: (a) full view; (b) magnified 100x; (c) magnified 1000x; and (d) magnified 5000x.</i>	261

<i>Figure A.11 Loose rust sample from GS fastener region of Pole 8Z-2L at Site 5.....</i>	<i>262</i>
<i>Figure A.12 SEM micrographs for loose rust sample from GS fastener region of Pole 8Z-2L at Site 5: (a) full view; (b) magnified 100x; (c) magnified 1000x; and (d) magnified 5000x.....</i>	<i>262</i>
<i>Figure A.13 Loose rust sample from GS fastener region of Pole 8Z-2R at Site 5.....</i>	<i>263</i>
<i>Figure A.14 SEM micrographs for loose rust sample from GS fastener region of Pole 8Z-2R at Site 5: (a) full view; (b) magnified 100x; (c) magnified 1000x; and (d) magnified 5000x.....</i>	<i>263</i>
<i>Figure A.15 Loose rust sample from GS fastener region of Pole 11Z-6R at Site 5.....</i>	<i>264</i>
<i>Figure A.16 SEM micrographs for loose rust sample from GS fastener region of Pole 11Z-6R at Site 5: (a) full view; (b) magnified 100x; (c) magnified 1000x; and (d) magnified 5000x.....</i>	<i>264</i>
<i>Figure A.17 XRD spectrum for pack-rust sample from reflective tape region of Pole C1F-20 at Site 1.</i>	<i>265</i>
<i>Figure A.18 XRD spectrum for pole wall sample from Pole Q3C-1L at Site 2.....</i>	<i>266</i>
<i>Figure A.19 XRD spectrum for pack-rust sample from coating line region of Pole Q3C-1L at Site 2.</i>	<i>266</i>
<i>Figure A.20 XRD spectrum for pole wall sample from Pole Q3C-1R at Site 2.....</i>	<i>267</i>
<i>Figure A.21 XRD spectrum for pole wall sample from Pole Q3C-2L at Site 2.....</i>	<i>267</i>
<i>Figure A.22 XRD spectrum for pack-rust sample from coating line region of Pole Q3C-2L at Site 2.</i>	<i>268</i>
<i>Figure A.23 XRD spectrum for pole wall sample from Pole Q3C-2R at Site 2.....</i>	<i>268</i>
<i>Figure A.24 XRD spectrum for pack-rust sample from coating line region of Pole Q3C-2R at Site 2.....</i>	<i>269</i>
<i>Figure A.25 XRD spectrum for pole wall sample from Pole S3B-2L at Site 3.....</i>	<i>269</i>
<i>Figure A.26 XRD spectrum for pole wall sample from Pole S3B-3L at Site 3.....</i>	<i>270</i>
<i>Figure A.27 XRD spectrum for pole wall sample from Pole S3B-7L at Site 3.....</i>	<i>270</i>
<i>Figure A.28 XRD spectrum for pole wall sample from Pole S3B-7R at Site 3.....</i>	<i>271</i>
<i>Figure A.29 XRD spectrum for pole wall sample from Pole TL-1 at Site 4.</i>	<i>271</i>
<i>Figure A.30 XRD spectrum for inner pack-out sample from Pole TL-1 at Site 4.....</i>	<i>272</i>

<i>Figure A.31 XRD spectrum for pack-rust sample from deepest pit on Pole TL-1 at Site 4.....</i>	<i>272</i>
<i>Figure A.32 XRD spectrum for pole wall sample from Pole 8Z-2L at Site 5.</i>	<i>273</i>
<i>Figure A.33 XRD spectrum for loose rust sample from GS fastener region of Pole 8Z-2L at Site 5.</i>	<i>273</i>
<i>Figure A.34 XRD spectrum for pole wall sample from Pole 8Z-2R at Site 5.....</i>	<i>274</i>
<i>Figure A.35 XRD spectrum for loose rust sample from GS fastener region of Pole 8Z-2R at Site 5.</i>	<i>274</i>
<i>Figure A.36 XRD spectrum for pole wall sample from Pole 11Z-2L at Site 5.</i>	<i>275</i>
<i>Figure A.37 XRD spectrum for pole wall sample from Pole 11Z-2R at Site 5.....</i>	<i>275</i>
<i>Figure A.38 XRD spectrum for pole wall sample from Pole 11Z-6R at Site 5.....</i>	<i>276</i>
<i>Figure A.39 XRD spectrum for loose rust sample from GS fastener region of Pole 11Z-6R at Site 5.</i>	<i>276</i>
<i>Figure A.40 ⁵⁷Fe Mössbauer spectra recorded for pack-rust sample from coating line region of Pole Q3C-2L at Site 2.</i>	<i>278</i>
<i>Figure A.41 ⁵⁷Fe Mössbauer spectra recorded for pole wall sample from Pole S3B-2L at Site 3.....</i>	<i>280</i>
<i>Figure A.42 ⁵⁷Fe Mössbauer spectra recorded for inner pack-out sample from Pole TL-1 at Site 4.</i>	<i>282</i>
<i>Figure A.43 ⁵⁷Fe Mössbauer spectra recorded for loose rust sample from GS fastener region of Pole 8Z-2L at Site 5.....</i>	<i>284</i>

CHAPTER 1.0 INTRODUCTION

Corrosion is a major instrument of degradation in steel transmission line structures, which are exposed to a broad range of aggressive outdoor environments. Direct exposure to moisture and airborne contaminants causes steel to corrode at rates that depend primarily on the exposure conditions and the characteristics of the steel (Morcillo et al. 2013). For the past three decades, the use of weathering steel (WS) has been a popular solution for corrosion-resistant transmission line poles Hoitomt (2002). When exposed to the atmosphere and allowed to routinely dry, WS forms a stable rust film that protects the steel surface beneath, thus offsetting the need for protective paint and coatings. However, significant corrosion problems have been documented on a number of WS transmission line structures, including cases in which the protective layer never stabilized and corrosion developed steadily (Li et al. 2008). As a result, uncertainty exists on the durability of WS transmission line structures, some of which have been recently installed.

Limited life-cycle data are available for WS transmission line poles compared to structures made of other materials such as wood (Tallavo et al. 2013). Information on age, population, structure type, and materials is currently not available in extents that are sufficient for meaningful life-cycle evaluations. Utilities, and possibly some contractors, may have pertinent information but it has yet to be compiled as part of an industry-wide survey and evaluation. This lack of data inevitably translates into knowledge gaps on how WS transmission line structures perform, and mirrors the substantial lack of standards and regulations on corrosion assessment, prevention and remediation.

Corrosion data from the literature are widely scattered (Morcillo et al. 2014). There are several factors that explain why all corrosion test results, not just those for WS, are scattered. For example, minor impurities in a steel alloy can have an effect on corrosion rates. Each of the elements included in WS alloys possess their own mechanical, chemical, and physical properties and, therefore, can corrode in different manners (Moroishi and Satake 1973). Furthermore, corrosion behavior is the result of complex interactions between a metallic surface and its adjacent environment. Corrosion data are usually specific to the environments where they are collected. There are a vast number of operational environments to which transmission lines can be exposed over their service life, and each can pose potential problems (Oh et al. 1999). Thus, corrosion data from a given source can seldom be used to predict corrosion rates in other field applications. For these reasons, the most dependable predictors of practical corrosion performance are the owners' and inspectors' experience, and results and data from field testing, for specific environments and variations thereof (Roberge 2008).

The overarching goal of the research project presented in this report is to provide utilities with comprehensive and up-to-date information on:

- Corrosion behavior of WS transmission poles vis-à-vis operating environments.
- Best practices for corrosion assessment, prevention and remediation.

Accordingly, the objectives of this report are to draw salient conclusions based on evidence gathered using a variety of field assessment and laboratory characterization techniques, and offer case-specific recommendations for prevention and remediation as it applies to WS transmission line poles located in diverse and representative environments.

CHAPTER 2.0 WEATHERING STEEL TRANSMISSION LINE POLES

This chapter presents an overview of WS with an emphasis on corrosion resistance in overhead transmission line structures. Section 2.1 summarizes the historical development of WS and provides information on representative WS alloys and their salient physical and mechanical properties. Section 2.2 describes the primary WS alloying elements and their functions, with an emphasis on implications for corrosion resistance. Section 2.3 overviews the corrosion behavior of WS based on the results drawn from long-term experimental programs reported in archival literature. Section 2.4 discusses the durability of WS transmission line structures based on representative examples of corrosion damage encountered in the field, also leveraging the direct experience of the authors.

2.1 Historical Development

The creation of WS follows the development of copper (Cu)-bearing steels. In the early 20th century, the idea of combining copper and iron to form steel was explored by the newly formed American Society for Testing and Materials (ASTM). Based on empirical evidence from tests on 50×100 mm samples exposed to industrial (coke) atmospheres in Pennsylvania, and marine environments in Atlantic City, NJ, thickness losses in Cu-bearing steels were reported to be 1.5 to 2.0 times smaller than those of carbon steel (CS) counterparts (Buck 1913). In particular, it was noted that corrosion resistance was maximized for Cu amounts in the range 0.15-0.25% in weight (Buck 1915). As a result, US Steel started to manufacture and sell Cu-bearing steel sheets. The appeal of Cu-bearing steel prompted more research in alloy optimization and, starting from the early 1920s, US

Steel Corporation developed high-strength low-alloy (HSLA) steels that were intended primarily for the railroad industry (Albrecht and Hall 2003). The development of WS as a spinoff of HSLA steel research dates back to the 1930s (Chen et al. 2005).

In 1933, US Steel patented the first marketable WS under the trademark USS Cor-Ten steel. The name identifies the two properties that distinguish WS from CS and Cu-bearing steel, i.e., corrosion resistance (“Cor”) and superior tensile (“Ten”) yield and ultimate strength, respectively (Albrecht and Hall 2003). In fact, as a result of the inclusion of Cu, chromium (Cr), phosphorus (P), and nickel (Ni), the corrosion by-products that form on the surface of WS coexist as crystalline and partially as amorphous structures, producing a more adherent and compact oxide film compared to standard CS (Albrecht and Hall 2003, Revie and Uhlig 2008). In regard to strength, the minimum specified mechanical properties for modern Cor-Ten steel used in transmission line structures are those set forth in ASTM A242 (ASTM 2013a) and ASTM A588 (ASTM 2015a) for HSLA structural steel, including a 345 MPa (50 ksi) minimum yield point for thicknesses up to 100 mm (3.9 in.).

Early types of WS contained Cu, Cr, and P as the primary alloying elements. Nickel was subsequently introduced to enhance corrosion resistance in chloride-laden (e.g., marine) environments. In 1941, the first WS standard was issued as ASTM A242 (ASTM 2013a), introducing a chemical composition comparable to that of modern Cor-Ten A steel (Table 2.1). ASTM A242 WS offered superior resistance to atmospheric corrosion, with thickness losses that were reported as four times smaller than those experience in standard CS. A significant shortcoming of ASTM A242 WS was the fact that iron phosphide (FeP_3) would form during the welding process, decreasing weldability and increasing brittleness. Therefore, the composition of ASTM A242 WS was amended to limit the amount of P to

less than 0.15% in weight, and a subsequent standard, ASTM A588 (ASTM 2015a), was published in 1968 to address this issue by specifying a weight content of P of less than 0.04% (Table 2.1). ASTM A588 WS, which is comparable to modern Cor-Ten B steel, possesses less resistance to atmospheric corrosion due to its reduced P content compared to ASTM A242 WS but offers better weldability.

A Canadian WS variation, labeled “Atmospheric Corrosion Resistant Steel,” was developed as an alternative to Cor-Ten steel. This variation was standardized in 1978 by the Canadian Standards Association (CSA) under CSA G40.21 (CSA 2013) as “Type AT” steel (Table 2.1). It noted that the standard asserts that the atmospheric corrosion resistance of this WS is superior to that of CS with or without copper.

Table 2.1 Chemical composition of modern WS alloys.

Designation	C	Mn	Cu	S	Cr	P	Ni	Si	V
	[% in weight]								
ASTM A242 (2013)	≤0.15	≤ 1.00	≥0.20	≤0.05	-	≤0.15	-	-	-
ASTM A588 (2010)	≤0.19	0.80-1.25	0.25-0.40	≤0.05	0.40-0.65	≤0.04	≤0.40	0.30-0.65	0.02-0.10
CSA G40.21 (2013)	≤0.20	0.75-1.35	-	≤0.04	≤0.70	≤0.03	-	0.70	-

Electric utilities have used weathering steel (WS) for nearly 50 years, leveraging its corrosion resistance and associated cost savings (Wong 2009). Introduced to utilities in the 1960s, WS was first used in the construction of two transmission towers in Massachusetts in 1961 and then in a 563-km (350-mile) transmission line in Pennsylvania (Goodwin and Pohlman 1993). In the US, WS has since been used in single poles and lattice towers. For example, Hoitomt (2002) reported that approximately 100,000 WS tubular structures had been used by utilities for transmission and distribution of electric

power, lighting of athletic fields and parking lots, highway interchange lighting, wind power generation and cellular communication structures.

In some instances, domestic and foreign utilities delayed using WS until more comprehensive data could be compiled to better understand performance and reliability. For example, until recently, utilities in China did not deploy WS in transmission towers due essentially to a lack of thoroughly tested and marketable products (Yang et al. 2009). In the US, problems with large WS structures arose in the 1970s. Notable architectural failures of WS structures include the Hawaii's Aloha Stadium (built in 1975), and the Omni Coliseum in Atlanta, GA (built in 1972). The Omni Coliseum was demolished after 25 years due to extensive corrosion damage in the structure. The Michigan Department of Transportation declared a moratorium on the use of WS in bridges due to corrosion concerns. The American Iron and Steel Institute (AISI) commissioned a study in 1982 to determine the nature of the problem (Barth and McConnell 2010). Approximately 100 WS bridges in West Virginia that covered a wide range of applications were inspected. It was determined that the bridges suffered the most severe problems when water infiltrated into or stagnated on WS members. It was recommended that careful consideration be paid to drainage systems and watertight connections to prevent corrosion damage. In fact, as extensively discussed in this report, inconsistent drying conditions hinder the exposure of WS surfaces to wet/dry cycles (e.g., rain/sun), which are necessary for the formation of an effective protective oxide film. This consideration is of primary importance in the design and detailing of WS transmission line poles.

2.2 Alloy Composition

This section presents a literature review on the alloy composition of WS. The primary alloying elements and their functions are discussed with an emphasis on implications for corrosion resistance. In fact, when alloyed with steel in small concentrations, Cu, Cr, P, and Ni are particularly effective in reducing corrosion. Significant knowledge gaps remain to understand the influence of WS alloying elements on corrosion resistance as most information is still based on empirical evidence (i.e., comparison of thickness loss of WS and CS counterparts) from exposure tests on flat steel coupons, which are hardly representative of actual structures, in selected environments.

2.2.1 Copper

Buck (1915) discovered that alloying mild steel with less than 0.25% Cu in weight resulted in an enhancement of atmospheric corrosion resistance. Based on the work of Larrabee and Coburn (1962), an optimal range for Cu was originally established as 0.05-0.20%. Copper influences the microstructure of oxides forming on the steel surface, resulting in larger density and a decrease in corrosion rate compared to standard CS. Copson (1945) noted that the increase in density of the oxide film is due to the formation of insoluble Cu complexes, $[\{Cu[(OH)_2Cu]_x\}SO_4]$, which contribute to filling the oxide pores, thereby increasing corrosion resistance irrespective of the exposure conditions (ranging from aggressive industrial to marine environments), as shown in Figure 2.1 (Larrabee and Coburn 1962).

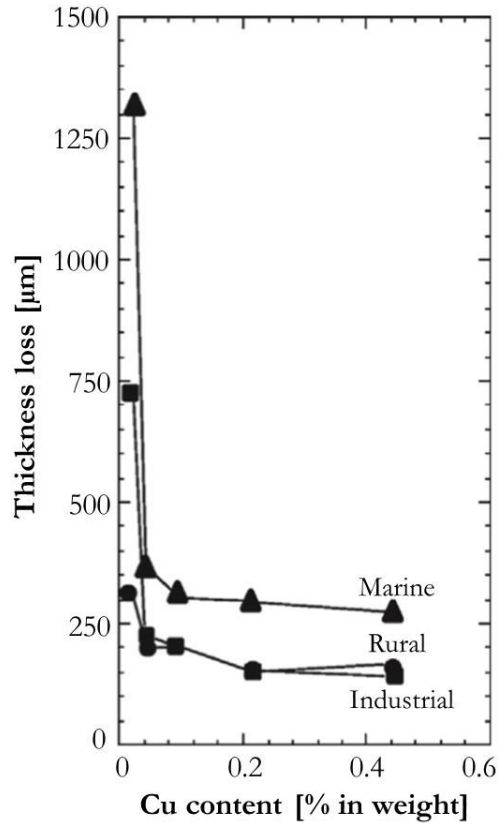


Figure 2.1 Effect of Cu content on corrosion-induced thickness loss of steel exposed to different aggressive environments for 15.5 years (Larrabee and Coburn 1962).

2.2.2 Chromium

The incorporation of Cr in steel is beneficial for atmospheric corrosion resistance provided that a sufficient amount of Cu is present, as indicated by the empirical data presented in Figure 2.2 (Copson 1960). In fact, the incorporation of relatively small amounts of Cr (<1%) may result in decreased durability as the Cu content is reduced to 0.01% (Larrabee and Coburn 1962). Copson (1960) suggested that the inclusion of Cu in amounts $\geq 0.1\%$ is desirable for corrosion resistance.

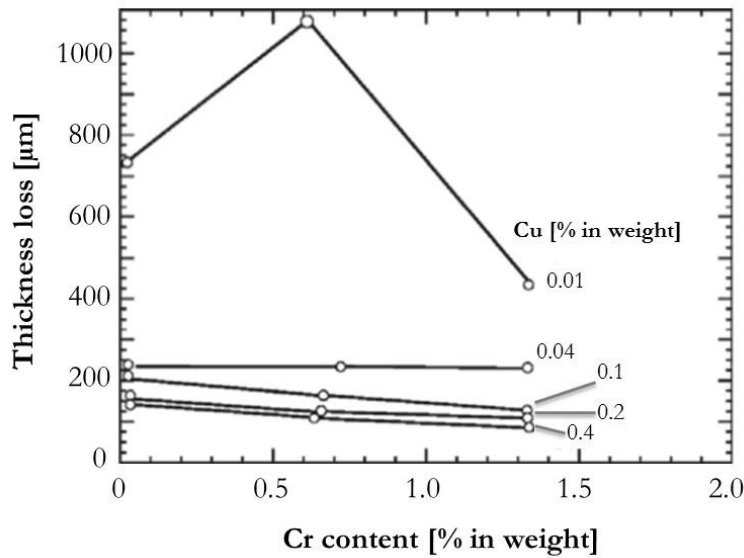


Figure 2.2 Effect of Cr content for different Cu contents on corrosion-induced thickness loss of steel exposed to industrial atmosphere for 18 years (Copson 1960).

Kamimura and Stratmann (2001) investigated the corrosion behavior of mild and Cr-bearing steel subjected to wet/dry cycles. The main influence of Cr on corrosion resistance appeared to lie in the inhibition of cathodic reactions. In addition, corrosion rates during drying decreased as the amount of Cr in the alloy increased. Qian et al. (2013) performed cyclic wet/dry tests to study the influence of Cr (in contents ranging from 0.8 to 9%) on the corrosion resistance of WS in a synthetic industrial atmosphere. Empirical evidence suggested that higher Cr contents facilitate the formation of a protective oxide film with enhanced passivation capabilities, mitigating the anodic dissolution of substrate alloys.

2.2.3 Phosphorus

When combined with Cu, P contributes to improving corrosion resistance. For example, the beneficial effect of adding up to 0.1% of P together with Cu is illustrated in Figure 2.3 (Larrabee and Coburn 1962). However, it is noted that P-bearing steel alloys

may experience either enhanced or impaired mechanical properties depending on the amount of P and the manufacturing process. Phosphorus is an effective hardener as less than 0.2% P may result in increases in the yield and tensile strength of steel by 60 MPa or greater. The associated tradeoff is the reduced fracture toughness and ductility. To offset embrittlement effects, the P content should be limited to 0.1% in structural steels to be directly exposed to potentially aggressive atmospheric conditions (Morcillo et al. 2014).

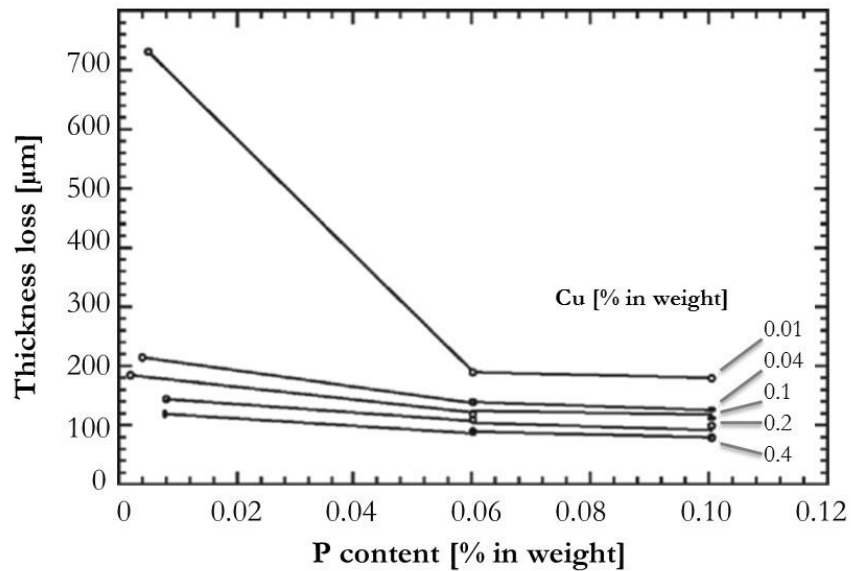


Figure 2.3 Effect of P content for different Cu contents on corrosion-induced thickness loss of steel exposed to industrial atmosphere for 15.5 years (Larrabee and Coburn 1962).

The corrosion resistance of an “economic” WS with a P content of 0.035% compared favorably with Cu-free CS and ASTM A242 WS (Hou and Liang 2002). The “economic” label was attributed as the WS variation entailed less expense on the alloying, and lacked the drawbacks that typically characterize P-bearing steel such as reduced bendability and weldability. A low-cost WS alloyed with Mn (1.38%), Cu (0.32%), and P (0.07%) also exhibited good corrosion resistance when subjected to wet/dry cyclic tests in

simulated industrial, coastal, and industrial-coastal atmospheres (Hao et al. 2011). The incorporation of P contributed to facilitating the formation of uniform and denser oxide films containing non-soluble phosphates, which offset the penetration of contaminants.

2.2.4 Nickel

Nickel is incorporated into WS alloys to curtail embrittlement during the hot-rolling process and improve resistance to atmospheric corrosion. The inclusion of Ni contributes to improving atmospheric corrosion resistance in both industrial and marine environments, as illustrated in Figure 2.4 for the latter case (Copson 1960). However, a higher Ni content is needed to attain comparable results to those attained through the incorporation of Cu. For example, a 1% Ni content is needed to yield similar enhancement in atmospheric corrosion resistance as produced by the addition of 0.5% Cu (Morcillo et al. 2014). Similar to Cr, the beneficial effects of Ni are enhanced by its combination with relatively small amounts of Cu (Larrabee and Coburn 1962).

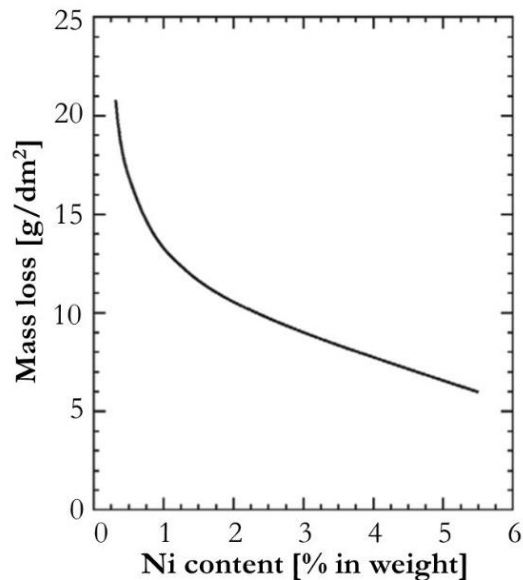


Figure 2.4 Effect of Ni content on corrosion-induced mass loss of steel exposed to marine atmosphere for 15.5 years (Copson 1960).

Nishikata et al. (1995) studied the corrosion rate of steels with different Ni contents (0, 2.5, 10, and 20%) under wet/dry cycles. The corrosion rate of standard CS and the 2.5% Ni-bearing steel were accelerated by the exposure to wet/dry cycles, and the corrosion rate of steel with at 5% or greater Ni content was less affected. However, the inclusion of Ni in amounts of 5% or greater produced a significant decrease of the corrosion rates of steel exposed to wet/dry cycles in chloride-laden environments.

2.2.5 Silicon

Based on empirical mass loss measurements, it has been reported that higher Si contents may result in greater corrosion resistance especially in environments with relatively low chloride levels (Gomez et al. 2011). In addition, evidence from X-ray diffraction measurements indicated that Si species do not replace iron in the goethite (α -FeOOH) microstructure of protective oxide films. Steel containing Cu (0.3%), Mn (0.5%), and Si (in the range 1-3%) was compared to standard CS by means of accelerated wet/dry cycles in aqueous 0.05 M and 0.5 M NaCl solutions. The formation of Fe oxides such as goethite, lepidocrocite (γ -FeOOH) and magnetite (Fe_3O_4) was observed. In the case of the Si-bearing steel alloys, superparamagnetic goethite was the main phase, suggesting that the presence of Si facilitates the formation of denser (i.e., having relative high goethite content) oxide films that mitigate corrosion effects (Gomez et al. 2012).

2.3 Corrosion Resistance

Corrosion protection is imperative for steel structures. When exposed to oxygen and moisture, especially in aggressive industrial and marine environments, steel may oxidize and corrode. The associated loss of surface material may result in a reduction of cross sectional area, thereby impairing both the strength and stability of transmission line

structural members (Matta et al. 2012, 2014). Since the introduction of WS, extensive research has been conducted to study the corrosion resistance of WS and other steel alloys. Relevant early examples include the work of Epstein and Horton (1949), Copson (1960), and Larrabee and Coburn (1962), which entailed atmospheric corrosion tests of steel specimens, as seen in Figure 2.5. These three comprehensive studies contributed towards the understanding (and subsequent improvement) of corrosion resistance and offered a major contribution to the knowledge base on HSLA steel and WS, particularly with regard to the correlation between alloying elements and corrosion performance, as well as corrosion mechanisms and their correlation with different environmental exposure conditions.

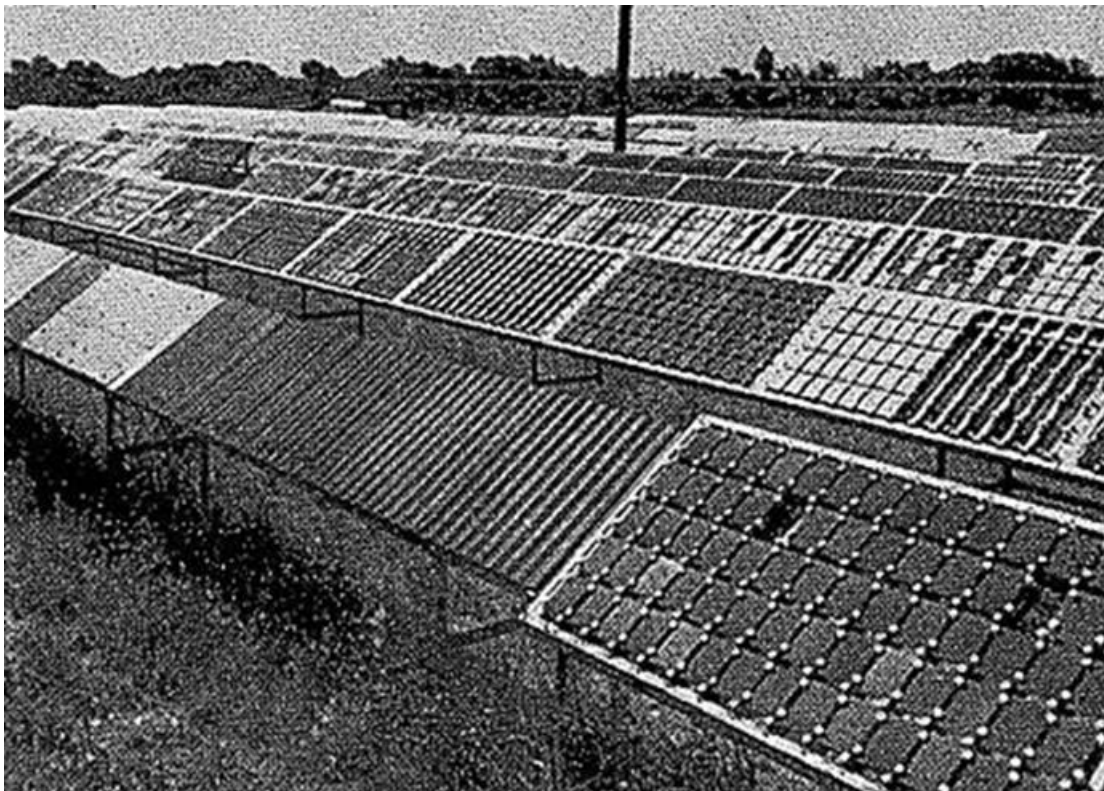


Figure 2.5 Atmospheric corrosion tests of steel specimens (Larrabee and Coburn 1962).

Epstein and Horton (1949) investigated atmospheric exposure effects on three base steel compositions containing various combinations of 15 different alloying elements. The base compositions were CS, Cu-bearing steel, and Mayari R steel (a proprietary high-strength low-alloy and corrosion-resistant steel produced by Bethlehem Steel Corporation, and an early competitor of Cor-Ten steel). The 15 alloying elements were aluminum (Al), arsenic (As), carbon (C), chromium (Cr), cobalt (Co), copper (Cu), manganese (Mn), molybdenum (Mo), nickel (Ni), phosphorus (P), silicon (Si), sulfur (S), tin (Sn), tungsten (W), and vanadium (V). Approximately 18,000 specimens of 300 different compositions were exposed to industrial atmospheres for periods of time between 7 and 16 years. The data generated from these experiments were used by Townsend (2002) to estimate the thickness loss of various WS compositions under different exposure conditions.

Copson (1960) performed atmospheric exposure tests on steel samples of 76 different compositions with diverse amounts of Cr, Cu, Ni, P, and Si. The test sites were located in Bayonne, NJ (industrial atmosphere), Block Island, RI, and Kure Beach, NC (marine atmosphere). The exposure times at the three sites were 18.1, 17.1, and 15.5 years, respectively. It was found that thickness losses for Cor-Ten A and Cor-Ten B steels were noticeably higher (up to 20%) for samples exposed to marine environments compared to industrial atmospheres (up to 5%). However, Cor-Ten steels outperformed CS and Cu-bearing steel.

Larrabee and Coburn (1962) subjected 270 different types of steel, also containing Cr, Cu, Ni, P, and/or Si, to the atmospheres of rural South Bend, PA, industrial Kearny, NJ, and marine Kure Beach, NC. Exposure times ranged from 0.5 to 15.5 years. Thickness loss trends as a function of time for CS, Cu-bearing steel, and WS (Cor-Ten B) samples

exposed to the industrial atmosphere of Kearny, NJ, are shown in Figure 2.6 (Larrabee and Coburn 1962). Cor-Ten B steel exhibited far superior corrosion resistance as a result of the formation of a stable and dense protective (self-passivating) oxide film, also known as patina, on the surface (Kamimura et al. 2002). It is noted that the corrosion index in ASTM G101 (2010) is based on the 15.5-year data from Kearny, NJ.

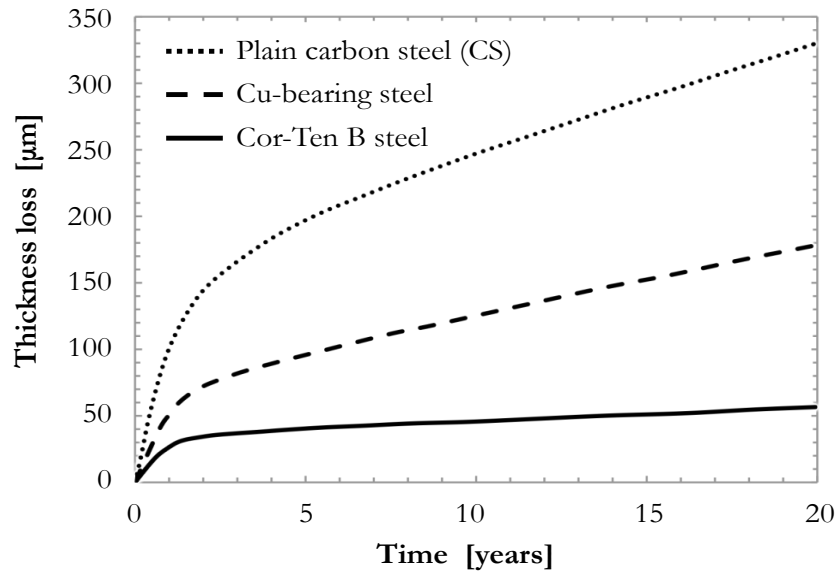


Figure 2.6 Corrosion thickness loss trend for CS, Cu-bearing and Cor-Ten B steel samples exposed to industrial atmosphere in Kearny, NJ (Larrabee and Coburn 1962).

In addition, Schmitt and Gallagher (1969) reported on evidence from Cor-Ten A steel samples that were tested under different exposure conditions. It was concluded that the quality of the patina in Cor-Ten A steel depends on the exposure to wet/dry cycles. It was also noted that surfaces shielded from cyclic wet/dry exposures are prone to forming a non-adherent oxide film whereas stable and dense films form on surfaces exposed to periodic wet/dry conditions. Matsushima et al. (1974) corroborated the conclusion that exposure to rain influences the formation of the protective film and studied the impact of drainage capabilities in areas where moisture was likely to collect. It was found that moisture

accumulation made the protective film less likely to form in environments with relatively higher pollution levels.

It is now widely recognized that the corrosion resistance of WS depends on the routine exposure to wet/dry conditions, and on different climate and environmental exposure conditions (Morcillo et al. 2014). The formation of protective oxide films is hindered by excess moisture, and presence of chlorides as well as sulfur dioxide. Ideal conditions entail a thorough washing of the steel surface, unimpeded drainage of built-up moisture, and rapid drying. Structures should be free of cracks and crevices, which facilitate an undesirable local stagnation of water. However, surface discontinuities resulting in crevices cannot be avoided entirely (e.g., in the case of mechanically-fastened connections), which may delay or hinder the formation of a protective oxide film. In fact, the use of bare WS in consistently wet environments or marine/industrial atmospheres should be discouraged (Kucera and Mattsson 1987). Settings where the corrosion performance of WS may be negatively impacted include atmospheres containing concentrated industrial fumes and coastal areas subject to chloride-laden sprays or fogs. Special maintenance considerations are also required for circumstances involving prolonged periods of rain, fog, and/or snow, and in the case of potential contact with aggressive chemicals such as agricultural fertilizers and herbicides (Hoitomt 2002).

2.4 Representative Corrosion Forms

In the case of WS transmission line poles, corrosion damage is typically attributed to “pack-rust” phenomena. Pack-rust can be formed as water penetrates between the initial oxide film and the underlying steel substrate. Once in contact with the water, the steel further oxidizes resulting in the formation of another oxide layer. This cyclic process may

continue with the formation of multiple non-adherent and unstable oxide films, thereby producing significant thickness losses as shown in the examples in Figure 2.7.

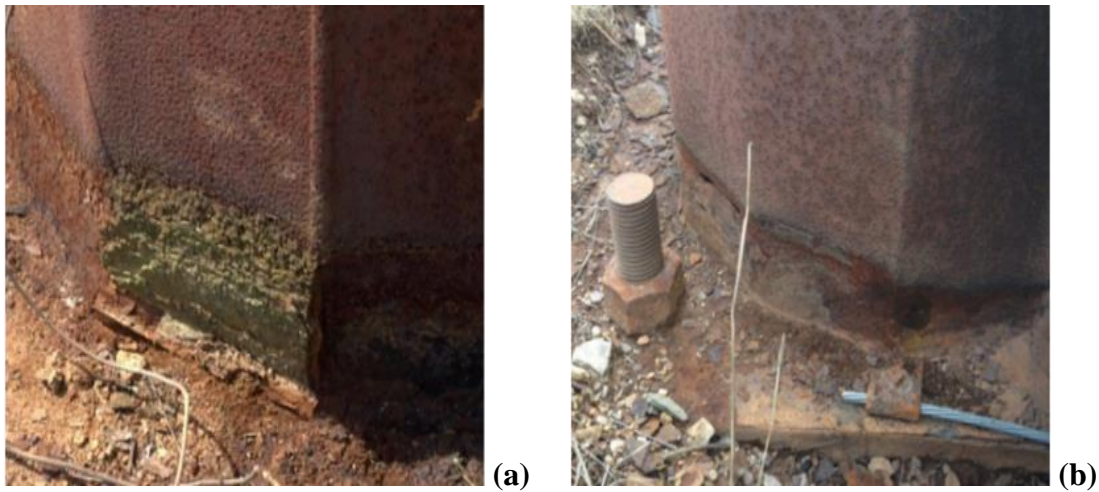


Figure 2.7 Examples of pack-rust damage near ground line of WS poles: (a) multiple layers stacking on one another; and (b) more severe thickness loss.

As highlighted in the photographs in Figure 2.7, corrosion damage in WS transmission line poles is more likely to occur near the ground line, irrespective of the type of foundation (i.e., direct embedment in soil or concrete foundation). In fact, a damp environment is formed as moisture collects at the ground line, thus hindering the formation of a protective oxide film. In particular, in the case of poles that are directly buried in soil, the steel is directly exposed to moist soil, which is an environment where WS steel (when unprotected) behaves similar to conventional CS from a corrosion standpoint. Corrosion can also be facilitated by the presence of surface flaws, changes in grades around the base of the pole after the pole is installed, uncontrolled growth of vegetation in the vicinity of (or in contact with) the pole, and sedimentation, which are all conditions that entail prolonged exposure to moisture as it is collected near the ground line. In these instances, the oxide film forming on the surface of WS may also be less adherent and stable than that

on conventional CS and a suitable protection (e.g., coating) should be considered (Misawa et al. 1974, Kamimura and Nasu 2000).

In WS structures, pack rust may build up at joints and crevices (e.g., between fasteners and steel plates), producing “pack-out” corrosion damage. In fact, pack rust has typically no room to flake off between adjacent steel surfaces in joints, and can build up. The volumetric expansion of the corrosion by-products results in significant pressures that are exerted on the adjoined steel elements, and may lead to structural damage due to large (plastic) deformations in addition to thickness losses (Dodson 2012). While this phenomenon is more likely to occur in WS lattice structures where mechanically-fastened connections are more common (Figure 2.8), it can also occur at discontinuities (e.g., coating lines) in WS transmission line poles.



Figure 2.8 Pack-out damage at connection in WS transmission line lattice structure. Note bent steel member.

Another form of corrosion damage that is of concern in WS transmission line poles is pitting. Pitting is a localized form of corrosion by which pits form in the metal substrate (Figure 2.9). Pitting is typically initiated by the occurrence of a local cathodic site within a

regular steel surface, and can be exacerbated by chemical or mechanical damage to the protective oxide film and damage to or poor application of protective coatings. The practical significance of pitting corrosion with respect to structural safety depends on the penetration rate and the thickness of the pole wall. The former generally decreases as the number of pits increases because the cathodic area of the pole, which controls the flow of corrosion current, is common to all adjacent pits. Pitting propagates as the penetration rate increases. Conversely, pits terminate if filled with corrosion products or the local cathode becomes covered in oxide film. Furthermore, the presence or absence of moisture will respectively facilitate or offset the development of pitting corrosion (Roberge 2008).



Figure 2.9 Widespread pitting over surface of WS pole wall.

Visual inspection is typically used to assess pitting levels in field applications. Because counting pits can be impractical, one can use rating charts from ASTM G46 (ASTM 2013c) to categorize pitting severity according to observed density (within 2 cm by 2 cm grids) and size, as shown in Figure 2.10. Within the context of this report, pitting damage levels are referred to accordingly by density and size. For example, pitting

corrosion with a density of 100,000/m² and average pit size of 2.0 mm² would be referred to as Level A4-B2.

When WS operates in a suitable service environment, approximately 60% of the protective oxide film forms within the first five years of exposure, consistent with the thickness loss trend shown in the example in Figure 2.6 (Larrabee and Coburn 1962), whereas negligible growth occurs after 25 years (Hoitomt 2002). The resulting corrosion resistance is reflected in a perceived life span for utilities in excess of 50 years (EPRI 2005). The life span of WS transmission line poles, however, may be drastically shortened should the corrosion examples described in this section manifest.











Level	<u>A</u>	<u>B</u>
	Density	Size
1	 2,500/m ²	 0.5 mm ²
2	 10,000/m ²	 2.0 mm ²
3	 50,000/m ²	 8.0 mm ²
4	 100,000/m ²	 12.5 mm ²
5	 500,000/m ²	 24.5 mm ²

Figure 2.10 Rating chart from ASTM G46 (ASTM 2013c) for pitting corrosion assessment.

In addition, design and construction flaws can also exacerbate corrosion problems. Representative cases include the use of poor materials (e.g., low-quality concrete in backfills, which allows soil moisture to reach the steel) and design practices (e.g., connections that trap and hold moisture). For example, the above-ground corrosion damage in WS poles may also be a consequence of poor sealing at the base and joints, leading to the collection of dirt and debris that absorb moisture, creating a damp environment that prevents the formation of protective oxide films. As a result, WS tends to corrode in a manner similar to CS.

CHAPTER 3.0 TEST SITES AND VISUAL ASSESSMENT OF POLE STRUCTURES

To assess the corrosion resistance of WS transmission line poles, field inspections were conducted at five test sites comprising diverse and significant operating environments and pole designs. These sites included three locations in Saskatchewan, Canada, and two sites in Florida, USA (Figure 3.1). This chapter will familiarize the reader with each test site by means of information collected via visual assessment.



Figure 3.1 Locations of test sites: (a) Saskatchewan, Canada; and (b) Florida, USA.

Visual assessment involved the use of photographs, videos, and field notes to document qualitative information on site location, environmental exposure conditions, pole design and detailing features, pre-existing corrosion prevention measures, and forms as well as severity of observable corrosion. Primary consideration was given to structural components from slightly above the ground line region to approximately 6-12 in. below ground since this is a critical area of concern for corrosion damage in transmission line poles. When evaluating corrosion forms, particular attention was given to the following: patina condition and color; evidence of pack-rust, pack-out, and pitting; galvanic corrosion effects; and steel condition at discontinuities and crevices.

Sections 3.1 through 3.5 provide the visual assessment outcomes for Sites 1 through 5, respectively. Section 3.6 compares all of the observed structures in terms of sustained corrosion damage and summarizes the most significant findings for each site. Section 3.7 summarizes the principal conclusions drawn for each test site from visual assessment.

3.1 Site 1 – Directly Embedded Pole in Rural/Urban Environment

Site 1 was situated on the outer edge of Regina, Saskatchewan (Figure 3.2), in between a steel manufacturing plant and Highway SK 11. The site was located adjacent to the steel plant's storage areas, approximately half a mile away from the manufacturing facilities, and removed from the city's more metropolitan areas by several miles. With this setting, Site 1 was considered to be exposed to a somewhat urban but predominantly rural environment and atmosphere. Inspection of Site 1 took place on 8 September 2015.

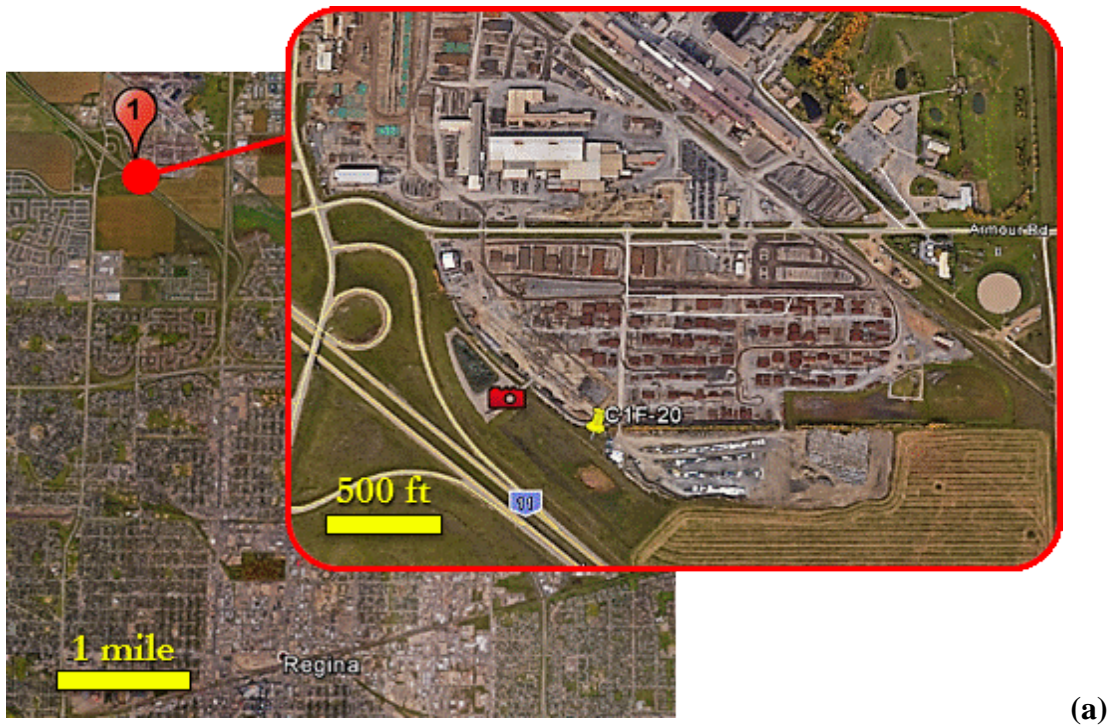


Figure 3.2 Site 1: (a) map indicating site and pole location; and (b) photographic view.

At the time of inspection, the transmission line considered, Line C1F, operated at a voltage of 230 kV. The line, which was installed in 1998, consisted of pole structures. One pole at Site 1, labeled C1F-20, was inspected by the author (Figure 3.3). The naming convention for this pole (and all other inspected structures) is based on a combination of the name of transmission line and the pole's position in the line with respect to the powering

substation. At the base, Pole C1F-20 has a circular cross section with nominal diameter of 18 in. and thickness of 5/16 in. It is made of Type AT steel as defined by CSA Standard G40.21 (CSA 2013). The pole was coated with liquid-applied polyurethane coating, directly embedded into the ground, and surrounded by a gravel backfill (Figure 3.4a). The coating extended approximately 30 in. above the ground line.



Figure 3.3 Ground-level view of Pole C1F-20 at Site 1.

Pole C1F-20 utilized a 10-ft galvanized steel (GS) grounding rod electrode for grounding protection. A grounding electrode conductor (GEC) connected the pole to the ground rod electrode by means of a “neutral” seven-wire GS strand (Figure 3.4b). The GEC was itself bonded to the WS surface just above the coating. According to the U.S. National Electrical Code, the purpose of grounding an electrical system is to control the voltage to earth during normal operation and the voltage imposed by contact with high voltage lines or lightning events (NFPA 2014).

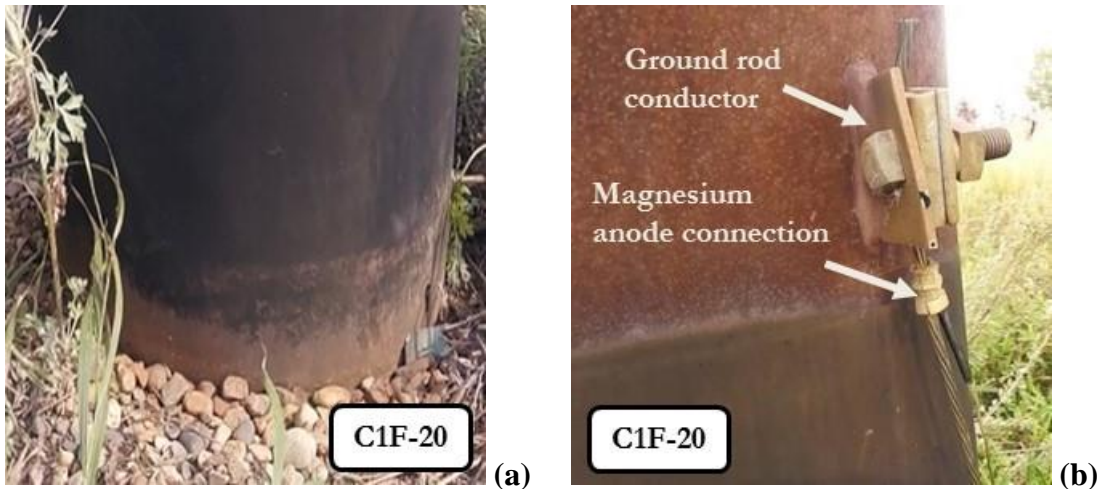


Figure 3.4 Corrosion prevention measures for Pole C1F-20: (a) polyurethane coating and rock backfill; and (b) GEC link to grounding rod and magnesium anode connection.

The structure was further protected from corrosion attack by a 32-lb magnesium anode that was installed at time of construction. The sacrificial anode was connected to the structure by means of a crimp that was fastened to the neutral wire used in the pole grounding system (Figure 3.4b). Magnesium anodes are used for cathodic protection of steel structures because magnesium has the greatest driving voltage of the materials used for sacrificial anodes. They are also favored for use in high-resistivity soils, as aluminum and zinc anodes are typically less economical in such electrolytic environments (Roberge 2008).

Pole C1F-20 was, for the most part, intact at the time of its inspection. The interface between the polyurethane coating and the WS substrate appeared to be intact. No delamination or visible signs of deterioration were present above the ground line and at the observed excavated portion. The oxide patina on the pole wall was relatively uniform with respect to smoothness, density, and dark-brown color. In addition to the ground level conditions being sound, no overhead damage was observed.

The major cause for concern was a green reflective tape that was applied to the circumference of the pole. In fact, only C1F-20 was inspected at Site 1 because repair efforts, including tape removal and cleaning of the underlying surfaces, had already been initiated on all other poles in the vicinity. Tape sections at two locations within reach were removed by slicing with a box cutter and peeling away from the surface. Underneath the top section, pitting was observed (Figure 3.5a) and classified via ASTM G46 (ASTM 2013c) as Level A3-B2. Below the bottom tape section, a thin layer of pack rust had formed (Figure 3.5b). This pack-rust would stick to the tape as it was removed, indicating that this oxide layer was not adherent to the pole wall nor protective.

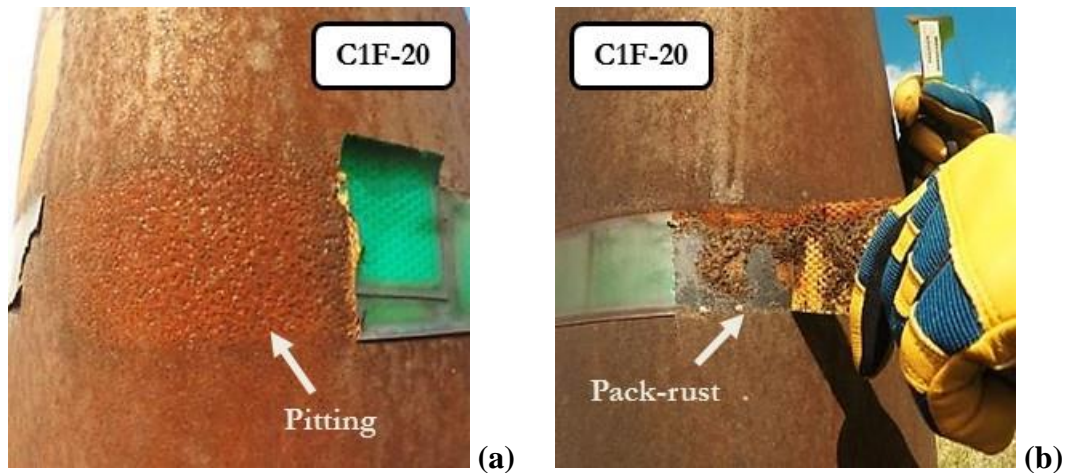


Figure 3.5 Corrosion damage under reflective tape on Pole C1F-20: (a) pitting; and (b) non-uniform pack rust.

Upon completion of visual inspection of Site 1, it was concluded that the localized forms of corrosion were likely due to continuous exposure to moisture that became entrapped between the tape and pole wall. Varying degrees of tape adhesion, and thus degrees of moisture penetration, are reasonable causes for the discrepancy in damage severity at different tape locations.

3.2 Site 2 – Directly Embedded Poles in Industrial Environment

Site 2 was located in Cory, Saskatchewan, approximately five miles southwest of Saskatoon, Saskatchewan (Figure 3.6), adjacent to a potash mine and the Cory Co-Gen Substation. Inspection of Site 2 took place on 9 September 2015.

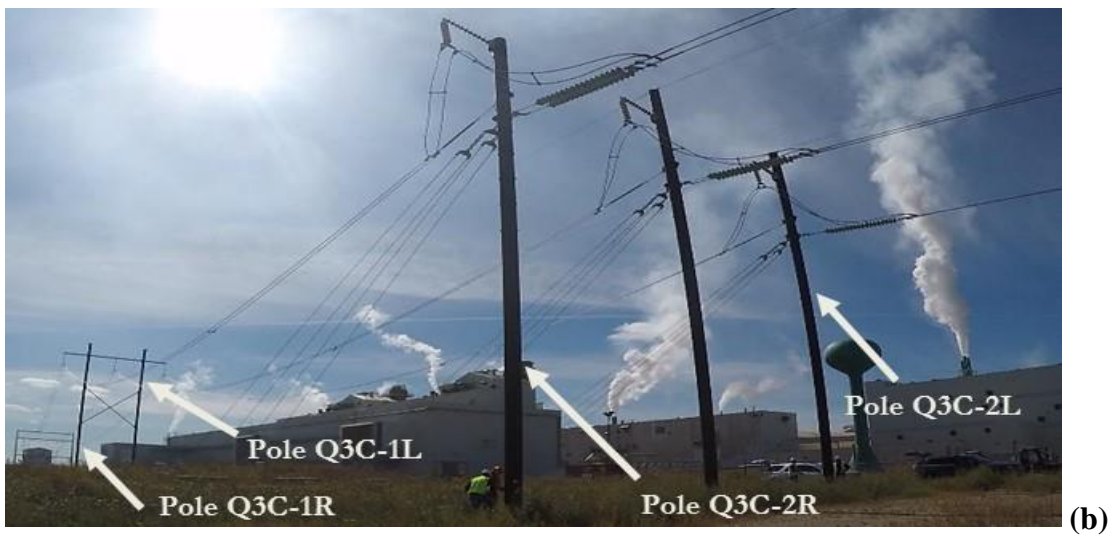
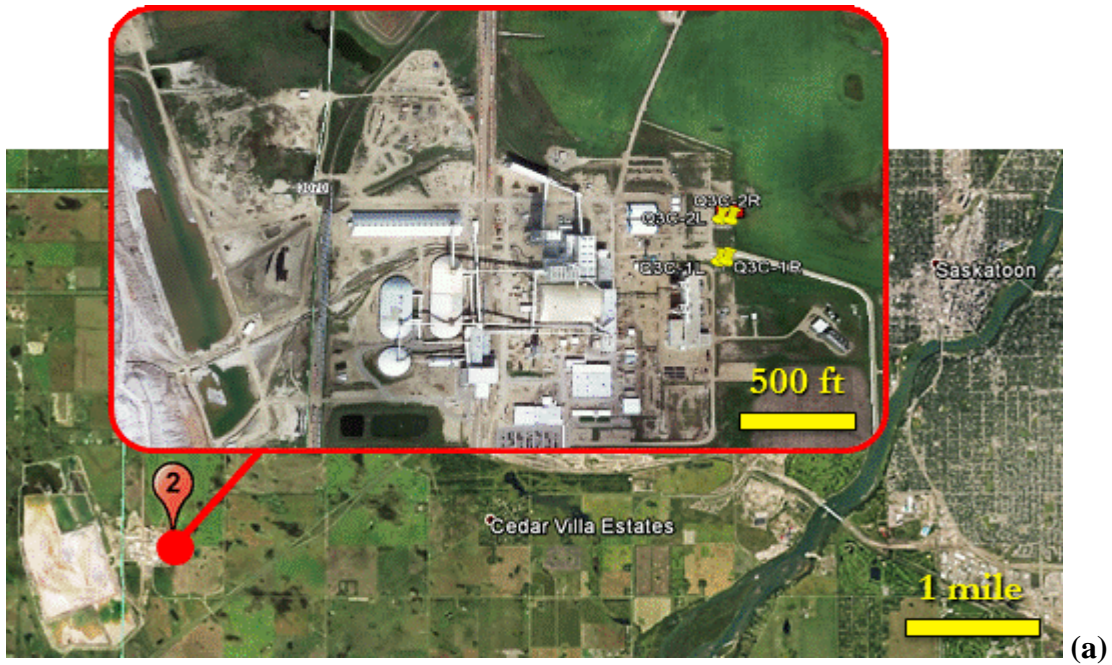


Figure 3.6 Site 2: (a) map indicating site and pole locations; and (b) photographic view.

The transmission line poles were located less than 100 ft from the mine processing facilities, which emitted smoke likely to contain corrosive pollutants. Due to the close proximity to these facilities, the poles were deemed to be exposed to an industrial atmosphere.

At the time of inspection, the transmission line at Site 2, Line Q3C, operated at a voltage of 138 kV. This line was installed in 2002. Out of five WS poles on site, one pole (Q3C-2R) was assessed based on visual inspection, and three poles (Q3C-1L, Q3C-1R, and Q3C-2L) were inspected using the full spectrum of field test methods detailed in Chapters 4.0 and 5.0. Poles Q3C-1L and Q3C-1R together formed an H-frame structure, while the other poles were split into single pole structures (Figure 3.6b). All four poles at Site 2 were made of Type AT steel (CSA 2013) and had a circular cross section at the base, with a nominal diameter of 18 in. Poles Q3C-1L and Q3C-1R had a nominal wall thicknesses of 5/16 in., and Poles Q3C-1L and Q3C-1R had a nominal wall thicknesses of 3/8 in. These four structures are shown in Figure 3.7.

All four poles were grounded using a similar type of grounding rod electrode system and GEC configuration (Figure 3.8). Poles Q3C-1L, Q3C-2L, and Q3C-2R utilized 32-lb magnesium anodes, which were installed at time of construction, as supplementary cathodic protection. Pole Q3C-1R did not feature a magnesium anode connection because the anode attached to Pole Q3C-1L was designed to protect both poles, which were connected to form an H-frame.

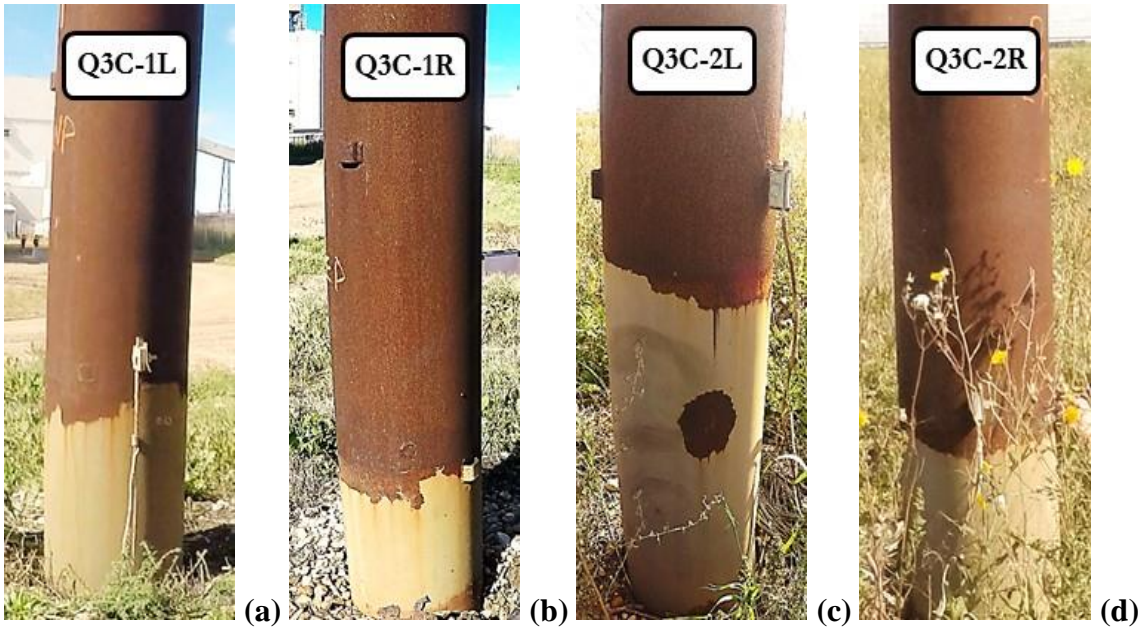


Figure 3.7 Site 2 poles: (a) Q3C-1L; (b) Q3C-1R; (c) Q3C-2L; and (d) Q3C-2R.



Figure 3.8 Corrosion prevention measures seen on Site 2 poles, including GEC link to grounding rod and magnesium anode connection.

The four poles were coated with a 3M Skotchkote 352 polyurethane coating (Johnson 2013), directly embedded into the ground, and backfilled with gravel. The use of this particular coating has since been discontinued. At their highest positions, the coatings extended above the ground line approximately 18 in. for Poles Q3C-1R and Q3C-2R, 24

in. for Pole Q3C-1L, and 30 in. for Pole Q3C-2L. Severe degradation was evident as significant coating lip delamination was observed around the entire circumference of each pole. The worst case of coating lip delamination (on Pole Q3C-1L) had resulted in an 8-in. drop from the original coating height (Figure 3.9). Such defects facilitate moisture penetration and stagnation. As a result, pack rust was observed at these coating crevices and discontinuities.



Figure 3.9 Severely delaminated coating line accompanied by widespread pack rust and pack out on ladder clip.

On some poles, bands of discolored orange-brown rust (indicative of non-protective patina) were seen to stretch from the lips to the level where the coatings originally terminated. Pitting was also common around this region, generally at a severity of Level A3-B4 per ASTM G46 (ASTM 2013c). One way that coating delamination was seen to propagate was through the formation of pack-out rust at the pole wall-coating interface, which is clearly evident on Poles Q3C-2L and Q3C-2R (Figure 3.10). This pack-out damage results in steel section losses while at the same time prying the coating from the pole. These phenomena are reasonably attributed to repetitive moisture entrapment

underneath the protective coatings. Wherever pack-out rust forms, it opens up a new gap for water to stagnate, leading to more oxidation and coating delamination. Debonding from the WS substrate was also observed within the bodies of some coatings. Multiple near-circular holes, spanning up to 6 in. across, were present in the coating of Pole Q3C-2L. One such defect was located at only 3 in. from the ground line (Figure 3.7). These issues may generate due to material quality, adhesion, and installation procedures.

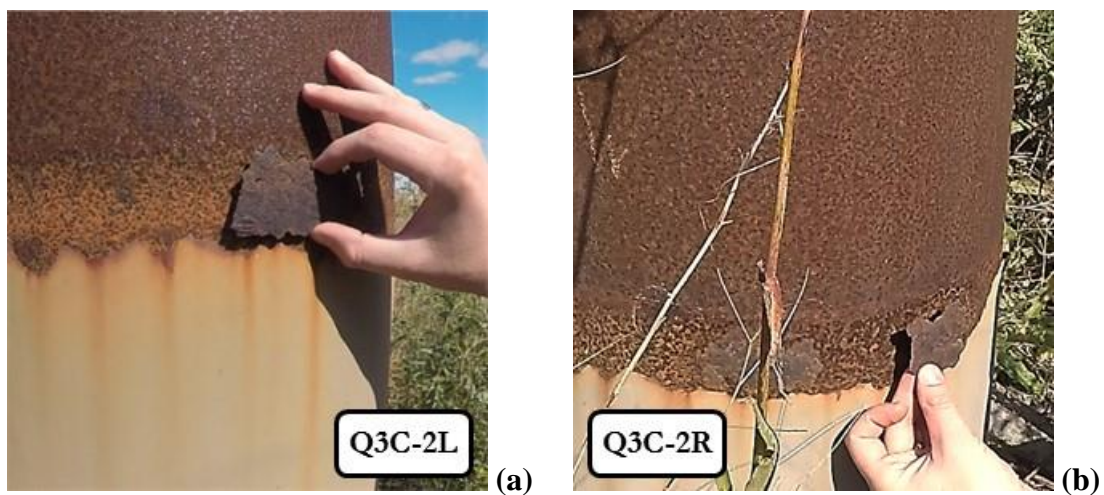


Figure 3.10 Pack-out corrosion damage: (a) rust removed from coating line; and (b) easily removed rust layer, with pack rust still visible along coating line.

Problems were not isolated to the coating and ground-line regions. While the patina for each pole was dark-brown for the most part, grain size and roughness of the patina visibly increased on surfaces closer to the potash plant. This increase in coarseness was an indicator of the non-adherence of the patina. In fact, the plant-side outer oxide layers on Poles Q3C-1L and Q3C-1R would slough off 2-5 mm rust pieces by simply running a hand across the WS surface (Figure 3.11).

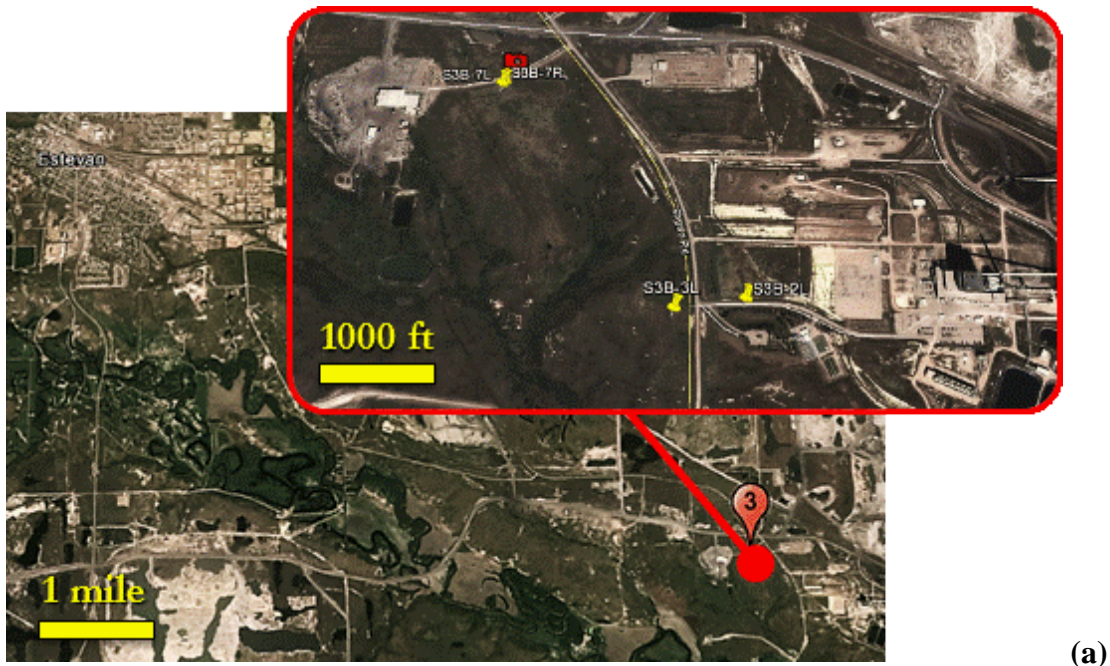


Figure 3.11 Non-adherent patina sloughing off with light rubbing of pole wall surface.

These instances of corrosion damage pointed to the formation of a non-protective oxide layer due to the continuous exposure to an industrial atmosphere. The adjacent potash mine provided a ready source of corrosive sulfur dioxide (SO_2) with the dust and exhaust fumes from its processing facilities. It is noted that the potash produced here has primarily been of the potassium chloride variety (PotashCorp 2015). A relevant implication is that, as a result of potash processing, atmospheric chlorides have also contributed to the environmental corrosivity of Site 2, lowering the effectiveness of the protective patina of nearby WS structures. This is highlighted since, to the best of the authors' knowledge, no study has been published on this type of corrosive environment, different from atmospheric chlorides at marine locations and from the use of deicing salts.

3.3 Site 3 – Directly Embedded Poles in Rural/Industrial Environment

Site 3, which is illustrated in Figure 3.12, was located almost five miles southeast of Estevan, Saskatchewan, and situated between a coal company and a coal-fired power station. Inspection of Site 3 took place on 10 September 2015.



(a)



(b)

Figure 3.12 Site 3: (a) map indicating site and pole locations; and (b) photographic view.

The actual coal mines were at least one mile away from each of the inspected structures. The power station was closer, but its smokestacks were still roughly 1000 ft away from the nearest pole. Because the structures were located in a pastoral area, the site was considered to be exposed to a rural atmosphere, with possible industrial influences.

The transmission line considered at Site 3, Line S3B, was installed in 1988 and possesses a voltage capacity of 230 kV. Four poles on this line were inspected, namely: S3B-2L, S3B-3L, S3B-7L, and S3B-7R (Figure 3.13). Each pole is part of a two-pole tubular H-frame structure made of Type AT steel (CSA 2013), and has a circular cross section with a nominal diameter of 18 in. Poles S3B-2L and S3B-3L have a nominal wall thickness of 3/16 in., and Poles S3B-7L and S3B-7R have a nominal thickness of 3/8 in.

Similar to Sites 1 and 2, the poles at Site 3 were constructed from Type AT steel (CSA 2013). Poles S3B-2L and S3B-3L were coated with a polyurethane coating similar to that used on Pole C1F-20, while Poles S3B-7L and S3B-7R utilized the same Skotchkote variety used on the poles in Site 2. All poles were directly embedded into the ground and surrounded by dirt backfills. Coating heights ranged from the ground line level in the case of Pole S3B-2L (Figure 3.13a), to nearly 36 in. above ground (Figure 3.13b). These structures were grounded with 10-ft GS ground rods, and were cathodically protected by 32-lb magnesium anodes that were installed at time of construction (Figure 3.14). Similar to Pole Q3C-2R in Site 2, Pole S3B-7R did not possess a direct magnesium anode connection as it is part of an H-frame system with Pole S3B-7L. The oxide films observed on the poles at Site 3 were a purple-brown mix that was, for the most part, in acceptable shape. Different levels of corrosion damage were evident on the four structures inspected.

Pole S3B-2L was seen to have sustained slightly more corrosion damage than the other poles at Site 3. The coating itself was readily delaminating. In addition, the directly embedded pole was installed such that the coating barely reached above the surrounding vegetation and soil and, in some spots, was not visible above ground (Figure 3.14a). The lack of a protective coating near the ground level led to corrosion damage in the form of

non-uniform thickness loss at the ground line. Widespread pitting occurred on the entire above-ground WS surface. The worst Level A4-B4 pitting (ASTM 2013c) was observed on the side facing the power station, as shown in Figure 3.15a.

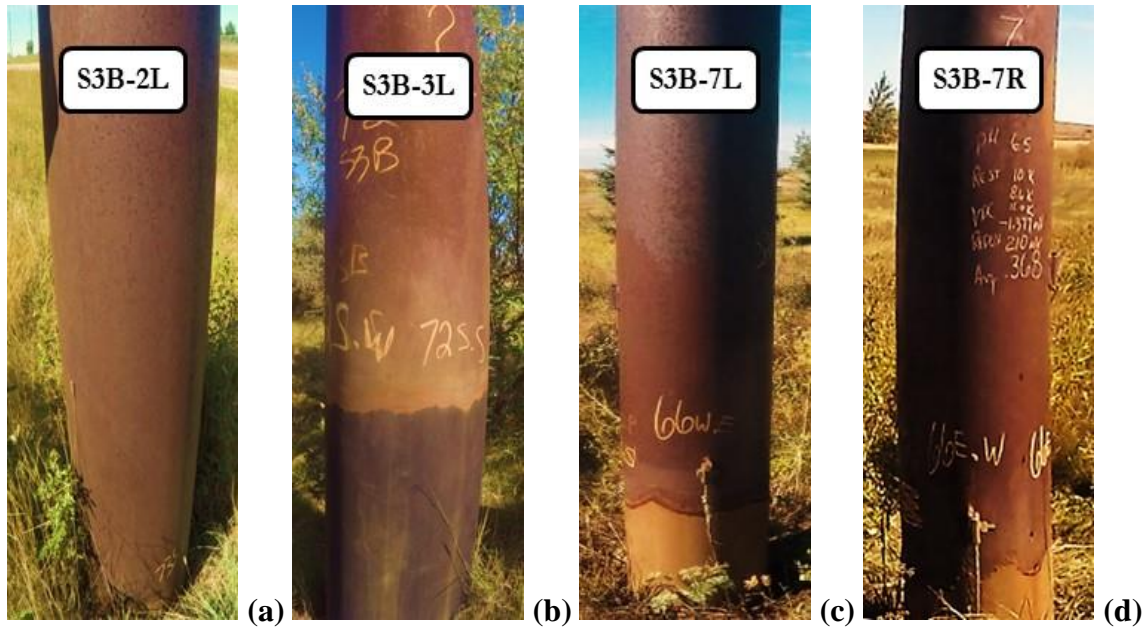


Figure 3.13 Site 3 poles: (a) S3B-2L; (b) S3B-3L; (c) S3B-7L; and (d) S3B-7R.

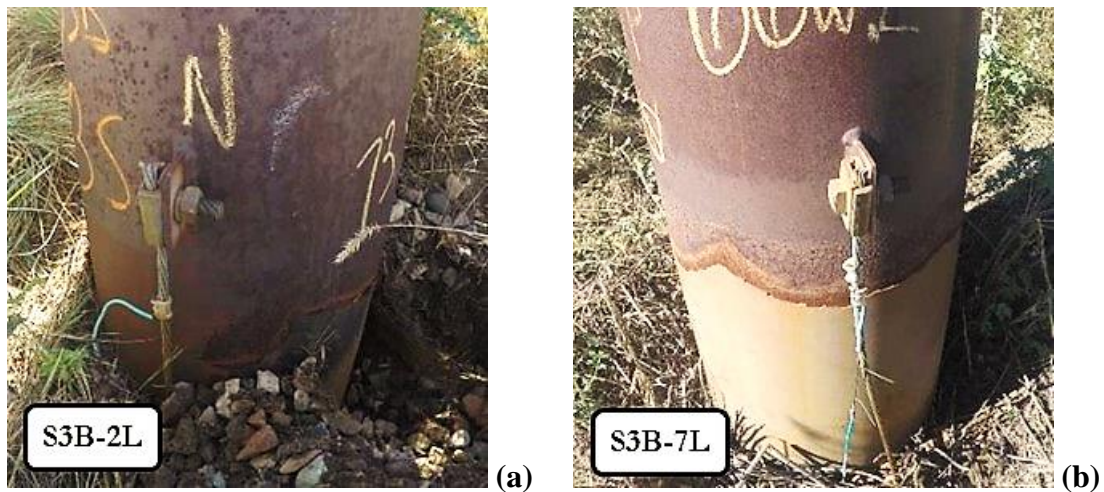


Figure 3.14 Site 3 pole bases showing corrosion prevention measures and: (a) coating barely extending above ground line; and (b) steady delamination of coating due to pack rust.



Figure 3.15 Dense pitting sites on pole wall surfaces: (a) Pole S3B-2L facing power station; and (b) Pole S3B-7R facing coal company.

Poles S3B-7L (Figure 3.14b) and companion Pole S3B-7R exhibited similar corrosion damage. Pitting sites were noted on both poles, with the most severe pitting reaching Level A4-B4 (ASTM 2013c) as evidenced in Figure 3.15b for Pole S3B-7R. The most severe pitting occurred on pole walls facing the coal company facility, which oversaw transportation and storage of mined coal, suggesting that proximity to and orientation toward coal trucks and storage yards may lead to enhanced pitting damage. Both poles also experienced disbonding and uniform pack-rust damage at the coating lips, which terminated at only 12 in. above the ground line.

Pole S3B-3L (Figure 3.16) demonstrated that WS poles can offer satisfactory corrosion resistance if located far enough away from buildings. The patina was dense, uniform, and without pits. Minor delamination at the coating lip did occur, but the adjacent rust layer was more stable than those seen in other poles (e.g., Pole S3B-7L in Figure 3.14b). Also, the coating lip reached approximately 36 in. above the ground line (Figure 3.16), thus minimizing concerns for ground line corrosion damage.



Figure 3.16 Pole S3B-3L showing minor coating delamination but overall dense and adherent patina.

It is emphasized that Site 3 offered substantially different exposure conditions within the same area. Poles S3B-7L and S3B-7R are adjacent to the coal company coal storage facilities whereas Poles S3B-2L and S3B-3L are located about 2800 ft away, and are separated from the power station by approximately 500 and 1000 ft, respectively. The local coal mines are separated from the inspected poles by at least 1 mile, with potentially less relevant implications for atmospheric corrosivity (it was not possible to inspect structures closer to any of the mines as those grounds are off-limits). Instead, the proximity of the power station could affect the corrosion resistance either because of its smokestacks, which yield fumes from the processing required to convert coal into energy, or stray currents, which may be released from the plant. These considerations would help explain why Pole S3B-2L appears to be the most heavily damaged of the four structures. In particular, atmospheric corrosivity may contribute to the widespread pitting, and stray currents may exacerbate the effects of ground-line corrosion. These hypotheses are further discussed in Section 4.1, Section 4.2, and Section 5.2, based on evidence on atmospheric corrosivity, soil corrosivity, and corrosion potential measurements, respectively.

3.4 Site 4 – Directly Embedded Pole in Marine Environment

Site 4 is located on Melbourne Beach, Florida (Figure 3.17), alongside the Atlantic Ocean. It is situated approximately 300 ft from the seawater at high tide. This proximity to the coast allows Site 4 to be classified as a marine environment. Inspection of Site 2 took place on 27 October 2015.



Figure 3.17 Site 4: (a) map indicating site and pole location; and (b) wide photographic view.

Site 4 did not feature an active transmission line but a test line instead. The line was installed in 1993 to assess the impact the marine atmosphere has on the quality and lifespan of its transmission structures. All structures on the line were single-pole structures. Two poles were inspected: one made of WS, labeled TL-1 (Figure 3.18a), and one made of galvanized steel (GS), labeled TL-2 (Figure 3.18b). Since WS has been shown to be susceptible to corrosion in marine atmospheres (Cano et al. 2014), a direct comparison was made between WS and GS poles with respect to corrosion resistance in a marine (chloride-laden) environment. Both poles have a dodecagonal cross section with nominal diameter of 19 in. at the base, where each flat has a nominal width and thickness of 5 in. and 0.25 in., respectively.

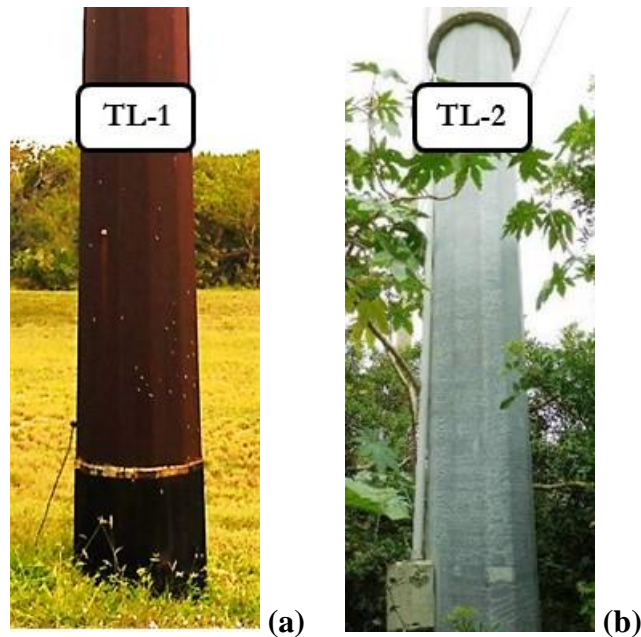


Figure 3.18 Ground-level view of Site 4 poles: (a) TL-1 and (b) TL-2.

Pole TL-1 was made from Cor-Ten B WS (ASTM 2015a). It was directly embedded into the ground and, for protection from the soil, covered with a welded-on steel ground

sleeve and then coated with a coal-tar epoxy (Figure 3.19a). The coating extended approximately 24 in. above the ground line. Pole TL-1 was grounded but not cathodically protected. The only physical barrier between the pole and the ocean was a tree line approximately 15-ft high, which partially obstructed the wind.

As a GS counterpart, Pole TL-2 was assessed only via visual inspection. This pole was protected by means of a polyurethane coating and a bolted-on ground sleeve, and was grounded similarly to Pole TL-1 (Figure 3.19b). Unlike Pole TL-1, Pole TL-2 was surrounded by dense vegetation that blocked a clear path to the sea (Figure 3.18b).

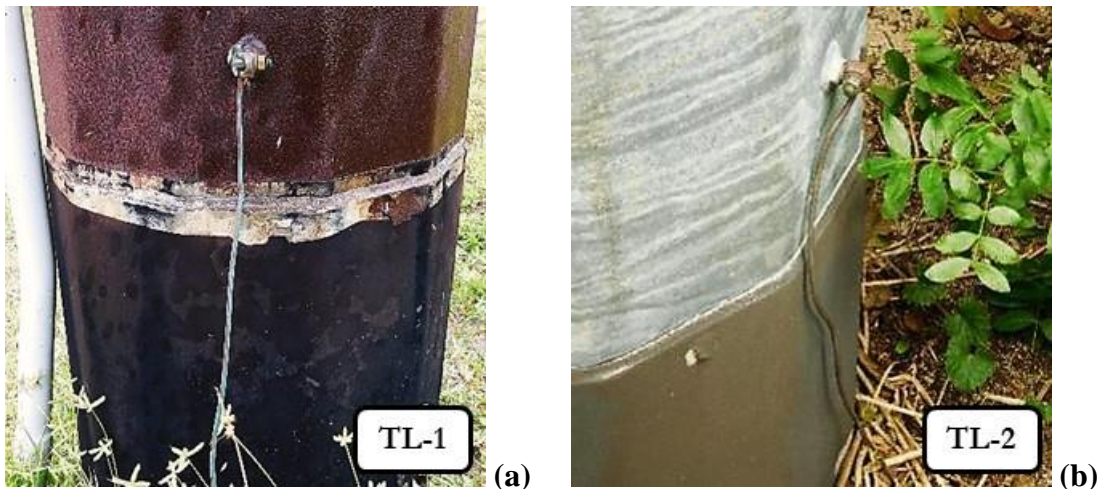


Figure 3.19 Ground-line coating on poles at Site 4: (a) Pole TL-1; and (b) Pole TL-2.

Pole TL-1 suffered from a number of apparent corrosion damage forms (Figure 3.20 through Figure 3.22). First, the ground line area of the pole, which was protected by both the additional WS sleeve and epoxy coating, was in a state of disrepair. The coating could be seen to fade in regions, exposing the underneath sleeve, and was experiencing delamination at several spots around its lip. Four deep cratering pits were also present in and around the coating region. These pit depths are discussed in Section 5.1 based on

thickness measurements. Examining the ground line regions of Pole TL-2, it was noted that the coating appeared to be stable, outside of a few regions near the lip. In these regions, the pole displayed crevice corrosion issues near the bolts fastening the ground line sleeve to the pole wall (Figure 3.20c-d).

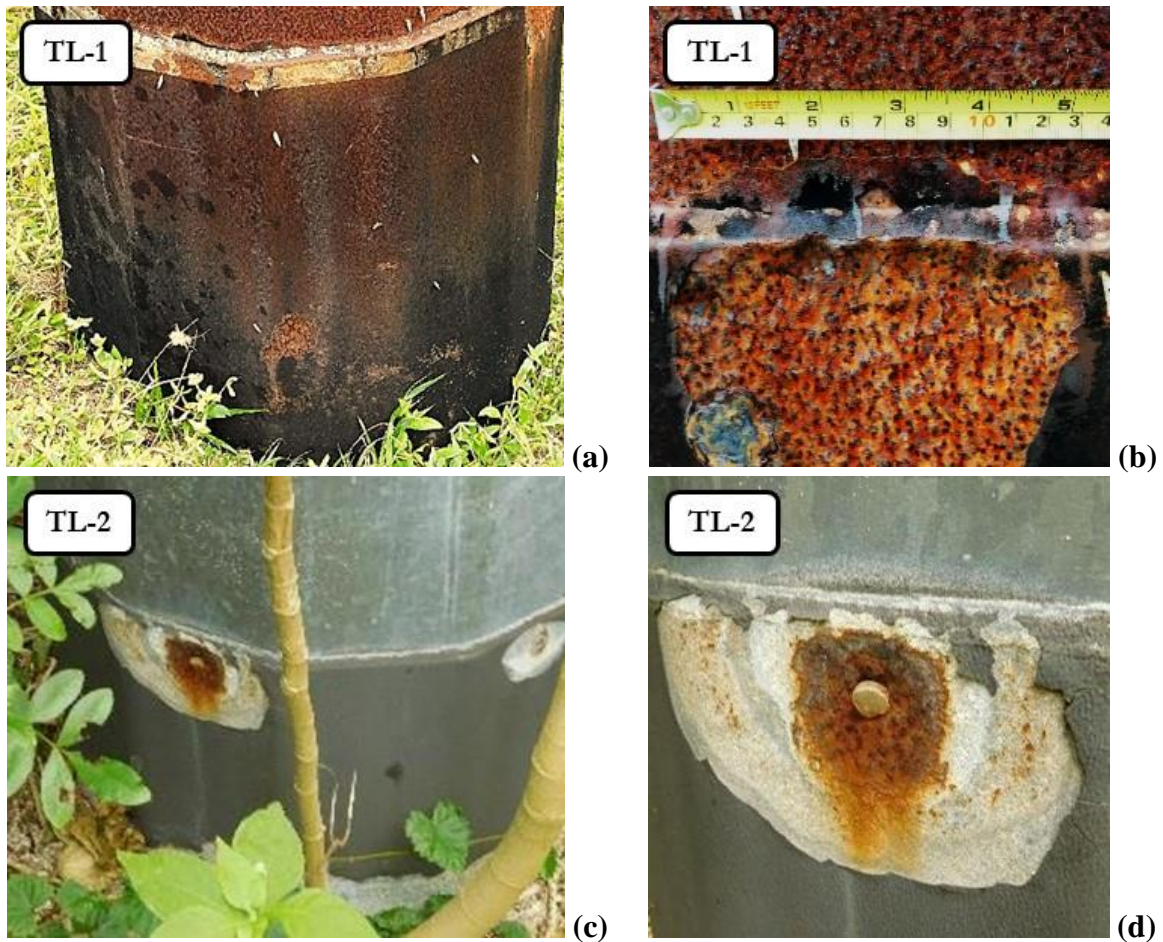


Figure 3.20 Damage around coating region in WS Pole TL-1 and GS Pole TL-2 near ocean: (a) deterioration of Pole TL-1 coating with visible pits; (b) pitting and pack-rust corrosion damage at Pole TL-1 coating lip; (c) coating delamination around bolted sleeve on Pole TL-2; and (d) crevice corrosion on Pole TL-2.

Smaller and denser pitting zones of Level A5-B4 (ASTM 2013c) were noted over most of the WS surface of Pole TL-1. Much of the pole wall patina displayed a more orange-purple color (which is indicative of a less protective patina) mix than a brown hue

(which is indicative of a more stable and adherent patina). For Pole TL-2, no damage could be observed besides some “tiger striping” (i.e., streaking of the protective zinc exterior). This surface defect is typically a consequence of improper transportation or storage of GS poles, and may lead to accelerated dissolution of the zinc film with negative implications for its protective ability (Zamanzadeh et al. 2006).

Both poles possessed a connected junction box, roughly 5-ft off the ground. The box on Pole TL-1 was located on the pole side opposite the ocean, while on Pole TL-2 the box was oceanside. This detail proved especially alarming for Pole TL-1. In fact, a sizable chunk of pack-out rust was present between the junction box and the pole, extending from the pole wall nearly 2 in. and covering the entire region behind the box, nearly 0.5 ft² (Figure 3.21a-c). It was by no means adherent as it was easily removed by hand. Removal of the pack-out rust revealed a 3-in. diameter hole, highlighting the fact that a portion of the entire pole wall had been consumed. Here, the orientation of the box may negatively contribute to corrosion resistance since it is located in a low-pressure region where: (a) moisture and chloride contaminants stagnate under winds blowing from the ocean; and (b) the WS surface is shielded from rain, which facilitates the formation of chloride deposits. In this environment, as expected, GS largely outperformed WS as no such corrosion damage was observed on Pole TL-2. (Figure 3.21d).

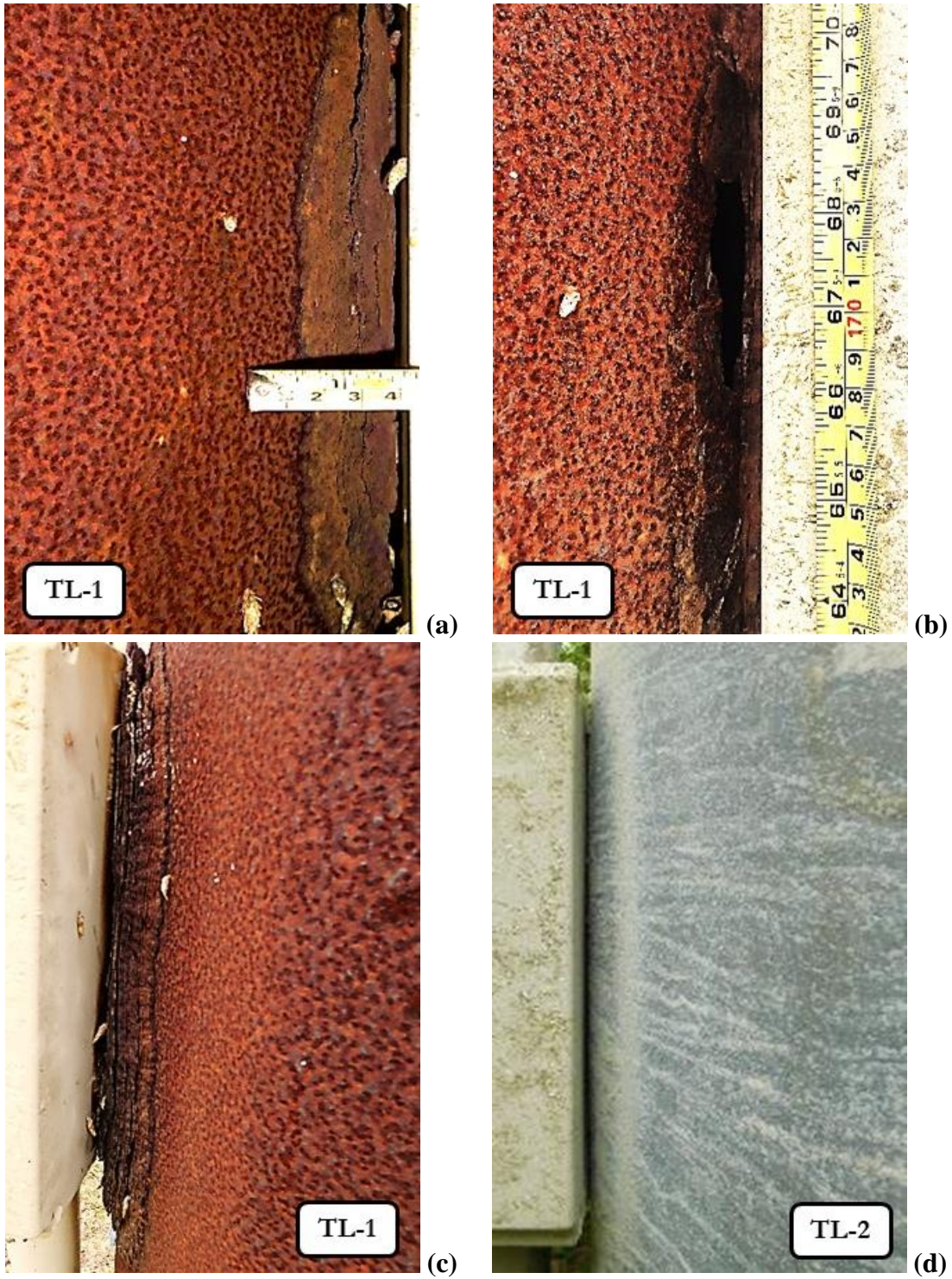


Figure 3.21 Corrosion behind junction boxes: (a) thick pack-out rust on Pole TL-1; (b) hole in WS pole wall exposed after removing pack-out rust; (c) pack-out damage from other side stretching length of junction box; and (d) no damage on Pole TL-2.

By looking overhead, another marked difference between the two poles was noted. At the slip-joint intersection of the pole sections about half-way up Pole TL-1, pack-rust damage could be identified from the ground (Figure 3.22a). For Pole TL-2, such joint was bolted and exhibited only some faint brown spotting, with no evidence of corrosion damage as in the case of Pole TL-1 (Figure 3.22b).

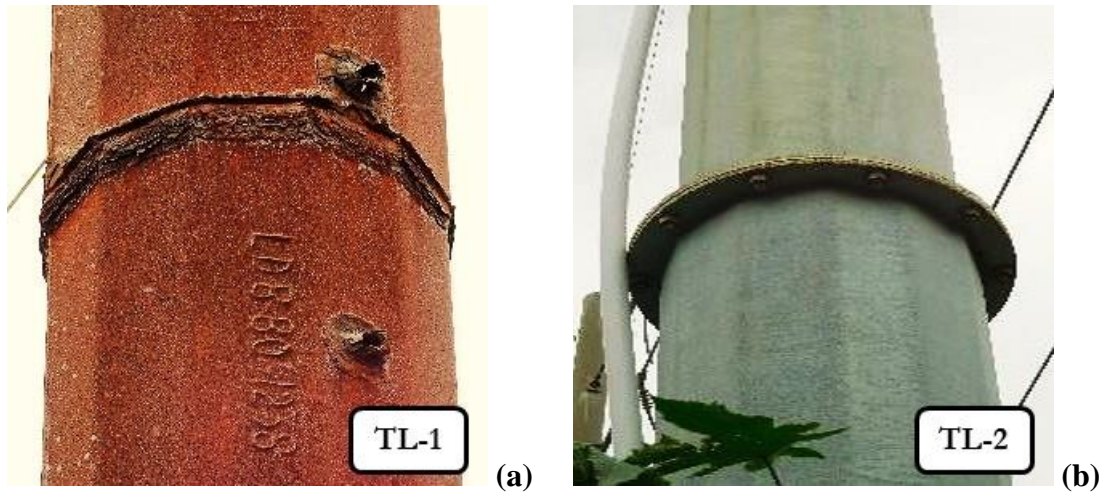


Figure 3.22 Condition of overhead slip joints near saltwater: (a) pack-rust damage on WS Pole TL-1 sections; (b) apparently sound, corrosion-free GS Pole TL-2.

Because of the extent and degree of corrosion damage observed on Pole TL-1, the possibility of moisture penetration into the pole (and subsequent internal corrosion phenomena) was further investigated by inspecting the interior walls using a borescope camera (model IPLEX LX, Olympus Corp., Figure 3.23). The process of using a borescope to inspect tubular poles, shown in Figure 3.24, consists of: pole wall grinding; drilling; surface cleaning; hole threading; insertion of the borescope camera; examination of pole interior; and plugging the hole after inspection with a threaded bolt. This bolt is left to rust over in order to fill the newly made hole in the pole wall.



Figure 3.23 IPLEX LX borescope camera (Olympus Corp.).

The pole interior did not exhibit signs of corrosion damage (Figure 3.25). The patina was only partially developed due to the lack of exposure to wet/dry cycles. This spotty oxide layer was interspersed with the steel substrate and appeared to be adherent (Figure 3.25a). No moisture accumulation was observed at or near the base of the pole. Overall, the pole at time of inspection was found to be in satisfactory condition with regard to its interior. However, the presence through-thickness steel loss due to pack-out corrosion (Figure 3.21a-c) may facilitate moisture penetration and should be addressed.

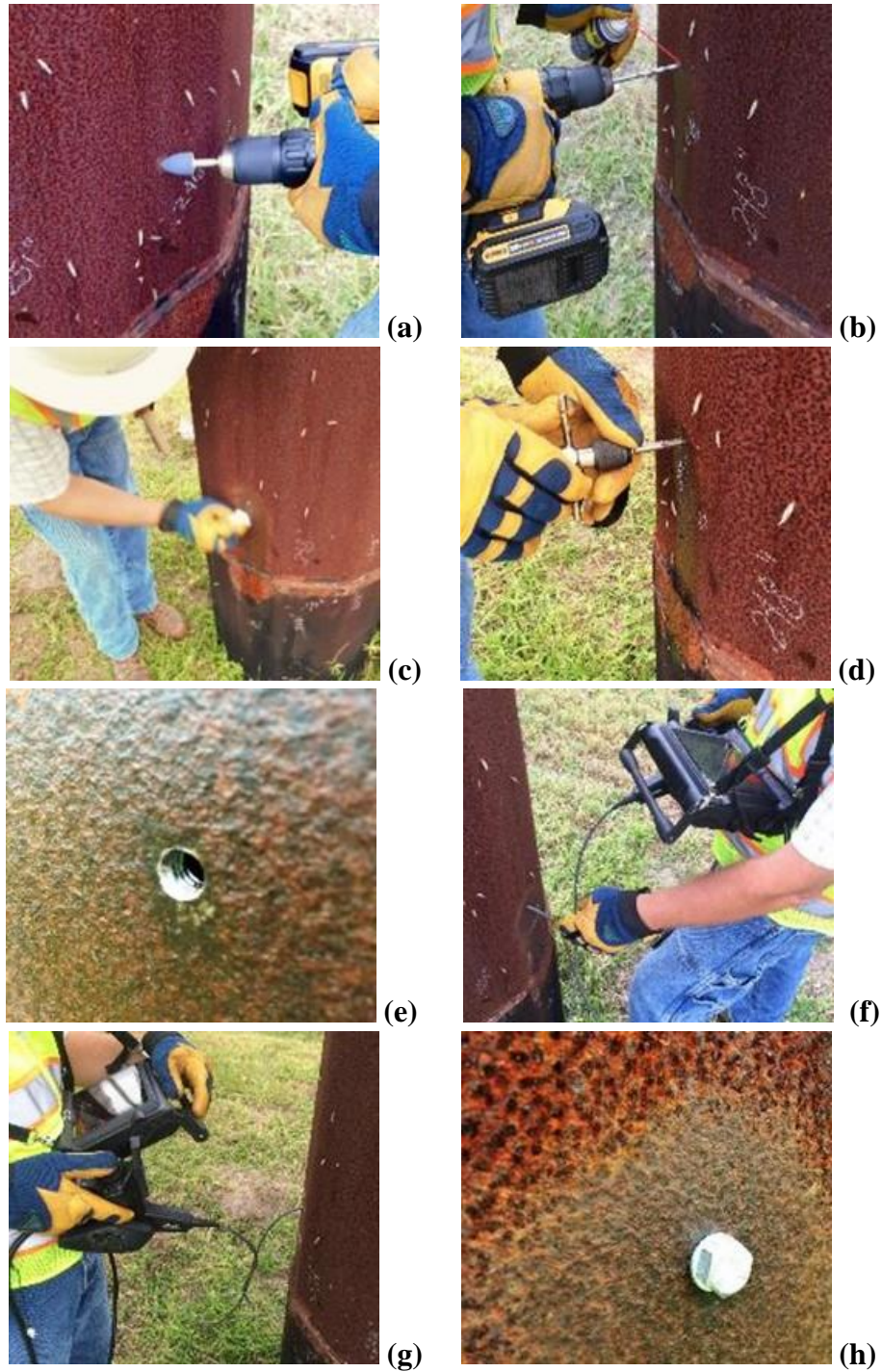


Figure 3.24 Interior inspection of Pole TL-1 at Site 4 via borescope: (a) grinding pole wall; (b) drilling; (c) cleaning surface; (d) threading hole; (e) close-up image of hole; (f) inserting borescope camera; (g) examining pole interior; and (h) plugging hole after inspection.

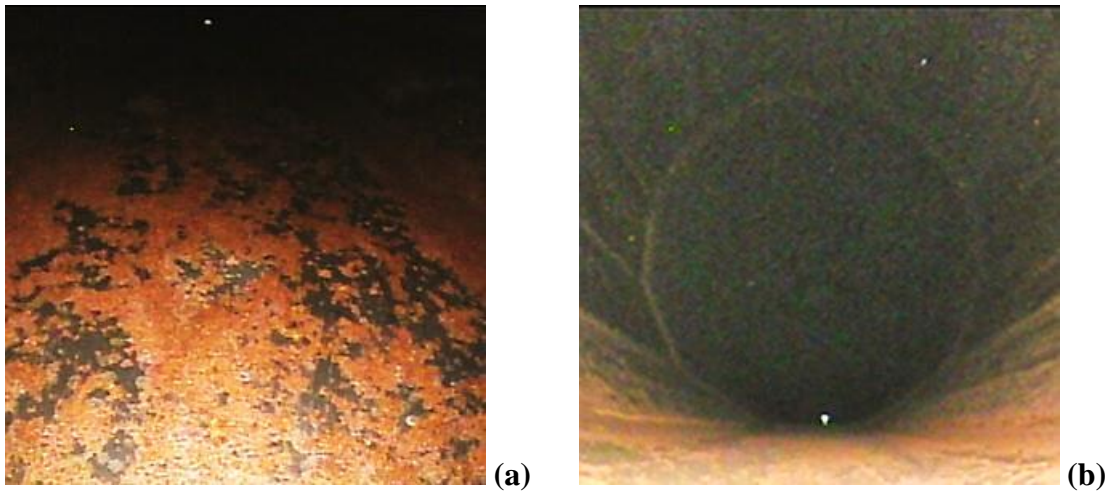


Figure 3.25 Borecope images of interior of Pole TL-1: (a) uneven patina due to lack of wet/dry cycles; and (b) view of pole interior.

The visual assessment of the test line located at Site 4 provides compelling evidence of the impracticality of using WS in transmission line structures located in close proximity to saltwater. Under these conditions, GS is unquestionably a more suitable choice.

3.5 Site 5 – WS Poles on Caisson Foundations in Rural Environment

Site 5 was located off of Highway FL-520, approximately 10 miles away from Indian River and 3 miles from Lake Poinsett (Figure 3.26). Here, winds may be able to carry airborne chlorides from the coast line. Site 5 was also roughly 20 miles east of the nearest major city, Orlando, and no industrial facilities were in the vicinity. Thus, the site was considered to be exposed to a rural atmosphere. In addition, the vicinity to the coast line raises the question of whether chloride exposure is of concern, thus making WS an unsuitable choice for overhead transmission line structures, as shown for the case of Pole TL-1 on Site 4 (Figure 3.21a-c and Figure 3.22a). Inspection of Site 5 took place on 27 October 2015.

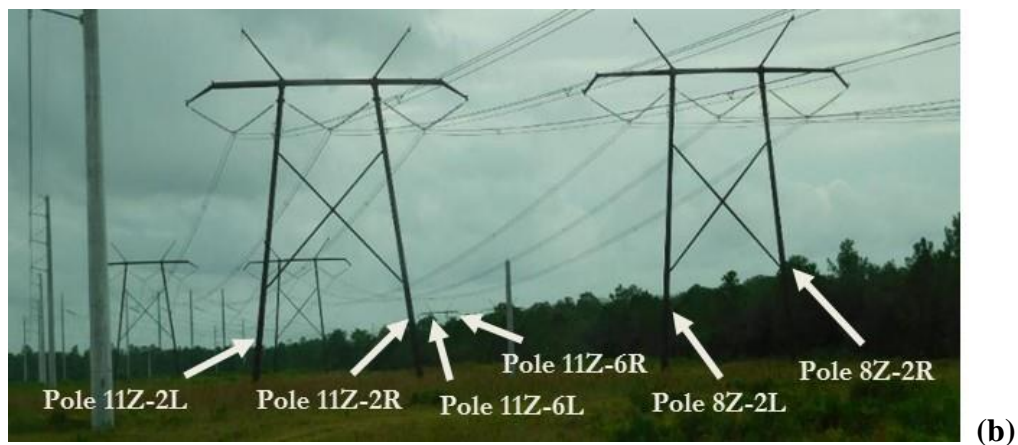


Figure 3.26 Site 5: (a) map indicating site and pole locations; and (b) wide photographic view.

Two parallel transmission lines, Lines 8Z and 11Z, were inspected. These 230 kV lines were installed in 1990 and consisted of two-pole tubular H-frame structures with slightly angled poles. Six poles were inspected, namely: for Line 8Z, Poles 8Z-2L and 8Z-2R, having circular cross section with nominal diameter of 21 in. at the base, and wall thickness of 5/16 in. (Figure 3.27); and, for Line 11Z, Poles 11Z-2L, 11Z-2R, 11Z-6L, and 11Z-6R, having a dodecagonal cross section with nominal diameter of 21 in. at the base,

flat width of 5.5 in., and wall thickness of 5/16 in. (Figure 3.28). It is noted that the poles of Line 11Z had welded-on sacrificial WS sleeves with 6-in. wide flats, which increased the diameter at the base from 21 in. to approximately 23 in.

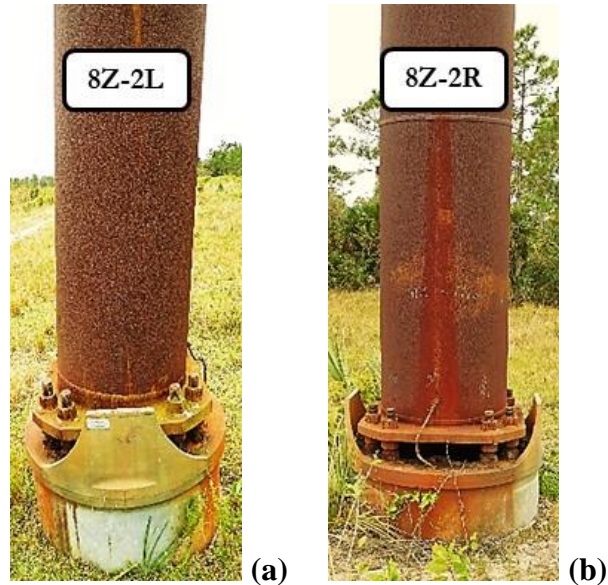


Figure 3.27 Ground-level view of poles: (a) 8Z-2L and (b) 8Z-2R.

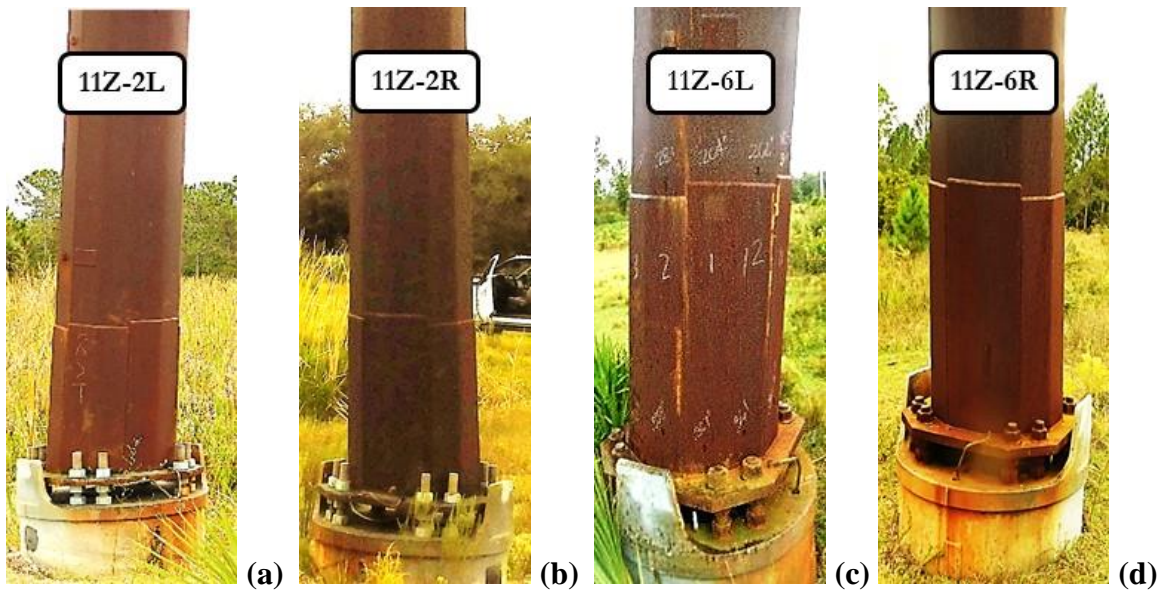


Figure 3.28 Ground-level view of Site 5 poles of Line 11Z: (a) Pole 11Z-2L; (b) Pole 11Z-2R; (c) Pole 11Z-6L; and (d) Pole 11Z-6R.

All poles were made of Cor-Ten B WS (ASTM 2015a). The poles at Site 5 are different from all other poles inspected since they have GS vibratory caisson foundations instead of being directly embedded in the ground (Figure 3.29). The poles were connected to the caissons by way of WS base plates that were welded to each pole, and 2-in. diameter GS bolts. In each pole, a seven-wire GS strand was also used to connect the poles and caissons, providing a grounding link and possibly cathodic protection by means of a voltage loop between the caisson and the pole surface. This strand was connected the walls of Line 8Z poles and base plates of Line 11Z poles. No coatings were applied to the WS poles since they were not directly embedded into the ground.

The caissons had been stained brown to different extents due to rain run-off from the WS pole surfaces. Vegetation build-up was noted around some of the pole bases, creating an environment that may facilitate moisture retention instead of wet/dry cycles. Different forms of corrosion damage were observed (Figure 3.29). Poles 8Z-2L and 8Z-2R (Figure 3.29a) exhibited large streaks of discoloration on their walls. In addition, their nuts and bolts at the base plate connections were no longer galvanized and were heavily corroding. Poles 11Z-6L and 11Z-6R (Figure 3.29b) exhibited a smooth and adherent patina, but their nuts and bolts at the base plate connections were also corroding. Conversely, Poles 11Z-2L (Figure 3.29c) and 11Z-2R seemed to be good condition with respect to the quality of the patina and the galvanized layer on the GS fasteners. To this end, it is important to note that these two poles had been remediated within the past five years by filling the caisson foundations with concrete, replacing corrosion-damaged GS fasteners, and introducing cathodic protection in the form of two magnesium anodes connected to the caisson foundation of Pole 11Z-2L.



(a)



(b)



(c)

Figure 3.29 Visual assessment of poles at Site 5: (a) discolored patina, corroding fasteners, and vegetation build-up around Pole 8Z-2R; (b) uniform patina but corroding fasteners on Pole 11Z-6R; and (c) uniform patina and GS fasteners on Pole 11Z-2L.

Upon closer inspection, fairly uniform corrosion damage in the form of a relatively rough patina was noted on the walls of all poles, and the WS repair sleeves of the poles of Line 11Z, as shown for example in Figure 3.30a-b. In addition, pitting was present at certain sections of all poles at moderate densities and sizing corresponding to Level A3-B3 per ASTM G46 (ASTM 2013c). Such damage suggests that the environment of Site 5 contributes significantly to corrosion processes in WS poles due to consistent exposure to moisture (from the high TOW and the presence of stagnating water in the hollow GS caisson foundations, as discussed later in this section), and perhaps due to the presence of chlorides that are transported to the site from the coast (e.g., by wind). The impact of chlorides on Site 5 poles was assessed further using both field and laboratory techniques, as described respectively in Sections 4.1 and 0. More research is needed to understand practical cut-off distances where chloride contamination should not be considered of concern for the formation of a stable and adherent patina on WS surfaces.

Among the poles at Site 5, Poles 11Z-2L (Figure 3.30a) and 11Z-2R possessed the roughest patinas, and powder samples could be easily removed from these pole surfaces as discussed in Section 6.2 (which supports the decision for expedited remediation made by the owner). Poles 11Z-6L and 11Z-6R also possessed rough patinas but these were more adherent than those of Poles 11Z-2L and 11Z-2R. Spots of orange discoloration could be seen to occur on all Line 11Z poles at the intersection of the pole wall and repair sleeve, most notably on Pole 11Z-6L (Figure 3.30b). The poles of Line 8Z, having circular cross section, possessed more uniform and adherent patinas than the dodecagonal poles of Line 11Z. The patina of Pole 8Z-2L was fairly consistent over the entire pole surface (Figure 3.30c). Pole 8Z-2R exhibited a similar patina, which was disrupted only by a red streak of

rust, centered on the seven-wire GS strand connection, that ran down the lowest section (about 36-in. long) of the cylindrical pole (Figure 3.30d). This area did not pose concerns since the patina was not different than the rest of the pole wall with regard to texture and uniformity. However, it is noted that the streak width increased in the vicinity to the GS strand connection, suggesting that the potential difference between the WS pole and GS caisson played a role (albeit minor until this time) on the formation of the protective oxide at this location.

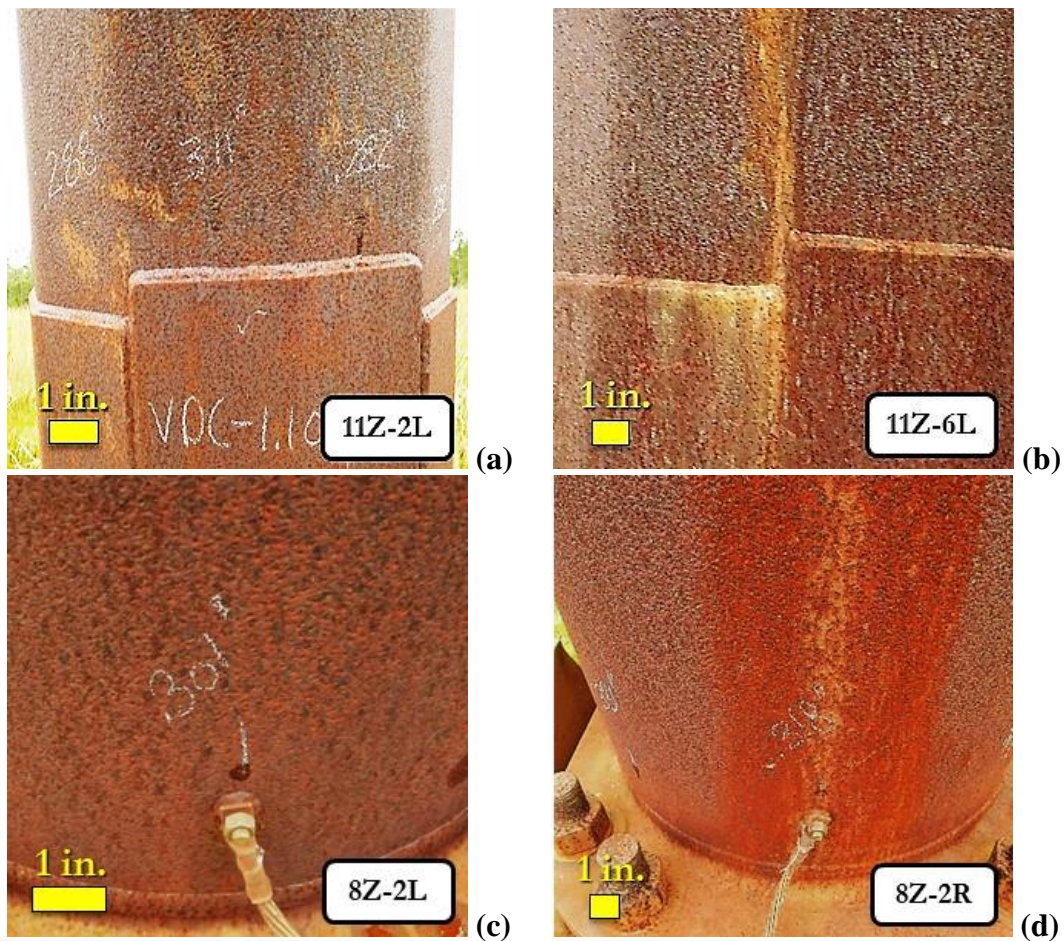


Figure 3.30 Close-up view of patinas on Site 5 poles: (a-b) rough and non-adherent patina with areas of discolored rust and pitting on wall and repair sleeves of Poles 11Z-2L and 11Z-6L; (c-d) smoother and more adherent patina than Line 11Z on wall of Pole 8Z-2L and Pole 8Z-2R, in addition to pitting.

Another instance of the impact of voltage differences could be seen in the corrosion damage of the GS fasteners at the base of each pole. Such damage is attributed primarily to galvanic corrosion effects suffered by the protective zinc layers on the fasteners, which act as sacrificial anodes protecting the connected WS poles. The fasteners of Line 11Z poles (Figure 3.31) were not as heavily corroded as those of Line 8Z poles (Figure 3.32), possibly because the attachment locations of the seven-wire strands led to sacrificial prioritization of the caissons and fasteners respectively. Regardless, the mechanism is concerning because the galvanized layer on the fasteners appeared to have been entirely consumed and, as a result, these connections are essentially made of unprotected plain carbon steel. This evidence highlights the importance of design and detailing solutions, especially at the pole base, as well as the selection of steel materials, with consideration to the potential for galvanic coupling.

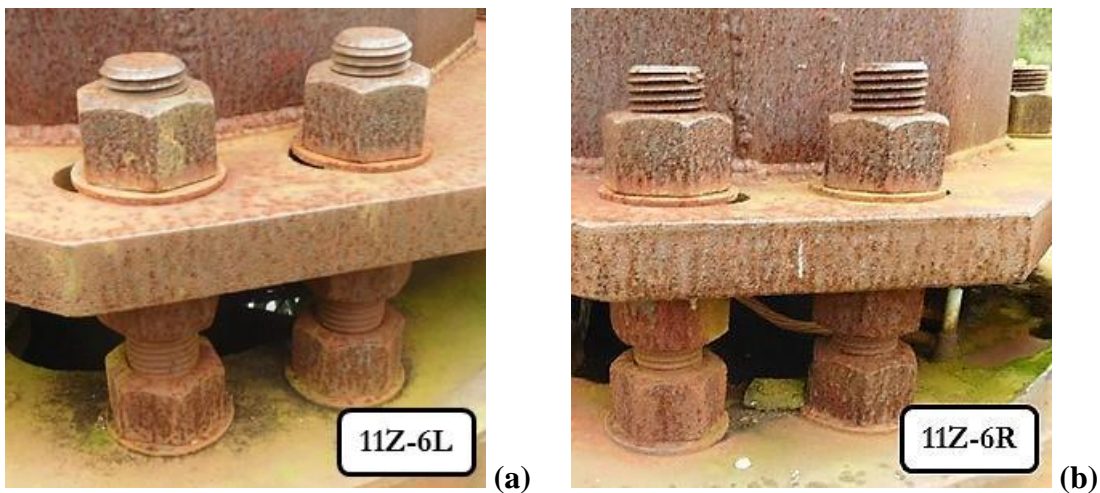


Figure 3.31 Corrosion of GS fasteners connecting WS pole to GS caisson for Line 11Z poles at Site 5: (a) depletion of protective zinc layer on GS nuts of Pole 11Z-6L; and (b) pack-rust damage on bottom GS nuts of Pole 11Z-6R.

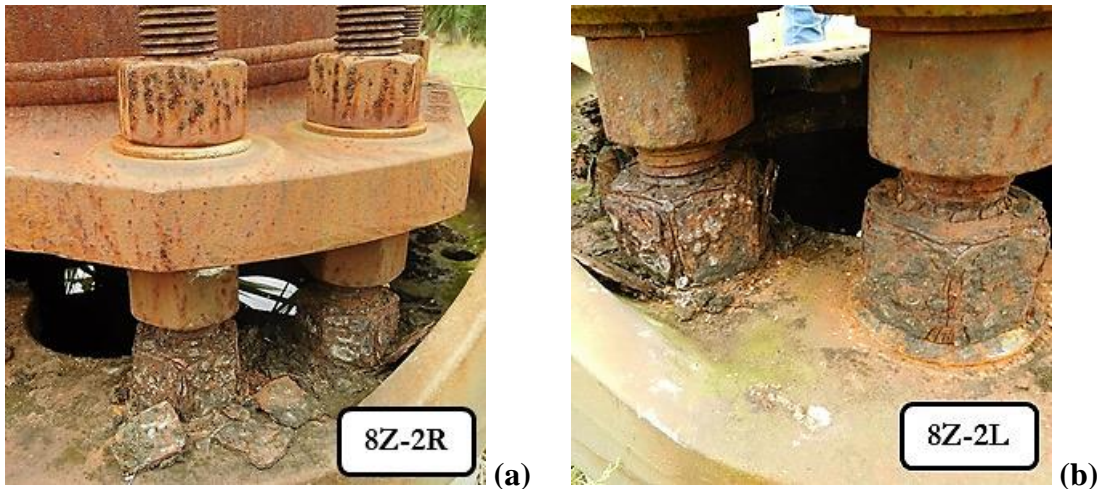


Figure 3.32 Corrosion of GS fasteners connecting GS caissons to WS poles of Line 8Z at Site 5: (a) Pitting on top nuts and pack-rust damage on bottom GS nuts of Pole 8Z-2R; and (b) pack-rust damage on bottom GS nuts of Pole 8Z-2L.

Serious concerns are posed by the original design that called for hollow caisson foundations. In fact, moisture from the groundwater table penetrated into the interior of the caissons of Poles 8Z-2L, 8Z-2R, 11Z-6L, and 11Z-6R, filling to their brims with water (Figure 3.33). This consistently moist environment promotes the growth of sludge and moss that also facilitate corrosion attack (Figure 3.33a), and provides the necessary electrolyte for corrosion to occur (Figure 3.33b). It is noted that the caisson foundations for Poles 11Z-2L and 11Z-2R were filled as part of the recent remediation, when the original GS fasteners were replaced.

Inspection of this area revealed that none of the WS poles were sealed at their bases. As a result, dense pitting of Level A4-B2 (ASTM 2013c) was noted on the interior of all poles of Lines 8Z and 11Z (Figure 3.34a-b), and pack-rust damage was noted on the lower inner ledge of the poles of Line 11Z (Figure 3.34b-d). These types of corrosion damage was observed for all poles with caisson foundations, irrespective of whether the caissons were hollow (Poles 8Z-2L, 8Z-2R, 11Z-6L, and 11Z-6R) or filled (Poles 11Z-2L and 11Z-

2R). This evidence clearly suggests that caisson foundations should be avoided because pole interiors are readily exposed to the atmosphere and moisture (especially when using hollow caissons) but not to sunlight, thus hindering the occurrence of the drying cycles that are needed to form a protective patina on WS.

Poles 11Z-6L and 11Z-6R had been retrofitted by replacing corroded fasteners with new GS nuts and bolts, applying cathodic protection, and filling the hollow caisson foundations with concrete (Figure 3.35). Here, the choice to continue using GS nuts and bolts to fasten a WS pole is questionable since these fasteners may eventually act again as sacrificial anodes. However, the magnesium anodes may offset this mechanism as zinc is nobler than magnesium in the galvanic scale. Similar remediation measures, in addition to filling the hollow caissons, sealing the WS poles at the base, and introducing cathodic protection, are recommended for other Site 5 structures.

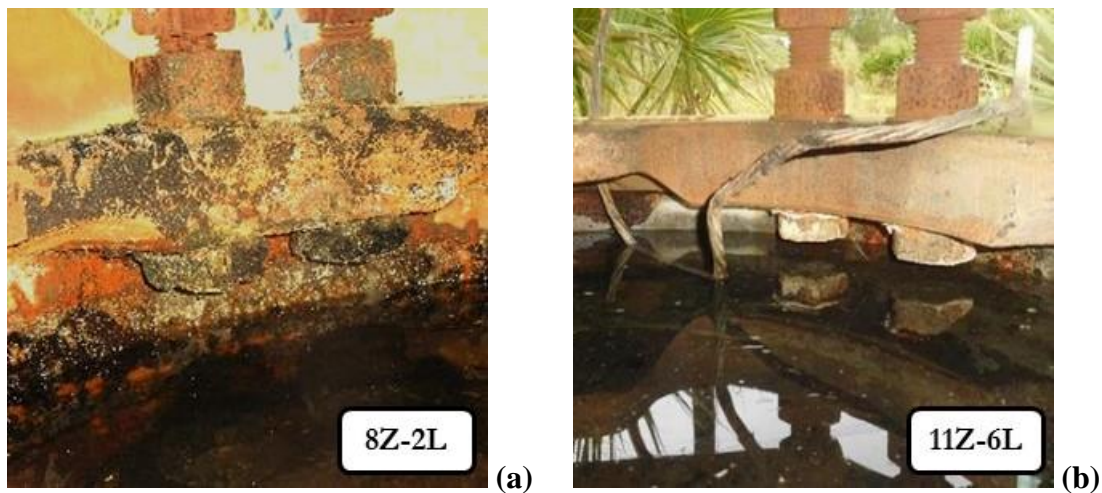


Figure 3.33 Water pooling in GS caisson foundations leading to: (a) sludge build-up; and (b) pack-rust damage on GS nuts.

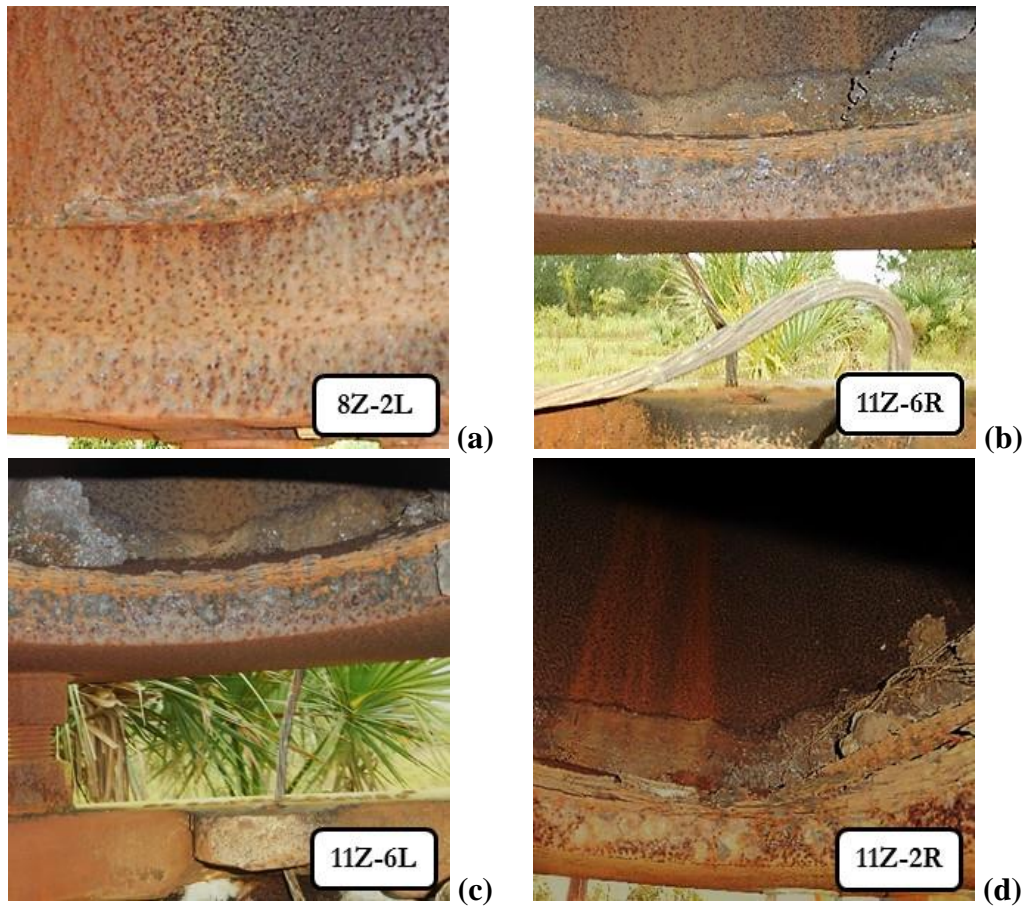


Figure 3.34 Corrosion damage on interior of unsealed WS poles at Site 5: (a) dense pitting on Pole 8Z-2L; (b) pitting and pack rust on Pole 11Z-6R; (c) pitting and pack rust on Pole 11Z-6L; and (d) severe pack rust on Pole 11Z-2R.

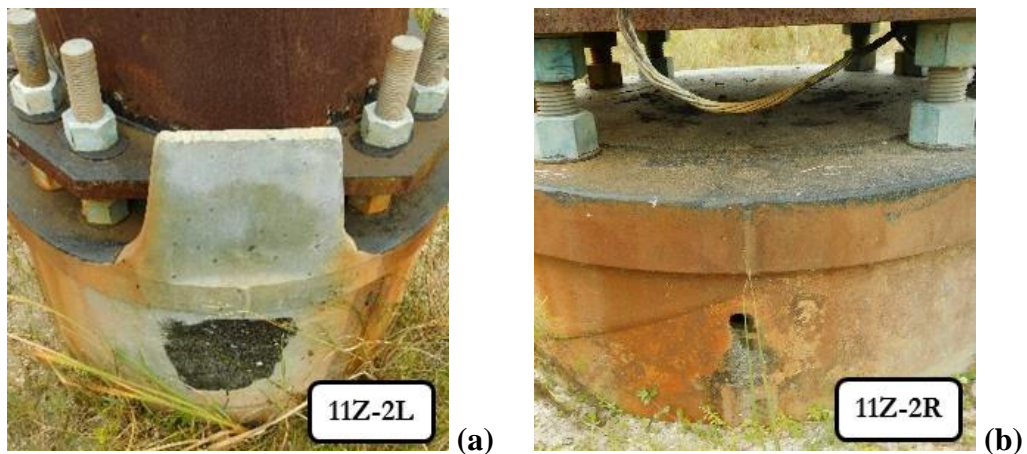


Figure 3.35 Recent remediation of Poles 11Z-2L and 11Z-2R at Site 5: (a) new GS fasteners and cathodic protection for GS caisson; and (b) concrete filling for hollow GS caisson.

The visual inspection of overhead areas highlighted the need for additional repair measures on two poles due to: corrosion-induced failure of a connection securing a utility ladder to Pole 11Z-6L (Figure 3.36a); and the formation of a large crack near the junction of the cross-arms joining Poles 8Z-2L and 8Z-2R (Figure 3.36b), which may have occurred due to fatigue loading (e.g., wind), with an exacerbating contribution from stress corrosion mechanisms.

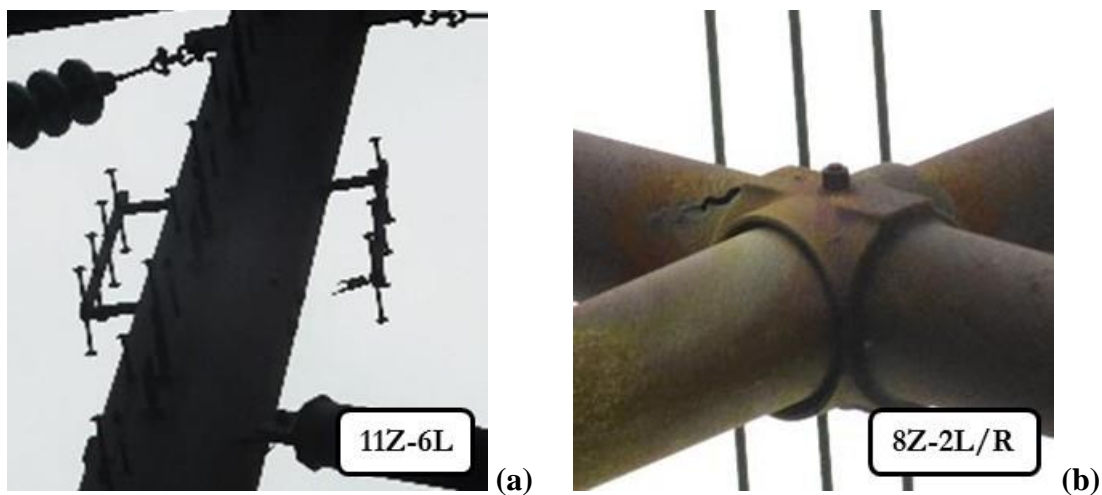


Figure 3.36 Overhead corrosion damage on WS poles at Site 5: (a) failure of ladder-wall connection on Pole 11Z-6L; and (b) crack at cross-arm connection of Poles 8Z-2L and 8Z-2R.

It is noted that both these failures occurred at geometric discontinuities where water ponding is facilitated, and where the presence of atmospheric chlorides from the nearby coastline is highly likely to exacerbate corrosion damage.

3.6 Damage Assessment based on Visual Inspection

The specific setting of each site, hypothesized environmental classification, and pole structures inspected, are summarized in Table 3.1. Based on the visual assessment presented in this chapter, the poles are then sorted in order of increasing corrosion damage

in Table 3.2. The inspected poles encompassed a wide range of damage levels, and they are grouped accordingly into four categories ranging from ‘Negligible’ to ‘Severe’ damage. It is noted that pitting levels are reported in conformance with the criteria set forth in ASTM G46 (ASTM 2013c), which depend only on pit density and size (diameter), as illustrated in Figure 2.10. Therefore, it is emphasized that these visual assessment criteria do not account for pit depths, which are key information to quantitatively assess thickness losses and associated corrosion rates. This task can be accomplished by means of thickness measurements, as demonstrated and documented in Section 5.1.

Table 3.1 Pertinent identification details on field testing sites and structures.

Site	Location	Coordinates	Setting	Environment	Pole	Year Installed
1	Regina, SK	50°30'49" -104°37'55"	Between steel plant and SK 11 highway	Rural/urban	C1F-20	1998
2	Cory, SK	52°05'39" -106°50'56"	Adjacent to potash mine	Industrial	Q3C-1L	2002
					Q3C-1R	2002
					Q3C-2L	2002
					Q3C-2R	2002
3	Estevan, SK	49°05'40" -102°52'55"	Rural area near coal mines and power station	Rural/industrial	S3B-2L	1988
					S3B-3L	1988
					S3B-7L	1988
					S3B-7R	1988
4	Melbourne Beach, FL	27°56'14" -80°29'32"	~300 ft from Atlantic Ocean	Marine	TL-1	1993
					TL-2*	1993
5	Orange County, FL	28°22'46" -80°54'56"	Off FL-520 highway	Rural	8Z-2L	1990
					8Z-2R	1990
					11Z-2L	1990
					11Z-2R	1990
					11Z-6L	1990
11Z-6R	1990					

* Pole TL-2 is a test structure made of galvanized steel (herein denoted as “GS”).

Table 3.2 Assessment of visible corrosion damage in inspected poles.

Damage Level	Site	Pole	Corrosion damage*
Negligible	1	C1F-20	Minimal pack rust and pitting (A3-B2) under tape
	3	S3B-3L	Minimal coating lip delamination
Minor	3	S3B-7L	Minor coating lip delamination, pronounced pitting (A4-B4)
		S3B-7R	Minor coating lip delamination, pronounced pitting (A4-B4)
	5	11Z-2L	Rough patina, pitting (A3-B3), pack rust on interior
		11Z-2R	Rough patina, pitting (A3-B3), pack rust on interior
		11Z-6L	Failed ladder connection, pitting (A3-B3), pack rust on interior
Moderate	2	Q3C-1R	Coating deterioration, rough patina, pack rust
	3	S3B-2L	Missing coating at base, ground-line pack rust, pronounced pitting (A4-B4)
	5	8Z-2L	Losses from galvanic corrosion of fasteners, cross arm crack, pitting (A3-B3), pitting (A4-B2) on interior
		8Z-2R	Losses from galvanic corrosion of fasteners, cross arm crack, pitting (A3-B3), pitting (A4-B2) on interior
		11Z-6R	Rough patina, losses from galvanic corrosion of fasteners, pitting (A3-B3), pack rust on interior
Severe	2	Q3C-1L	Severe coating deterioration, rough patina, pack-rust and pack-out damage, pitting (A3-B4)
		Q3C-2L	Severe coating deterioration, rough patina, pack-rust and pack-out damage, pitting (A3-B4)
		Q3C-2R	Severe coating deterioration, rough patina, pack-rust and pack-out damage, pitting (A3-B4)
	4	TL-1	Severe coating deterioration, rough patina, pack-rust and pack-out damage, severe pitting (A5-B4), hole in WS wall at junction box

* Pitting levels are reported in conformance with ASTM G46 criteria (ASTM 2013c).

This visual assessment classification will be further verified and discussed in the following chapters based on evidence gathered from other state-of-the-art assessment methodologies. The objective is to understand to what extent utilities can rely on careful visual inspection to make informed decisions on prioritized maintenance and remediation.

3.7 Concluding Remarks

Based on the visual inspection of the WS pole structures inspected at Site 1 through Site 5, the following concluding remarks are noted.

- Site 1: an adherent patina forms on WS pole surfaces in this rural-urban environment. The occurrence of localized corrosion damage underneath reflective tape demonstrates the importance of preventing the introduction of (even small) geometric discontinuities where water can stagnate. In fact, water stagnation prevents the formation of a protective patina, and facilitates the occurrence of corrosion damage by acting as an electrolyte.
- Site 2: exposure to an industrial atmosphere (potash mine) can cause moderate to severe corrosion damage to WS pole structures. It is also hypothesized that the presence of atmospheric chlorides contribute to such damage. The selection, installation and detailing of a suitable coating system are critical to ensure that the ground line is protected from corrosion damage.
- Site 3: exposure to a rural/industrial environment (coal mine and coal-fired power station) can result in negligible to moderate corrosion damage. In particular, pitting severity reasonably depends on the distance between the WS structure and industrial facilities, and appears to be exacerbated for WS pole walls that face directly potential contaminant sources (e.g., smokestacks, coal trucks and storage yards). In addition, stray current effects may be of concern for structures in proximity to power stations. Under these conditions, corrosion damage can be exacerbated by incorrect detailing of the coating at the ground level (e.g., insufficient height above ground).

- Site 4: direct exposure to a marine (chloride-laden) environment inevitably results in severe corrosion on WS transmission line structures. Corrosion forms range from extensive and heavy pitting to pack-out damage, where the latter is facilitated in areas that are more likely to be interested by water stagnation or moisture retention, and formation of chloride deposits. In this environment, WS is not a sound choice for transmission line structures. Instead, GS may be considered.

- Site 5: WS appears to be a viable choice in coastal areas for structures located a few miles from saltwater. However, the formation of a relatively unstable patina may still be attributed to the exposure to atmospheric chlorides. More research is needed to understand practical cut-off distances where the use of WS should be discouraged. While the service environment is a critical factor to consider for corrosion assessment, there are instances where pole design and detailing become more important. For example, at this site, poor design and detailing choices (e.g., unsealed poles, coupling between WS and GS) resulted in severe corrosion damage.

CHAPTER 4.0 ASSESSMENT OF ENVIRONMENTAL CORROSIVITY

A comprehensive quantitative assessment of the environmental (both atmospheric and soil) corrosivity was performed in each of the test sites presented in Chapter 3.0. Section 4.1 discusses atmospheric corrosivity with an emphasis on implications for WS transmission line structures, since WS is often chosen over other steel alloys because of its expected corrosion resistance when exposed to outdoor environments. Most utility poles, including the majority of those encountered in this study, are directly embedded into the ground. Therefore, Section 4.2 discusses soil corrosivity and implications thereof. First, each section reviews the influencing factors for WS transmission line structures, standard classification methods for environmental corrosivity, and state-of-the-art test methods as implemented in each test site. Then, the field test results are presented and analyzed. Finally, Section 4.3 summarizes salient conclusions on the impact of atmospheric and soil corrosivity on the WS poles exposed to the representative environments of Site 1 through Site 5.

4.1 Atmospheric Corrosivity

The main factors that influence atmospheric corrosivity for WS alloys are moisture, presence of airborne contaminants, especially sulfur dioxide and chloride (Sereda 1960), and temperature. The five test sites covered in this study offer a representative and significant range of exposure environments, as illustrated in Figure 4.1. In fact, Sites 1, 3, and 5 generally exhibit rural atmospheres but each has peculiarities that may significantly affect corrosion behavior, such as: proximity to a metropolitan area and steel plant (Site 1),

coal mines and a power station (Site 3), and a highway a few miles away from saltwater bodies (Site 5). In addition, Site 2 features WS poles that are adjacent to a potash mine with a potentially aggressive industrial atmosphere, and Site 4 is facing the ocean in a hot and humid area.



(a)



(b)



(c)



(d)



(e)

Figure 4.1 Photographs illustrating atmospheric exposure of WS pole structures in: (a) Site 1; (b) Site 2; (c) Site 3; (d) Site 4; and (e) Site 5.

4.1.1 *Influence of Moisture*

The most important factor affecting the atmospheric corrosivity of WS is moisture. When WS is exposed to prolonged wetness or stagnant moisture, protective oxide films cannot form and the corrosion rate is typically comparable to that of CS. Representative examples of permanently moist aggressive environments for WS structures include:

- Regions with long periods and/or heavy amounts of rain, fog, or snow.
- Coastal atmospheres with intense sprays or gusts of salt water.
- Areas that are sheltered from sunlight.
- Terrain with pronounced vegetation growth or sedimentation.

Permanently moist environments can also form in areas of transmission poles, like:

- Pits or crevices.
- Poorly sealed joints.
- Ground lines.
- Hollow caisson foundations.

Exposure to stagnant moisture facilitates the volumetric expansion of corrosion by-products, which exerts pressures that may result in large deformations and damage (Dodson 2012) in the case of pack-rust phenomena. Based on experiments performed by Larrabee (1953), significant corrosion-induced thickness losses on both WS and CS were measured as a result of exposure in a wet tunnel where steel coupons remained constantly damp. In particular, 12 months of exposure to acidic moisture resulted in thickness losses in WS that

were 11 times greater than those measured on the same type of WS under open exposure in an industrial environment.

The potential impact of moisture on corrosion processes is typically quantified based on “time of wetness” (TOW). This parameter depends primarily on the following climatic factors: relative humidity of the atmosphere, frequency and duration of rain, melting snow, fog, dew, air currents, direct radiation from the sun (affecting drying cycles), and temperature of air and steel surface (Mendoza and Corvo 1999). The onset of corrosion depends on the formation of and prolonged exposure to a thin moisture (electrolyte) film on the steel surface. While such film may be invisible to the naked eye, the corrosive contaminants it contains can reach relatively large concentrations, particularly under conditions of alternating wetting and drying. In fact, in the absence of moisture, most contaminants would have little to negligible effects on corrosion. Wind can also be a contributing factor, for example in the case of sea breeze carrying moisture and chlorides.

Relative humidity (RH) is defined as the ratio of the quantity of water vapor present in the atmosphere to the saturation quantity at a given temperature. It is expressed as a percentage. The thickness of the adsorbed layer of water on a material surface increases with RH and corrosion rates increase with the thickness of the adsorbed layer (Roberge et al. 2001). However, beyond a certain thickness of the moisture layer, corrosion reactions would be mitigated or prevented due to the resulting barrier against oxygen diffusion. The critical RH level depends on the intrinsic properties of the corroding material, the predisposition of corrosion products to absorb moisture, and the direct exposure to atmospheric pollutants. When such %RH level is reached, it may prompt corrosion as water lingers on the surface, increasing contaminant concentrations (Mendoza and Corvo 1999).

Surface moisture from condensation can also be harmful. Rain carries pollutants while adding moisture to the steel surface. If moisture from rain collects in pits or crevices, the prolonged wetness may accelerate the corrosion process in these areas. Similarly, dew can be detrimental to corrosion resistance if it results in stagnant condensation. In particular, dew that is saturated with acid sulfates or chlorides constitutes an aggressive electrolyte. However, rain that does not result in stagnant moisture can have a positive effect as it washes atmospheric pollutants away from the exposed steel surface. The washing effect of rain results in reduced corrosion rates when the dry contaminant deposition is greater than the wet contaminant deposition. This effect has been especially noticeable in marine atmospheres. Conversely, in areas where air has a limited concentration of atmospheric contaminants, corrosion rates tend to increase due to exposure to rain and wetness (Popov 2015).

Sunlight also plays an important role for WS. In fact, the formation of a protective patina on WS requires a consistent exposure to wet/dry cycles, and radiations from sunlight facilitate moisture evaporation and surface drying.

4.1.2 Influence of Airborne Contaminants

The most critical atmospheric contaminants are gaseous sulfur dioxide (SO₂) and atmospheric chlorides and, to a lesser extent, nitrogen oxides (NO_x) and phosphates. Atmospheric corrosion damage is of concern in areas with relatively high concentration of SO₂ or aggressive salts. In fact, exposure to these airborne contaminants deeply affects the composition of the patina that forms on WS surfaces (Singh et al. 2008). As a result, atmospheric corrosion typically occurs in industrial and marine environments, and is exacerbated by the presence of particles (e.g., dirt, dust, soot) on the WS surface as

moisture and contaminants are retained for a longer period of time (Albrecht and Hall 2003).

It is also noted that atmospheric contaminants are often distributed by way of aerosols. Aerosols are substances that are expelled from the earth's surface (e.g., sea spray, wind-blown dust) or created via physical and chemical reactions in the atmosphere. For example, SO₂ and nitrogen oxides can react through moisture and sunlight to form chemicals that can be transported as aerosols. A representative example of this type of aerosols is the haze cladding densely populated urban areas. Up to 50% of such haze is a combination of sulfuric and nitric acids (Tanner et al. 1981). As a result, the interaction of SO₂ with NO₂ and/or O₃ may lead to higher deposition rates of SO₂ and, consequently, more severe corrosion-induced thickness losses (Oesch 1996).

4.1.2.1 Sulfur Dioxide

Sulfur dioxide is one of the most noteworthy air pollutants contributing to corrosion of structural steel. SO₂ is the gaseous product of the combustion of fuels that contain sulfur such as coal, gasoline, diesel fuel, and natural gas. Gaseous SO₂ adsorbs into the surface of an electrolytic layer and is hydrolyzed, producing bisulfite (HSO₃⁻), which is the conjugate base of sulfurous acid. Oxygen interacts with HSO₃⁻ yielding SO₃ by decreasing the heat of reaction, and is then rapidly converted into sulfuric acid (H₂SO₄). These processes are shown in Equations 4-1 through 4-3.



There are still significant gaps in the understanding of the influence of gaseous SO₂ on the corrosion behavior of WS. Some researchers contend that WS is less vulnerable to SO₂ than CS, especially for relatively longer exposure times (Wang et al. 2013), others make the case that exposure to modest concentrations of SO₂ may actually facilitate the formation of a protective patina on WS (Wang et al. 1997). While a certain amount of SO₂ or sulfate aerosol deposits may contribute to the formation of a protective oxide film, excessive amounts can result in severe acidification of the aqueous layer, causing dissolution and impeding precipitation (Diaz et al. 2012). Moroishi and Satake (1973) observed a noticeable correlation between one-year corrosion damage (thickness loss) and SO₂ levels, although this correlation was no longer apparent after five years of exposure.

Knotkova et al. (1982) conducted experiments in various atmospheres to study the effect of SO₂ on the atmospheric corrosion of an ASTM A242 WS. Salient results are illustrated in Figure 4.2. Relatively low rates of corrosion were recorded in less polluted rural atmospheres (i.e., with deposits of less than 40 mg SO₂/m²d on the steel surface). The oxide film forming on WS in rural environments was described as a compact structure with a dark brown to violet color. In urban and/or moderate industrial atmospheres (i.e., with deposits in the range 40-90 mg SO₂/m²d on the steel surface), the oxide film on WS was also dark brown to violet in color but was less stable than that of WS exposed to low-pollution atmospheres. Higher corrosion rates were noted in heavily polluted industrial atmospheres (i.e., with deposits in excess of 90 mg SO₂/m²d on the steel surface), indicating that unstable oxide films formed and were routinely damaged. The appearance of oxide films on WS exposed to polluted industrial atmospheres were for the most part dark brown, but largely non-adherent and unstable.

Corrosion rate in WS appears to be a function of SO_2 concentration, increasing as the SO_2 concentration rises. After further long-term testing and analysis, Knotkova et al. (1982) suggested a maximum level of $90 \text{ mg SO}_2/\text{m}^2\text{d}$ for atmospheres where WS may be used without protective coatings. The supporting trend of corrosion mass loss measured as a function of SO_2 concentration is presented in Figure 4.3, highlighting the change in the rate of increase of mass loss at approximately $90 \text{ mg SO}_2/\text{m}^2\text{d}$.

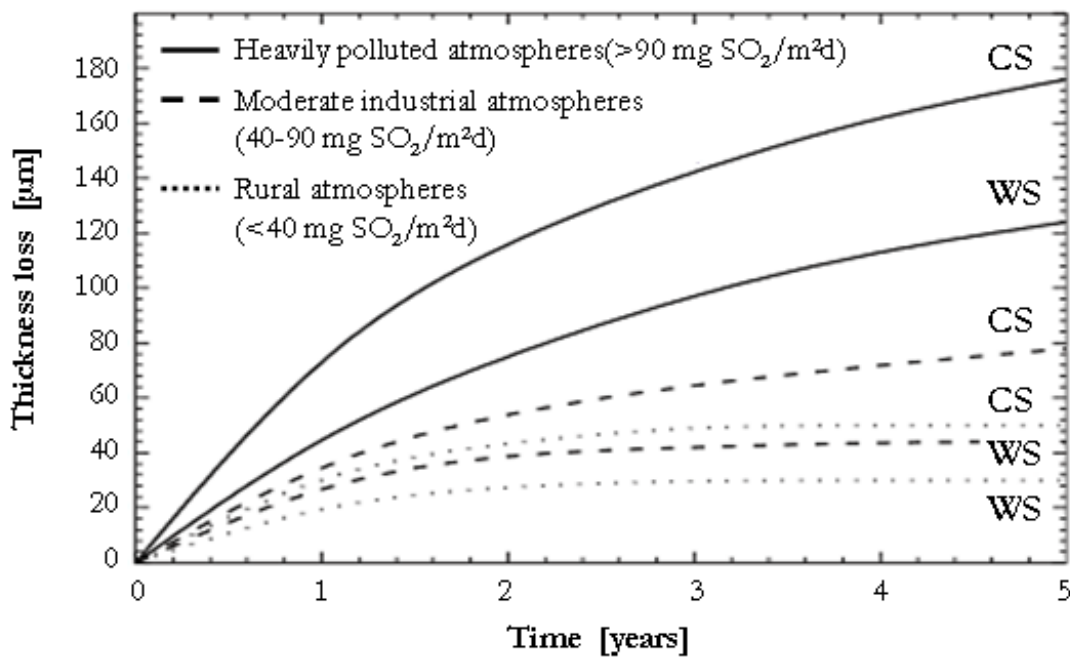


Figure 4.2 Corrosion-induced thickness loss in atmospheres with different SO_2 content for WS and plain CS (Knotkova et al. 1982).

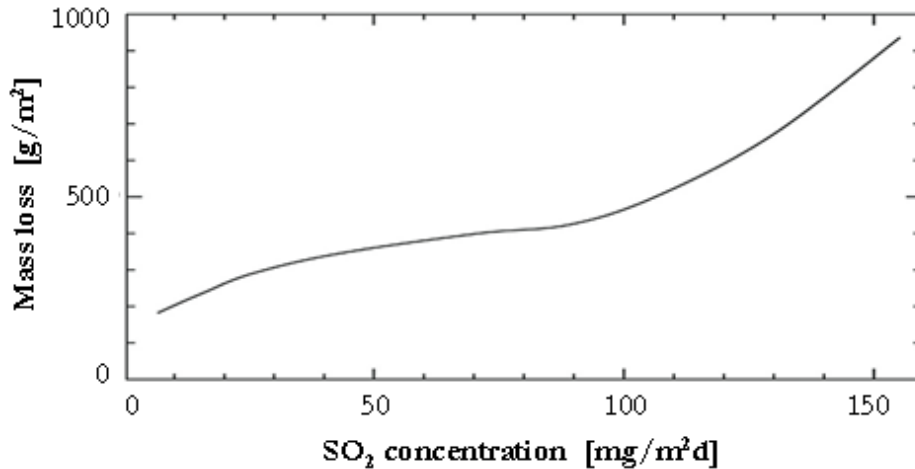


Figure 4.3 Corrosion of WS as function of SO₂ concentration (Knotkova et al. 1982).

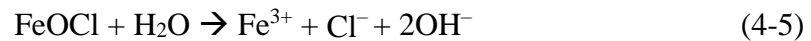
Consideration of other studies yields a similar comparison between atmospheres with various SO₂ concentrations. Fairly low corrosion rates, in the range 1-3 $\mu\text{m}/\text{year}$, were measured by Wang et al. (2013) for WS specimens in rural atmospheres. In urban atmospheres, WS displayed slightly higher steady-state corrosion rates, in the range 2-6 $\mu\text{m}/\text{year}$ (Oh et al. 1999). For comparison, it is noted that CS was characterized by decidedly greater corrosion rates in urban conditions. WS corrosion rates have been shown to be considerably larger in heavily industrial atmospheres than in rural or urban environments, indicating that the effectiveness of protective oxide films fades under increasing SO₂ concentrations. Yet, corrosion rates in WS have been consistently determined as smaller than those in CS when exposed to similar industrial atmospheres (Morcillo et al. 2013).

4.1.2.2 Chlorides

Chlorides from airborne salt significantly affect the atmospheric corrosion of steel in marine environments. Corrosive chloride-laden environments can also accrue from the production of hydrochloric acid (HCl) from burning fossil fuels, the emission of chlorine

from industrial processes, and the use of deicing salts (Amrhein et al. 1992) such as sodium chloride (NaCl) and calcium chloride (CaCl₂). Chloride-induced corrosion of steel depends on the specific exposure conditions and environment, alloy composition, oxidizer concentration and dissolved oxygen levels.

In WS, chloride ions adsorb on the outer surface of the surface patina, permeate into it, and interact with the underlying substrate. The outermost layers of the passive film are displaced due to the catalytic formation of FeOCl, which dissociates to Fe³⁺ when it is placed in contact with a relatively high concentration of chlorides. These processes are illustrated in Equations 4-4 and 4-5.



In marine environments, chloride contamination is a major concern for the corrosion resistance of WS. Limited data have been reported on the effect of airborne salts in marine atmospheres. However, Morcillo et al. (2013) discussed the relation between the long-term (i.e., steady-state) corrosion rate of steel and atmospheric salinity based on empirical data as summarized in Figure 4.4. The statistical sample considered included steels with oxide film of adherent and non-adherent quality. Figure 4.4 clearly shows that steels with non-adherent oxide films exhibit far greater steady-state corrosion rates compared to steels with adherent (i.e., protective) oxide films.

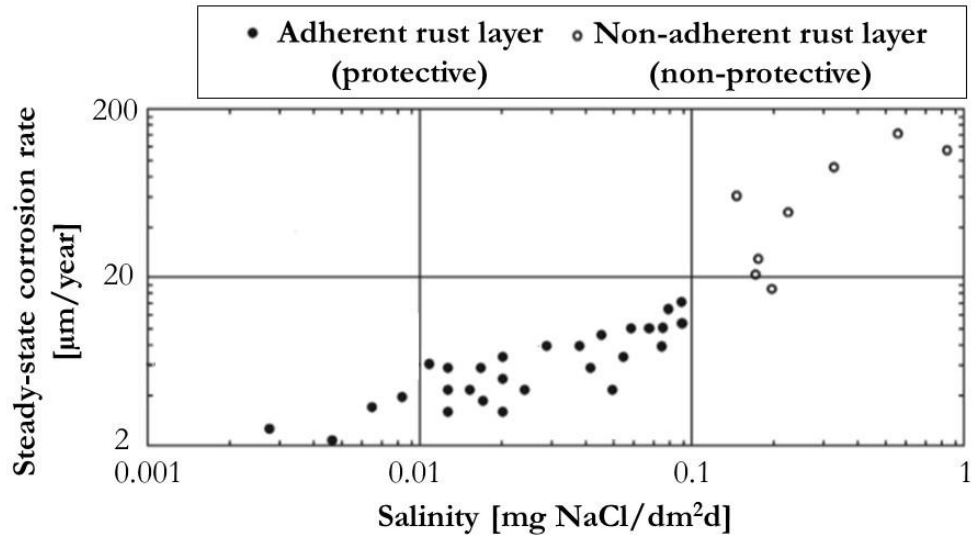


Figure 4.4 Impact of airborne salinity on corrosion rate of WS (Morcillo et al. 2013).

Typical corrosion rates have been reported in the range 6-20 $\mu\text{m}/\text{year}$ and as high as 50 $\mu\text{m}/\text{year}$ for WS located in close proximity to seashores (Oh et al. 1999). In fact, the formation of protective oxide films is undermined by the disruptive presence of FeOCl and/or Fe^{3+} . In particular, WS surfaces that are shielded from rain are at greater risk due to the potential for the build-up of chloride patinas, which can contribute to creating a highly corrosive environment.

4.1.3 Influence of Temperature

Temperature typically affects the atmospheric corrosion of steel in two manners. First, temperature has a strong and nearly logarithmic correlation with corrosion activity. The corrosion rate of metals increases with an increase in temperature in humid environments. For example, a 10°C increase in temperature may result in a 100% increase in corrosion activity (Sereda 1960). On the other hand, the %RH tends to decrease as temperature increases, which is likely to positively contribute to corrosion resistance.

Second, steel experiences a temperature lag as the ambient temperature fluctuates as it cools and heats slower than air does. For example, as ambient temperature drops in the evening, steel surfaces tend to remain warmer and do not begin to collect condensation until after the dew point is reached. When the surrounding air begins to reheat, the cooler steel tends to act as a condenser, preserving a layer of moisture on its surfaces. As a result, the condensation process is extended for longer than the time the ambient air is at or below the dew point, which indicates the equilibrium condition of condensation and evaporation from a surface. Typically, the wetting cycle is prolonged when the temperature lies below the dew point, and corrosion may be facilitated if the temperature remains approximately 15°C or less above the dew point (Popov 2015).

4.1.4 Categorization of Atmospheric Corrosivity

Outdoor atmospheres and exposure environments are typically sorted into one of three principal categories. In ascending order of corrosivity, these are rural, industrial, and marine atmospheres. Urban atmospheres can vary from city to city, ranging from more rural to more industrial, and so are difficult to explicitly define. Figure 4.2 illustrates a direct comparison of the trend of corrosion damage (i.e., thickness loss) over time for WS and CS in rural, urban, and industrial environments where corrosivity is related to the concentration of SO₂ (Knotkova et al. 1982).

For the specific case of WS, corrosion-induced thickness loss trends for ASTM A242 (Cor-Ten A) and ASTM A588 (Cor-Ten B) steels subjected to different open exposure conditions are illustrated in Figure 4.5 (Schmitt and Gallagher 1969) and Figure 4.6 (Zoccola 1982), respectively. Schmitt and Gallagher (1969) clearly demonstrated the favorable corrosion response of WS in rural environments. Cor-Ten A was also noted to

perform better in industrial Kearny, NJ, than in the marine atmosphere of Kure Beach, NC, after the initial year of exposure. The industrial atmosphere of Bethlehem, PA, was shown to be more corrosive than Kure Beach over the initial four years of exposure of Cor-Ten B specimens, but the marine environment again proved more corrosive in the long-term. Remarkably, exposure to an urban highway in Newark, NJ, produced elevated corrosion rates in the first year, but ultimately lower corrosion rates than even rural Saylorsburg, PA.

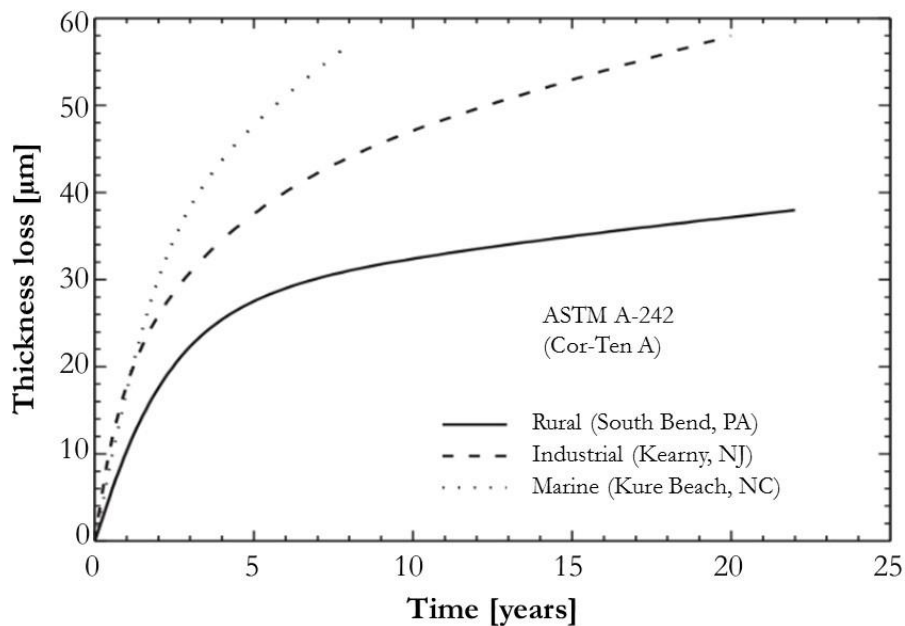


Figure 4.5 Corrosion-induced thickness loss history for ASTM A242 (Cor-Ten A) WS under different exposure conditions (Schmitt and Gallagher 1969).

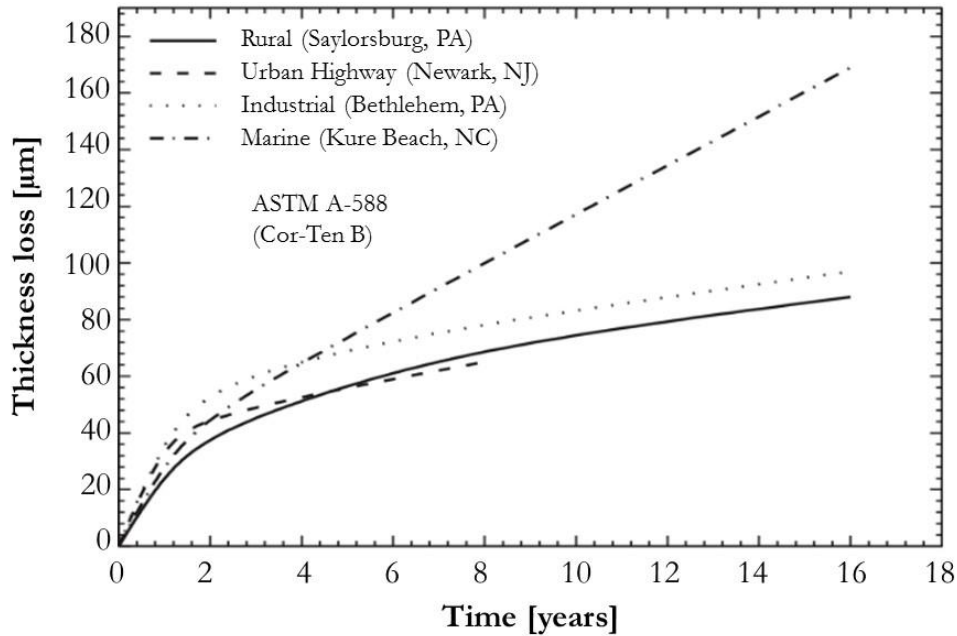


Figure 4.6 Corrosion-induced thickness loss history for ASTM A588 (Cor-Ten B) WS under different exposure conditions (Townsend and Zoccola 1982).

Atmospheric corrosivity may be classified based on qualitative and quantitative corrosivity attributes (e.g., airborne SO₂ and chloride concentration). The International Standards Organization (ISO) has standardized an atmospheric corrosivity categorization method, ISO 9223 (ISO 2012b) as a means to assess the combined impact of corrosivity parameters on the corrosion performance of steel alloys (Dean 1993). This methodology (ISO 2012b) relies on the assumption that corrosion rates are governed by time of wetness (TOW for %RH > 80% and temperature > 0°C) and concentration of certain atmospheric pollutants (SO₂ and chlorides). The categorization of TOW, SO₂ deposition (SD) rate and chloride deposition (CD) rate is summarized in Table 4.1, Table 4.2 and Table 4.3, respectively (ISO 2012b, Roberge et al. 2001). The standard (ISO 2012b) specifies how to combine TOW categories (T_1 through T_5) with SD (P_0 through P_3) and CD (S_0 through S_3)

categories to yield atmospheric corrosivity categories (C_1 through C_5 in ascending order of severity), as summarized in Table 4.4.

Table 4.1 Time of wetness categories per ISO 9223 (ISO 2012b).

TOW category	TOW [hr/year]	Examples of environments
T_1	$TOW \leq 10$	Indoor with climatic control
T_2	$10 < TOW \leq 250$	Indoor without climatic control
T_3	$250 < TOW \leq 2500$	Outdoor in dry, cold climates
T_4	$2500 < TOW \leq 5500$	Outdoor in other climates
T_5	$TOW > 5500$	Damp climates

Table 4.2 Sulfur dioxide deposition rate categories per ISO 9223 (ISO 2012b).

SD category	SO₂ deposition rate [mg/(m²d)]
P_0	$SD \leq 10$
P_1	$11 \leq SD \leq 35$
P_2	$36 \leq SD \leq 80$
P_3	$81 \leq SD \leq 200$

Table 4.3 Chloride deposition rate categories per ISO 9223 (ISO 2012b).

CD category	Chloride deposition rate [mg/(m²d)]
S_0	$CD \leq 3$
S_1	$4 \leq CD \leq 60$
S_2	$61 \leq CD \leq 300$
S_3	$301 \leq CD \leq 1500$

For example, category C_1 in Table 4.4 can be associated with a dry indoor environment without relevant airborne contaminants, and category C_5 can be associated with a moist and/or chloride- or sulfate-contaminated environment. Therefore, the ISO 9223 methodology (ISO 2012b) provides a rational approach to categorize atmospheric

corrosivity for transmission line steel structures although the margins of improvement remain significant (Roberge et al. 2001). In fact, addressing the following limitations may be critical for the practical corrosion assessment of WS transmission line structures:

- Potentially relevant corrosive pollutants – albeit less frequently encountered than SO₂ and chlorides – such as NO_x, hydrogen sulfide, chlorine gas and acid rain are not considered.
- Different temperatures above 0°C, wind conditions, sheltering (e.g., Figure 3.21b) and exposure angle are also not considered as variables, although they can contribute to corrosion, and should be accounted for separately on a case-by-case basis.
- Localized corrosion mechanisms are not explicitly considered, and should be accounted for separately on a case-by-case basis. Representative examples relevant to WS structures include severe pitting, crevice corrosion, galvanic corrosion (e.g., Figure 3.32), localized pack-rust damage (e.g., Figure 3.21a-c) and stress corrosion cracking (e.g., Figure 3.36).

However, the state-of-the-art knowledge base presented in this chapter provides a solid foundation towards the field investigation reported herein, which is aimed at probing the corrosion behavior of WS transmission line structures exposed to different environments.

Table 4.4 Categorization of atmospheric corrosivity per ISO 9223 (ISO 2012b).

TOW category	CD category	SD category	Corrosivity category
T_1	S_0 or S_1	P_1 or P_2	C_1
		P_3	C_1 or C_2
	S_2	P_1 or P_2	C_1
		P_3	C_1 or C_2
	S_3	P_1 or P_2	C_1 or C_2
		P_3	C_2
T_2	S_0 or S_1	P_1	C_1
		P_2	C_1 or C_2
		P_3	C_2
	S_2	P_1	C_2
		P_2	C_2 or C_3
		P_3	C_3
	S_3	P_1 or P_2	C_3 or C_4
		P_3	C_4
T_3	S_0 or S_1	P_1	C_2 or C_3
		P_2	C_3 or C_4
		P_3	C_4
	S_2	P_1 or P_2	C_3 or C_4
		P_3	C_4 or C_5
	S_3	P_1	C_4
		P_2	C_4 or C_5
		P_3	C_5
	T_4	S_0 or S_1	P_1
P_2			C_4
P_3			C_5
S_2		P_1 or P_2	C_4
		P_3	C_5
S_3		P_1, P_2 or P_3	C_5
T_5	S_0 or S_1	P_1	C_3 or C_4
		P_2	C_4 or C_5
		P_3	C_5
	S_2	P_1, P_2 or P_3	C_5
	S_3	P_1, P_2 or P_3	C_5

4.1.5 Test Methods

Standard test methods are available to monitor atmospheric properties. Galvanic cell monitoring can be enlisted to estimate TOW per ASTM G84 (ASTM 2012c). Likewise, sulfation plate tests can be used to estimate the deposition rate of SO₂ in accordance with ASTM G91 (ASTM 2011b), and the “wet-candle” method can be used to measure chloride deposition rates in accordance with ASTM G140 (ASTM 2014a). In addition, different test specimens, experimental setups and protocols, and measurement methodologies can be enlisted to evaluate the corrosion resistance of WS materials and structures vis-à-vis atmospheric environments and exposure conditions. Steel panel specimens are typically considered for atmospheric corrosion testing, in addition to standard tensile specimens for basic mechanical characterization and, when needed, stress corrosion cracking (SCC) specimens (Roberge 2008). Panel specimens should be prepared, cleaned (e.g., using acetone), and evaluated in accordance with ASTM G1 (ASTM 2011a). These specimens are typically mounted in racks that are inclined with respect to the horizontal plane and face the source of corrosive atmosphere, as shown in Figure 2.5 (Larrabee and Coburn 1962) and Figure 4.7 (Roberge 2008). Representative panel specimen dimensions are 100-150 mm in width and length with thickness of 2 mm. The specimens are electrically insulated from the racks and arranged to prevent cross-contamination with adjacent panels (Albrecht and Hall 2003).



Figure 4.7 Steel panel specimens mounted on inclined rack for corrosion testing in chloride-laden atmosphere (Roberge 2008).

Atmospheric corrosion tests on steel (including WS) panels are typically performed in accordance with ASTM G50 (ASTM 2015b). Depending on the test objectives, specimens may be fully exposed or partially sheltered. In most exposure experiments, a relatively large number of specimens are used to enable a comprehensive characterization of corrosion damage (e.g., including the chemical composition of the protective oxide film as reviewed in Section 1.1) at different test times such as 1, 2, 7, and 20 years or 2, 5, 10, and 20 years, whereas short-term experiments are of lesser use as they are likely to yield evidence that is inconclusive or difficult to interpret in a meaningful fashion.

Soft and hard data that are routinely collected may include appearance, mass or thickness loss, average and maximum pit depth, and residual tensile strength (Roberge 2008). Important factors to consider for atmospheric corrosion testing and data analysis, interpretation and comparison with historical databases include specimen material,

geometry and orientation, shading and sheltering, elevation, atmospheric pollutants and corrosive agents (Morcillo et al. 2013). Empirical data collected from panel tests can be evaluated based on a comparison of the performance of WS with that of CS subjected to similar exposure conditions. For example, Morcillo et al. (2013) used data from a worldwide bibliographic survey of atmospheric corrosion data for WS, as discussed further in Section 5.1.1. A reduction factor, R , was calculated as the ratio of the steady-state corrosion rate of ASTM A242 WS to that of plain CS. The resulting R values range from 0.29 to 0.57, indicating that WS was significantly less susceptible to atmospheric corrosion damage than CS.

Natural exposure experiments, while informative, entail relatively long test durations (of the order of years or decades) to yield usable data. To overcome this drawback for the purpose of obtaining preliminary data (for example for a comparative evaluation of different materials subjected to specific aggressive environments), accelerated corrosion methods have been implemented using synthetic laboratory environments (e.g., environmental chambers) as well as impressed currents, and are based on prior determination of governing corrosion factors. There are numerous techniques to accelerate corrosion but none have been found to realistically simulate real-world corrosion damage, for example with respect to the actual composition of corrosion by-products. This shortcoming is also well known for the case of steel corrosion in concrete (Poursaee and Hansson 2009).

Panel tests in general may be suitable to simulate exposure of WS surfaces, but they cannot provide meaningful results to evaluate corrosion resistance in the case of details with geometric discontinuities and crevices, where stagnant moisture becomes a major

concern as it hinders the formation of an adherent and chemically stable protective oxide film. Albrecht and Hall (2003) detailed environmental conditions under which fully-exposed WS structural members tend to undergo more severe corrosion damage than WS panel specimens mounted on inclined supports. In general, any exposure condition and structural detail that may contribute to prolonging the time of wetness on a WS member (e.g., sheltering, orientation, angle of exposure, build-up of debris, airborne pollutants, clearance from vegetation and ground, and geometric discontinuities such as structural joints) facilitates corrosion phenomena. Therefore, while evidence from long-term experiments on panel specimens is precious, the interpretation of results (let alone any extrapolation) to predict the corrosion resistance of actual structural members should be based on a careful assessment of these conditions.

To yield meaningful outcomes, long-term tests under realistic exposure conditions should be used to produce data that can be analyzed as a function of exposure time, service environment, and alloy composition (Oh et al. 1999). However, similar to what owners and inspectors would be typically experiencing, the author was tasked with inspecting pole structures, and collecting information to attempt an assessment of exposure conditions and environmental corrosivity consistent with ISO 9223 (ISO 2012b), based on relatively short field investigations (one to two days per site). The results of this effort are presented and discussed in Section 4.1.6 and Section 4.1.7.

4.1.6 Estimation of Atmospheric Corrosivity Parameters from Short-Term Field Tests

To produce results that could be evaluated per the ISO 9223 classification scheme presented in Section 4.1.4 (ISO 2012b), tailored strategies had to be devised to define

TOW, SD and CD rates using short-term field test data. These strategies are presented in the following two sub-sections.

4.1.6.1 Time of Wetness

TOW is defined as the amount of time (hr/year) in which RH exceeds 80% and temperature exceeds 0°C (32°F). For each test site, hourly RH and temperature measurements could have been taken using a hygro-thermometer to obtain reference data points. However, this approach would have provided an unrepresentative short-term (one- to two-day) sample size since RH and temperature vary widely over the course of the year. Therefore, a more realistic course of action was followed where TOW was estimated based on data of high/low RH and high/low temperature values as recorded at weather stations near each testing site. These open datasets are presented in Figure 4.8 through Figure 4.12 (WeatherSpark 2015a-e) for Site 1 through Site 5, respectively, where: the bold lines indicate the average high and low daily values; the inner, darker-shaded bands indicate a 50% confidence interval; and the outer, lighter-shaded bands indicate an 80% confidence interval. Based on the data available, the parameter TOW was estimated as follows:

$$\text{TOW} = 730 \left[(M, t > 32^\circ\text{F}) + \frac{1}{2} (M, t < 32^\circ\text{F}, T > 32^\circ\text{F}) \right] \frac{R - 80}{80 - r} \quad (4-6)$$

where M = number of months, t = average low temperature (°F), T = average high temperature (°F), R = highest recorded value for average high RH (%), and r = lowest recorded value for average low RH (%). In Equation 4-6:

- The first multiplier is a conversion factor to obtain units of hr/year from months/year.

- The second multiplier is given by the sum of all months in which the average low temperature exceeds the freezing temperature, and half of the months in which only the average high temperature rises above 32°F (0°C).
- The third multiplier is based on the assumption that the amount of time in which RH exceeds 80% can be estimated as the ratio of the differences between this threshold and most extreme RH values recorded.

4.1.6.2 Deposition Rate for Atmospheric Chlorides and Sulfates

Estimating deposition rates for atmospheric chlorides and SO₂ based on evidence from single-day field tests is a challenge that, if addressed in a practical and robust fashion, would demonstrate a methodology that owners and inspectors may consider. Deposition rates are most accurately measured via standardized monitoring techniques such as ASTM G91 (ASTM 2011b) for SD, and ASTM G140 (ASTM 2014a) for CD, as presented in Section 4.1.5. However, given the short duration of the field inspections performed as part of this project, a different procedure for estimating physical deposition data (in mg/m²) was devised. The procedure: (a) considers soluble chlorides and sulfates, where the latter are reasonably assumed to be a correlatable by-product of gaseous SO₂ deposition; and (b) is intended to be repeated at a later time, or the initial data would be extrapolated, to determine deposition rates.

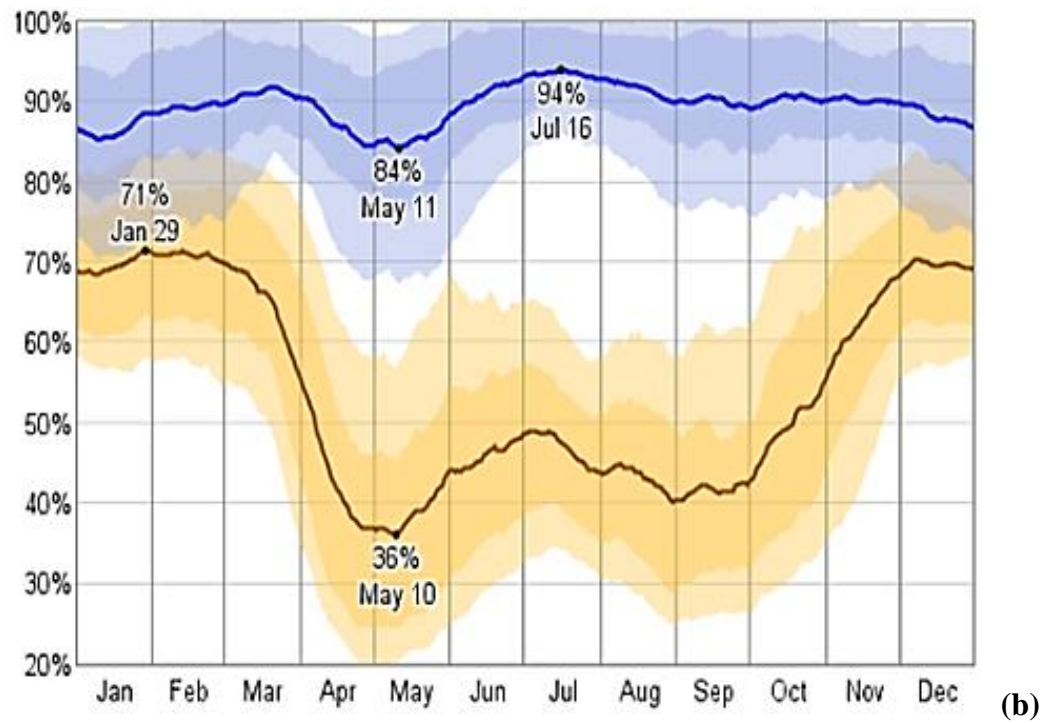
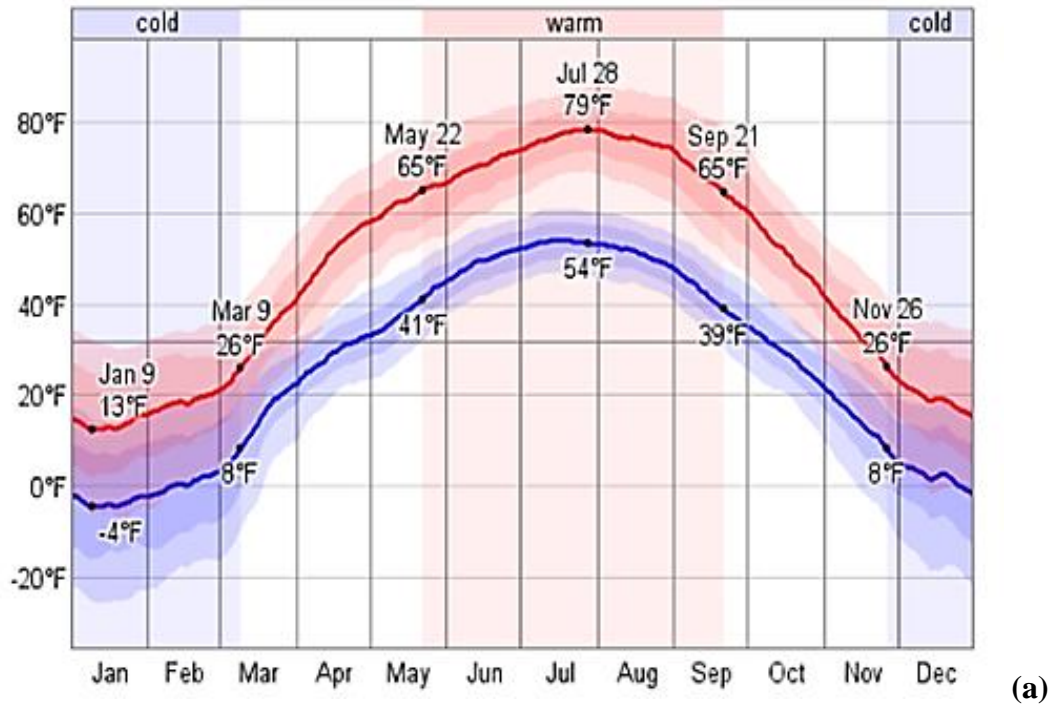


Figure 4.8 Weather data collected for Site 1 from Regina International Airport (Regina, SK) weather station: (a) high and low temperature averages; and (b) high and low RH averages (WeatherSpark 2015d).

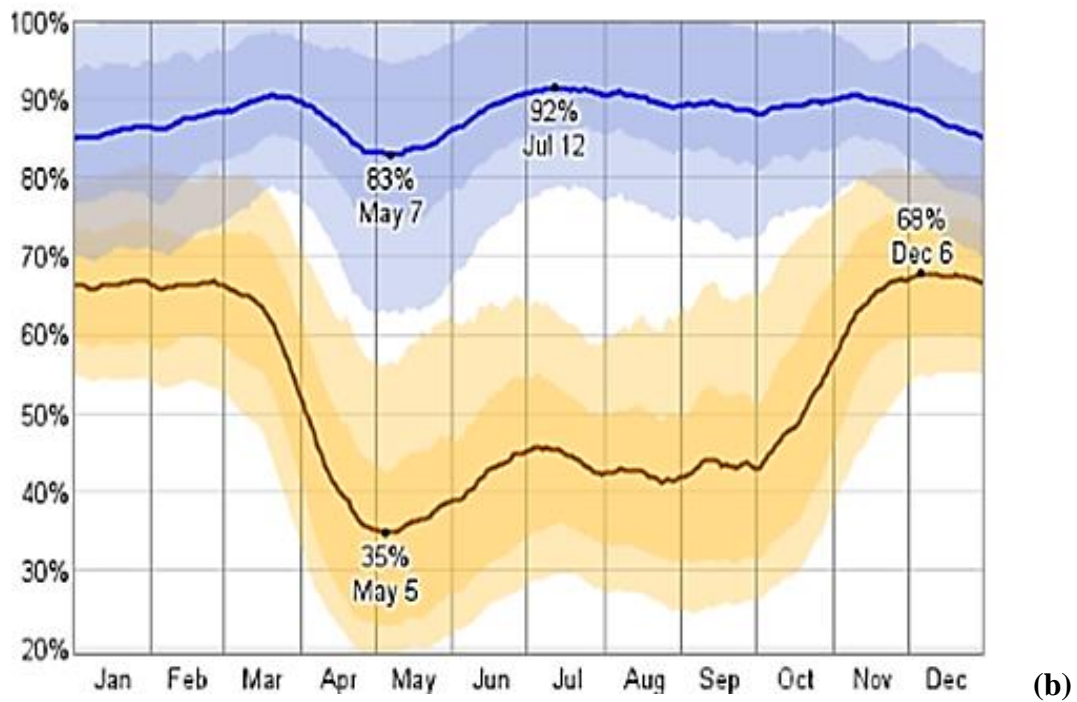
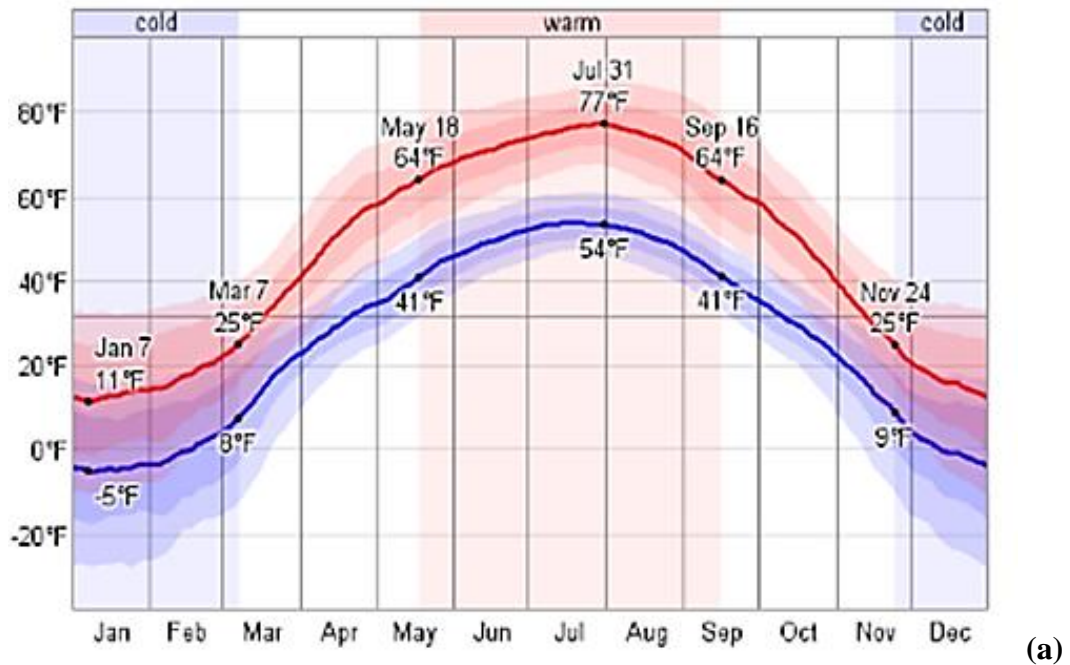


Figure 4.9 Weather data collected for Site 2 from Saskatoon John G. Diefenbaker International Airport (Saskatoon, SK) weather station: (a) high and low temperature averages; and (b) high and low RH averages (WeatherSpark 2015e).

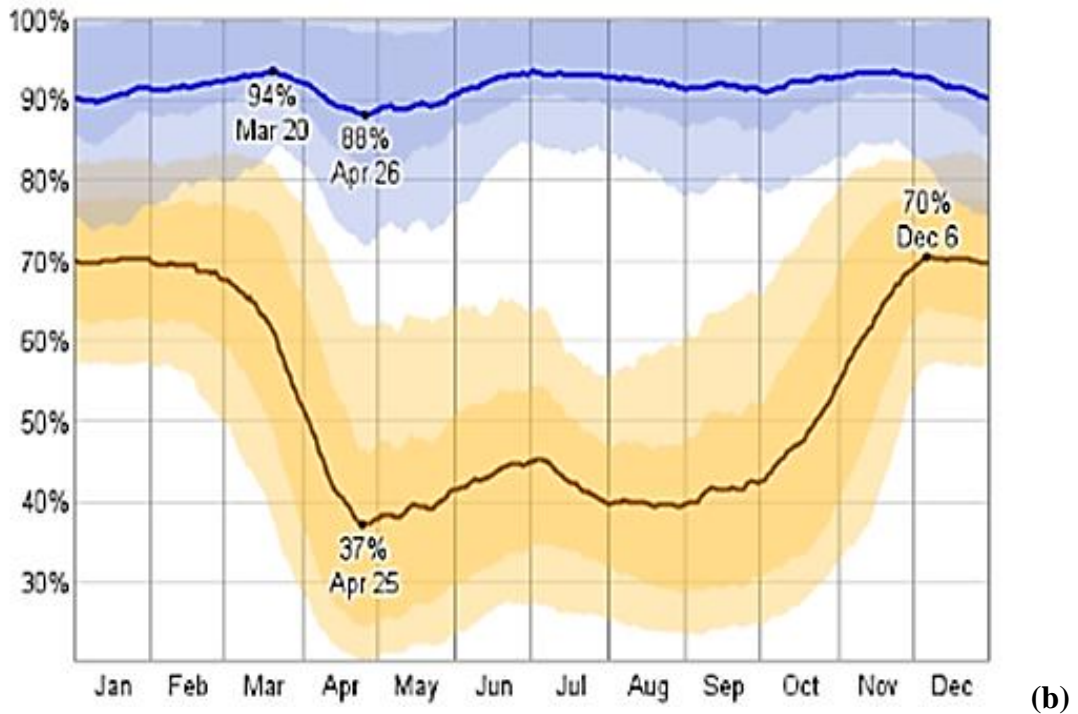
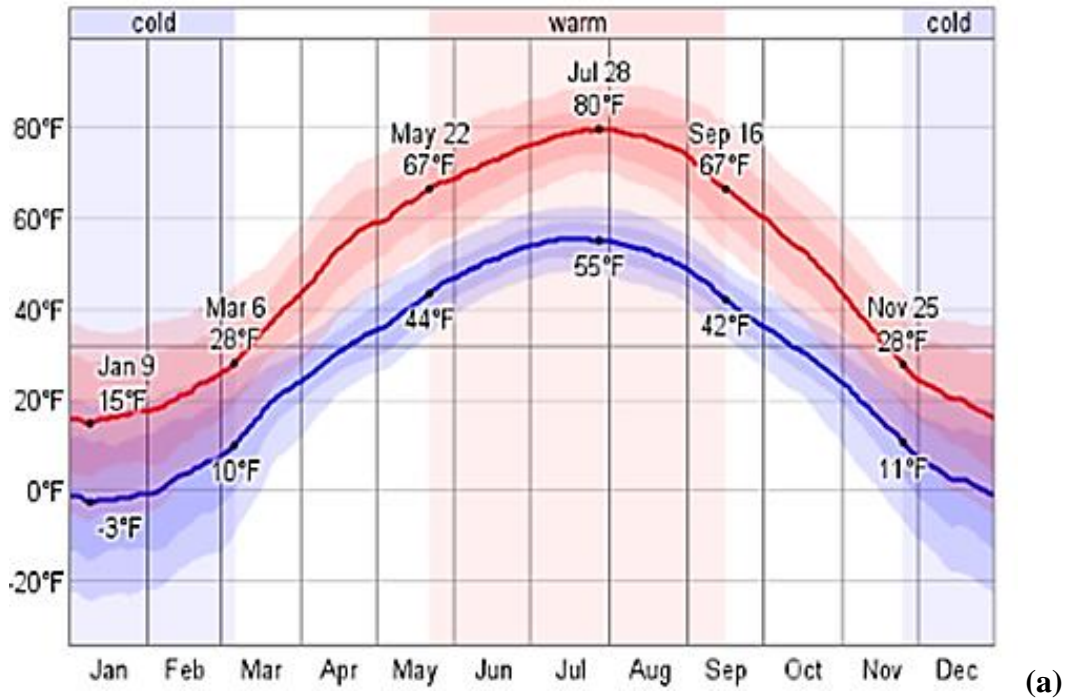


Figure 4.10 Weather data collected for Site 3 from Estevan Regional Aerodrome (Estevan, SK) weather station: (a) high and low temperature averages; and (b) high and low RH averages (WeatherSpark 2015b).

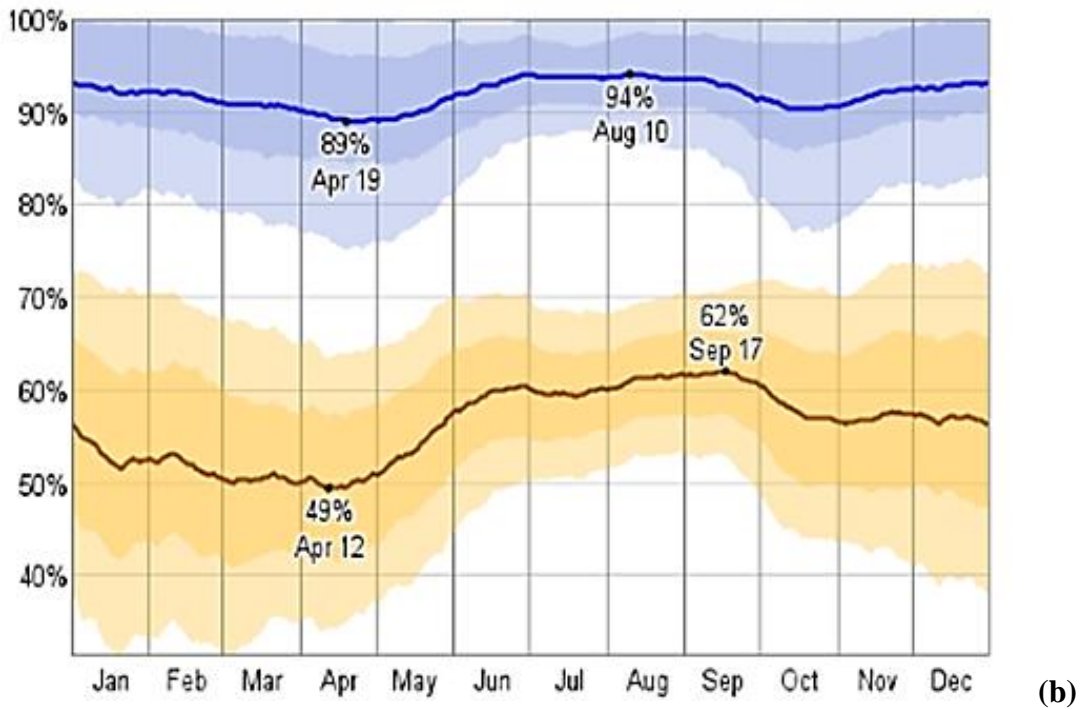
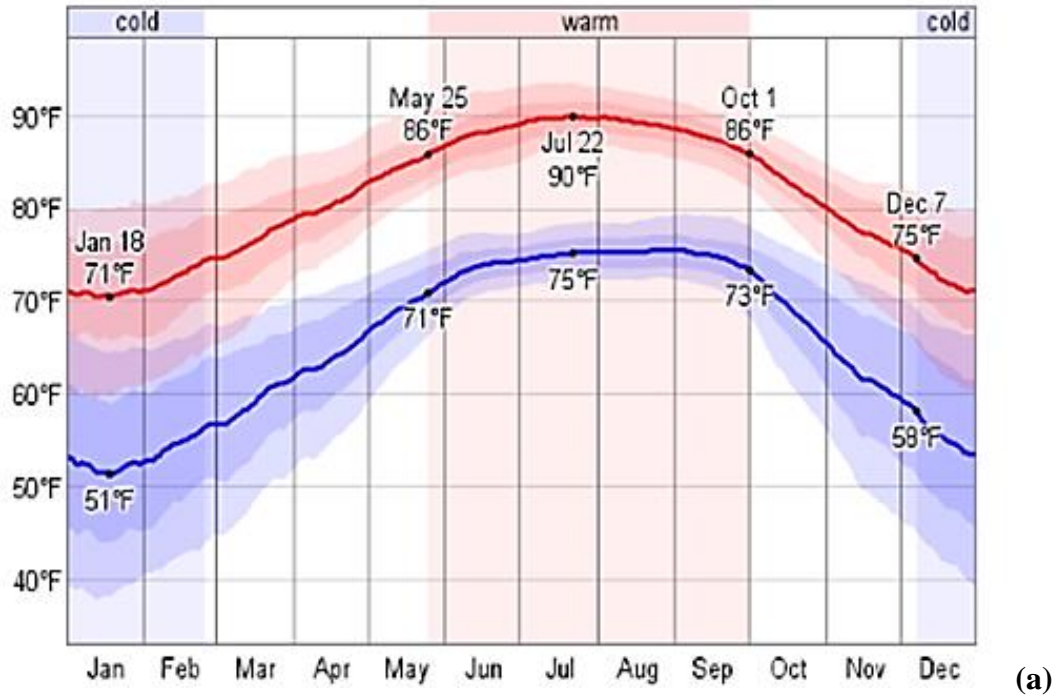


Figure 4.11 Weather data collected for Site 4 from Melbourne International Airport (Melbourne, FL) weather station: (a) high and low temperature averages; and (b) high and low RH averages (WeatherSpark 2015c).

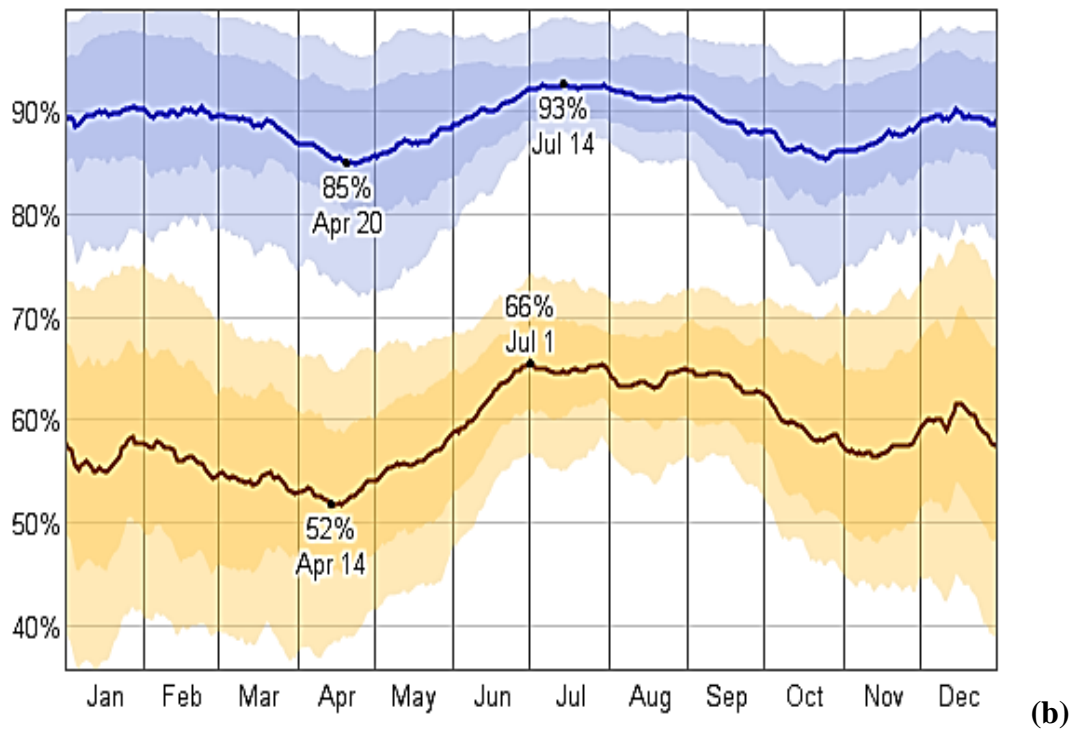
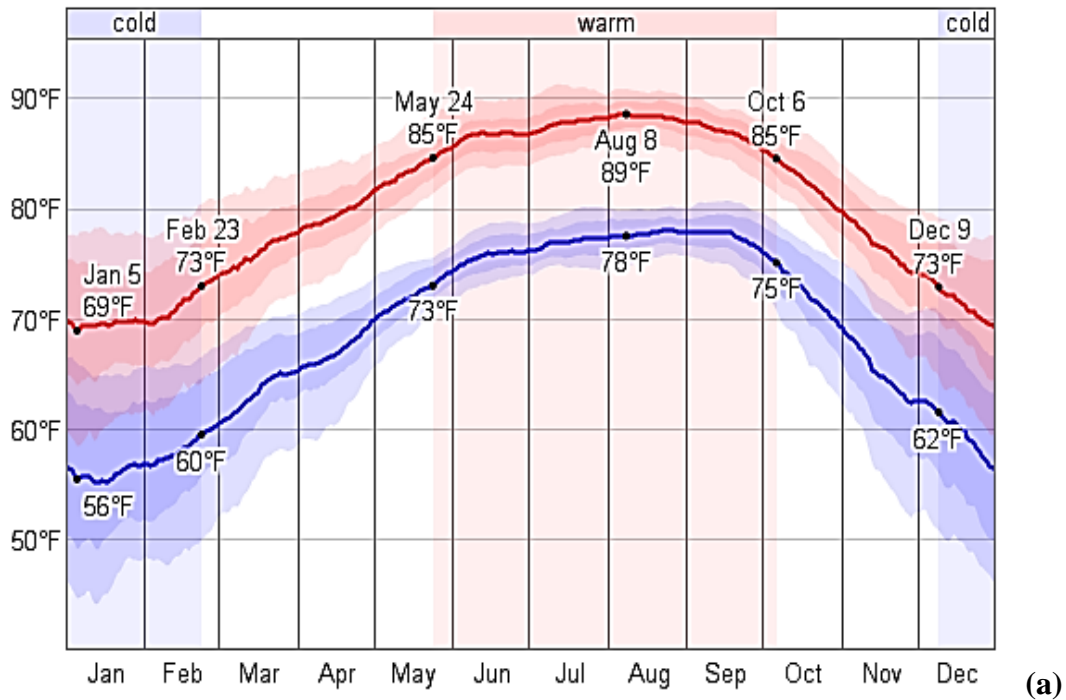


Figure 4.12 Weather data collected for Site 5 from Patrick Air Force Base (Cocoa Beach, FL) weather station: (a) high and low temperature averages; and (b) high and low RH averages (WeatherSpark 2015a).

Flores et al. (1994) examined two field test strategies for measuring soluble salt depositions on steel, namely surface swabs and the Bresle, or plastic-patch, method prescribed by ISO 8502-6 (ISO 2006). Contaminant extraction was quantified using indicator test strips for each contaminant, and concentrations were reported in mg/m². It was determined that both techniques were appropriate for use on steel surfaces, although they led to underestimating concentrations of deposits on oxidized steel surfaces (similar to the patina that forms on WS). Consequently, data collected using either method would underestimate deposition rates and, in turn, atmospheric corrosivity.

Surface-swab tests were chosen as the means for quantifying contaminant deposition. In fact, surface swabbing seemed to be more expedited and repeatable than Bresle patch tests and, more importantly, allow to collect chloride as well as sulfate samples whereas the Bresle patch method is not applicable to sulfate depositions. Surface-swab chemical inspection kits (Figure 4.13) were obtained from MSES Consultants, Inc. (Clarksburg, WV). These kits were used to quantify chloride as well as sulfate concentrations on pole surfaces at each test site using color-indicator strips, expressing the results in contaminant mass per liter of deionized water (DI) (Figure 4.14). In fact, sulfate depositions originate from SO₂ that has reacted with other elements (Ferm et al. 2006), and serve as an indicator of the presence of atmospheric SO₂. It is also noted that these kits allow to quantify pH, and iron, sulfide, nitrite, nitrate, carbonate, calcium, and manganese depositions.



Figure 4.13 Surface-swab testing for chloride and sulfate deposition: (a) test kit by MSES Consultants, Inc.; (b) pole swabbing; and (c) on-site analysis of swab samples.

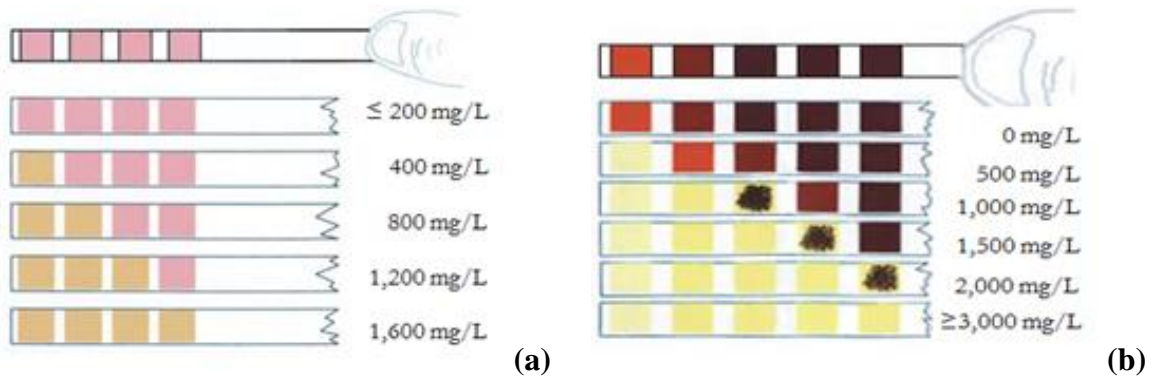


Figure 4.14 Color-coded criteria for indicator strips in swab test kit: (a) sulfates and (b) chlorides. Results expressed in contaminant mass per liter of aqueous solution.

Three swab tests were conducted on each WS pole. For each test, a 100 mm × 100 mm (0.01 m²) area of pole wall surface was swabbed, and contaminant concentration analysis was carried out following the kit manufacturer's instructions. The indicator strips provided the chloride and sulfate concentration in milligrams per liter of DI water (mg/L). The actual amount of ionic particulates extracted from a pole surface was obtained by multiplying this concentration by the volume of DI water (0.025 L) in each test vessel. For example, if a sulfate indicator strip read 200 mg/L, then 5 mg of sulfate were extracted. Knowing the size of the area swabbed, contaminant depositions was determined in a straightforward fashion (e.g., 5 mg sulfate from a 0.01 m² area are equivalent to a deposition of 500 mg/m²).

In order to convert the deposition values (mg/m²) to deposition rates in mg/m² per day (mg/m²d), two alternative approaches were tested. The first approach had the author leave additional test kits with the personnel overseeing the inspected structures. Follow-up tests were conducted for each structure after a period of three months, and the data were compared. Similar results to the initial data were obtained for all structures. Since no appreciable changes in deposition values were observed, a second conversion approach was followed based on the reasonable assumption that the measured depositions were attained primarily over relatively short time spans (after rainfalls). In fact, recent rainfall (i.e., within up to two weeks prior to testing) had occurred at all test sites before the field inspections, likely washing contaminants from the pole surfaces. Therefore, a deposition time of two weeks was considered for estimating deposition rates. In other words, it was assumed that, in the span of two weeks, a pole wall with no concentration of surface contaminants yields usable deposition data for chlorides and sulfates in a given atmosphere.

4.1.7 Results and Discussion

For each test site, the TOW values calculated using Equation 4-6 are summarized in Table 4.5, together with the associated TOW categories based on Table 4.4 (ISO 2012b). These outcomes appear to be sensible representations of the TOW values expected for each test site, consistent with the environment examples presented in Table 4.1. The average chloride and sulfate concentration data collected for each pole and the associated deposition rate estimates are presented in Table 4.6.

Sulfate concentrations ranged from 200 mg/L to 800 mg/L whereas no chloride concentration levels above 500 mg/L were detected. In fact, chlorides were only detected on the ocean-facing side of Pole TL-1 at Site 4. This single result was considered for Pole TL-1 in lieu of the average concentration to yield a more conservative (i.e., worst-case scenario) deposition estimate. The calculated deposition rate of 89 mg/m²d corresponds to the second most severe (*S*₂) CD category given in Table 4.3. In fact, a high deposition rate was expected given the proximity to saltwater. For the other poles that were located in areas not as directly exposed to chloride-laden atmospheres, it is noted that the detection of chloride depositions on WS surfaces may be difficult to accomplish via swab testing because chloride ions rapidly react with the iron oxides in WS (Asami and Kikuchi 2003), as discussed in detail in Section 1.1. From a practical standpoint, based on the chloride swab test results, it is suggested that future attempts consider the Bresle patch method (ISO 2006) when chloride depositions are of interest.

Table 4.5 TOW values and categories for each test site.

Site	M ($t > 32^{\circ}\text{F}$)	M ($t < 32^{\circ}\text{F}$, $T > 32^{\circ}\text{F}$)	R [%]	r [%]	TOW [hr/year]	TOW category
Site 1	5	3	94	36	1,510	T_3
Site 2	5	3	92	35	1,265	T_3
Site 3	5	3	94	37	1,544	T_3
Site 4	12	0	94	49	3,956	T_4
Site 5	12	0	93	52	4,067	T_4

Table 4.6 Contaminant concentrations and estimated deposition rate for WS poles.

Site	Pole	Chlorides		Sulfates	
		Concentration* [mg/L]	Average deposition rate [mg/m ² d]	Concentration* [mg/L]	Average deposition rate [mg/m ² d]
1	C1F-20	0 (0, 0, 0)	0	300 (300, 300, 300)	54
2	Q3C-1L	0 (0, 0, 0)	0	533 (600, 600, 400)	95
	Q3C-1R	0 (0, 0, 0)	0	500 (600, 500, 400)	89
	Q3C-2L	0 (0, 0, 0)	0	467 (500, 500, 400)	83
	Q3C-2R	0 (0, 0, 0)	0	300 (300, 300, 300)	54
3	S3B-2L	0 (0, 0, 0)	0	200 (200, 200, 200)	36
	S3B-3L	0 (0, 0, 0)	0	200 (200, 200, 200)	36
	S3B-7L	0 (0, 0, 0)	0	300 (300, 300, 300)	54
	S3B-7R	0 (0, 0, 0)	0	300 (300, 300, 300)	54
4	TL-1	500 (0, 500, 0)	89	300 (300, 300, 300)	54
5	8Z-2L	0 (0, 0, 0)	0	333 (400, 300, 300)	60
	8Z-2R	0 (0, 0, 0)	0	333 (400, 300, 300)	60
	11Z-2L	0 (0, 0, 0)	0	333 (400, 300, 300)	60
	11Z-2R	0 (0, 0, 0)	0	333 (400, 300, 300)	60
	11Z-6L	0 (0, 0, 0)	0	300 (300, 300, 300)	54
	11Z-6R	0 (0, 0, 0)	0	300 (300, 300, 300)	54

*Average value (of three values for different pole locations provided between parentheses).

The sulfate concentration results were more informative. The highest concentrations were found at Site 2 due to the exposure to an industrial atmosphere. Three out of four poles yielded sulfate concentrations greater than 450 mg/L, corresponding to a deposition rate of 81 mg/m²d, with the most corrosive SD category (i.e., P_3) defined in

Table 4.2. Only Pole Q3C-2R, the structure farthest from the potash mine, displayed lower values. The lowest concentrations (200-300 mg/L) were found at Site 3 for Poles S3B-2L and S3B-3L, the poles closest to the power station. This is thought to be due to the exposure to a predominantly rural atmosphere and suggests that the pitting damage observed on the pole walls near the power station does not necessarily accrue from sulfate exposure. Comparable sulfate concentrations were recorded at Sites 1, 4, and 5. Here, the most commonly observed concentration (300 mg/L) corresponds to a deposition rate of 54 mg/m²d and SD category *P*₂. Sites 1, 4, and 5 were all interestingly located near heavily trafficked roads; at these locations, no corrosion damage was clearly attributable to sulfate exposure.

The estimated CD and SD rates and associated categories (based on the criteria in Table 4.2 and Table 4.3) were paired with the TOW categories in Table 4.5 to comprehensively assess the atmospheric corrosivity for each WS pole based on. To this end, the ISO 9223 (ISO 2012b) criteria presented in Table 4.4 were applied. The resulting corrosivity categories are presented in Table 4.7. The numerous instances in which the poles are exposed to medium- and high-corrosivity (category *C*₃ to *C*₄) atmospheres highlight the significance of the selected sites. In these locations, using corrosion-resistant alloys is a reasonable proposition.

Site 1 lies within a corrosivity category *C*₃ to *C*₄, which suggests that atmospheric corrosivity at this location may shift depending on a more direct exposure to the city (urban atmosphere) or nearby steel plant (industrial atmosphere). Based on the visual observations of Pole C1F-20, the more rural corrosivity category *C*₃ appears to be the most suitable choice for this site.

Similar results can be seen for Pole Q3C-2R at Site 2 and Poles S3B-7L and S3B-7R at Site 3 (corrosivity category C_3 to C_4), which are located in areas with mixed rural-industrial atmospheres. The rest of the poles at Site 2 are shown to be exposed to a clearly industrial atmosphere due to the proximity to a potash mine, yielding a corrosivity category C_4 . Instead, the open (rural) spaces of Site 3 appear to outweigh the impact of the power station, resulting in a less concerning corrosivity category C_2 to C_3 for Poles S3B-2L and S3B-3L. However, Pole S3B-2L at Site 3 proved to be susceptible to corrosion due to reasons other than the specific exposure atmosphere (possibly stray currents and coating detailing), as discussed in Section 3.3.

Table 4.7 Atmospheric corrosivity categories based on ISO 9223 (ISO 2012b).

Site	Pole	TOW category	CD category	SD category	Corrosivity category
1	C1F-20	T_3	S_0	P_2	C_3 to C_4
2	Q3C-1L	T_3	S_0	P_3	C_4
	Q3C-1R	T_3	S_0	P_3	C_4
	Q3C-2L	T_3	S_0	P_3	C_4
	Q3C-2R	T_3	S_0	P_2	C_3 to C_4
3	S3B-2L	T_3	S_0	P_1	C_2 to C_3
	S3B-3L	T_3	S_0	P_1	C_2 to C_3
	S3B-7L	T_3	S_0	P_2	C_3 to C_4
	S3B-7R	T_3	S_0	P_2	C_3 to C_4
4	TL-1	T_4	S_2	P_2	C_4
5	8Z-2L	T_4	S_0	P_2	C_4
	8Z-2R	T_4	S_0	P_2	C_4
	11Z-2L	T_4	S_0	P_2	C_4
	11Z-2R	T_4	S_0	P_2	C_4
	11Z-6L	T_4	S_0	P_2	C_4
	11Z-6R	T_4	S_0	P_2	C_4

It is noted that both the high-TOW atmospheres of Sites 4 and 5 are characterized by a corrosivity category C_4 , despite the substantial difference in chloride deposition rates. This finding suggests that all WS poles located along the coast line at the Florida sites are

susceptible to corrosion damage, irrespective of the CD category, and that moisture is the dominant factor affecting atmospheric corrosivity. In fact, a moist environment facilitates water stagnation, thereby hindering exposure to much needed wet/dry cycles. However, the deterioration observed on Pole TL-1 clearly indicates that a direct exposure to a chloride-laden environment near saltwater exacerbates any moisture-related corrosion damage. To this end, it is also emphasized that swab tests seem to underestimate the presence of chlorides on WS surfaces due to the chlorides reactivity with iron oxides on WS (Asami and Kikuchi 2003). Therefore, it is likely that Site 4 possesses a more corrosive (i.e., C₅) atmosphere. The evidence presented in this chapter for Sites 4 and 5 reinforces the conclusion of visual assessment presented in Section 3.7, that is, WS is not a sound choice for transmission line structures operating near saltwater. In these chloride-laden environments where the atmospheric corrosivity may call for the use of a corrosion-resistant alternative, GS is a more sensible choice.

4.2 Soil Corrosivity

Transmission line poles made of WS are typically fitted with coatings or set upon elevated foundations in order to prevent a direct contact between WS and soil, which would hinder the formation of a chemically stable and adherent patina. However, there are practical instances where WS surfaces are not adequately protected from the surrounding soil. For example, soil corrosivity becomes a concern as coatings deteriorate or when poles are installed improperly, as documented in Figure 4.15 for Pole Q3C-2L at Site 2 and Pole S3B-2L at Site 3, respectively.

4.2.1 Influencing Factors

Below-ground corrosion depends on several variables, including soil type, moisture content, aeration levels, redox potential, acidity, resistivity, presence of soluble ionic species (salts), and microbiological activity (Ismail et al. 2009). Water is an essential electrolyte that supports electrochemical corrosion reactions in moist soils. Water retention is strongly dependent on the texture of the soil. For example, coarse sands tend to retain relatively low moisture whereas fine clay soils store can retain relatively large amounts of water, thereby creating more corrosive environments.

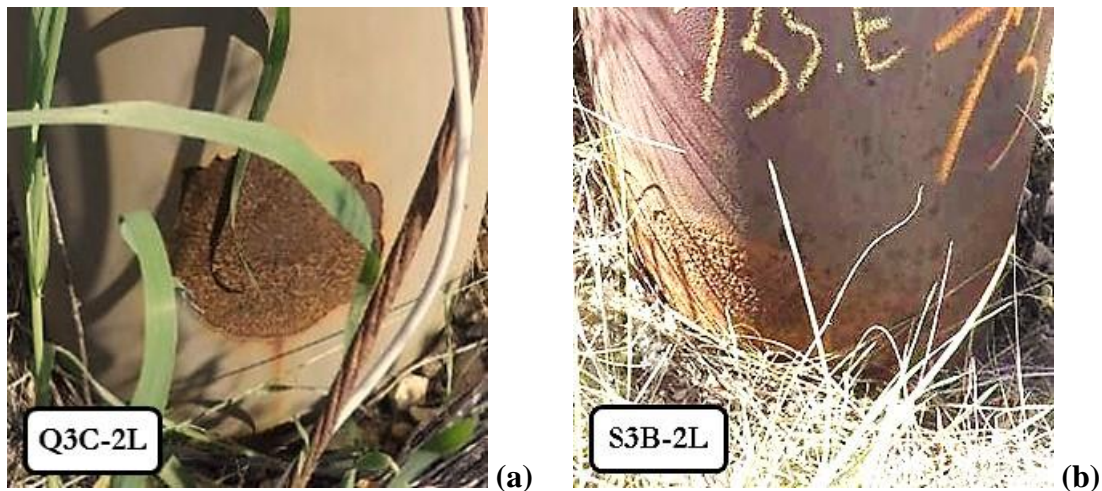


Figure 4.15 Areas of soil corrosivity concern: (a) coating deterioration near ground line of Pole Q3C-2L; and (b) pack rust at uncoated ground line of Pole S3B-2L.

Aeration is defined as the process by which air is circulated through, mixed with, or dissolved in a liquid or substance. With regard to soil corrosion, aeration refers to the oxygen concentration, or amount of trapped air, in soil. Soil size and gradation play a pivotal role in determining the degree of aeration. Oxygen transport is higher in coarse soils than in fine ones. Well-aerated soil typically displays lower moisture content and increased evaporation rates (Roberge 2008). Oxygen concentration characteristically

decreases with increasing soil depth. Redox (also known as oxidation-reduction) potential is a measure of the activity of oxidizers and reducers in relation to their concentration. Increasing redox potentials are associated with soils having higher oxygen contents where soils tend to passivate metals. As the redox potential decreases, steel becomes more susceptible to oxidation (Ismail et al. 2009).

Soils exhibit pH that can range between 2.5 and 10 although the pH of most soils typically lies within the range 5-8 (Roberge 2008). In this range, pH is not considered a major variable in assessing corrosion rates since more neutral pH values mitigate the likelihood of corrosion damage. In acidic soils where the pH is below 5, corrosion and pitting rates of steel are likely to increase. More acidic soils are produced by industrial wastes, acid rain, mineral leaching, decomposition of acidic plants, and some forms of microbiological activity. Conversely, alkaline soils are typically characterized by relatively high sodium, potassium, magnesium, and calcium contents. The presence of the latter two elements can facilitate the formation of protective calcareous deposits on buried structures (Roberge 2008).

Soil resistivity is a measure of the capability of soil to impede or resist the flow of electric current through it. Because ionic current flow is associated with soil corrosion reactions, high soil resistivity typically hinders the occurrence of corrosion phenomena. Resistivity varies due to changes in soil composition and moisture content. Sandy soils are typically characterized by relatively higher resistivity whereas clay soils, particularly those contaminated with saltwater, exhibit lower resistivity. Increased moisture contents can reduce soil resistivity and increase the possibility for corrosion (Roberge 2008).

Similar to atmospheric corrosion, which is heavily influenced by the presence of airborne contaminants, soil corrosivity also depends on the presence soluble ionic species such as chlorides and sulfates. Chlorides may be found naturally in soils as a result of contact with brackish groundwater and sea beds, or from external sources such as deicing salts. Chloride ions can participate in the anodic dissolution reactions of buried steel, and also tend to decrease the soil resistivity. Sulfate ions are generally considered less threatening to metal structures than chlorides with regard to corrosivity. Benign sulfate ions, however, can be converted into highly corrosive sulfides by anaerobic sulfate-reducing bacteria (Roberge 2008).

4.2.2 *Classification of Soil Corrosivity*

Soil resistivity is widely considered to be the dominant indicator of soil corrosion severity. Generally adopted corrosion severity ratings based on soil resistivity, as reported by Roberge (2008), are given in Table 4.8. Because soil resistivity measurements alone are likely to yield an incomplete account of soil corrosivity, a classification scheme that incorporated the full range of factors listed in Section 4.2.1 was sought for the purpose of estimating soil corrosivity for Site 1 through Site 5.

Table 4.8 Soil corrosivity classification based on soil resistivity (Roberge 2008).

Soil corrosivity rating	Soil resistivity (Ω-cm)
Extremely corrosive	< 1,000
Highly corrosive	1,000-3,000
Corrosive	3,000-5,000
Moderately corrosive	5,000-10,000
Mildly corrosive	10,000-20,000
Essentially noncorrosive	> 20,000

The American Water Works Association developed the standard AWWA C-105 as a means to assess soil corrosivity (AWWA 2010). This standard specifies soil corrosivity ratings based on accumulation of corrosivity “points.” The collective value depends on soil moisture condition, redox potential, pH, resistivity, and sulfide content. These parameters and their associated points are given in Table 4.9. The criteria for soil corrosivity classification per AWWA C-105 (AWWA 2010) are presented in Table 4.10. A total point value of 0-13 defines non-corrosive soils whereas higher values define corrosive soils.

More comprehensive point-based soil corrosivity assessment criteria are defined by the German Technical and Scientific Association for Gas and Water (DVGW 2011), as summarized in Table 4.11 and Table 4.12. Here, soil corrosivity is a function of soil composition, ground water level, moisture content, pH, resistivity, concentration of carbonates, chlorides, sulfates and sulfides, and presence of cinder and coke. The associated corrosivity points are presented in Table 4.11. The criteria for soil corrosivity categorization are presented in Table 4.12. Positive cumulative values indicate non-corrosive soils whereas negative values indicate slightly to very corrosive soils for which active protection measures such as cathodic protection should be considered (DVGW 2011).

Table 4.9 Soil corrosivity parametric criteria per AWWA (2010).

Soil parameter value or classification	Assigned points
Moisture condition	
Poor drainage (soil continuously wet)	2
Fair drainage (soil generally moist)	1
Good drainage (soil generally dry)	0
Redox potential [mV]	
< 0	5
0 – 50	4
50 – 100	3.5
> 100	0
pH	
0 – 2	5
2 – 4	3
4 – 6.5	0
6.5 – 7.5	0
7.5 – 8.5	0
> 8.5	3
Resistivity [Ω-cm]	
< 700	10
700 – 1,000	8
1,000 – 1,200	5
1,200 – 1,500	2
1,500 – 2,000	1
> 2,000	0
Sulfide content	
Positive	3.5
Trace	2
Negative	0

Table 4.10 Soil corrosivity classification per AWWA (2010).

Total assigned points per Table 4.9	Soil corrosivity classification
0 to 13	Non-corrosive
14 and above	Corrosive

Table 4.11 Soil corrosivity parametric criteria per DVGW (2011).

Soil parameter value or classification	Assigned points
Soil composition	
Calcareous, sandy marl, not stratified sand	+2
Loam, sandy loam (loam content $\leq 75\%$), sandy clay soil (silt content $\leq 75\%$)	0
Clay, mainly clay, humus	-2
Peat, thick loam, marshy soil	-4
Ground water level at buried position	
None	0
Present	-1
Variable	-2
Moisture content [%]	
$\leq 20\%$	0
$> 20\%$	-1
pH	
≥ 6	0
< 6	-2
Resistivity [Ω-cm]	
$> 10,000$	0
10,000 – 5,000	-1
5,000 – 2,300	-2
2,300 – 1,000	-3
$< 1,000$	-4
Carbonate concentration [%]	
≥ 5	+2
5 – 1	+1
< 1	0
Chloride concentration [mg/L]	
≤ 100	0
> 100	-1
Sulfate concentration [mg/L]	
< 200	0
200 – 500	-1
500 – 1,000	-2
$> 1,000$	-3
Sulfide concentration	
None	0
Traces	-2
Present	-4
Cinder and coke content	
None	0
Present	-4

Table 4.12 Soil corrosivity classification per DVGW (2011).

Total assigned points per Table 4.11	Soil is classified as:
≥ 0	Non-corrosive
-1 to -4	Slightly corrosive
-5 to -9	Corrosive
≤ -10	Very corrosive

The test method deployed to assess soil corrosivity as part of this project were tailored to allow the application of both the AWWA (2010) and the DVGW (2011) approach, as covered in Section 4.2.3 and Section 4.2.4.

4.2.3 Test Methods

Soils were initially evaluated by considering the predominant soil types of each testing region, namely silty clays at the sites in Saskatchewan (Site 1, Site 2 and Site 3) and sandy loams at Florida locations (Site 4 and Site 5). Moisture content and groundwater presence were evaluated based on visual inspections, likening soil with good or fair drainage (AWWA 2010) to a lack of ground water and moisture content $\leq 20\%$ (DVGW 2011), and soil with poor drainage to presence of ground water and moisture content $> 20\%$.

Redox potential measurements were obtained using a digital potential meter (M.C. Miller Co., Inc., Sebastian, FL) with copper/copper sulfate reference electrode (CCSRE), which is shown in Figure 4.16. The DPM can register potential ranges of 0-2 V and 0-20 V DC with $\pm 0.5\%$ accuracy and 20 M Ω input resistance on both ranges in accordance with ASTM G200 (ASTM 2014b). The use of a CCSRE is typically favored over other reference electrodes for potential measurements of systems buried in soils due to its relatively constant half-cell potential. The half-cell potential of a CCSRE is dependent only upon the electrochemical equilibrium of Cu and its ions, which is stable under most conditions.



Figure 4.16 Digital potential meter with CCSRE (M.C. Miller Co., Inc.).

The single-measurement probe testing meter shown in Figure 4.17 (model SRM-100, MSES Consultants, Inc., Clarksburg, WV) was utilized to measure soil pH and resistivity. This instrument can register an acidity range of 3-10 standard pH units with $\pm 0.5\%$ accuracy, and a resistivity range of 0-1.5M Ω -cm with $\pm 5\%$ accuracy in accordance with ASTM G51 (ASTM 2012a). This instrument can utilize either a bell-hole probe or a subsurface probe, and essentially acts as a two-pin resistivity-measuring device where both electrodes are mounted on a single rod, similar to the two-pin testing method defined in ASTM G187 (ASTM 2012d). While this method is less accurate than the four-pin Wenner method defined in ASTM G57 (ASTM 2012b), it has the benefit of producing resistivity readings more quickly, thus lending itself to field testing.

The swab test data from Section 4.1.7 (Table 4.6) were used to estimate soluble chloride and sulfate contaminant concentrations in soil, assuming similar deposition rates to those on WS pole walls. Carbonate and sulfide surface concentrations were also obtained for up to two poles per test site because associated testing strips for these contaminants

were included in the full swab-based chemical kits. The carbonate color-indicator strip, expressing the results in contaminant mass per liter of deionized water (DI), is shown in Figure 4.18.



Figure 4.17 Soil pH and resistivity meter (SRM-100, MSES Consultants, Inc.).

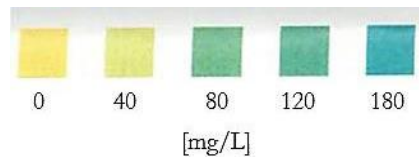


Figure 4.18 Color-coded criteria for carbonate indicator strip in swab test kit.

The strip for sulfide is not pictured because it simply turns from plain white to brown or black in the presence of sulfide. No field tests were performed to quantify cinder and coke depositions. However, since these contaminants are by-products of coal processes, their presence may affect soil corrosivity at Site 3.

4.2.4 Results and Discussion

The selected digital potential meter and soil pH and resistivity meter, which are pictured in a field test in Figure 4.19, are employed in practice by Osmose Utility Services, Inc. on a regular basis. The soil inspection tests were performed for each structure in up to 30 minutes.



Figure 4.19 Field testing of soil corrosivity.

Table 4.13 identifies the following soil corrosivity parameters for each WS pole, including soil type, moisture content, redox potential, pH, and resistivity. It is noted that resistivity was measured at three different locations around each pole, up to a distance of 3 m, to obtain representative averages together with information on parameter variability.

4.2.4.1 Soil Type and Moisture Content

The soils at Sites 1, 2, and 3 consisted of a majority of silt (0.002-0.05 mm particle size) and clay (<0.002 mm particle size) particles, while those encountered at Sites 4 and 5 were determined to be primarily medium-fine sands (0.10-0.50 mm particle size). All

soils were observed to be generally dry (i.e., demonstrating fair to good drainage) with the exception of the soil of Poles 11Z-2L and 11Z-2R, which was wet. These two poles were located adjacent to, but not within, a marshy terrain that retained a visible expanse of water above the ground, which was due in part to the rainfall occurring in the preceding days.

Table 4.13 Soil corrosion parameter measurements.

Pole	Soil type	Moisture condition (content [%])	Redox potential [mV]	pH	Soil resistivity [Ω -cm]			
					Test 1	Test 2	Test 3	Average
C1F-20	Clay	Dry (<20)	+153	8.0	2,900	2,500	2,500	2,633
Q3C-1L	Clay	Dry (<20)	+125	7.5	7,500	7,500	7,500	7,500
Q3C-1R	Clay	Dry (<20)		7.5				
Q3C-2L	Clay	Dry (<20)	+128	6.5	18,200	4,700	4,700	9,200
S3B-2L	Clay	Dry (<20)	+201	7.0	10,600	6,300	6,900	7,933
S3B-3L	Clay	Dry (<20)	+189	6.0	9,300	8,200	11,700	9,733
S3B-7L	Clay	Dry (<20)	+210	6.5	10,000	8,600	11,000	9,867
S3B-7R	Clay	Dry (<20)		6.5				
TL-1	Loam	Dry (<20)	+168	5.0	38,900	250,000	116,000	134,967
8Z-2L	Loam	Moist (<20)	+168	5.5	104,000	20,700	143,900	89,533
8Z-2R	Loam	Moist (<20)		5.5				
11Z-2L	Loam	Wet (\geq 20)	+168	5.5	7,900	10,500	7,600	8,667
11Z-2R	Loam	Wet (\geq 20)		5.5				
11Z-6L	Loam	Dry (<20)	+168	4.5	56,500	23,400	20,000	33,300
11Z-6R	Loam	Dry (<20)		4.5				

4.2.4.2 Redox Potential

Standard redox potential refers to a standard hydrogen electrode (SHE), which is arbitrarily given a potential of 0.000 V. Therefore, since redox potentials were measured originally against a CCSRE, they were converted by adding 0.318 V to the CCSRE potential to compare with a SHE. The measured redox potentials ranged from +125 mV vs. SHE for Site 2 to +210 mV vs. SHE for Site 3. While the DVGW (2011) approach does not specifically account for redox potential readings, AWWA C-105 (AWWA 2010) notes

that redox potentials above +100 mv vs. SHE generally indicate non-corrosive soils. Thus, no recorded redox potential value raises particular concerns with regard to soil corrosivity. Interestingly, all redox potential measurements at the Florida locations (Sites 4 and 5) yielded the same result of +168 mV vs. SHE, possibly indicating that these more porous sandy loams tend to possess similar aeration levels.

4.2.4.3 pH and Soil Resistivity

The soils at Sites 4 and 5 (Florida, USA) tended to be more acidic than those at Sites 1, 2 and 3 (Saskatchewan, Canada). The pH values at Sites 4 and 5 ranged from 4.5 to 5.5 whereas the lowest pH value measured in Canada was 6.0, and was recorded near Pole S3B-3L (Site 3). The other soils at Sites 2 and 3 had a pH between 6.5 and 7.5. The soil near Pole C1F-20 (Site 1) was found to be slightly alkaline, with a pH = 8.0, which suggests that it has low corrosivity. However, this soil was also characterized by the lowest soil resistivity (i.e., highest corrosivity) among all sites inspected, with an average value of (2,633 Ω -cm in Table 4.13). The highest soil resistivity measurement (250,000 Ω -cm) was made near Pole TL-1 (Site 4), consistent with the presence of well-drained non-cohesive (sandy) soil. However, it is noted that a low resistivity may not be, per se, sufficient proof of low corrosivity, which may be exacerbated by low pH values as well as presence of soluble contaminants such as chlorides for Pole TL-1. It is noted that all average resistivity values for soils in Sites 1, 2 and 3 (Saskatchewan) fall below 10,000 Ω -cm whereas the only soils in Sites 4 and 5 (Florida) to do so were the wet soils surrounding Poles 11Z-2L and 11Z-2R. The other soils in Sites 4 and 5 exhibited relatively high resistivity values that are consistent with a non-corrosive rating in every classification system considered in Section 4.2.2 (Roberge 2008, AWWA 2010, DVGW 2011).

4.2.4.4 Contaminant Concentration

The soil contaminant concentrations are summarized in Table 4.14. The concentrations of chlorides and sulfates on the soil surface surrounding each poles were reasonably assumed to be equal to the concentrations on the WS pole walls (Table 4.6), which were used to estimate deposition rates. The chloride concentration for Pole TL-1 (Site 4), which contributes to atmospheric corrosivity, also contributes to soil corrosivity. The impact of sulfate concentration can be broken down into similar categories as those observed in Table 4.7 for atmospheric corrosivity. For example, Poles Q3C-1L, Q3C-1R and Q3C-2L (Site 2) are more heavily influenced by sulfates, which highlights the potential implications of industrial atmospheres on soil corrosivity in the absence of a proper ground-level protection (e.g., coating). Instead, Poles S3B-2L and S3B-3L (Site 3) are the least influenced by sulfates. This is important information since Pole S3B-2L is particularly susceptible to ground-level damage due to insufficient height of the coating (Figure 3.14a).

Table 4.14 Concentrations of soluble soil contaminants from field tests.

Site	Pole	Chloride [mg/L]	Sulfate [mg/L]	Carbonate [mg/L]	Sulfide [mg/L]
1	C1F-20	0	300	80	0
2	Q3C-1L	0	533	60	0
	Q3C-1R	0	500	-	-
	Q3C-2L	0	467	-	-
	Q3C-2R	0	300	-	-
	S3B-2L	0	200	-	-
3	S3B-3L	0	200	20	0
	S3B-7L	0	300	20	0
	S3B-7R	0	300	-	-
	TL-1	500	300	40	0
5	8Z-2L	0	333	-	-
	8Z-2R	0	333	-	-
	11Z-2L	0	333	40	0
	11Z-2R	0	333	-	-
	11Z-6L	0	300	40	0
	11Z-6R	0	300	-	-

Swab tests yielded different carbonate concentrations for each test site. Sites 1, 2 and 3 exhibited concentrations of 80, 60 and 20 mg/L, respectively. Sites 4 and 5 exhibited concentrations of 40 mg/L. None of these values were high enough to register on the DVGW (2011) rating scale (Table 4.11). Negligible sulfide amounts were detected on all pole surfaces and surrounding soil, which is encouraging since sulfides are more corrosive than sulfates (Roberge 2008).

4.2.4.5 Classification per Roberge (2008), AWWA (2010) and DVGW (2011)

Based on the soil field test data presented above, the soil corrosivity was classified in conformance with the criteria set forth in Roberge (2008), AWWA (2010), and DVGW (2011) for all WS poles except Pole Q3C-2R at Site 2. The soil surrounding this pole was not tested using all test procedures described in Section 4.2.3. However, it is reasonable to expect similar results to those obtained for the companion Pole Q3C-2L. The classifications are summarized in Table 4.15 and Table 4.16. For AWWA (2010) and DVGW (2011), the cumulative value is followed, between parentheses, by the point values for each influencing factor in the same order of Table 4.9 and Table 4.11, respectively.

Significant discrepancy exists between different classification methods. For example, the soil around Pole C1F-20 (Site 1) is classified as: highly corrosive based on its resistivity (Roberge 2008); corrosive based on the DVGW (2011) criteria; and non-corrosive based on the AWWA (2010) criteria. It is also noted that all soils tested are classified as non-corrosive based on the AWWA (2010) criteria whereas the outcomes are more consistent based Roberge (2008) and DVGW (2011). However, the DVGW (2011) criteria have the merit to more comprehensively account for the influence of soluble contaminants by assigning specific points to as a function of carbonate, chloride, sulfate,

Table 4.15 Soil corrosivity classification of Sites 1, 2 and 3 (Saskatchewan, Canada) according to Roberge (2008), AWWA (2010) and DVGW (2011).

Site	Pole	Roberge (2008) classification	AWWA (2010) points	AWWA (2010) classification	DVGW (2011) points	DVGW (2011) classification
1	C1F-20	Highly corrosive	0 (0, 0, 0, 0, 0)	Non-corrosive	-5 (-2, 0, 0, 0, -2, 0, 0, -1, 0, 0)	Corrosive
2	Q3C-1L	Moderately corrosive	0 (0, 0, 0, 0, 0)	Non-corrosive	-5 (-2, 0, 0, 0, -1, 0, 0, -2, 0, 0)	Corrosive
	Q3C-1R	Moderately corrosive	0 (0, 0, 0, 0, 0)	Non-corrosive	-5 (-2, 0, 0, 0, -1, 0, 0, -2, 0, 0)	Corrosive
	Q3C-2L	Moderately corrosive	0 (0, 0, 0, 0, 0)	Non-corrosive	-4 (-2, 0, 0, 0, -1, 0, 0, -1, 0, 0)	Slightly corrosive
3	S3B-2L	Moderately corrosive	0 (0, 0, 0, 0, 0)	Non-corrosive	-3 (-2, 0, 0, 0, -1, 0, 0, 0, 0, 0)	Slightly corrosive
	S3B-3L	Moderately corrosive	0 (0, 0, 0, 0, 0)	Non-corrosive	-3 (-2, 0, 0, 0, -1, 0, 0, 0, 0, 0)	Slightly corrosive
	S3B-7L	Moderately corrosive	0 (0, 0, 0, 0, 0)	Non-corrosive	-4 (-2, 0, 0, 0, -1, 0, 0, -1, 0, 0)	Slightly corrosive
	S3B-7R	Moderately corrosive	0 (0, 0, 0, 0, 0)	Non-corrosive	-4 (-2, 0, 0, 0, -1, 0, 0, -1, 0, 0)	Slightly corrosive

Table 4.16 Soil corrosivity classification of Sites 4 and 5 (Florida, USA) according to Roberge (2008), AWWA (2010) and DVGW (2011).

Site	Pole	Roberge (2008) classification	AWWA (2010) points	AWWA (2010) classification	DVGW (2011) points	DVGW (2011) classification
4	TL-1	Non-corrosive	0 (0, 0, 0, 0, 0)	Non-corrosive	-4 (0, 0, 0, -2, 0, 0, -1, -1, 0, 0)	Slightly corrosive
5	8Z-2L	Non-corrosive	1 (1, 0, 0, 0, 0)	Non-corrosive	-3 (0, 0, 0, -2, 0, 0, 0, -1, 0, 0)	Slightly corrosive
	8Z-2R	Non-corrosive	1 (1, 0, 0, 0, 0)	Non-corrosive	-3 (0, 0, 0, -2, 0, 0, 0, -1, 0, 0)	Slightly corrosive
	11Z-2L	Moderately corrosive	2 (2, 0, 0, 0, 0)	Non-corrosive	-6 (0, -1, -1, -2, -1, 0, 0, -1, 0, 0)	Corrosive
	11Z-2R	Moderately corrosive	2 (2, 0, 0, 0, 0)	Non-corrosive	-6 (0, -1, -1, -2, -1, 0, 0, -1, 0, 0)	Corrosive
	11Z-6L	Non-corrosive	0 (0, 0, 0, 0, 0)	Non-corrosive	-3 (0, 0, 0, -2, 0, 0, 0, -1, 0, 0)	Slightly corrosive
	11Z-6R	Non-corrosive	0 (0, 0, 0, 0, 0)	Non-corrosive	-3 (0, 0, 0, -2, 0, 0, 0, -1, 0, 0)	Slightly corrosive

sulfide concentration, and presence of cinder and coke. This information suggest that greater consideration may be given to the DVGW (2011) criteria for the practical as well as accurate assessment of soil corrosivity especially when exposure to soluble contaminants, cinder, coke, and combinations thereof, is of concern.

The field tests performed provide numerous examples supporting the hypothesis that the DVGW (2011) criteria are more practical for a comprehensive assessment of soil corrosivity.

- At Site 2, Poles Q3C-1L, Q3C-1R and Q3C-2L exhibited significant corrosion damage and coating deterioration near the ground line (e.g., Figure 4.15a). In fact, these structures are surrounded by the soil with the highest corrosivity rating based on the DVGW (2011) criteria, whereas a “moderately corrosive” classification is determined based on resistivity only (Roberge 2008). Here, it appears that the DVGW (2011) classification enables one to more effectively capture the influence of sulfate depositions (Table 4.14).
- At Site 3, there is a reasonable possibility that Poles S3B-2L, S3B-7L and S3B-7R are directly exposed to coal from the local mines, although quantitative evidence of depositions is not available. Accounting for such exposure would lead to a significantly smaller number of cumulative points, between –7 and –8, per DVGW (2011). In fact, coals in western North America (e.g., Montana, Wyoming, Saskatchewan) are typically low in sulfur and high in alkalis, and related coal ash contains alumina, silica, and calcium oxide. The corrosivity of environments with such coal ash for various steel alloys, including advanced ferritic steel and high-Ni alloys, has been reported to be significantly higher

than that found in similar environments lacking ash (Zeng et al. 2014). These considerations can contribute to explain why visible corrosion damage was noted at the uncoated base of Pole S3B-2L (Figure 4.15b), further highlighting the importance of coating detailing.

- At Site 4, the soil surrounding Pole TL-1 is rated as non-corrosive based on its high resistivity (Roberge 2008). Instead, this soil ranks close to the most corrosive soils at Sites 2 and 5 due to its low pH and exposure to chlorides based on DVGW (2011). This latter classification is more reflective of the severe corrosion damage that was observed at the ground line (Figure 3.20a). Cathodic protection should be considered.

4.3 Concluding Remarks

Based on the state-of-the-art review of environmental (atmospheric and soil) corrosivity and results of field tests presented in this chapter, the following conclusions are drawn.

- Atmospheric corrosivity is a key measurable indicator of the susceptibility of WS transmission line structures to corrosion damage. The main contributing factors are moisture, which can be conveniently quantified as “time of wetness”, and presence of airborne contaminants, with an emphasis on sulfur dioxide (e.g., sulfates in industrial atmospheres) and chlorides (e.g., near saltwater or due to direct exposure to deicing salts). It appears that exposure to nearby heavily trafficked roads is, per se, not of concern as far as corrosion resistance of WS poles (as noted for Sites 1, 4 and 5).

- Soil corrosivity is an important indicator of susceptibility to corrosion damage for directly embedded WS surfaces when the protective coating does not sufficiently extend above ground, and when a deteriorating coating is present at and below the ground line (e.g., with non-adherent and disrupted areas). This issue is less relevant for well-coated WS surfaces. Soil corrosivity is largely influenced by moisture content and presence of ionic species such as sulfates and chlorides (which also depend on their concentration in the atmosphere).
- For the case studies presented in this report, classification of soil corrosivity using the AWWA (2010) criteria appears less effective than those based on soil resistivity (Roberge 2008) and the DVGW (2011) criteria. In particular, the DVGW (2011) criteria yields classifications that are more consistent with field observations especially in environments with soluble and airborne contaminants, irrespective of the resistivity level (e.g., case of Pole TL-1 exposed to a chloride-laden environment at Site 4).
- Both atmospheric and soil corrosivity should be considered when planning field inspections. In fact, exposure to a corrosive atmosphere may facilitate coating deterioration and delamination on directly embedded WS surfaces, and thus the occurrence of corrosion damage at and below the ground line.
- Both atmospheric and soil corrosivity are highly dependent on moisture contents, which heavily depend on the location and orientation of a given WS structure, and exposure to damp soils that act as low-resistivity electrolytes. Under these circumstances, exposure to a corrosive soil (e.g., a damp soil acting as a low-resistivity electrolyte) may further exacerbate corrosion damage, and

excavation may be considered to assess below-ground WS surfaces with respect to unintended direct exposure to stagnant moisture and water penetration.

- Detrimental exposure to excess moisture also depends on structural designs and detailing that facilitate moisture retention (e.g., geometric discontinuities, mechanical connections without seamless transitions) and, in worst-case scenarios, water ponding (e.g., unfilled caisson foundations, especially in conjunction with unsealed poles). These aspects must be considered at the design stage, especially for WS structures that are expected to operate in aggressive environments.
- Site 1 (and, in part, Site 3) offers evidence on the corrosion behavior of a WS transmission line pole operating in a rural environment. This environment tends to exhibit a low-corrosivity atmosphere. Yet, corrosion damage of WS pole surfaces can still occur due to moisture accumulation and stagnation resulting from seemingly inoffensive details that create geometric discontinuities, such as the reflective tape attached on Pole C1F-20.
- Site 2 and Site 3 offer evidence on the corrosion behavior of WS transmission line poles operating in an industrial environment. Site 2 is characterized by relatively high atmospheric and soil corrosivity, where it is reasonable to expect that the latter be influenced by the exposure to atmospheric contaminants. For example, elevated sulfate deposition levels on WS surfaces appear to be correlated with atmospheric corrosivity as well as soil corrosivity and corrosion damage. Instead, direct exposure to coal may be of concern at Site 3.

- Site 4 offers evidence of the ineffective corrosion resistance of a WS transmission line pole operating in a chloride-laden marine environment. In these instances, cathodic protection should be considered. However, galvanized steel appears to be a more sensible choice.
- With regard to atmospheric corrosivity characterization in field inspections, it is noted that it may be impractical to detect of chloride depositions on WS surfaces through swab tests, and Bresle patch tests (ISO 2006) may provide more reliable data. However, chlorides are difficult to detect as they rapidly react with the patina on WS surfaces, possibly resulting in relatively small chloride depositions. Therefore, an elemental analysis of the surface oxide composition based on laboratory tests seems a more rational strategy to understand whether the presence of chlorides in the atmospheres is such that the corrosion resistance of WS is impaired, as demonstrated in Chapter 6.0. This may reasonably be the case for Pole TL-1 at Site 4 as well as other structures located less close to saltwater.
- Site 5 offers evidence on the corrosion behavior of WS transmission line poles operating in a rural and humid environment, albeit at a relatively small distance from saltwater. Here, atmospheric moisture is the dominant factor affecting atmospheric corrosivity, irrespective of the exposure to airborne contaminants. One additional concern is the possibility of exposure to chlorides carried by winds from the nearby coastline, as remarked in Section 3.7.

CHAPTER 5.0 ASSESSMENT OF CORROSION RATE AND POTENTIAL

The quantification of the corrosion rates of the WS poles inspected provides the means to practically understand the combined impact of the environmental corrosivity parameters examined, together with other factors influencing corrosion behavior (e.g., design and detailing). In addition, the quantification of the corrosion potential provides owners and inspectors with robust evidence to understand present and future susceptibility to corrosion damage, for example as a result of the formation of unstable and non-adherent surface oxides. This information can be leveraged for diagnosis and prognosis purposes, thereby enabling owners to make informed decisions on allocating and prioritizing prevention and remediation resources. For the WS poles inspected, Section 5.1 demonstrates the quantification of corrosion rates based on thickness loss measurements performed in the field. Section 5.2 examines the corrosion potential of each WS pole to quantitatively assess present and future susceptibility to corrosion damage. Section 5.3 summarizes the main findings from these tasks.

5.1 Corrosion Rate

Thickness loss measurements have been utilized to estimate the rate of corrosion for WS poles surfaces. These measurements were taken at representative locations to evaluate maximum and average corrosion rates for all the WS poles inspected. Section 5.1.1 introduces a relevant standard classification, and Section 5.1.2 reviews testing equipment and procedures. Section 5.1.3 reports on the thickness loss data that were collected during the field inspections, and discusses the resulting corrosion rates for each WS pole.

5.1.1 Assessment Strategies

The ISO 9223 standard (ISO 2012b) that was utilized to assess the atmospheric corrosivity (Table 4.4) has a companion standard, ISO 9224 (ISO 2012c), which provides guiding values to associate atmospheric corrosivity categories (Table 4.7) to practical corrosion rate (CR) ranges for standard carbon steel. The correlation between atmospheric corrosivity category (C_1 through C_5) and corrosion rates is given in Table 5.1 (ISO 2012b).

Table 5.1 Atmospheric corrosivity and corrosion rates for carbon steel (ISO 2012b).

Atmospheric corrosivity	Corrosion rate (CR) based on thickness loss measurements [mils/year]
C_1	$CR \leq 0.05$
C_2	$0.05 < CR \leq 1.0$
C_3	$1.0 < CR \leq 2.0$
C_4	$2.0 < CR \leq 3.25$
C_5	$CR > 3.25$

The time required for WS to reach steady-state corrosion rates and form a protective patina varies depending on numerous variables including exposure time, atmospheric corrosivity, exposure to wet/dry cycles, and type and amount of corrosion by-products. As a result, it has been reported that protective oxide films can form on WS in six weeks to eight years (Diaz et al. 2012), although it may take a few months or years of patina build-up before quasi steady-state conditions are attained (Figure 2.6). Matsushima et al. (1974) reported on stabilization times of one to five years for corrosion by-products at various locations in structures in industrial and urban environments. However, unsurprisingly, no stabilization was attained at locations that experienced water stagnation. Morcillo et al. (2013) conducted a worldwide bibliographic survey of atmospheric corrosion data for WS, examining records from over 70 test sites throughout North America and Europe. In this

analysis, decreases of 10% or greater in one-year corrosion rates were associated with steady-state conditions. Based on a classification of atmospheric corrosivity categories in conformance with ISO 9223 (ISO 2012b), it was noted that the patina stabilization time decreased for more corrosive atmospheres. Average stabilization times ranged from six to eight years in relatively mild atmospheres (i.e., resulting in C_2 and low C_3 corrosivity categories) to four to six years in more aggressive atmospheres (high C_3 , C_4 and C_5 corrosivity categories). It is noted that a shorter stabilization time does not necessarily entail a more protective patina. For example, while stabilization occurs more rapidly in marine environments, the resulting oxide films are not as effective as those formed in non-marine atmospheres (rural, urban, or industrial) where stabilization times are typically longer. Average steady-state corrosion rates for both marine and non-marine atmospheres increased as the atmospheric corrosivity increased (Morcillo et al. 2013).

In order to ensure the effectiveness of a WS structure, steady-state corrosion rates must be limited to a sufficiently low threshold for which essentially no maintenance is required. Larrabee and Coburn (1961) recommended a CR limit of 5 $\mu\text{m}/\text{year}$ (0.20 mils/year). Based on data reviewed by Albrecht and Hall (2003), Cook (2007) noted that WS may be suitable for exposures to medium corrosivity environments resulting in thickness losses up to 120 μm (4.72 mils) during the first 20 years of exposure, i.e., for an average maximum CR of 6 $\mu\text{m}/\text{year}$ (0.24 mils/year). From a practical standpoint, it is noted that for a steady-state long-term corrosion rate of more than 5-6 $\mu\text{m}/\text{year}$ there is a theoretically negligible advantage in using WS instead of plain carbon steel in aggressive atmospheres. Average steady-state corrosion rates for non-marine environments exceeded this limit for first-year corrosivity categories of C_3 or greater. Instead, the corrosion rates

for marine environments exceeded 5-6 $\mu\text{m}/\text{year}$ irrespective of the first-year corrosivity category (Morcillo et al. 2013), highlighting the vulnerability of WS to chloride-laden atmospheres.

Empirical data from atmospheric corrosion tests on steel coupons can serve to define a power model relating thickness loss with time, as specified in ASTM G101 (ASTM 2015c), in the form:

$$C = At^n \quad (5-1)$$

which can also be rendered as a “bi-logarithmic power model” in the form $\log C = \log A + n \log t$, where C is the corrosion-induced thickness loss at time t , and A and n are empirical coefficients. Representative examples for weathering steel alloys are provided in Figure 4.2, Figure 4.5 and Figure 4.6. The corrosion damage model in Equation 5-1 is often enlisted to estimate atmospheric corrosion resistance for extended exposure times. Pourbaix (1980) noted that this model may be applicable to diverse metals and atmospheres, and contended that results from four-year tests could be used to estimate 20-30 year corrosion damage. When A and n are known for a given steel and exposure condition, estimating future corrosion damage for exposed WS wall surfaces becomes feasible. However, it is noted that the definition of these variables requires that thickness loss measurements be taken on WS samples over an extended period of time whereas short-term field tests are unsuitable to define A and n for use in power models for prognosis purposes. More research, largely based on simple field measurements, is needed to define these parameters for WS as a function of operating environment and pole age.

5.1.2 Test Methods

Ultrasonic thickness (UT) gages offer a practical means to accurately and non-destructively measure the thickness of steel pole walls, as demonstrated for corroding GS poles by Matta et al. (2014). Thickness losses were measured at representative locations on the WS pole surfaces, which were previously cleared of loose particles. The measurements were taken using a UT gage (model 45MG, Olympus Corp., USA) that is compliant with ISO 16831 (ISO 2012a), as illustrated in Figure 5.1. The instrument can measure thicknesses between 0.040 and 1.500 in. (1 and 37 mm) with an accuracy of $\pm 0.1\%$ over a temperature range of 14 to 122°F (−10 to 50°C).

Thickness measurements were recorded around the perimeter of each pole at Sites 1 through 4 within a distance of 6 in. (152 mm) above the coating termination. The thickness of the ground sleeves on Pole TL-1 was also measured. For the WS poles of Line 11Z at Site 5, thickness measurements were taken within a distance of 6 in. (152 mm) above and below the termination of the WS repair sleeves. For the poles of Line 8Z at Site 5, wall thickness measurements were taken within 6 in. (152 mm) above the WS base plates. It is noted that these areas either experienced the most visible corrosion damage (e.g., pack rust at the coating lip as in Figure 3.10 and Figure 4.15b) or are representative of such damage (e.g., more uniform deterioration due to exposure to aggressive atmospheres as in Figure 3.30), with the exception of the deep pits on the coated base of Pole TL-1 at Site 4. For round poles, measurements were taken at 90° increments, for a total of four measurements per pole. For paneled poles, measurements were taken at each flat, for a total of 12 measurements per pole. It is noted that for 12 benchmark measurements (t_0) were also taken at seemingly undamaged areas where remarkably

negligible differences were noted (i.e., within the accuracy of the UT gage) in each WS pole.

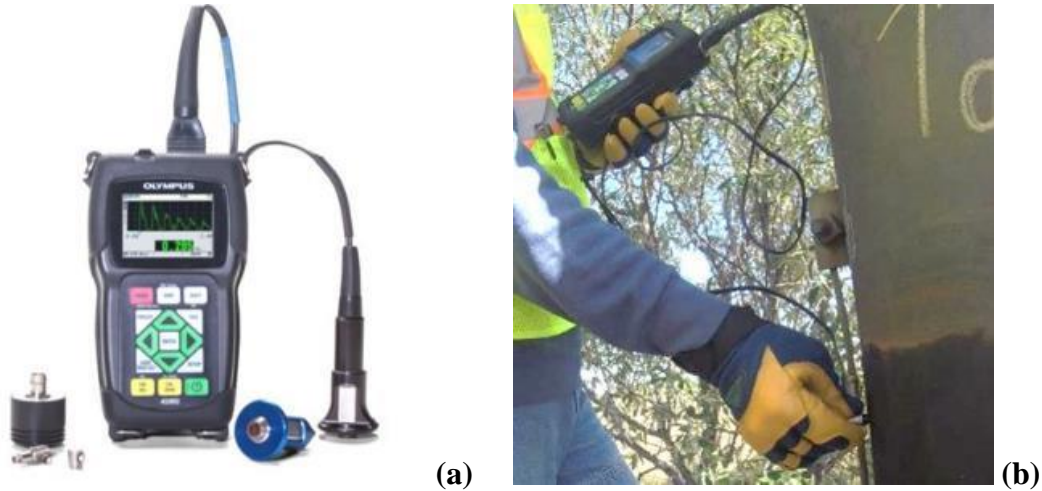


Figure 5.1 Ultrasonic thickness gage measurements: (a) instrument used (model 45MG, Olympus Corp.); and (b) measurement being performed on Pole S3B-3L.

The maximum pit depths at the base of Pole TL-1 (Figure 3.20a-b) were measured using a pipe pit gage (W.R. Thorpe & Co., Bixby, OK), as illustrated in Figure 5.2. The gage can be used to measure thicknesses up to 0.625 in. (15.9 mm) with an accuracy of ± 0.005 in. (0.127 mm).

The thickness of the protective coating (t_c) was measured using a dry-film thickness (DFT) pen gage (model PenTest, ElektroPhysik, Cologne, Germany), as illustrated in Figure 5.3. The DFT pen gage is designed for quick-check measurements on steel panels in compliance with ISO 2178 (ISO 2016). The gauge works by placing the tip onto the coated steel surface, applying firm contact with the thumb, and carefully pulling up the black slide until the magnet lifts off from the coating surface. Coating thicknesses can be measured within a range of 1 to 30 mils (25 to 700 μm) with an accuracy of $\pm 10\%$ over a temperature range of 14 to 176°F (-10 to 80°C).



(a) (b)

Figure 5.2 Deep pit measurement: (a) pit gage (W.R. Thorpe & Co.); and (b) measurement being performed on Pole TL-1.



(a) (b)

Figure 5.3 Coating thickness measurement: (a) thickness gage (model PenTest, ElektroPhysik); and (b) measurement being performed on Pole S3B-7R.

5.1.3 Results and Discussion

Table 5.2 through Table 5.4 summarize the thickness measurement data as well as the associated corrosion rates and corrosivity category per ISO 9223 (ISO 2012b). The maximum and average thickness losses were estimated for each pole to provide quantitative information on the extent and severity of the damage (e.g., predominance of

either pitting or more uniform thickness loss. For the most damaged area or flat in each pole, the maximum thickness loss, Δt_{\max} , was calculated as:

$$\Delta t_{\max} = t_0 - t_{\min} \quad (5-2)$$

where t_0 is the original non-corroded thickness, and t_{\min} is the minimum thickness measured. For a given pole, average thickness loss, Δt_{avg} , was calculated as:

$$\Delta t_{\text{avg}} = \frac{\sum_{i=1}^{i=n} (t_0 - t_i)}{n} \quad (5-3)$$

where t_i represents an individual thickness measurement, and n is the total number of measurements taken around a pole circumference. The maximum and average corrosion rates were determined by dividing the maximum and average thickness losses by the age (in years) of each pole, respectively:

$$\text{CR}_{\max} = \frac{\Delta t_{\max}}{\text{Age}} \quad (5-4)$$

and

$$\text{CR}_{\text{avg}} = \frac{\Delta t_{\text{avg}}}{\text{Age}} \quad (5-5)$$

The results summarized in Table 5.2 through Table 5.4 are discussed in the following subsections.

Table 5.2 Thickness measurements on circular WS poles at Sites 1, 2 and 3 (Saskatchewan, Canada).

Site		1	2		3		
Pole		C1F-20	Q3C-1L	Q3C-2L	S3B-2L	S3B-3L	S3B-7L
Age [years]		18	14	14	28	28	28
Area of Measurement		Pole Wall	Pole Wall	Pole Wall	Pole Wall	Pole Wall	Pole Wall
t_c [in] ($\pm 10\%$)		0.030	0.032	0.030	0.030	0.020	0.028
t_o [in] ($\pm 0.1\%$)		0.323	0.318	0.385	0.188	0.185	0.368
t_i [in]	1	0.320	0.385	0.168	0.190	0.370	0.325
	2	0.318	0.380	0.190	0.184	0.366	0.321
	3	0.317	0.385	0.189	0.185	0.368	0.323
	4	0.318	0.388	0.192	0.182	0.369	0.323
Δt_{max} [mils]		2.00	1.00	5.00	20.0	3.00	2.00
Δt_{avg} [mils]		0.00 ± 1.63	0.00 ± 1.26	0.50 ± 3.32	3.25 ± 11.2	0.00 ± 3.40	0.00 ± 1.71
CR_{max} [mils/year]		0.11	0.07	0.36	0.71	0.11	0.07
CR_{avg} [mils/year]		0.00 ± 0.09	0.00 ± 0.09	0.04 ± 0.24	0.12 ± 0.40	0.00 ± 0.12	0.00 ± 0.06
Corrosivity based on CR		C_1 to C_2	C_1 to C_2	C_1 to C_2	C_2	C_1 to C_2	C_1 to C_2
Atmospheric corrosivity (Table 4.7)		C_3 to C_4	C_4	C_4	C_2 to C_3	C_2 to C_3	C_3 to C_4

Table 5.3 Thickness measurements on paneled WS poles at Sites 4 and 5 (Florida, USA).

Site		4			5							
Pole		TL-1			11Z-2L		11Z-2R		11Z-6L		11Z-6R	
Age [years]		23			26		26		26		26	
Area of Measurement		Pole Wall	Ground Sleeve	Sleeve Pits	Pole Wall	Repair Sleeve	Pole Wall	Repair Sleeve	Pole Wall	Repair Sleeve	Pole Wall	Repair Sleeve
t_c [in] ($\pm 10\%$)		0.028	-	-	-	-	-	-	-	-	-	-
t_0 [in] ($\pm 0.1\%$)		0.251	-	-	0.284	-	0.268	-	0.281	-	0.264	-
t_i [in]	1	0.246	0.216	-0.200	0.271	0.368	0.235	0.367	0.264	0.367	0.261	0.390
	2	0.251	0.215	-	0.256	0.373	0.257	0.375	0.281	0.358	0.258	0.362
	3	0.244	0.211	-0.180	0.251	0.360	0.243	0.378	0.281	0.360	0.262	0.362
	4	0.241	0.218	-	0.262	0.363	0.254	0.381	0.269	0.360	0.261	0.361
	5	0.241	0.221	-	0.260	0.370	0.258	0.361	0.270	0.359	0.271	0.363
	6	0.240	0.210	-0.110	0.259	0.366	0.241	0.366	0.261	0.359	0.252	0.371
	7	0.246	0.220	-	0.284	0.358	0.275	0.369	0.268	0.359	0.257	0.375
	8	0.241	0.210	-	0.282	0.359	0.273	0.367	0.250	0.358	0.262	0.362
	9	0.251	0.210	-	0.282	0.374	0.279	0.365	0.249	0.359	0.264	0.362
	10	0.244	0.211	-	0.311	0.374	0.272	0.368	0.266	0.363	0.263	0.366
	11	0.243	0.212	-	0.288	0.360	0.273	0.364	0.266	0.365	0.264	0.365
	12	0.248	0.216	-0.170	0.292	0.358	0.272	0.364	0.266	0.361	0.268	0.366
Δt_{\max} [mils]		11.00			33.0		33.0		32.0		12.00	
Δt_{avg} [mils]		6.33 \pm 3.82			9.17 \pm 17.93		7.00 \pm 15.15		15.08 \pm 9.78		2.08 \pm 4.94	
CR_{\max} [mils/year]		0.48			1.27		1.27		1.23		0.46	
CR_{avg} [mils/year]		0.28 \pm 0.17			0.35 \pm 0.69		0.27 \pm 0.58		0.58 \pm 0.38		0.08 \pm 0.19	
Corrosivity based on CR		C_2			C_2 to C_3		C_2 to C_3		C_2 to C_3		C_2	
Atmospheric corrosivity (Table 4.7)		C_4			C_4		C_4		C_4		C_4	

Table 5.4 Thickness measurements on circular poles at Sites 4 and 5 (Florida, USA).

Site		5	
Pole		8Z-2L	8Z-2R
Age [years]		26	26
Area of Measurement		Pole Wall	Pole Wall
t_c [in] ($\pm 10\%$)		-	-
t_0 [in] ($\pm 0.1\%$)		0.294	0.330
t_i [in]	1	0.294	0.330
	2	0.301	0.310
	3	0.284	0.321
	4	0.240	0.318
Δt_{max} [mils]		54.0	20.0
Δt_{avg} [mils]		14.25 \pm 27.4	10.25 \pm 8.26
CR _{max} [mils/year]		2.08	0.77
CR _{avg} [mils/year]		0.55 \pm 1.05	0.39 \pm 0.32
Corrosivity based on CR		C ₂ to C ₄	C ₂
Atmospheric corrosivity (Table 4.7)		C ₄	C ₄

5.1.3.1 Corrosion Rate and Corrosivity Category

In Table 5.2 through Table 5.4, for each WS pole, CR_{max} and CR_{avg} values are presented together with the associated corrosivity category per ISO 9223 (2012b), and the corrosivity category as it would be expected for standard carbon steel exposed to the local atmosphere (from Table 4.7). It is noted that the corrosivity categories based on actual CR_{max} values are typically, and often largely, better than those based on the atmospheric corrosivity assessment presented in Section 4.1 (Table 4.7). This evidence indicates that WS should largely outperform uncoated carbon steel in the representative environments of Sites 1 through 5. The only exception is Pole 8Z-2L at Site 5 (corrosivity category C₄), which highlights the extent to which a damp environment can negatively influence the corrosion resistance of WS surfaces. Based on the maximum thickness loss data and the associated corrosion rates, CR_{max}:

- Four WS poles (C1F-20 at Site 1, Q3C-1L at Site 2, and S3B-3L and S3B-7L at Site 3) exhibit $CR_{\max} < 0.20$ mils/year ($5 \mu\text{m}/\text{year}$), thus lying within a low corrosivity category C_2 . For these poles, it is noted that Δt_{\max} may also be justified due to pole wall manufacturing tolerances rather than actual corrosion damage.
- Five poles (Q3C-2L at Site 2, S3B-2L at Site 3, TL-1 at Site 4, and 8Z-2R and 11Z-6R at Site 5) exhibit CR_{\max} in the range 0.20-1 mils/year ($5\text{-}25 \mu\text{m}/\text{year}$), thus lying within a medium to high corrosivity category C_2 especially for poles exposed to relatively corrosive environments. However, it is noted that these results cannot account for the severe damage suffered by Pole TL-1 in areas where chloride depositions were more likely to accumulate (i.e., between the pole wall and the junction box in Figure 3.21a-c).
- Four poles (11Z-2L, 11Z-2R, 11Z-6L and 8Z-2L at Site 5) exhibit $CR_{\max} > 1$ mils/year ($25 \mu\text{m}/\text{year}$), up to a maximum of 2.08 mils/year for Pole 8Z-2L, thus lying within corrosivity category C_3 to C_4 . These results clearly indicate that the WS poles at Site 5 are more prone to localized thickness loss than poles at any other sites.

The evidence from Site 4 (Pole TL-1) and Site 5 reinforces the conclusion that while an aggressive environment is not desirable for overhead WS transmission line structures, susceptibility to corrosion can be critically exacerbated by questionable design and detailing practices. Relevant examples are the aforementioned junction box location for Pole TL-1 (Figure 3.21a-c) and, for the poles at Site 5, the direct coupling of WS and

galvanized steel through mechanical fastening (Figure 3.32), using hollow caisson foundations that facilitate water ponding (Figure 3.33), and leaving the WS poles unsealed at the base (Figure 3.34).

Based on the average thickness loss data summarized in Table 5.2 through Table 5.4, and the associated corrosion rates, CR_{avg} , and corrosivity categories per ISO 9223 (2012b):

- Five poles (C1F-20 at Site 1, Q3C-1 and Q3C-2L at Site 2, and S3B-3L and S3B-7L at Site 3) exhibit negligible values of CR_{avg} , corresponding to corrosivity category C_1 .
- Eight poles (S3B-2L at Site 3, TL-1 at Site 4, and all the poles at Site 5) exhibit CR_{avg} in the range 0.1-0.6 mils/year (2.5-15 $\mu\text{m}/\text{year}$), thus lying within a low to medium corrosivity category C_2 .

Therefore, none of the WS poles inspected experienced a uniform corrosion damage of concern. In other words, based on the results of average and maximum thickness loss measurements, it appears that for the representative pole ages and environments covered in Sites 1 through 5, any relevant corrosion damage accrues from localized corrosion mechanisms. A relevant example is Pole TL-1 at Site 4 at areas where chloride deposition is facilitated (Figure 3.21a-c), which may also explain the occasional areas with deteriorated sleeve coating (Figure 3.20a-b) and pit depths up to 0.2 in. (5 mm) (Table 5.3). Another compelling example is offered by the WS poles at Site 5 where a questionable foundation design and pole detailing were implemented (Figure 3.32, Figure 3.33 and Figure 3.34), and where the likely exposure of unsealed poles to a consistently humid

environment due to water stagnation in the open caisson foundations (Figure 3.33) hindered the formation of a stable and adherent patina (Figure 3.30). This conclusion is also significant because it highlights:

- The criticality of using actual overhead transmission line structures to generate empirical evidence for corrosion studies. Instead, WS coupons (e.g., Larrabee and Coburn 1961, Oh et al. 1999, Kamimura et al. 2006, Li et al. 2008, Cano et al. 2014) become a viable choice to study the corrosion response over time for flat and undisturbed surfaces on a more fundamental level, with the understanding that these specimens are unlikely to be representative of practical worst-case scenarios. This important point was also made by Albrecht and Hall (2003) in regard to weathering steel bridge structures. While WS poles were investigated as part of this project, the same consideration certainly applies to transmission towers. In fact, WS tower structures include numerous details (e.g., mechanically-fastened joints, geometric discontinuities) that facilitate water stagnation, and thus the occurrence of pack-rust and pack-out corrosion damage.
- The practical motivation for the fact that corrosion prevention and remediation strategies for WS transmission line poles, as presented in Chapter 7.0, are better suited for areas of localized corrosion damage as opposed to more uniform damage.

5.1.3.2 Comparison between Average and Maximum Corrosion Rates on Pole Walls

For all WS poles inspected, a graphical comparison of CR_{avg} and CR_{max} is presented in Figure 5.4 where the error bars indicate the positive standard deviation resulting from all thickness measurements that were taken for a given pole.

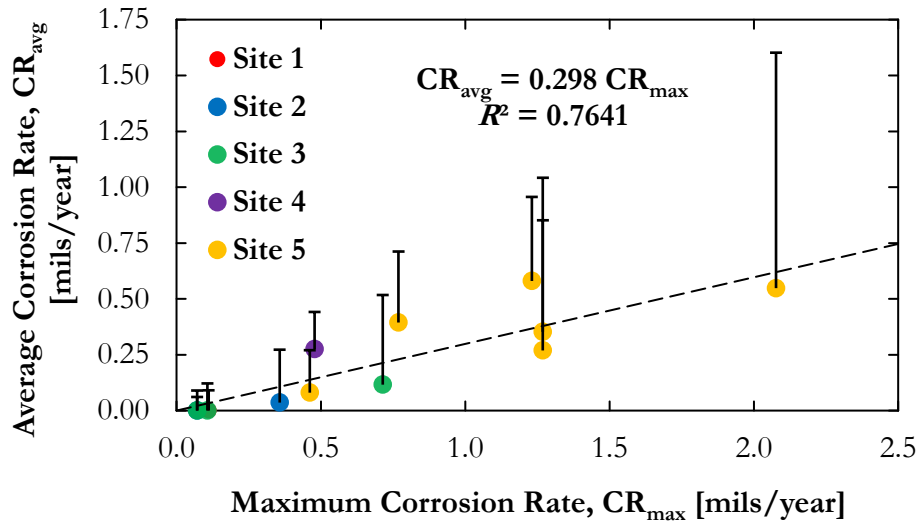


Figure 5.4 Comparison of average and maximum corrosion rate for all WS poles.

Utilizing Figure 5.4 shows that a consistent ($R^2 = 0.7641$) linear correlation exists between CR_{avg} and CR_{max} in the form:

$$CR_{avg} = 0.298 CR_{max} \quad (5-6)$$

For the range of WS pole age, environments and corrosion rate covered in Sites 1 through 5, Equation 5-6 suggests that the average corrosion rate consistently amounts to about 30% of the maximum corrosion rate for corrosion damage that is primarily controlled by atmospheric influences (e.g., humidity), regardless of corrosion rate magnitude.

Therefore, while corrosion rates can vary widely for a given pole (as highlighted by the standard deviation bars), most of the pole surface may tend to corrode at lower rates than at the most damaged surface areas. However, the fact that the trend is essentially confirmed up to about $CR_{avg} \sim 0.5$ mils/year ($13 \mu\text{m}/\text{year}$) and $CR_{max} \sim 2$ mils/year ($51 \mu\text{m}/\text{year}$) for Pole 8Z-2L at Site 5 suggests that no further acceleration of localized corrosion mechanisms (e.g., transition to severe pitting or pack-rust damage) takes place on pole wall areas that are located away from corrosion-prone areas and details (e.g., Figure 3.21a-c and Figure 3.32).

5.1.3.3 Influence of Environment and Pole Age on Corrosion Rates

Equation all WS poles inspected at Sites 1 through 5, Figure 5.5 and Figure 5.6 illustrate the maximum and average corrosion rates as functions of the pole age. The objective is to present a visual comparison of corrosion rates to further understand the influence of environmental exposure and pole age. It is noted that such corrosion damage is associated with thickness measurements that were aimed at assessing the corrosion resistance of the pole wall surfaces (see Section 5.1.2) instead of critical details (e.g., Figure 3.21a-c).

For Site 1, Pole C1F-20 exhibits $CR_{max} = 0.11$ mils/year and $CR_{avg} = 0$ mils/year. These minimal to negligible corrosion rates are consistent with the assessment outcomes based on visual inspection (Table 3.2) and atmospheric corrosivity analysis (Table 4.7), and reflect an expected corrosion behavior for WS structures operating in an essentially rural environment. However, the fact that negligible corrosion damage is expected in this environment reinforces the emphasis that should be placed on an attentive study of details that may facilitate localized water stagnation. In fact, this issue is highlighted by the

significant pack-rust damage that was imparted by a seemingly inoffensive reflective tape (Figure 3.5).

For Site 2, Pole Q3C-1L exhibits relatively low maximum corrosion rate ($CR_{\max} = 0.07$ mils/year) and a negligible average corrosion rate ($CR_{\text{avg}} = 0$ mils/year), which are associated with the presence of a rough but adherent pack-rust layer (Figure 3.9). Instead, Pole Q3C-2L exhibits a maximum corrosion rate greater than 0.20 mils/year ($CR_{\max} = 0.36$ mils/year) and a low average value ($CR_{\text{avg}} = 0.04$ mils/year), which are consistent with notable with pack-out corrosion damage (Figure 3.10a). The companion Pole Q3C-2R, on which thickness loss measurements were not taken, was in a similar state to that of Pole Q3C-2L, as documented in Figure 3.10b. This evidence reflects the exposure of the WS poles to an industrial environment with a C_4 corrosivity category (Table 4.7), where higher corrosion rates are expected compared to Site 1 despite of the younger age of the poles. Relatively high sulfate depositions were measured at this site (Table 4.6). In addition, exposure to chlorides is also a reasonable possibility due to the presence of a potash mine, as verified through the laboratory investigation of pack-out rust samples presented in Chapter 6.0. The ISO 9223 (ISO 2012b) corrosivity category associated with the maximum corrosion rate estimates is C_2 (Table 5.2), which does not raise concerns. However, given the relatively young age of these WS poles and the particularly aggressive environment at Site 2, it is recommended that routine assessments be prioritized.

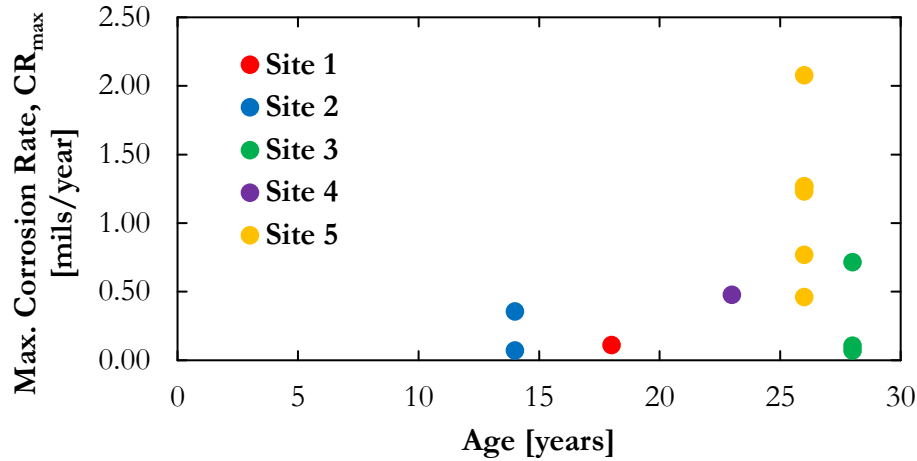


Figure 5.5 Maximum corrosion rates as a function of age for all WS poles.

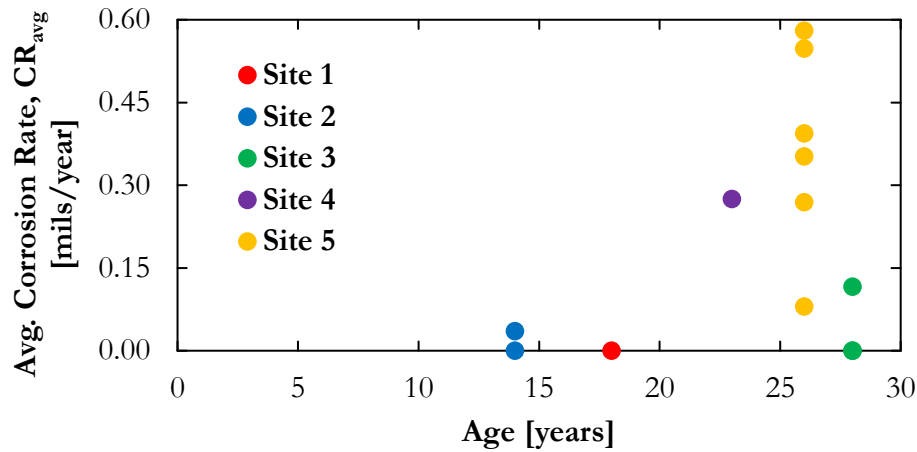


Figure 5.6 Average corrosion rates as a function of age for all WS poles.

For Site 3, Poles S3B-3L and S3B-7L exhibit relatively low maximum corrosion rates ($CR_{max} = 0.11$ and 0.07 mils/year, respectively) and negligible average corrosion rates ($CR_{avg} = 0$ mils/year), which reflects the exposure to a rural environment with corrosivity category C_2 to C_3 (Table 4.7). Instead, Pole S3B-2L is corroding at a relatively low average rate ($CR_{avg} = 0.12$ mils/year) but exhibits a significant maximum corrosion rate ($CR_{max} = 0.71$ mils/year) on the WS wall facing the nearby power station (Figure 3.14a and Figure 3.15a). This CR_{max} value is higher than that of Pole TL-1, which was located near saltwater

at Site 4. Since corrosion damage was sustained primarily on the pole wall facing the nearby power station, while atmospheric corrosivity does not appear of concern (Table 4.6 and Table 4.7), it is reasonable to hypothesize that such damage can be attributed to other instruments of corrosion associated with the proximity to the power station, such as stray currents. This hypothesis was further verified because of the difficulties encountered while measuring the corrosion potential for Pole S3B-2L, as discussed in Section 5.2. This finding highlights the importance of understanding the implications of the proximity of industrial sites (e.g., power station) to prioritize the routine inspection of specific WS poles as well as the corrosion protection systems in place (e.g., Figure 3.14a).

For Site 4, the maximum corrosion rate of Pole TL-1 ($CR_{max} = 0.48$ mils/year) is double the value of 24 mils/year suggested by Cook (2007). This threshold is also exceeded by the average corrosion rate based on the thickness measurements reported in Table 5.3 ($CR_{avg} = 0.28$ mils/year). It is noted that Pole TL-1 exhibits the greatest CR_{avg} / CR_{max} ratio of all the WS poles inspected. This evidence indicates that a chloride-laden and humid environment (TOW category T_4 from Table 4.5) is especially penalizing for the corrosion resistance of WS pole wall surfaces. In fact, the average corrosion rate of the 23-year-old Pole TL-1 is also comparable to that of some of the poles at Site 5, which are older (26 years). It is also emphasized that the estimated CR_{max} for Pole TL-1 does not account for the large and deep pits within the WS ground sleeve (Figure 3.20a-b), which exhibited depths up to 0.2 in. (5.1 mm) as reported in Table 5.3, nor the major through-thickness losses behind the junction box (Figure 3.21b). Therefore, this evidence indicates that areas where moisture and chlorides are likely to accumulate may experience extreme corrosion rates. In addition, this evidence raises concerns on the effectiveness of the hand-sprayed

coal tar epoxy coating used on the ground sleeves of Pole TL-1, although more evidence is needed to test this hypothesis and, if so, understand the influence of the material itself and the possibly non-uniform coating thickness resulting from the hand-spraying process.

For Site 5, the WS poles exhibit both the greatest average and maximum corrosion rates of all the WS poles inspected, up to 0.58 mils/year and 2.08 mils/year, respectively. These CR values far exceed those for the poles at Site 3, which are two years older, and often exceed those for Pole TL-1 at Site 4, which is three years younger and is exposed to a chloride-laden atmosphere. Rather than to the humid atmosphere itself (Table 4.5 and Table 4.7), this outcome is attributed primarily to some questionable design choices such as using unsealed WS pole structures and hollow (and water-filled) caisson foundations (Figure 3.33 and Figure 3.34). It is reasonable to conclude that the exposure of both the pole exterior and interior to a consistently moist environment effectively caused the steel substrate to be attacked from both sides, calling for the remediation measures that were recently deployed (Figure 3.35).

5.1.3.4 Coating Thickness

Coating thickness measurements, t_c , are summarized in Table 5.2 and Table 5.3 for the WS poles at Sites 1 through 5. It is noted that coatings on directly embedded WS poles were consistently measured at thicknesses at or near 30 mils, with the exception of Pole S3B-3L for which a 20-mil coating was measured. However, Pole S3B-3L was one of two directly embedded poles (the other being Pole C1F-20) for which little to no coating deterioration nor corrosion damage around the coating region were observed, and a negligible average corrosion rate was estimated. Therefore, it appears that a relatively thinner coating film is not of concern for this 28-year old pole that is exposed to a low- to

medium-corrosivity atmosphere (Table 4.7), and a slightly corrosive soil (Table 4.15). Greater attention should be given to the coatings of all poles at Site 2, Pole S3B-2L at Site 3 (Figure 4.15b), and Pole TL-1 at Site 4 (Figure 3.20a-b), due to the corrosivity of the local soil as discussed in Section 4.2.4.5 (e.g., due to the presence of sulfates at Site 2, and a low pH at Site 4).

5.2 Corrosion Potential

Corrosion potential is a key parameter for corrosion assessment since it can be used to evaluate present and future susceptibility to corrosion damage. Section 5.2.1 discusses how corrosion potential measurements can be used for assessment, and Section 5.2.2 presents related test methods. Then, Section 5.2.3 reports on the measurement results for all the WS poles inspected.

5.2.1 Assessment Strategies

Corrosion potential is measured as the potential difference between a metallic surface (i.e., WS pole walls) and a reference electrode. Both the metallic surface and reference electrode must be in contact with a known electrolyte. In the case of transmission line poles, soil can be used as the electrolyte. Different reference electrodes can be used to measure corrosion potential, including standard hydrogen electrodes (SHE), silver/silver chloride half-cells, and calomel electrodes. Copper/copper sulfate reference electrodes (CCSRE) are typically used for measurements on steel structures that are in contact with soils (Roberge 2008).

Corrosion potentials are reported indicating voltage magnitude and sign. Greater values of corrosion potential (i.e., more positive or less negative) are associated with greater susceptibility to corrosion damage. NACE SP0169 (formerly RP0169) (NACE

2013) stipulates that a corrosion potential reading of -0.85 V vs. CCSRE or less indicates full cathodic protection of steel structures in soil. Therefore, in the field measurements reported herein, a threshold of -0.85 V vs. CCSRE was considered as indicative of whether or not a given WS pole was adequately protected from corrosion currents. A background discussion of cathodic protection is provided in Section 7.2.3.

The author is cognizant that a cathodic polarization (i.e., corrosion potential shift) of 100 mV as a result of applying cathodic protection may indicate satisfactory protection of steel structures (NACE 2013). In addition, a polarized potential (i.e., sum of corrosion potential and cathodic polarization) of -0.85 V vs. CCSRE or less may also indicate satisfactory protection (NACE 2013). Assessment using these criteria may prevent unnecessary cathodic protection expansion or remediation (Barlo 2001). However, polarization is measured by disrupting the current flow from any applied cathodic protection, which makes this time-consuming operation impractical for short-term field inspections (Holtsbaum 2003) such as those presented in this report.

Potential-pH (Pourbaix) diagrams can be used to effectively represent the effects of exposure environments on metals, indicating three possible states for a metal, namely: immune, passive, or corroding. A metal is considered to be:

- Immune from corrosion attack when the potential of the metal in contact with a given electrolyte is smaller than the equilibrium potential associated with oxidation. By forcing a cathodic shift, cathodic protection brings the potential of a metal closer to immunity.
- Passive when the metal substrate is coated with an oxide or hydroxide film whose protectiveness depends on the exposure environment. In WS poles, a

dense, stable and adherent patina prevents a direct contact between unprotected steel and the atmosphere.

- Corroding when the metal takes the form of ionic (soluble) products and becomes susceptible to corrosion attack. The type and extent of corrosion attack must be determined by other means as demonstrated in Sections 3.0, 5.1 and 6.0.

The information gained from Pourbaix diagrams can be used to predict whether or not corrosion is likely to occur on WS structures, estimate the type of oxides that are likely to form (and thus the quality of the protective patina), and compare the results from different sites to understand the influence of specific service environments on corrosion resistance.

5.2.2 Test Method

The corrosion potential of steel transmission line poles, also referred to as “structure-to-soil potential” (SSP), is the potential measured between a structure and a reference electrode. The soil itself possesses no standard value against which to compare voltage readings and simply serves as the electrolyte. The SSP results from the electrolytic reaction that occurs between the pole structure and the surrounding soil. SSP measurements are made using a high-impedance voltmeter that enables one to observe and record small voltages without requiring significant current flow (which can affect measurement accuracy).

As part of the field inspections at Sites 1 through 5, corrosion potentials were measured using the digital potential meter (M.C. Miller Co., Inc., Sebastian, FL) with

copper/copper sulfate reference electrode (CCSRE) that was also used to measure redox potentials (Figure 4.16), as reported in Section 4.2.3. A photograph documenting the SSP measurement on a WS pole at Site 2 is shown in Figure 5.7.

For structures with added cathodic protection, the digital potential meter was electrically attached to the magnesium anode connection (instead of the WS structure itself) to account for the influence of cathodic protection on the SSP. Otherwise, the digital potential meter was attached to a low-lying ladder clip to ensure good electrical connection, thereby providing measurements for the WS surface region and above-ground height that were covered in the visual inspections and thickness measurements.



Figure 5.7 Measurement of structure-to-soil potential on WS pole at Site 2.

5.2.3 Results and Discussion

The measured corrosion potential for each pole (in reference to both CCSRE and SHE) are summarized in Table 5.5. This table also provides information on whether or not cathodic protection was in place, whether or not the SSP value is equal to or smaller than

the NACE (2013) protection threshold of -0.85 V vs. CCSRE (i.e., “Adequately protected?”), and the pH values of the soil around each WS pole (to be used in the construction of the Pourbaix diagram).

Table 5.5 Structure-to-soil corrosion potential (SSP) for WS poles inspected.

Site	Pole	Soil pH	SSP [mV vs. CCSRE]	SSP [mV vs. SHE]	Adequately Protected?
1	C1F-20	8.0	-0.768	-0.450	No
2	Q3C-1L	7.5	-0.345	-0.027	No
	Q3C-1R	7.5	-0.345	-0.027	No
	Q3C-2L	6.5	-0.487	-0.169	No
3	S3B-2L	7.0	-0.240	+0.078	No
	S3B-3L	6.0	-0.185	+0.133	No
	S3B-7L	6.5	-1.389	-1.071	Yes
	S3B-7R	6.5	-1.377	-1.059	Yes
4	TL-1	5.0	-0.487	-0.169	No
5	8Z-2L	5.5	-0.811	-0.493	No
	8Z-2R	5.5	-0.797	-0.479	No
	11Z-2L	5.5	-1.109	-0.791	Yes
	11Z-2R	5.5	-1.181	-0.863	Yes
	11Z-6L	4.5	-0.834	-0.516	No
	11Z-6R	4.5	-0.781	-0.463	No

* SSP is close to the -0.85 V vs. CCSRE threshold (NACE 2013). The flow of corrosion current may not be expected to significantly hinder the effects of cathodic protection.

** SSP is close to the -0.85 V vs. CCSRE threshold (NACE 2013). The flow of corrosion current does not hinder the protective action provided by the GS fasteners, which act as sacrificial anodes. However, the fasteners exhibit visible corrosion damage.

Cathodic protection in the form of magnesium anodes was installed on all the directly embedded WS poles in Sites 1 through 3 to lower their corrosion potential. No cathodic protection was deployed on Pole TL-1 at Site 4. At Site 5, cathodic protection was deployed only on the recently remediated Pole 11Z-2L, which is connected to Pole 11Z-

2R by means of cross-bracings (Figure 3.26). No magnesium anode cables were disconnected from their respective structures. Yet, of the 15 poles tested, 11 failed to satisfy the NACE (2013) protection threshold, although five exhibited SSP values that are close to (within 100 mV) the -0.85 V vs. CCSRE threshold.

5.2.3.1 Corrosion Potential Measurements

At Site 1, Pole C1F-20 registered a corrosion potential reading of -0.768 V vs. CCSRE. This value is fairly close to the -0.85 V vs. CCSRE threshold (NACE 2013), and the flow of corrosion current is not expected to significantly hinder the effects of cathodic protection. In fact, Pole C1F-20 displayed a dense and adherent patina except beneath the reflective tape (Figure 3.5), and exhibited negligible average and maximum corrosion rates (Table 5.2). Further inspections may be considered to understand if the magnesium anode is intact but unable to overcome the natural flow of current from the structure into the soil, or if the magnesium anode has deteriorated due to the direct exposure to a corrosive soil (Table 4.15) in which it resides. The latter possibility is realistic since the local soil had the lowest soil resistivity of all other sites (Table 4.13).

At Site 2, Poles Q3C-1L, Q3C-1R and Q3C-2L exhibited ineffective corrosion potentials. It is noted that a similar SSP value of -0.345 V vs. CCSRE was recorded for Poles Q3C-1L and Q3C-1R since the two poles are part of a H-frame structure, and Pole Q3C-1L had a connected magnesium anode (Figure 3.7a). Pole Q3C-2L, which also had a connected magnesium anode (Figure 3.8), exhibited a slightly better SSP of -0.487 V vs. CCSRE, which might suggest that better corrosion potentials are attained at larger distances from the nearby potash mine. This hypothesis reflects the possibility that stray currents originating from the potash mine may be disrupting the flow of protective current between

the WS poles and their anodes. In fact, corrosion potential measurements were somewhat difficult for the poles at Site 2 as the digital potential meter hovered around 0 mV for some time (about 2-3 minutes instead of the typical 15-20 seconds) before providing a stable potential reading. The WS poles at Site 2 would benefit from a more effective cathodic protection, as further supported by the discussion on the Pourbaix diagram representation in Section 5.2.3.2.

At Site 3, similar difficulties to those of Site 2 were encountered when measuring the corrosion potential of Poles S3B-2L and S3B-3L. The digital potential meter could not provide consistently stable potential values for these poles. For Pole S3B-2L, it was also necessary to reattach the probe. Poles S3B-2L and S3B-3L exhibited corrosion potentials of -0.240 V and -0.185 V vs. CCSRE, respectively. These values were the highest (i.e., worst) of all WS poles inspected. It is reasonable to hypothesize that stray currents originating from the nearby power station and/or coal mines can disrupt SSP readings and hinder cathodic protection. This hypothesis is consistent with the evidence from visual assessment (Figure 3.15a) and the corrosion rate estimates (Table 5.2) for the Pole S3B-2L wall facing the power station. The difference in coating quality may be the main reason why Pole S3B-2L suffered extensive pitting (Figure 3.15a) and significant thickness losses (with $CR_{\max} = 0.71$ mils/year) whereas Pole S3B-3L experienced negligible corrosion damage (Figure 3.16) and thickness losses ($CR_{\text{avg}} = 0$ mils/year). In addition, a suitable coating appears to compensate for the inadequate cathodic protection for possible corrosion damage at or below the ground line (e.g., soil corrosion, stray-current corrosion). In fact, while the SSP of Pole S3B-3L is greater (i.e., worse) than that of Pole S3B-2L, the coating on Pole S3B-3L extended about 3 ft above ground, and protected the pole from soil and

stray-current corrosion. Instead, Pole S3B-2L was largely uncoated at the ground line and thus more susceptible to soil and stray-current corrosion (Figure 4.15b). Further insight on stray currents and their effect on cathodic protection is offered in Section 7.2.3.

Of the directly embedded WS poles inspected, only Pole S3B-7L at Site 3 possessed a magnesium anode (Figure 3.14b) that resulted in a safe corrosion potential (-1.389 V vs. CCSRE). The cathodic protection system installed on Pole S3B-7L also provided ample support to Pole S3B-7R (-1.377 V vs. CCSRE) through the H-frame connection. These SSP values help explain the minor amount of visible damage that was sustained by both poles (Table 3.2), and the negligible corrosion rate of Pole S3B-7L (Table 5.2). This evidence shows that cathodic protection is capable of effectively protecting multiple connected structures (in this instance in the form of an H frame), provided that suitable ground-line coating is used. This evidence also demonstrates that magnesium anodes can last for decades (i.e., 28 years for Pole S3B-7L and its anode) in a moderately corrosive soil (Table 4.15).

At Site 4, Pole TL-1 exhibited a corrosion potential of -0.487 V vs. CCSRE. This value is similar to or better than those of the cathodically protected WS poles at Sites 2 and 3, despite the fact that Pole TL-1 is not cathodically protected. This notable difference is attributed primarily to the high resistivity of the soil at Site 4 (up to $250,000$ Ω -cm) (Table 4.13). Such high resistivity is expected to alleviate the flow of corrosion currents. Yet, the installation of a cathodic protection system should be recommended if this pole was in service instead of being part of a test line.

At Site 5, the WS poles are not directly embedded in soil. Instead, they are mechanically connected to GS caisson foundations by means of GS fasteners. In this

configuration, the protective zinc layer on the GS caissons and fasteners are expected to act as sacrificial anodes, thereby protecting the WS structure against corrosion. As a result, the potential of WS is expected to shift toward the protective threshold of -0.85 V vs. CCSRE (NACE 2013) at the expense of the GS fasteners, as shown in Figure 3.32. In fact, the highest (i.e., worst) SSP reading recorded at Site 5 was -0.781 V vs. CCSRE for Pole 11Z-6R. This corrosion potential does not meet the NACE (2013) requirement for satisfactory protection but is fairly close to the -0.85 V vs. CCSRE threshold. A similar result was obtained for Poles 8Z-2L, 8Z-2R and 11Z-6L. Therefore, the sacrificial action of zinc-protected components appears somewhat insufficient to adequately protect the WS poles. In fact, only the recently remediated Poles 11Z-2L and 11Z-2R (which are the only cathodically protected poles at Site 5) exhibited satisfactory corrosion potentials. For these two poles, which are part of the same H-frame structure, the connection of two magnesium anodes to the GS caisson of Pole 11Z-2L (Figure 3.35a) contributed to shift the SSP for this pole to -1.109 V vs. CCSRE, and to -1.181 V vs. CCSRE for Pole 11Z-2R. This evidence suggests that the deployment of cathodic protection to the other WS poles at Site 5, together with other necessary corrective remediation (i.e., replacing the GS fasteners, filling the GS caissons, and sealing the pole bases), would greatly alleviate the high corrosion rates that were estimated based on thickness measurements (Table 5.3 and Table 5.4).

5.2.3.2 Pourbaix (Corrosion Potential – Soil pH) Diagram

Figure 5.8 illustrates the Pourbaix diagram for iron (Fe) at 25°C . In the diagram, the corrosion potential – soil pH domain is subdivided considering the possible reactions associated with iron, and excluding dry corrosion products such as magnetite (Fe_3O_4) and

ferric oxide (Fe_2O_3). For all WS poles inspected, the results for soil pH and SSP summarized in Table 5.5 are plotted in Figure 5.8, together with the -0.85 V vs. CCSRE (-0.53 V vs. SHE) cathodic protection threshold (NACE 2013).

This representation helps explain why this SSP threshold (NACE 2013) is generally accepted as indicative of a protected steel pole. If the corrosion potential of a WS pole is more negative than this threshold, then the iron by-products will more likely be stable (i.e., non-ionic “Fe”) and effectively “immune” from corrosion for soil pH values up to approximately 9. For example, this is a typical case for the interior surface of well-sealed WS poles, or exterior surfaces of cathodically protected WS poles. In fact, soils rarely exhibit pH values above 8 (Roberge 2008). Instead, iron is expected to oxidize if it is stable in its ferrous ion form (Fe^{2+}) or ferric ion form (Fe^{3+}), that is, at corrosion potential values greater than -0.92 V vs. CCSRE (-0.6 V vs. SHE) and soil pH values below 9 (or less at increasing corrosion potential values).

Conversely, WS poles with a well-developed protective patina are expected to plot in the “passivation” region of the Pourbaix diagram where iron tends to form more stable ferric hydroxides, $\text{Fe}(\text{OH})_3$ and – for very alkaline soils that are not typically relevant for transmission line structures – ferrous hydroxides, $\text{Fe}(\text{OH})_2$, and complex HFeO_2^- ions.

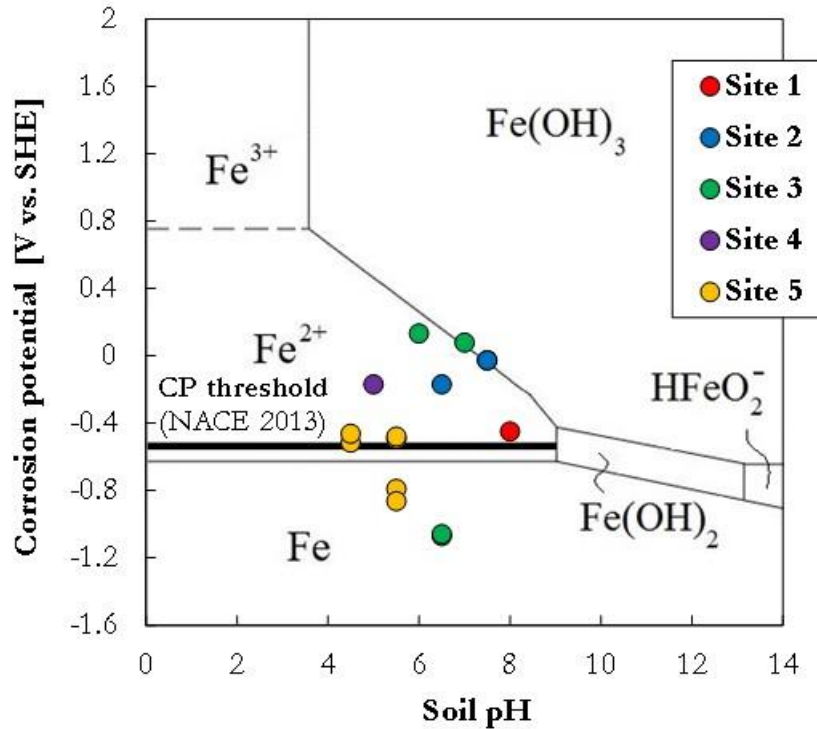


Figure 5.8 Pourbaix diagram of Fe with NACE (2013) cathodic protection threshold and corrosion potential-soil pH markers for WS poles at Sites 1 through 5.

Figure 5.8 illustrates the importance of an adequate cathodic protection for WS transmission line poles. Representative examples are discussed as follows. It is noted that a detailed list of remediation measures recommended for the WS poles at Sites 1 through 5 is discussed in Section 7.3.

- Poles S3B-7L and S3B-7R have most likely possessed adequate cathodic protection throughout their lifetimes. In fact, these poles are marked in green well below the NACE (2013) protection threshold, and within the stable “Fe” domain of the Pourbaix diagram (i.e., similar to the recently remediated Poles 11Z-2L and 11Z-2R at Site 5). These results are consistent with the evidence from both visual assessment (Table 3.2) and corrosion rate estimates (Table 5.2).

- Despite the sacrificial action contributed by the GS components at the base of Poles 8Z-2L, 8Z-2R, 11Z-6L and 11Z-6R at Site 5, the SSP-soil pH coordinates for these poles lie slightly above the NACE (2013) protection threshold marked in Figure 5.8. These coordinates place these four poles in the “Fe²⁺” domain where corrosion is expected to occur, as reflected in the significant corrosion damage documented in Section 3.5, and corrosion rates reported in Table 5.3 and Table 5.4. Therefore, also based on the evidence offered by the recently remediated Poles 11Z-2L and 11Z-2 at Site 5, it is reasonable to expect that providing additional cathodic protection would decidedly mitigate corrosion effects on Poles 8Z-2L, 8Z-2R, 11Z-6L and 11Z-6R.
- For Pole C1F-20 at Site 1, cathodic protection is not necessarily adequate. However, as noted in Section 5.2.3.1, the corrosion potential is close to the NACE (2013) threshold, and the corrosion current may not be expected to result in significant corrosion damage. In addition, the service environment does not pose major issues as reflected in the results of visual inspection (Table 3.2) and corrosion rate estimates (Table 5.2).

Most WS poles inspected fall into the “Fe²⁺” domain or at the boundary with the passive “Fe(OH)₃” domain of the Pourbaix diagram (Figure 5.8). Representative examples are discussed as follows.

- Pole TL-1 at Site 4 (23-year old) and Pole Q3C-2L at Site 2 (14-year old) lie well within the “Fe²⁺” domain, and thus are expected to suffer corrosion damage beyond the formation of a protective oxide film. This observation is

substantiated by evidence from visual inspection (Table 3.2) and corrosion rate estimates (Table 5.2 and Table 5.3). This outcome was anticipated for Pole TL-1, which is part of a test line that has been consistently exposed to a marine atmosphere, and where no cathodic protection is in place.

- For Pole Q3C-2L at Site 2 (and the companion Pole Q3C-2R, for which the SSP was not measured), it is noted that relatively large pack-out rust layers were easily removed from the WS surface (Figure 3.10), thus suggesting that it is unlikely for the corrosion potential to increase over time to levels compatible with the passive “Fe(OH)₃” domain. Therefore, cathodic protection should be re-examined and corrected on these poles, perhaps after assessing the presence of stray currents.
- Pole S3B-3L at Site 3 lies within the “Fe²⁺” domain but close to the boundary with the passivation [Fe(OH)₃] domain. Here, the issue of insufficient cathodic protection is overcome by the fact that the ground-line coating is adequate and the exposure environment is not of concern. In fact, this pole features a dense and adherent patina (Figure 3.16). Instead, Pole S3B-2L at Site 3, which lies at the boundary between the “Fe²⁺” and the passive domains, exhibits corrosion damage that may be attributed to stray currents from the nearby power plant, as discussed in Section 3.3 and Section 5.2.3.1. Here, while cathodic protection may be re-examined and corrected (perhaps after assessing the presence of stray currents), extending the coating above the ground line may be sufficient.
- Poles Q3C-1L and Q3C-1R at Site 2 lie at the boundary between the “Fe²⁺” and the passivation [Fe(OH)₃] domains, and operate in a corrosive rural/industrial

atmosphere [category C_4 per ISO 9223 (2012b) as reported in Table 4.7]. This case is indicative of the fact that such position in the Pourbaix diagram (Figure 5.8) is not sufficient to assume full passivity under relatively corrosive environments, although severe corrosion damage may not occur. In fact, the walls of these WS poles feature pack rust deposits (Figure 3.9) and a somewhat low-quality patina (Figure 3.11). It is noted that this patina is far more adherent than that of Poles Q3C-2L and Q3C-2R, from which pack-out rust layers were easily removed (Figure 3.10). In addition, negligible corrosion rates were estimated (Table 5.2), different than for Pole Q3C-2L (and, presumably, for Pole Q3C-2R if thickness measurements were made). However, it is emphasized that exposure to an aggressive environment can exacerbate corrosion effects associated with water stagnation at geometric discontinuities, such as in the case of the pack-out damage documented at a ladder clip on Pole Q3C-1L (Figure 3.9). Therefore, cathodic protection should be re-examined and corrected on these poles, perhaps after assessing the presence of stray currents.

In perspective, the fact that none of the five WS poles without cathodic protection lies clearly in the “ $\text{Fe}(\text{OH})_3$ ” (passivation) domain further highlights the importance of investing resources in field inspections, and in the development of shared knowledge base and best practices for owners and inspectors.

5.3 Concluding Remarks

Based on the evidence from thickness loss and corrosion potential measurements presented in this chapter, the following conclusions are drawn:

- The quantification of corrosion rates allows for a better understanding of the combined impact of the environment, design and detailing on WS poles. The quantification of corrosion potentials allows for the assessment of present and future susceptibility to corrosion damage. This information can be leveraged for diagnosis and prognosis purposes, thereby enabling owners to prioritize and allocate prevention and remediation resources.
- For the different exposure environments covered in Sites 1 through 5, the inspected WS poles exhibit corrosion rates that are typically correlated with low to medium corrosivity classifications per ISO 9223 (ISO 2012b). Comparison of these classifications and those determined based on atmospheric corrosivity (Chapter 4.0), indicates that WS is expected to perform far better than standard carbon steel. In fact, none of the WS poles inspected experienced a uniform corrosion damage of concern. Based on the results of average and maximum thickness loss measurements, it appears that for the representative pole ages and environments covered in Sites 1 through 5, any relevant corrosion damage accrues from localized corrosion mechanisms, especially due to moisture stagnation.
- Corrosion damage in WS pole walls may be accurately predicted using semi-empirical analytical models that are calibrated based on thickness loss measurements that are collected over an extended period of time. Short-term field inspections are unsuitable to define empirical parameters for such models. More research is needed to define such parameters for WS as a function of exposure environment and pole age.

- Of the 15 poles tested for corrosion potential, 11 failed to satisfy the NACE (2013) protection criterion based on the -0.85 V vs. CCSRE threshold. Five poles did exhibit potential values that are close (within 100 mV) to the -0.85 V vs. CCSRE threshold. Examining corrosion potential (and soil pH) data via the Pourbaix diagram illustrates the importance of adequate cathodic protection for WS poles. It is noted that none of the five WS poles without cathodic protection lies clearly in the passivation domain of the diagram. This outcome highlights the importance of routine checks on the health of cathodic protection systems.
- Site 1: Pole C1F-20 exhibits negligible maximum and average corrosion rates, which are consistent with the presence of a dense and adherent patina, and a low-corrosivity atmosphere. Therefore, the corrosion potential is not of concern although it is slightly greater than the NACE (2013) threshold. However, it is noted that severe corrosion damage can still occur at locations where water can stagnate. The damage observed beneath the reflective tape is indicative of the susceptibility of WS to corrosion damage at geometric discontinuities.
- Site 2: cathodic protection should be re-examined and corrected on all WS poles (perhaps after assessing the presence of stray currents). In fact, the exposure to an aggressive industrial atmosphere makes it unlikely for a stable and adherent patina to develop, and exacerbates any corrosion damage accruing from moisture stagnation (e.g., at coating lips). It is recommended that routine assessments be prioritized at Site 2.
- Site 3: despite the non-corrosive (rural) atmosphere, Pole S3B-2L experienced significant thickness losses on the surface facing the nearby power station, and

exhibited insufficient cathodic protection. These issues likely stem from the combination of: (a) exposure to stray currents emanating from the power station, as highlighted by the difficulties to measure corrosion potentials; and (b) inadequate above-ground extension of the coated area. In fact, Pole S3B-3L, for which the coating area extends well above the ground line, exhibits a similarly inadequate cathodic protection together with negligible corrosion rates. Therefore, for Pole S3B-2L, while cathodic protection may be re-examined and corrected after assessing the presence of stray currents, extending the coating above the ground line may be sufficient. Instead, the 28-year old Poles S3B-7L and S3B-7R are located far away from the power station and exhibited excellent cathodic protection. The resulting low maximum corrosion rate demonstrates that cathodic protection can effectively protect multiple connected structures and last for decades, provided that suitable coating is used.

- Site 4: the chloride-laden and humid environment hinders the corrosion resistance of WS wall surfaces of Pole TL-1, as reflected in the corrosion rate estimates. However, far more severe damage may occur at locations where moisture and chlorides can accumulate, as demonstrated by the completely consumed WS substrate behind the junction box. For existing WS poles located near saltwater, installing cathodic protection should be recommended.
- Site 5: a number of questionable design choices are reflected in high corrosion rates. These design issues (hollow GS caisson foundations, unsealed pole bases, galvanic coupling of GS and WS steel elements) should be remediated. Based on the evidence offered by Poles 11Z-2L and 11Z-2R, which were recently

remediated, it is reasonable to expect that adding cathodic protection to the other WS poles at Site 5 would be beneficial for corrosion resistance.

- The uncoated WS surface of interest in pole structures lies above ground instead of in direct contact with the soil. Therefore, more research is needed to understand the applicability of the NACE (2013) threshold to above-ground WS surfaces. Based on the results of this study (e.g., for Pole C1F-20 at Site 1), some adjustments are needed to increase the -0.85 V vs. CCSRE (-0.53 V vs. SHE) cathodic protection threshold (NACE 2013), which applies to steel surfaces in direct contact with soil (e.g., buried pipes).
- The use of WS poles connected by steel bracings (e.g., forming H-frames such as in the case of Poles S3B-7R and S3B-7L in Figure 3.12) should be discouraged. In fact, connecting multiple WS poles may accelerate corrosion damage due to differential potentials, thus forcing some adjoining structures to act as sacrificial anodes. To prevent this event, single poles or non-conductive (e.g., glass fiber-reinforced polymer) connections are recommended.
- Corrosion studies on WS coupons are unlikely to provide comprehensive conclusions with regard to practical worst-case scenarios (e.g., focusing on corrosion-sensitive details). Investigating actual transmission line structures exposed to significant environments is important to generate hard evidence. To this end, extending the scope of the project reported herein from WS poles to WS lattice towers should be considered. In fact, tower structures include numerous corrosion-sensitive details, such as mechanically-fastened joints and other geometric discontinuities that are difficult to protect with coatings.

CHAPTER 6.0 ASSESSMENT OF OXIDE MICROSTRUCTURE AND COMPOSITION

This chapter reports on laboratory tests that were aimed at characterizing the microstructure and chemical composition of powder oxide (patina) samples that were collected at representative locations on the WS pole walls, and larger rust samples that were removed from more corroded areas. The test methods deployed included scanning electron microscopy (SEM), energy-dispersive X-ray spectroscopy (EDX), X-ray diffraction (XRD), and Mössbauer spectroscopy (MS). The overarching objective is to verify whether peculiar oxide phases are present in low-quality patinas and in oxides that form on WS surfaces exposed to particularly aggressive environments.

Section 1.1 presents a literature review on the composition of WS surface oxides. Section 6.2 presents the collection of oxide samples from the WS poles in Sites 1 through 5. Section 6.3 reports on the use of SEM imaging and EDX analysis to visualize the microstructure and identify the elemental composition of the solid rust samples collected in the field. Section 6.4 reports on the use of XRD as well as MS to quantify different iron oxide species in the powder and solid rust samples collected in the field. Then, Section 6.5 introduces a new analytical model that uses quantitative data obtained through laboratory characterization of iron oxides to assess the quality of the protective patina and iron oxides that form on WS pole surfaces. This “Protective Ability Index” model is then verified vis-à-vis evidence from visual assessment (Chapter 3.0) and atmospheric corrosivity assessment (Chapter 4.0). Salient conclusions are summarized in Section 6.6.

6.1 Literature Review of Microstructure and Composition of Surface Oxides

The fundamental understanding of corrosion mechanisms and reasons thereof (e.g., undesirable atmospheres and exposure conditions) requires knowledge of the chemical composition of surface oxide films on WS, and factors influencing their adherence to the steel substrate, density, chemical stability, and resulting steady-state (long-term) corrosion rates. The corrosion resistance of WS depends on the formation of an adherent and dense surface patina. Such patina may consist of different ferric oxides, hydroxides and amorphous phases, which are summarized in Table 6.1. Specific proportions depend on the composition of the steel alloy, service environment, and age of the structure (i.e., duration of exposure). The influence of different alloying elements (Cu, Cr, P, Ni, Si) on the corrosion resistance of WS is reviewed in Section 2.2.

Table 6.1 Iron oxides and hydroxides typically found in WS surface patina.

Designation	Composition
Oxides	
Hematite	α -Fe ₂ O ₃
Maghemite	γ -Fe ₂ O ₃
Magnetite	Fe ₃ O ₄
Ferrihydrite	Fe ₅ HO ₈ ·4H ₂ O
Hydroxides	
Goethite	α -FeOOH
Akaganeite	β -FeOOH
Lepidocrocite	γ -FeOOH
Feroxyhyte	δ -FeOOH

Numerous compositions of oxide films on WS have been hypothesized, and there has been much debate on their physical structure (Misawa 1988). Yamashita et al. (1998) proposed a detailed concept for the morphology and composition of WS patinas as illustrated in Figure 6.1 (Morcillo et al. 2014). The main phases include goethite (α -

FeOOH) and lepidocrocite (γ -FeOOH) and, to a smaller extent, maghemite (γ -Fe₂O₃) and magnetite (Fe₃O₄). Akaganeite (β -FeOOH) is uncommon in corrosion-resistant WS but may form in highly corrosive chloride-laden environments (Li et al. 2008). A simple two-layer structure (Figure 6.1a) was proposed where goethite and lepidocrocite are located in an inner and outer layer, respectively (Yamashita et al. 1998). In some instances, an alternating-band structure may form (Figure 6.1b), with goethite being present also in a third (outermost) layer, and with maghemite/magnetite inclusions in the goethite and lepidocrocite areas.

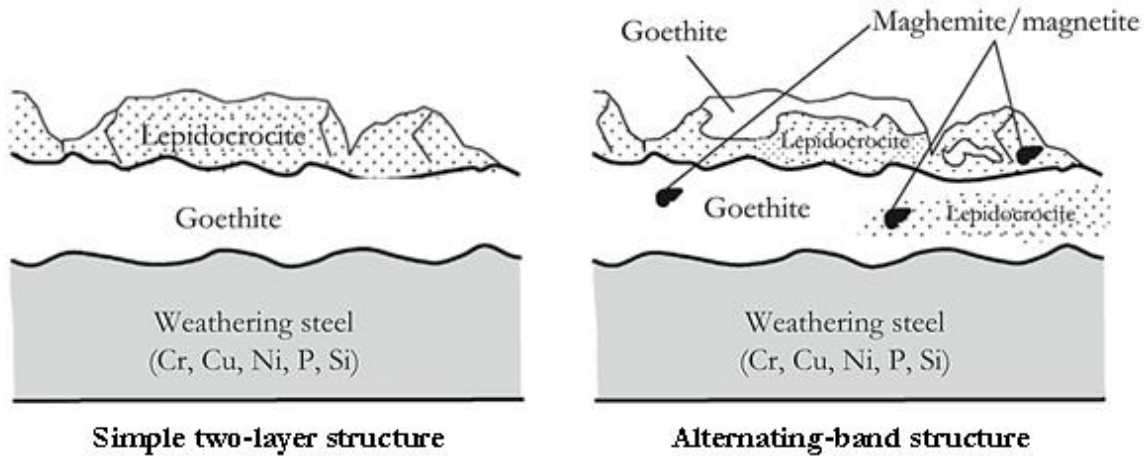


Figure 6.1 Schematic of structure of protective oxide film in WS steel (Morcillo et al. 2014).

Several other iron compounds can form depending on the exposure environment. In urban and industrial atmospheres containing sulfur, melanterite [FeSO₄·7H₂O], rozenite [Fe²⁺SO₄·4(H₂O)], and Fe (III) sulfate [Fe₂(SO₄)₃] may form. In marine atmospheres, chloride-containing compounds such as Fe (II) chloride (lawrencite, FeCl₂), Fe (II) chloride tetrahydrate [FeCl₂·4(H₂O)], and Fe (III) chloride hexahydrate [FeCl₃·6(H₂O)], may also form. In the case of WS, the protective patina can be idealized as consisting of an inner and

an outer layer, where the former is generally considered as the primary contributor to corrosion resistance (Morcillo et al. 2014).

SEM micrographs of representative corrosion by-products are shown in Figure 6.2. These iron oxides and hydroxides have specific crystallite characteristics and tend to form relatively large microstructural assemblies whose morphology is unique to each species. Goethite takes the form of elongated rod-like particles, and exhibits a tendency towards lateral (i.e., stacking) aggregation, resulting in the formation of dendritic microstructures (Figure 6.2a). Its crystallites measure approximately 1 μm in length, with widths of 50 nm or less (Zic et al. 2007). Lepidocrocite is typically found as deposits of randomly oriented particles that are normally less than 200 nm in length (Figure 6.2b), with relatively large pores (Antony et al. 2004). Magnetite exhibits monodispersed sphere-like grains with size in the range 40-50 nm (Figure 6.2c) (Topal and Aksan 2016). Maghemite typically takes the form of homogeneous and approximately spherical nanoparticles with a diameter of 20-30 nm (Figure 6.2d) (Mozaffari et al. 2015). Akaganeite crystals (e.g., Figure 6.2e) can take different crystallite forms, including spindle-shaped, tubular, or rod-like, characteristically making up large phase particles with diameter in the range 10-50 μm (Roque-Malherbe et al. 2015).

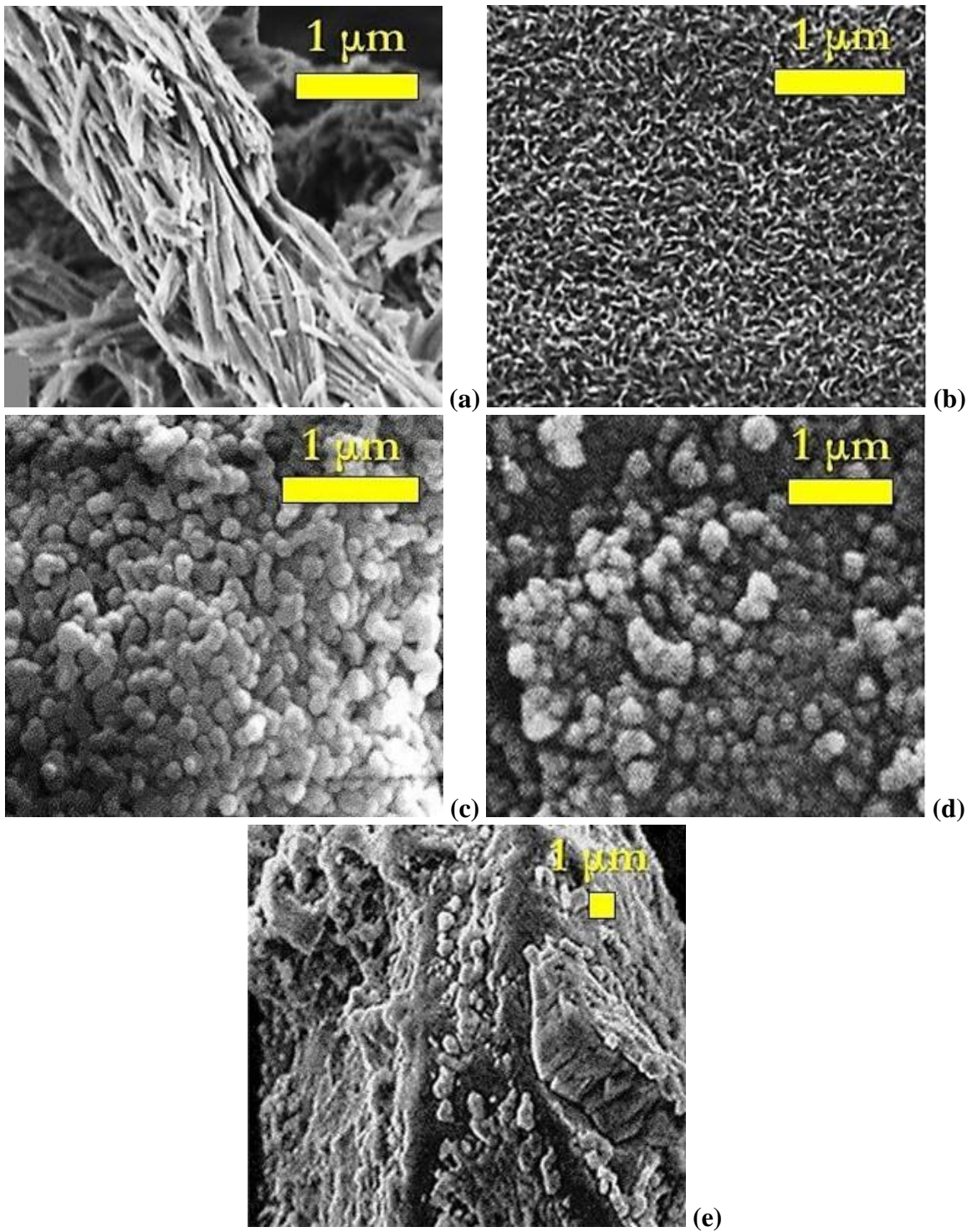


Figure 6.2 SEM micrographs of iron oxides and hydroxides in WS patina: (a) goethite (Zic et al. 2007); (b) lepidocrocite (Antony et al. 2004); (c) magnetite (Topal and Aksan 2016); (d) maghemite (Mozaffari et al. 2015); and (e) akaganeite (Roque-Malherbe et al. 2015).

It is noted that the composition of oxide films in WS can greatly vary depending on the surface electrolytes and type of atmospheric exposure. Lepidocrocite (γ -FeOOH) appears to be the most frequently encountered crystalline corrosion by-product, while goethite (α -FeOOH) appears to be the most stable ferric hydroxide (Morcillo et al. 2014).

Goethite has been identified as the key component of the heterogeneous protective film in combatting corrosion, acting as a dense barrier against the infiltration of corrosive agents (Morcillo et al. 2014). In slightly acidic solutions, lepidocrocite transforms into goethite through a process that depends on sulfate concentration and temperature. The conversion of lepidocrocite into goethite, which has been shown to occur in industrial environments over extended periods of time, has a beneficial influence on the corrosion resistance of the oxide film (Wang et al. 1996).

The mass ratio of goethite (α -FeOOH) to all other ferric compounds in the oxide layer (γ -FeOOH, β -FeOOH, and Fe_3O_4), which is denoted as α/γ^* , increases with the exposure time (Kamimura et al. 2006). There is a strong correlation between the increase in α/γ^* ratio and decreases in corrosion rate in marine environments, where all four ferric compounds are found, and rural and industrial environments, where typically only α -FeOOH and γ -FeOOH form. For example, in the case of marine environments, this correlation is illustrated in Figure 6.3 (Kamimura et al. 2006).

Kamimura et al. (2006) suggested that the parameter α/γ^* can serve as a “protective ability index” with the aim of quantifying the quality of WS oxide composition; in fact, corrosion rates greater than 0.01 mm/year were not observed for $\alpha/\gamma^* > 1$, i.e., when a sufficient amount of goethite forms with respect to the combined amounts of the other phases. This rationale is consistent with the identification of goethite as a particularly stable

phase that is primarily responsible for the stability and adherence of the protective patina on WS surfaces (Li et al. 2008). In contrast, comparatively greater amounts of akaganeite (β -FeOOH) are present in WS oxide films that form in chloride-laden environments where corrosion damage is typically more severe (Li et al. 2008).

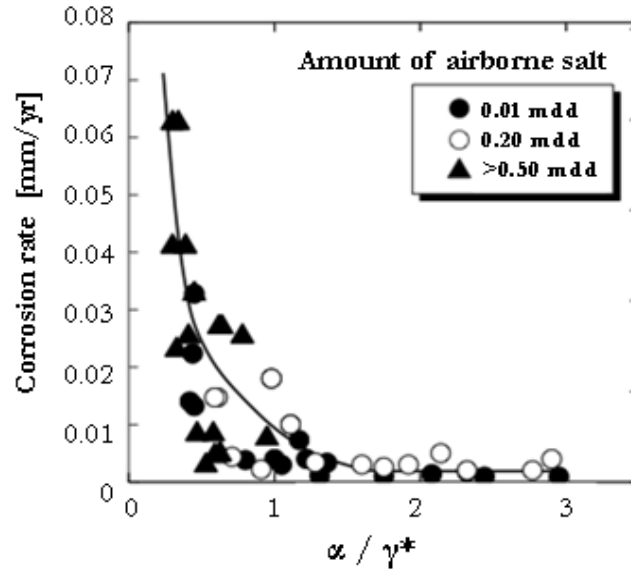


Figure 6.3 Corrosion rates in WS for different atmospheric chloride concentrations (in mg/dm²-day or m d d) as function of α/γ^* (Kamimura et al. 2006).

Magnetite (Fe_3O_4) is also one of the main oxide constituents. It is typically present in inner rust layers and tends to chemically bond onto the surface of WS upon prolonged exposure to the atmosphere. Magnetite and akaganeite appear to be negatively correlated (Asami and Kikuchi 2003) as the latter tends to form on WS that is exposed to marine environments, indicating that chloride ions may react with magnetite to create akaganeite, thereby decreasing the corrosion-protection effectiveness of the oxide film (Li et al. 2008). Here, akaganeite is typically found in the outermost layer of the oxide film that develops in early corrosion stages by oxidation of FeCl_2 or hydrolysis of FeCl_3 in the presence of Fe (Cano et al. 2014).

Maghemite ($\gamma\text{-Fe}_2\text{O}_3$) was also identified on WS surfaces exposed to different types of atmospheres. Oh et al. (1999) found traces of maghemite in WS, CS, and Cu-bearing steel exposed to rural, industrial, and marine environments. Conversely, in the case of marine environments, only large particles of maghemite on plain CS were observed, suggesting that the alloying elements in Cu-bearing and weathering steels may hinder the formation of maghemite.

In addition, hematite ($\alpha\text{-Fe}_2\text{O}_3$) is not a by-product that is often encountered but has been found on plain CS in industrial atmospheres (De la Fuente et al. 2011), and ferrihydrite ($\text{Fe}_5\text{HO}_8\cdot 4\text{H}_2\text{O}$) may be detected in atmospherically corroded steels. Oxide deposits formed on steel in an artificially polluted atmosphere at 100% RH consisted of substantial amounts of lepidocrocite and ferrihydrite (Leidheiser et al. 1984). Also, the amorphous ferric hydroxide, ferrihydrite ($\delta\text{-FeOOH}$), may influence – albeit marginally – the composition of WS patinas (De la Fuente et al. 2011).

The characterization of the types, proportions and distribution of corrosion by-products that form on WS can be used to identify corrosion mechanisms associated with specific environmental exposures. To this end, suitable characterization techniques that are often enlisted (Morcillo et al. 2014) include SEM, XRD, infrared (IR) spectroscopy, and MS. When a more refined depiction of the corrosion by-product microstructure is sought, Raman microspectroscopy and X-ray microdiffraction may be considered (Morcillo et al. 2014).

6.2 Oxide Sampling from WS Pole Structures

Oxide samples for laboratory characterization were collected from WS poles at each test site, in conformance with ASTM G1 (ASTM 2011a), as summarized in Table 6.2.

The samples included:

- Oxide (patina) powder samples, which were collected from each WS pole by scraping the wall surface (Figure 6.4a) throughout a maximum area of 1 ft² (1 ft by 1 ft) for no more than ten minutes. For each sample in Table 6.2, 0.1 g were used for XRD and MS analysis.
- Larger solid rust samples, which were removed by tool or hand from pack-rust and pack-out deposits (Figure 6.4b). These larger rust samples were obtained from seven WS poles at Sites 2, 4 and 5 (Table 6.2). Portions of these samples were: (a) used to extract small samples (i.e., with the surface smaller than that of a circle with diameter of 0.5 in., and thickness up to 0.2 in.) for SEM/EDX analysis; and (b) ground into powder using a sterilized agate mortar and pestle to obtain 0.1 g samples suitable for XRD and MS analysis.

The removal of oxide samples was performed using a forged high-carbon steel chisel scraper and/or a hardened, tempered, and polished steel putty knife. Specimens were then transferred to sterile sealable plastic containers using nitrile gloves, and were kept in these containers until testing.



Figure 6.4 Collection of surface oxide samples: (a) scraping of patina to obtain powder sample; and (b) pack-out rust sample removed by hand from junction box area of Pole TL-1.

For each WS pole inspected, Table 6.2 summarizes the type and amount of oxide samples that were collected during the field inspections, along with the area from which each sample was acquired.

At Site 1, two powder samples were obtained from Pole C1F-20. A mass of 0.22 g was scraped from an undamaged section of the pole wall, and 0.31 g of powder was collected from the pack rust that accumulated under the reflective tape (Figure 3.5b).

Table 6.2 Surface oxide samples collected from WS poles inspected.

Site	Pole	Source Location	Type	Mass [g]
1	C1F-20	Pole wall	Powder	0.22
		Reflective tape	Powder	0.31
2	Q3C-1L	Pole wall	Powder	1.05
		Coating line	Solid	1.82
	Q3C-1R	Pole wall	Powder	0.34
	Q3C-2L	Pole wall	Powder	0.87
		Coating line	Solid	20.90
	Q3C-2R	Pole wall	Powder	1.33
Coating line		Solid	12.81	
3	S3B-2L	Pole wall	Powder	0.11
	S3B-3L	Pole wall	Powder	0.16
	S3B-7L	Pole wall	Powder	0.47
	S3B-7R	Pole wall	Powder	0.42
4	TL-1	Pole wall	Powder	1.65
		Inner pack out	Solid	451.53
		Outer pack out	Solid	468.18
		Pit (Figure 3.20b)	Solid	2.50
5	8Z-2L	Pole wall	Powder	0.35
		GS fasteners	Solid	178.08
	8Z-2R	Pole Wall	Powder	0.27
		GS fasteners	Solid	174.01
	11Z-2L	Pole wall	Powder	1.21
	11Z-2R	Pole wall	Powder	1.09
	11Z-6L	Pole wall	Powder	0.23
	11Z-6R	Pole wall	Powder	0.61
GS fasteners		Solid	36.46	

At Site 2, Poles Q3C-1L and Q3C-2R each yielded over 1 g of powder oxide. A sizable powder sample (0.87 g) was also collected from Pole Q3C-2L. Poles Q3C-1L, Q3C-2L, and Q3C-2R yielded pack-out rust samples from their coating line regions. A 1.82 g pack-rust sample was collected from Pole Q3C-1L (Figure 3.9) whereas Poles Q3C-2L and Q3C-2R yielded larger pack-out rust samples of 20.90 g and 12.81 g, respectively

(Figure 3.10). A powder sample with a mass of 0.34 g was collected from Pole Q3C-1R where no harvestable deposits of pack rust were noted. These mass quantities suggest that Poles Q3C-1L and Q3C-1R possessed more adherent patinas than Poles Q3C-2L and Q3C-2R. This outcome is consistent with the position of each pole in the Pourbaix diagram (Figure 5.8). In fact, Poles Q3C-1L and Q3C-1R lie near the passivation $[\text{Fe}(\text{OH})_3]$ region whereas Pole Q3C-2L (and, reasonably, its companion Pole Q3C-2R) lies well within the corrosion (Fe^{2+}) region.

At Site 3, 0.47, 0.42, 0.11 and 0.16 g of powder samples were collected from Poles S3B-7L, S3B-7R, S3B-2L and S3B-3L, respectively. These mass values are consistent with the atmospheric corrosivity classifications from Table 4.7. These classifications suggest that Poles S3B-7L and S3B-7R are exposed to an atmosphere (C_3 to C_4) with similar corrosivity to Site 1 (C_3 to C_4) and less corrosivity than Site 2 (C_4), and that the nearby Poles S3B-2L and S3B-3L are exposed to a slightly less corrosive atmosphere (C_2 to C_3). The corrosion rate estimates summarized in Table 5.2 may lead one to expect larger samples from Pole S3B-2L. However, the thickness losses sustained by this structure are caused primarily by pitting corrosion (Figure 3.15a), possibly due to stray currents as discussed in Section 5.2.3.1. Furthermore, with regard to Poles S3B-2L and S3B-3L, the combination of low-corrosivity atmosphere and corrosion potential near the passivation region of the Pourbaix diagram (Figure 5.8) seems to favor the formation of adherent patinas on WS wall surfaces.

At Site 4, Pole TL-1 produced the largest powder oxide sample (1.65 g) of all poles inspected. It also provided by far the largest amount of solid rust samples as over 900 g of pack-out rust was collected from the junction box area (Figure 3.21). In Table 6.2, the rust

removed from the outer half of the pack-out deposit (approximately 3/4 in. in thickness) was distinguished from the rust removed from the inner layers to assess differences (if any) in microstructure and chemical composition. In addition, 2.50 g of pack rust was collected from the pit near the coating lip shown in Figure 3.20b.

At Site 5, Poles 11Z-2L and 11Z-2R yielded the largest powder masses at over 1 g each, which may help explain why these structures were considered for remediation over the others at Site 5. Solid oxide samples were collected from Poles 8Z-2L, 8Z-2R and 11Z-6R. These samples were completely detached from the GS fasteners that secured the WS poles to their GS caisson foundations (Figure 3.31 and Figure 3.32). Poles 8Z-2L and 8Z-2R possessed severely damaged fasteners, and each yielded over 170 g of solid rust. The GS fasteners of Pole 11Z-6R were far less damaged and yielded a solid rust sample of 36.46 g.

6.3 Microstructure Characterization via SEM and EDX Analysis

Scanning electron microscopy (SEM) imaging was used in conjunction with energy-dispersive X-ray spectroscopy (EDX) to analyze the microstructure of the solid rust samples. The morphology of each specimen was captured via SEM imaging, and the associated chemical (elemental) composition was determined via EDX analysis. In all, eight representative samples were tested, i.e., one from each WS pole from which solid samples were collected at Sites 2, 4 and 5, except for Pole TL-1, for which two samples (from the inner and outer pack-out rust removed) were considered.

6.3.1 SEM/EDX Methodology

SEM/EDX imaging and analysis were performed at the University of South Carolina Electron Microscopy Center using a variable pressure microscope (model Vega3

LMU, Tescan, Brno, Czech Republic). The microscope is equipped with a backscattered electron detector and EDX capabilities. The solid samples were sprayed with gas duster to minimize the amount of loose particles on the scanning surfaces, and then placed on test tabs having a 12-mm diameter. SEM micrographs and EDX data were acquired for magnifications up to 5,000x, allowing comprehensive analysis and comparison of the morphology and elemental composition of the oxides present in the samples with those available in the literature (e.g., Figure 6.2 for SEM and Table 6.3 for EDX).

Table 6.3 Elemental compositions of iron oxides and hydroxides.

Oxide	Composition		Proportion
	Iron (Fe) [wt%]	Oxygen (O) [wt%]	[Fe/O]
Goethite	62.85	36.01	1.75
Lepidocrocite	62.85	36.01	1.75
Akaganeite	55.75	33.83	1.65
Magnetite	72.36	27.64	2.62
Maghemite	69.94	30.06	2.33

Representative SEM micrographs are presented and discussed in Section 6.3.2. In addition, for significant samples from poles at Sites 2, 4 and 5, Appendix A.1 documents photographs of the samples and SEM micrographs in four scales. These SEM micrographs are provided to document the observation of representative iron oxides. In addition, the elemental composition data obtained through EDX analysis (in weight %, or wt%) were used to identify specific iron oxides by comparing the amounts of iron and oxygen as well as their proportion (Fe/O) with well-known indicative values (Table 6.3). To this end, it is noted that the presence of chlorine was also treated as an indicator to identify akaganeite, whose empirical formula can be written as $\beta\text{-FeOOH}$ or $\text{Fe}^{3+}_{7.6}\text{Ni}_{0.4}\text{O}_{6.4}(\text{OH})_{9.7}\text{Cl}_{1.3}$.

The aim is to demonstrate that relevant oxides were identified. However, it is shown that the key practical outcome is that the evidence from SEM/EDX testing is typically incomplete or insufficient to gain a satisfactory insight to assess the corrosion by-products vis-à-vis the results of visual assessment (Chapter 3.0), atmospheric corrosivity (Chapter 4.0), corrosion rate estimates and corrosion potential measurements (Chapter 5.0). This drawback is reasonably attributed to the fact that: (a) it is unrealistic to effectively map the oxide phases in relatively large rust samples by observing only the visible surfaces using a scanning electron microscope; and (b) EDX data only enable one to quantify elements rather than oxide species. These limitations were resolved by resorting to XRD and MS testing, as presented and discussed in Section 6.4.

6.3.2 SEM/EDX Results and Discussion

Representative SEM micrographs from the pack-rust samples collected at Site 2, pack-out samples from Site 4, and fastener rust samples from Site 5 are shown in Figure 6.5 through Figure 6.7. For each micrograph in Figure 6.5 through Figure 6.7, associated EDX results are provided in Table 6.4.

6.3.2.1 Site 2

The microstructure in Figure 6.5a occurred throughout the sample from Pole Q3C-1L but was not observed in the samples from Poles Q3C-2L or Q3C-2R. Based on the position of Pole Q3C-1L in the Pourbaix diagram (Figure 5.8) and the small mass of its sample compared with those of Poles Q3C-2L and Q3C-2R (Table 6.2), the microstructure in Figure 6.5a is most likely goethite or lepidocrocite. Its microstructure consists of peaked, inter-locking particles with random orientations (Figure 6.5a), thus resembling lepidocrocite. The larger and less dense microstructure compared to that in Figure 6.2b

(Antony et al. 2004) may be due in part to the corrosivity of the industrial environment of Site 2 (Table 4.7). The composition includes 60.72 wt% of iron and 30.43 wt% of oxygen (Table 6.4) for a Fe/O ratio of 1.99, which exceeds the Fe/O ratio of 1.75 for lepidocrocite (Table 6.3). Thus, it is reasonable to hypothesize that other iron oxides with higher Fe/O ratios, such as magnetite or maghemite, contribute to the composition of this sample. This hypothesis is consistent with the alternating-band microstructure configuration for WS oxides illustrated in Figure 6.1b (Morcillo et al. 2014).

A substantially different microstructure was observed on the sample collected from Pole Q3C-2L (Figure 6.5b). This microstructure consists primarily of deposits of somewhat round particles with size (diameter) of approximately 1 μm or less. This microstructure is typical of magnetite or maghemite, as seen in Figure 6.2c-d (Topal and Aksan 2016, Mozaffari et al. 2015). The Fe/O ratio from the associated EDX data (showing 64.59 wt% of Fe and 27.97 wt% of O in Table 6.4) is 2.31, which is nearly identical to that of maghemite (Table 6.3). However, one would expect that the sample from Pole Q3C-2L possess more magnetite than maghemite, based on the presence of Pole Q3C-2L in the “Fe²⁺” domain of the Pourbaix diagram (Figure 5.8). In fact, magnetite features Fe²⁺ and Fe³⁺ ions whereas maghemite only features Fe³⁺ ions. This evidence shows that it is difficult to distinguish between the two iron oxides, thereby providing supporting evidence to assess rust composition and related driving mechanisms. To this end, a technique that enables one to identify oxide composition instead of elemental composition becomes necessary. This hypothesis is explored further using XRD analysis, as reported in Section 6.4.

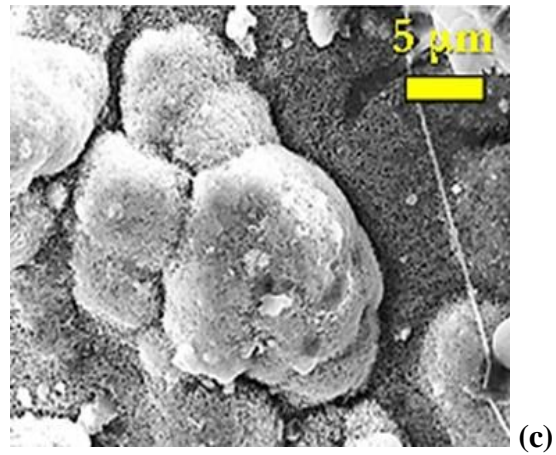
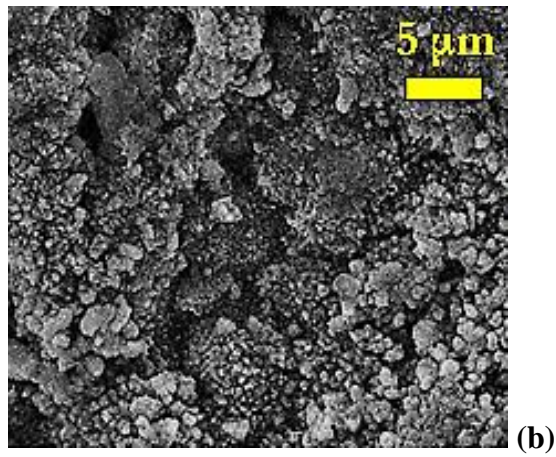
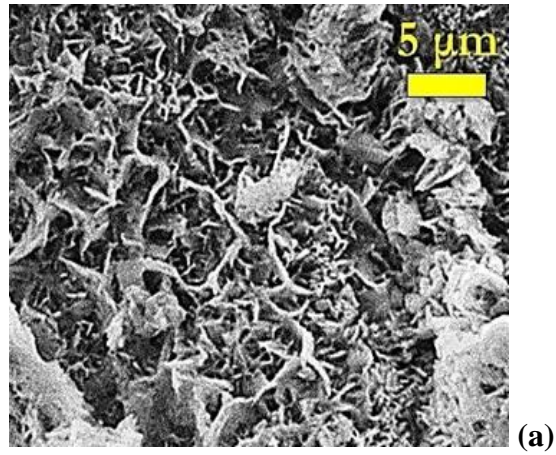


Figure 6.5 SEM micrographs of pack-rust samples collected from coating line region of WS poles at Site 2: (a) Pole Q3C-1L; (b) Pole Q3C-2L; and (c) Pole Q3C-2R.

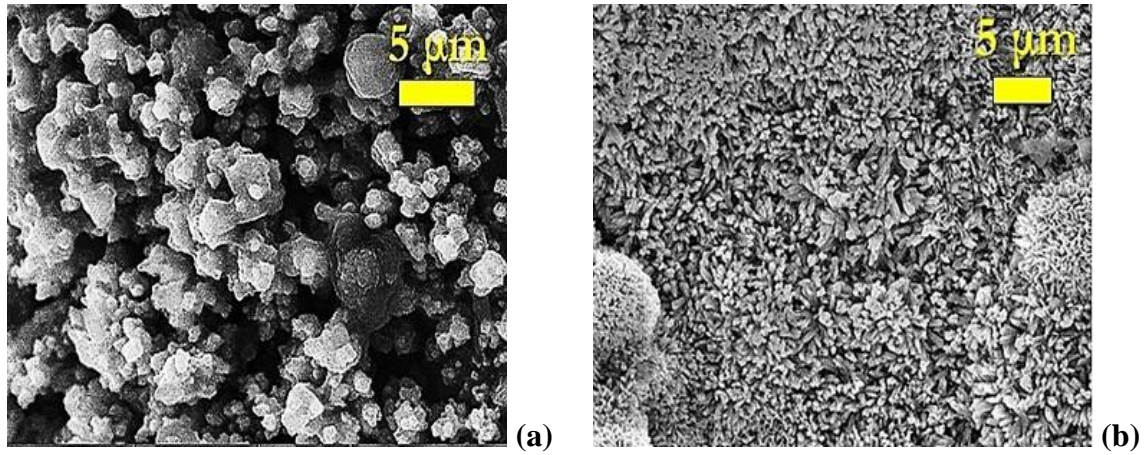


Figure 6.6 SEM micrographs of samples collected from Pole TL-1 at Site 4: (a) outer pack out; and (b) inner pack out.

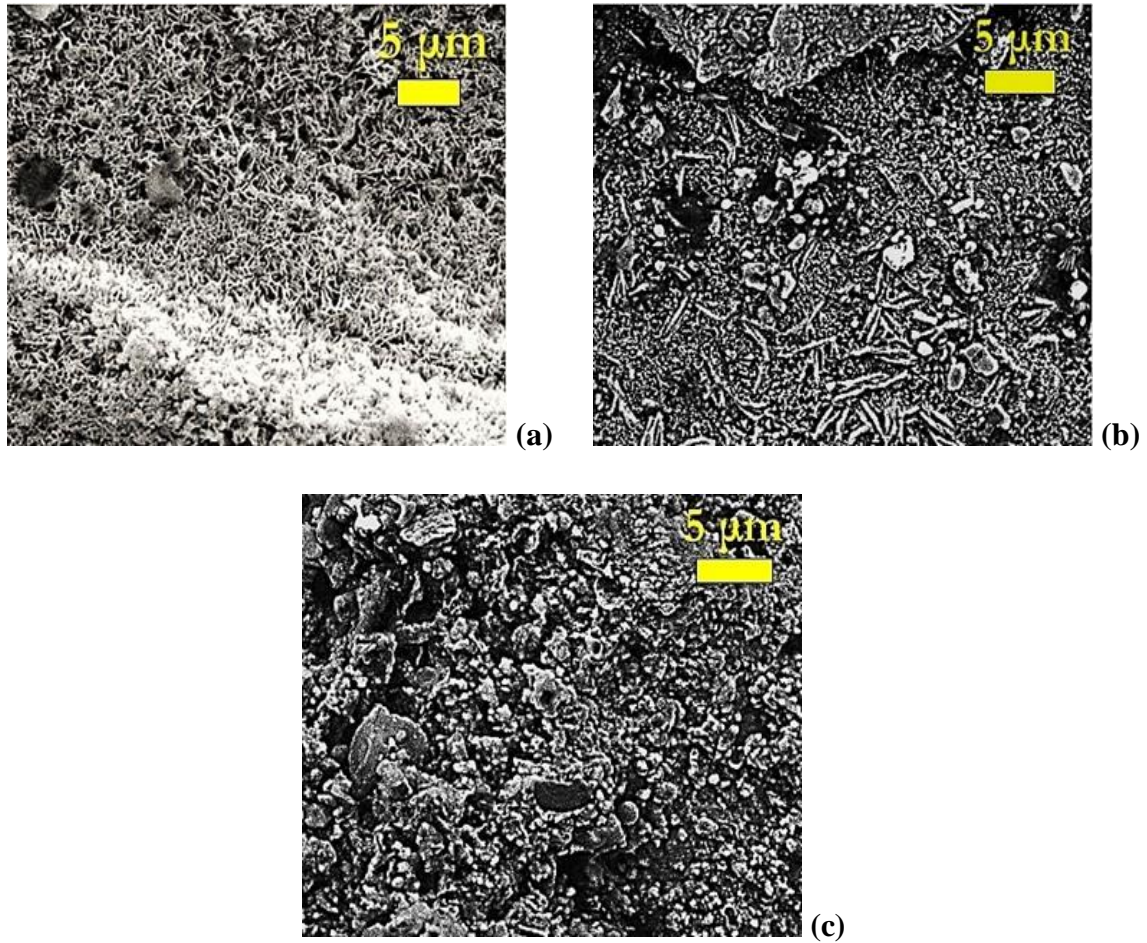


Figure 6.7 SEM micrographs of loose rust samples collected from GS fastener region of WS poles at Site 5: (a) Pole 8Z-2L; (b) Pole 8Z-2R; and (c) Pole 11Z-6R.

Table 6.4 EDX data for solid rust specimens collected from WS poles, including pack-rust samples from Site 2, pack-out samples from Site 4, and loose rust samples from Site 5.

Site		2			4		5		
Pole		Q3C-1L	Q3C-2L	Q3C-2R	TL-1		8Z-2L	8Z-2R	11Z-6R
Source Location		Coating line	Coating line	Coating line	Outer pack out	Inner pack out	GS fasteners	GS fasteners	GS fasteners
Elemental Composition [wt%]	Al	0.44 ± 0.09	-	0.27 ± 0.04	0.51 ± 0.04	0.66 ± 0.10	-	0.72 ± 0.08	0.85 ± 0.09
	C	4.03 ± 0.23	5.14 ± 0.49	6.33 ± 0.25	4.94 ± 0.33	6.12 ± 0.37	5.16 ± 0.34	19.16 ± 0.44	17.76 ± 0.49
	Ca	-	-	-	1.79 ± 0.08	0.54 ± 0.04	-	-	-
	Cl	-	-	0.48 ± 0.04	0.15 ± 0.03	-	-	-	-
	Fe	60.72 ± 0.44	64.59 ± 0.97	55.81 ± 0.44	57.12 ± 0.41	46.58 ± 0.46	64.17 ± 0.44	37.58 ± 0.34	40.24 ± 0.45
	K	0.19 ± 0.03	-	-	-	0.34 ± 0.03	-	0.18 ± 0.03	0.24 ± 0.03
	Mg	-	-	0.27 ± 0.05	0.51 ± 0.04	0.50 ± 0.05	-	0.23 ± 0.05	0.18 ± 0.05
	Mn	1.50 ± 0.09	1.56 ± 0.20	-	3.13 ± 0.19	15.67 ± 0.31	-	1.01 ± 0.14	9.65 ± 0.29
	Na	-	-	-	0.20 ± 0.08	-	-	-	-
	Ni	-	-	-	-	0.71 ± 0.11	-	-	-
	O	30.43 ± 0.25	27.97 ± 0.51	35.63 ± 0.28	30.78 ± 0.25	27.19 ± 0.27	30.37 ± 0.25	37.56 ± 0.35	27.19 ± 0.35
	P	-	-	0.08 ± 0.04	-	-	-	0.23 ± 0.03	-
	S	-	-	0.24 ± 0.04	-	-	-	-	0.23 ± 0.03
Si	2.68 ± 0.09	0.74 ± 0.08	0.89 ± 0.07	0.88 ± 0.06	1.16 ± 0.08	0.30 ± 0.05	1.70 ± 0.07	2.06 ± 0.08	
Zn	-	-	-	-	0.52 ± 0.16	-	1.46 ± 0.27	1.61 ± 0.19	
Total		100	100	100	100	100	100	100	100
[Fe/O]		2.00	2.31	1.57	1.86	1.71	2.11	1.00	1.48

The sample collected from Pole Q3C-2R featured microstructures similar to those of Pole Q3C-2L (Figure 6.5b) but also displayed a peculiar microstructure (Figure 6.5c). This microstructure includes particles with an equivalent diameter of approximately 20 μm , which is compatible with akaganeite (Figure 6.2e). The amounts of iron (55.81 wt%) and oxygen (35.63 wt%) in the microstructure, as well as the associated Fe/O ratio of 1.57 (Table 6.4), also compare favorably with the known values for akaganeite (Table 6.3). This conclusion is corroborated by evidence of presence of chlorides (0.48 wt% in Table 6.4), which can react with magnetite to create akaganeite, thereby hindering the effectiveness of the protective patina (Li et al. 2008). This evidence is important as it suggests that atmospheric chlorides in the vicinity of the potash mine do affect the corrosivity of the industrial atmosphere at Site 2, and are likely to contribute to the pack-out corrosion damage observed near the coating lips of Poles Q3C-2L and Q3C-2L (Figure 3.10b).

6.3.2.2 Site 4

Examination of the outer pack-out sample collected from Pole TL-1 presented evidence of a widespread microstructure (Figure 6.6a) consisting of polygonal particles between 1 and 5 μm in diameter, which did not closely resemble any of the common microstructures shown in Figure 6.2. These particles do tend to form larger deposits that may feature magnetite or maghemite. Instead, the EDX data include an iron content of 57.12 wt% (Table 6.4), which resembles the iron content of akaganeite at 55.75 wt% (Table 6.3). This hypothesis is supported by evidence of presence of chlorides (0.15 wt%). However, the Fe/O ratio is equal to 1.87, which is more consistent with goethite or lepidocrocite. This example of conflicting evidence illustrates how one may not always

identify specific iron oxide species in rust samples based on evidence from SEM/EDX analysis.

The inner pack-out sample collected from Pole TL-1 also possessed a common microstructure (Figure 6.6b) that could not be identified as a specific iron oxide species. This microstructure is primarily comprised of randomly oriented particles, each no bigger than 1 μm long, which is reminiscent of lepidocrocite (Figure 6.2b). Nonetheless, the individual particle shapes are unable to be distinguished on a 5 μm scale and could be goethite, which typically does not exceed 1 μm in diameter (Figure 6.2a). The amounts of iron (46.90 wt%) and oxygen (27.19 wt%) in the microstructure yield an Fe/O ratio of 1.72 (Table 6.4), which compares favorably with the Fe/O ratio for both lepidocrocite and goethite (Table 6.3). However, the specific iron content is lower than any known value in Table 6.3. This is likely due to the relatively large, round microstructures at the left and right fringes of Figure 6.6b, which seem to be mostly manganese, an alloying element for WS (Table 2.1). The amount of manganese in the inner pack-out sample is 15.67 wt% (Table 6.4), five times more than the manganese content of the outer pack-out sample (3.13 wt%). Such a high presence may indicate that manganese helps repel chloride ions, since no chlorine is observed in the inner pack-out sample (Table 6.4).

6.3.2.3 Site 5

SEM micrographs for the solid rust samples collected from the fasteners of Poles 8Z-2R and 11Z-6R are shown in Figure 6.7b-c. The presence of zinc (Table 6.4) confirms that these samples originate from oxidized GS (from the fasteners) and not WS (from the pole structure). Both samples were covered with organic material from the moss-like deposits that can be noted in Figure 3.31b and Figure 3.32a. This organic matter was

pervasive throughout the specimens, including areas where it was not visible without using a microscope. The EDX data reflect the presence of this organic matter. In fact, iron amounts (37.58 wt% for Pole 8Z-2R and 40.24 wt% for Pole 11Z-6R in Table 6.4) are smaller than those of any expected iron oxide or hydroxide (Table 6.3), while the carbon amount (19.16 wt% for Pole 8Z-2R and 17.76 wt% for Pole 11Z-6R) is much larger than that noted in samples from Sites 2 and 4, which lies in the range 4-6.5 wt% (Table 6.4). The formation of organic matter on the steel surface can be facilitated by the high moisture of the environment, which is due to the high TOW (Table 4.5) and water stagnation in the GS caissons (Figure 3.33), and also facilitates the stagnation of detrimental moisture on the surface of the GS fasteners. In this instance, the evidence from SEM/EDX analysis provides some valuable albeit rudimentary insight on the nature of the rust samples.

The sample collected from the fasteners of Pole 8Z-2L exhibited a microstructure (Figure 6.7c) similar to that of the coating line sample from Pole Q3C-1L (Figure 6.5a). This microstructure also consists of peaked particles with random orientations, although these particles are 1 μm or less in size, which is more consistent with the lepidocrocite micrograph in Figure 6.2b (Antony et al. 2004). Additionally, the Fe/O ratio of the microstructure in Figure 6.7c is 2.11. This is comparable to the Fe/O ratio of 2.00 observed for the microstructure in Figure 6.5a (Table 6.3). Such a Fe/O ratio suggests the presence of magnetite and/or maghemite, and there do appear to be slightly round particles interspersed throughout the microstructure in Figure 6.7c. Because the rust sample from Pole 8Z-2L was a by-product of the corrosion of the GS fasteners, it seems that GS with depleted galvanizing (Zn = 0 wt% in Table 6.4) effectively corrodes like WS and/or carbon steel. In fact, only four elements, Fe, O, C and Si, are observed in this microstructure. These

same four elements are also the only ones that are identified consistently for all rust samples (Table 6.4). Thus, it appears that the alloying element Si (Table 6.3) contributes to formation of outermost rust layers on steel in general.

6.4 Quantification of Oxide Composition via XRD and MS Analysis

X-ray diffraction (XRD) and Mössbauer spectroscopy (MS) analysis were enlisted to quantify the iron oxides and hydroxides in powder samples that were collected from each WS pole inspected in Sites 1 through 5 (Table 6.2). The results of XRD analysis are presented and discussed served as the primary means of analysis, are found in Section 6.4.1. The results of MS analysis of significant oxide samples are presented and discussed vis-à-vis the XRD ones in Section 6.4.2. It is noted that MS analysis may enable one to quantify the mass fraction of some iron oxides while taking into account the contribution of nano-sized phases whereas larger (non nano-sized) crystallites can be identified through XRD analysis. This is relevant as larger goethite fractions are indicative of a more protective oxide layer, and part of the goethite can be present as a denser (and thus more protective) nanophase that may be difficult to identify through XRD analysis (Cook 2005). However, MS testing is complex and time-consuming, and requires equipment that is not widely available whereas XRD facilities are relatively common. The results presented in this section are useful to understand whether XRD analysis is sufficient to gain an insight into oxide composition (and thus associated corrosion mechanisms and quality of the patina), or MS analysis is more appropriate.

6.4.1 XRD Methodology

XRD probes crystalline structure at the atomic level to characterize crystalline materials and determine of their structure. Each crystalline solid has a unique characteristic

X-ray powder pattern that can be used as a “fingerprint” for its identification. Once a material has been identified, X-ray crystallography determines the structure (i.e., how the atoms pack together in the crystalline state). The process works by having X-rays bombard a metal target, often copper (Cu) or molybdenum (Mo), with a beam of electrons emitted from a hot filament. The beam will ionize electrons causing X-rays to be emitted.

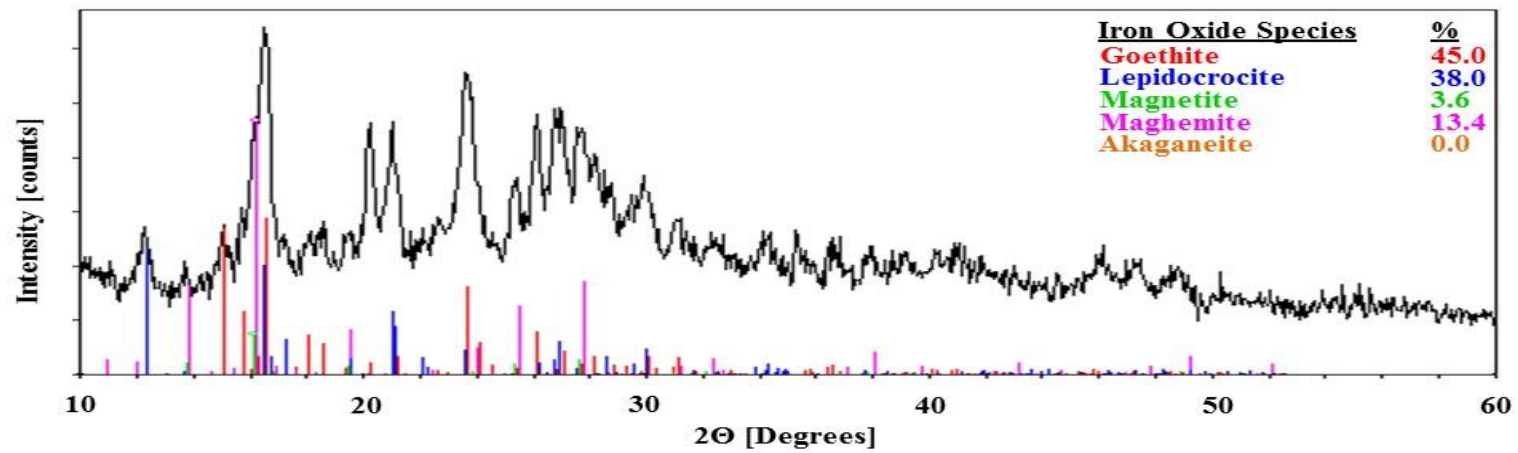
XRD equipment is available at the University of South Carolina. However, it utilizes a Cu target, which can cause complications in the identification of iron-based compounds due to fluorescence effects. Fluorescence effects are due to the fact that iron atoms fluoresce (i.e., emit secondary X-rays) when a copper target is used. Therefore, the author obtained access to suitable XRD equipment (as well as MS equipment, as reported in Section 6.4.3) through the National High Magnetic Field Laboratory. Measurement of powder diffraction patterns were made using an X-ray generator with a Mo target (model RU-H2R, Rigaku, Japan). Scans were performed over a $2\text{-}\Theta$ range of $10\text{-}60^\circ$ degrees using a scanning rate of $2^\circ/\text{min}$ and step width of 0.05° . Goethite ($\alpha\text{-FeOOH}$), lepidocrocite ($\gamma\text{-FeOOH}$), akaganeite ($\beta\text{-FeOOH}$), magnetite (Fe_3O_4), and maghemite ($\gamma\text{-Fe}_2\text{O}_3$) were identified by comparing the most intense peaks of the resulting XRD diffractograms against the Powder Diffraction File (PDF), a database maintained by the International Centre for Diffraction Data (ICDD 2015). It is noted that XRD analysis does not allow for the identification of amorphous or non-crystalline oxide phases. Therefore, the mass ratios estimated via XRD analysis are to be considered as approximate. Their validity is assessed by comparing XRD results on oxide composition with outcomes of field inspections and measurements (Chapters 3.0 through 5.0) in Section 6.4.2, and by comparing mass ratios of samples, as determined via XRD and MS analysis, in Section 6.4.4.

6.4.2 XRD Results and Discussion

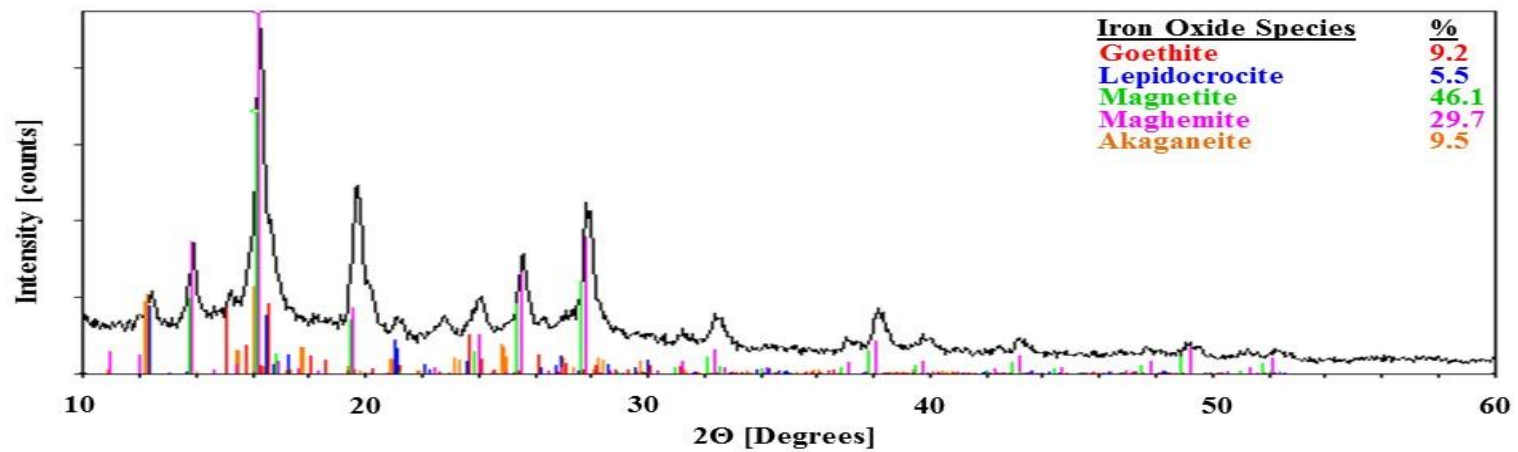
Representative examples of XRD spectra are presented in Figure 6.8, illustrating a best-case scenario (Figure 6.8a) for the powder scraped from the adherent patina on Pole C1F-20 at Site 1 (rural atmosphere) and a worst-case scenario (Figure 6.8b) for the large outer pack-out rust sample from Pole TL-1 at Site 4 (chloride-laden marine atmosphere).

In fact, a large discrepancy between all phase quantifications of these two specimens is noted. Goethite and lepidocrocite each compose over a third of the prior. Both hydroxides are seen to make up less than 10 wt% of the latter. Akaganeite is absent from the Pole C1F-20 sample, while it outnumbers goethite in the Pole TL-1 sample. Magnetite amounts to just 3.6 wt% of the Pole C1F-20 sample but constitutes nearly half of the Pole TL-1 sample.

The XRD spectra for all other samples (Table 6.2) can be found in Appendix A.2. The chemical oxide compositions for all powder specimens as determined by XRD are listed in Table 6.5. It is noted that the pole wall specimen for Pole 11-6L is excluded, as the XRD data collected for this sample only indicated the presence of magnetite and maghemite, likely signifying human error during testing. Compositions are reported as averaged values. Multiple ICDD database entries pertaining to the specific identification of each oxide species were considered, leading to a variety of calculated proportions. Variation can also be seen to occur within an individual specimen's spectrum itself, depending on the sharpness or broadness of the peaks observed. Sharp peaks indicate that a specimen consists of well-crystallized corrosion byproducts, whereas broader peaks suggest a decrease in the crystalline size. Broadened peaks are a signal that certain oxide species may be present that XRD is not capable of diagnosing.



(a)



(b)

Figure 6.8 XRD spectra for: (a) Pole C1F-20 wall sample; and (b) Pole TL-1 outer pack-out rust sample.

Table 6.5 Quantity of iron oxide and hydroxide species determined via XRD analysis.

Site	Pole	Area	Goethite [wt%]	Lepidocrocite [wt%]	Akaganeite [wt%]	Magnetite [wt%]	Maghemite [wt%]
1	C1F-20	Pole wall	45.03 ± 1.01	38.00 ± 0.92	0.00 ± 0.00	3.53 ± 1.59	13.43 ± 1.01
		Reflective tape	37.27 ± 1.00	24.23 ± 1.15	0.00 ± 0.00	15.20 ± 2.63	23.30 ± 3.29
2	Q3C-1L	Pole wall	23.07 ± 0.40	31.27 ± 0.15	19.10 ± 0.46	19.67 ± 0.55	6.90 ± 0.61
		Coating line	17.60 ± 0.75	12.73 ± 4.03	0.00 ± 0.00	41.47 ± 7.03	28.20 ± 8.99
	Q3C-1R	Pole wall	20.60 ± 2.07	34.27 ± 0.49	17.33 ± 3.04	18.80 ± 2.46	9.00 ± 2.91
	Q3C-2L	Pole wall	28.93 ± 0.40	24.90 ± 0.10	22.87 ± 0.31	12.13 ± 1.11	11.17 ± 1.07
		Coating line	14.40 ± 0.00	0.00 ± 0.00	0.00 ± 0.00	58.40 ± 0.00	27.20 ± 0.00
	Q3C-2R	Pole wall	24.10 ± 0.17	30.00 ± 0.53	28.07 ± 1.40	12.63 ± 0.47	5.20 ± 1.44
Coating line		8.60 ± 0.69	0.00 ± 0.00	3.97 ± 0.21	82.67 ± 2.94	4.77 ± 3.72	
3	S3B-2L	Pole wall	33.50 ± 0.00	42.10 ± 0.00	0.00 ± 0.00	24.40 ± 0.00	0.00 ± 0.00
	S3B-3L	Pole wall	42.53 ± 0.06	35.70 ± 0.00	0.00 ± 0.00	18.47 ± 0.06	3.30 ± 0.00
	S3B-7L	Pole wall	47.10 ± 0.00	30.87 ± 0.06	0.00 ± 0.00	13.83 ± 0.06	8.20 ± 0.00
	S3B-7R	Pole wall	35.40 ± 0.10	32.27 ± 0.06	0.00 ± 0.00	20.43 ± 0.38	11.90 ± 0.35
4	TL-1	Pole wall	29.17 ± 1.11	35.33 ± 1.55	16.73 ± 2.29	11.93 ± 1.70	6.83 ± 2.18
		Outer pack out	9.20 ± 0.70	5.43 ± 0.06	9.53 ± 2.48	46.13 ± 2.47	29.70 ± 1.97
		Inner pack out	21.30 ± 0.00	11.50 ± 0.00	0.00 ± 0.00	34.10 ± 0.00	33.10 ± 0.00
		Pit (Figure 3.20b)	29.20 ± 2.98	10.23 ± 0.21	11.37 ± 0.06	33.93 ± 4.41	15.27 ± 1.80
5	8Z-2L	Pole wall	34.07 ± 0.06	51.20 ± 0.17	0.00 ± 0.00	4.33 ± 0.06	10.40 ± 0.17
		GS fasteners	27.00 ± 2.69	14.07 ± 0.68	0.00 ± 0.00	43.83 ± 7.97	15.10 ± 10.8
	8Z-2R	Pole wall	30.80 ± 0.00	58.10 ± 0.00	0.00 ± 0.00	1.40 ± 0.00	9.70 ± 0.00
		GS fasteners	27.43 ± 0.84	16.70 ± 1.73	0.00 ± 0.00	46.80 ± 1.95	9.07 ± 0.92
	11Z-2L	Pole wall	39.60 ± 0.00	36.50 ± 0.00	0.00 ± 0.00	9.00 ± 0.00	14.90 ± 0.00
	11Z-2R	Pole wall	38.70 ± 0.46	42.20 ± 0.52	0.00 ± 0.00	7.17 ± 0.25	11.93 ± 0.29
	11Z-6R	Pole wall	35.30 ± 0.82	39.07 ± 0.15	0.00 ± 0.00	20.17 ± 0.71	5.47 ± 0.78
		GS fasteners	25.30 ± 0.00	14.40 ± 0.00	0.00 ± 0.00	44.50 ± 0.00	4.80 ± 0.00

Examination of Table 6.5 allows one to distinguish between the patina and damaged rust forms within individual structures and also compare the compositions observed for several structures at a single test site. Likewise, comparative observations can also be made between the sites themselves.

6.4.2.1 Site 1

Two samples were considered for Pole C1F-20, including a patina sample and a pack-rust sample from the tape section in Figure 3.5b. The pack-rust sample possesses less goethite (37.27 wt%) and lepidocrocite (24.23 wt%), and more magnetite (15.20 wt%) and maghemite (23.30 wt%), compared to the adherent patina sample (45.03, 38.00, 3.53 and 13.43 wt%, respectively). These values reflect the quality of these oxides as highlighted through visual assessment (Section 3.1). However, both samples display a relatively large presence of goethite. In fact, the mass ratio of goethite in the pack-rust sample exceeds that of 10 of the 15 pole patina samples examined (Table 6.2). This result suggests that the pack-rust damage that occurred on Pole C1F-20 due to the use of a reflective tape (Figure 3.5b) is of limited concern although it requires remediation. Thus, the position of Pole C1F-20 in the Pourbaix diagram (Figure 5.8) may be indicative of passivation or immunity, which is likely facilitated by the exposure to a low-corrosivity environment for WS (Table 5.2).

6.4.2.2 Site 2

The patina sample from Pole Q3C-2L possesses more goethite (28.93 wt%) and less lepidocrocite (24.90 wt%) than those from the other WS poles at Site 2. Of these four specimens, Pole Q3C-1R exhibits the lowest ratio of goethite (20.60 wt%) and highest ratio of lepidocrocite (34.27 wt%). The larger mass ratio of goethite in the patina of Pole Q3C-

2L is consistent with the slightly lower (i.e., better) corrosion potential than Poles Q3C-1L and Q3C-1R (Table 5.5). In fact, while Poles Q3C-1L and Q3C-1R lie at the boundary between the unstable “Fe²⁺” domain and the passivation [Fe(OH)₃] region of the Pourbaix diagram (Figure 5.8), the fact that these WS poles are located close to the potash mine at Site 2 makes it unlikely to form a protective patina with more goethite (i.e., transitioning into the [Fe(OH)₃] region over time). This consideration is consistent with the recommendation to re-examine and correct the currently inadequate cathodic protection, as discussed in Section 5.2.3.1.

It is also noted that the patina samples from the WS poles at Site 2 display higher levels of goethite and lepidocrocite and lower levels of magnetite than the pack-out rust samples collected from the coating line of the same poles (Figure 3.10). The pack-out rust samples from Poles Q3C-2L and Q3C-2R do not feature lepidocrocite while the sample from Pole Q3C-1L features a lepidocrocite mass ratio of only 12.73 wt%. This composition can be explained because lepidocrocite may exist as part of outer rust layers as illustrated in Figure 6.1 (Morcillo et al. 2014), which can be partially or fully removed as the coating peels away from the pole surface.

A remarkable outcome is the presence of akaganeite in five of the seven oxide samples collected at Site 2. In fact, this evidence suggests that atmospheric chlorides produced from the process of potash refinement contribute to the atmospheric corrosivity of Site 2, and to the corrosion damage of the WS poles. In addition, these XRD results illustrate the importance of using a suitable test method to recognize the influence of chloride contamination. In fact, no chloride depositions were found by swab-testing (Table 4.6), which is likely due to the fact that chloride ions rapidly react with the iron oxides in

WS (Asami and Kikuchi 2003), as noted in Section 4.1.7. The fact that akaganeite is missing from the pack-out rust samples collected at the coating line of Poles Q3C-1L and Q3C-2L) is reasonably attributed to the fact that akaganeite tends to form in the outermost rust layers on WS (Cano et al. 2014), and could have been stripped away as the coating delaminated. The greatest ratio of akaganeite was found on Pole Q3C-2R (28.07 wt%), which suggests that chloride contamination is not necessarily more severe for the poles located closer to the potash mine. Magnetite is present in much higher quantities in the pack-out rust samples (≥ 41.47 wt%) than in the patina samples (≤ 19.67 wt%), suggesting that the mass ratios of magnetite and akaganeite are negatively correlated, in agreement with Asami and Kikuchi (2003). In addition, greater amounts of maghemite also tend to form in pack-out rust as noted for the sample from Pole Q3C-1L, which displays the highest ratio of maghemite (28.20 wt%) at Site 2.

6.4.2.3 Site 3

The patina sample from Pole S3B-7L exhibits the highest goethite mass ratio (47.10 wt%) and the lowest lepidocrocite mass ratio (30.87 wt%) of all samples collected at Site 3. The patina samples from Pole S3B-3L also contain a significant amount of goethite (42.53 wt%), suggesting that a longer exposure to suitable environments facilitates the conversion of lepidocrocite into goethite (Wang et al. 1996), thereby enhancing corrosion resistance. In fact, the 28-year old WS poles at Site 3 are the oldest inspected in Sites 1 through 5. While Pole S3B-7R exhibits a smaller ratio of goethite (35.40 wt%) than the companion Pole S3B-7L, both poles feature adequate cathodic protection (Table 5.5), suggesting that both patinas are sufficiently protective.

The benefit of using WS is apparent for Pole S3B-3L (Table 4.7), for which the exposure to a mild environment seems to facilitate the formation of a protective patina despite the inadequate cathodic protection (Table 5.5). However, under these exposure conditions, other factors may contribute to hindering the formation of a protective patina. For example, different from Pole S3B-3L, Pole S3B-2L exhibits the lowest ratio of goethite (33.50 wt%) and the highest ratio of lepidocrocite (42.10 wt%) of the four patina samples collected at Site 3. In fact, Pole S3B-2L is the only structure at Site 3 that features less goethite than lepidocrocite, as well as more magnetite and less maghemite than the other WS poles at Site 3. In Section 5.2.3.1, stray-current corrosion was proposed as a reasonable explanation for the relatively high corrosion rate (Table 5.2) and poor corrosion potential (Table 5.5) of Pole S3B-2L, and may also affect this particular patina composition.

6.4.2.4 Site 4

The XRD oxide composition results for Pole TL-1 are consistent with the position in the middle of the “Fe²⁺” domain of the Pourbaix diagram (Figure 5.8), indicating susceptibility to corrosion damage. None of the four samples collected from Pole TL-1 (Table 6.2) exhibit goethite ratios of 30 wt% or greater. The patina sample is the only one that features less goethite (29.17 wt%) than lepidocrocite (35.33 wt%). This sample also exhibits the highest fraction of akaganeite (16.73 wt%) as well as the lowest fractions of magnetite (11.93 wt%) and maghemite (6.83 wt%). Interestingly, all four samples collected from Site 2 contain more akaganeite (≥ 17.33 wt%) than the patina sample from Pole TL-1. Somewhat surprisingly, these results suggest that it is possible that the chloride contamination attributed to the vicinity to the potash mine and processing facility at Site 2 yields more severe corrosion damage than that due to the proximity to saltwater. However,

the combination of chloride contamination and high-TOW at Site 4 (Table 4.7), together with the older age of Pole TL-1, determined a more visible damage (Table 3.2) and corrosion rates (Table 5.2 and Table 5.3). This comparison between Site 2 and Site 4 highlights the importance of carefully assessing atmospheric corrosivity near industrial facilities (which may appear less obvious than in marine environments) to inform decision making for planning and prioritizing routine inspections.

The two pack-out rust samples that were collected from the outer and inner layers (Figure 3.21a-c) exhibit notable dissimilarities. The outer pack-out rust sample features the lowest goethite fraction (9.20 wt%) and the lowest lepidocrocite fraction (5.43 wt%) of all samples from Pole TL-1, and includes akaganeite (9.53 wt%). The inner rust pack-out sample possesses mass ratios of goethite (21.30 wt%) and lepidocrocite (11.50 wt%) that are more than double those of the outer pack-out rust sample, and is the only sample from Pole TL-1 where akaganeite was not detected. These XRD data suggest that chloride penetration is mitigated at some point, albeit without beneficial effects on corrosion protection. In addition, areas that facilitate moisture retention and water stagnation (e.g., the junction box in Figure 3.21a-c) remain susceptible to pack-out corrosion damage.

The oxide sample from the pit shown in Figure 3.20b, which faces the ocean, features a comparable mass ratio of akaganeite (11.37 wt%) to that of the outer pack-out rust sample (9.53 wt%), which was collected from an area opposite the ocean. However, the pit sample features more goethite (29.20 wt%) than any other sample collected from Pole TL-1, which is consistent with the fact that corrosion damage is far less severe than that at the junction box (Figure 3.21a-c), where the outer pack-out rust sample includes only 9.20 wt% of goethite.

6.4.2.5 Site 5

The patina samples collected from the WS poles at Site 5 exhibit mass ratios of goethite in the range 30.80-39.60 wt% whereas the range for the GS fastener samples is 25.30-27.43 wt%. In particular, the recently remediated Poles 11Z-2L and 11Z-2R exhibit relatively high mass ratios of goethite (39.60 wt% and 38.70 wt%, respectively). This result reinforces the conclusion that adequate cathodic protection (Table 5.5) contributes to the formation of goethite in these poles, highlighting the effectiveness of the remediation measures described in Section 3.5 (Figure 3.35).

It is also noted that the patina samples exhibit much higher ratios of lepidocrocite (≥ 36.50 wt%) than the GS fastener samples (≤ 16.70 wt%). In fact, the patina samples from Poles 8Z-2L and 8Z-2R exhibit larger mass ratios of lepidocrocite than any other pole inspected (51.20 wt% and 58.10 wt%, respectively). It is possible that these relatively large lepidocrocite contents are associated with the galvanic activity in these poles, which is reflected in the severe corrosion damage of the GS fasteners (Figure 3.32) (that act as unintended sacrificial elements). The GS fastener samples feature significantly lower mass ratios of lepidocrocite (14.07-16.70 wt%) and significantly higher mass ratios magnetite (43.83-46.80 wt%) than those of the patina samples (36.50-58.10 wt% and 1.40-20.17 wt%, respectively), further highlighting the severity of the galvanic corrosion in the GS.

It is important to note that no akaganeite was detected in any of the oxide samples from Site 5. This finding suggests that chlorides from the coast may not reach locations more than 10 miles inland. Furthermore, this finding corroborates the outcome from visual assessment (Section 3.7) and atmospheric corrosivity assessment (Section 4.1) that more

research is needed to understand practical cut-off distances from saltwater where the use of WS should be discouraged.

6.4.2.6 General Composition Observations

The following observations are noted by examining the breakdown of all 25 oxide sample compositions in Table 6.5.

- Sixteen samples exhibit higher quantities of goethite than lepidocrocite. The other nine samples were collected from WS pole walls (i.e., patina). All ground-up solid (i.e., pack rust or pack-out rust) samples exhibited more goethite than lepidocrocite. In fact, two pack-out samples, which were collected from the coating line regions of Poles Q3C-2L and Q3C-2R, do not feature lepidocrocite. This indicates that a basic comparison of the ratio of goethite to lepidocrocite is insufficient to understand oxide quality on WS poles.
- Eight samples include akaganeite. These samples were collected from Sites 2 and 4, indicating that both the potash mine and processing facility at Site 2, and the saltwater environment at Site 4, generate chlorides that contribute to atmospheric corrosivity and corrosion damage on WS poles. From a practical standpoint, this finding highlights the importance of assessing atmospheric corrosivity also near industrial facilities to inform decision making for planning and prioritizing routine inspections.
- Nineteen samples exhibit higher values of magnetite than maghemite, and one sample collected from Pole S3B-2L does not include maghemite. Maghemite exceeded magnetite only at the rural environments of Site 1 (for both patina and pack-rust oxide samples) and Site 5 (for the patina samples of four out of five

WS poles). Considering that more SO₂ may be present in the atmosphere at Site 3 (attributed to the vicinity to the coal mines and power station) compared to the sulfate levels estimated via swab testing (Table 4.6), it is reasonable to expect that a lack of atmospheric contaminants facilitates the transformation of magnetite into maghemite as opposed to other forms. For example, magnetite can become akaganeite when WS is exposed to chlorides (Li et al. 2008).

- Certain oxide samples, especially those collected from damaged areas (e.g., coating line of Pole Q3C-1L, GS fasteners of Pole 8Z-2L), display significant variability in the mass ratios of magnetite and maghemite. In fact, standard deviations up to 7.97 wt% and 10.8 wt% were obtained for magnetite and maghemite, respectively, whereas the maximum standard deviation of 4.03 wt% was obtained for the other oxide species. These data suggest that magnetite and maghemite may be confused when performing XRD analysis, since these oxides share a similar microstructure (Yamashita et al. 1998). Hematite (α -Fe₂O₃), which was not considered during XRD spectra analysis because it is infrequently encountered in WS (De la Fuente et al. 2011), also possesses a composition similar to maghemite. With regard to XRD testing and analysis, more research is needed to differentiate between magnetite, maghemite, and hematite in WS oxides, and understand their correlation (if any) with quality of the patina, corrosion damage, service environment, and exposure conditions.

6.4.3 MS Methodology

MS is a practice that makes use of the resonant emission and absorption of gamma-ray photons by atomic nuclei in a solid without energy loss due to nuclear recoil. The

energy levels of an atomic nucleus are agitated by way of exchanges with its immediate surroundings. Through measurement of these minute fluctuations in the energies of nuclear levels, MS makes it possible for atomic nuclei to serve as probes for defining the proximate molecular environment.

All samples investigated by MS contained 10-30 mg of finely ground rust powder dispersed in an inert eicosane matrix. Temperature-dependent spectra were considered at 4.2 K, 100 K, 150 K, 200 K, and room temperature (RT). These spectra were recorded using a Mössbauer spectrometer equipped with a Janis 8DT Super Varitemp cryostat, which was outfitted with an 8 T superconducting magnet. The spectrometer was operated in a constant acceleration mode, used a ~100 mCi $^{57}\text{Co}(\text{Rh})$ source, and allowed for applied fields parallel to the observed γ -radiation. Isomer shifts are quoted against the centroid of a room-temperature spectrum recorded for a standard iron metal foil. Mössbauer spectral simulations were performed using WMOSS software and relied on using both the spin-Hamiltonian formalism and the Voigt-based model of assessing hyperfine field distributions developed by Rancourt et al. (1991).

Each Mössbauer spectrum was analyzed using the hyperfine field distribution (HFD) model developed by Rancourt et al. (1991). In the absence of dynamic effects, this approach allows for a distribution of hyperfine splitting parameters with an arbitrary shape to be described in terms of a discrete sum of individual Gaussian components. Each HFD component is described by three parameters, including a mass ratio (in wt%), and z (in kG) and dz (in kG) that denote the centroid and width of the Gaussian HFD, respectively. In addition, several parameters were needed to describe the elemental sextet spectra comprising the HFD, including: Γ (in mm/s), the full width at half maximum (FWHM) of

the intrinsic Lorentzian line shape; δ (in mm/s), the isomer shift; Δ (in mm/s), the electric field gradient (EFG) tensor component along the internal field. A representative example of ^{57}Fe Mössbauer spectra constructed using these parameters at different temperatures (in K) is presented in Figure 6.9.

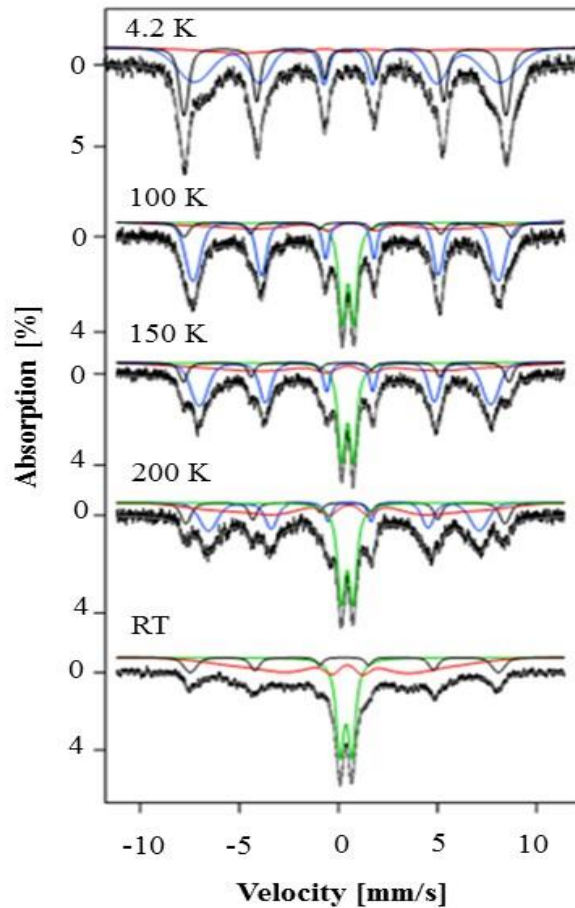


Figure 6.9 ^{57}Fe Mössbauer spectra for pack-rust sample from reflective tape of Pole C1F-20 at Site 1.

MS analysis was performed on five oxide samples, one from each test site. These five samples were selected because they are representative of a wide range of atmospheric and exposure conditions observed in the field. These samples were collected from underneath the reflective tape of Pole C1F-20 (Site 1), the coating line of Pole Q3C-2L

(Site 2), the pole wall (patina) of Pole S3B-2L (Site 3), the inner pack-out rust of Pole TL-1 (Site 4), and a GS fastener of Pole 8Z-2L (Site 5). In addition to the Mössbauer spectra presented in Figure 6.9, Appendix A.3 documents the complete set of Mössbauer spectra, and the associated data that support their construction).

6.4.4 *MS Results and Discussion*

The Mössbauer spectra recorded for the five oxide samples at RT exhibit an intense quadrupole doublet superimposed on a broad, sextet spectral component. The observation of hyperfine-split, six-line spectra for oxide samples magnetically ordered at RT is indicative of the presence of iron oxides. For the five samples analyzed, a comparison of Mössbauer spectra acquired at 4.2 K and at RT is presented in Figure 6.10 where the solid red lines overlaid on the experimental data (in black) are spectral simulations. While the simulations of the 4.2 K spectra provide the best estimates of the relative ratio of iron oxides present in these samples, those of the RT spectra yield most information about distribution with respect to particle sizes. Regardless of the sample considered, as the temperature is lowered the relative intensity of the central doublet decreases and that of the hyperfine split component increases such that, at 4.2 K, only the latter component is observed. This behavior is typical of magnetic nanoparticles and is associated with the presence of a superparamagnetic relaxation regime. Large portions of goethite can occur as superparamagnetic (<15 nm) particles, depending on environmental conditions (Cook 2005).

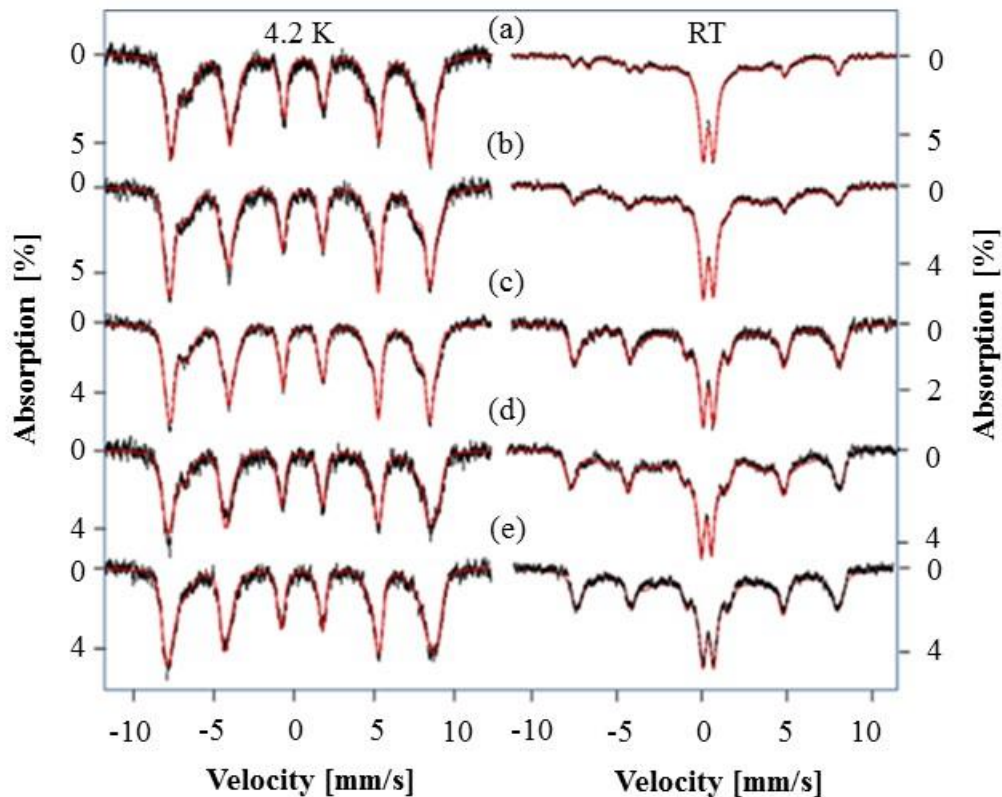


Figure 6.10 ^{57}Fe Mössbauer spectra for WS oxide samples from: (a) Pole S3B-2L; (b) Pole C1F-20; (c) Pole Q3C-2L; (d) Pole 8Z-2L; and (e) Pole TL-1.

Thus, the flip rate of the magnetic moment, or the relaxation of the magnetization of an individual nanoparticle, is shown to be temperature-dependent and is determined by the magnetic anisotropy of the respective nanoparticle. In turn, the magnetic anisotropy of a nanoparticle is proportional to its volume. Consequently, for a collection of nanoparticles of different sizes, one observes a distribution in relaxation rates. Nanoparticles for which the relaxation is fast, when compared to the nuclear Larmor precession of ^{57}Fe nuclei, yield a spectrum for which the averaged magnetic hyperfine interactions appear as a quadrupole doublet. Conversely, nanoparticles with a slow relaxation are observed as hyperfine split, sextet spectra (Greenwood 2012).

The relative ratio of different iron oxides present in the powder samples was determined from the simulations of the spectra recorded at 4.2 K. At this temperature, no quadrupole doublet is observed, which allows one to conclude that the relaxation rate of the magnetization of all iron-containing nanoparticles is slow regardless of their size. Therefore, the spectra observed at 4.2 K are essentially free of relaxational effects. Furthermore, the individual spectral components were determined by taking the difference between appropriate spectra recorded at various temperatures. This procedure is illustrated in Figure 6.11. The difference spectrum demonstrates that by cooling the sample from 180 K to 4.2 K, the spectral component associated with nearly 30% of the iron is converted from a quadrupole doublet to a six-line pattern).

By taking the difference between the spectra recorded for the patina sample from Pole S3B-2L at 4.2 and 180 K, the spectral component associated with goethite was isolated. Both the superparamagnetic behavior and the parameters obtained for this sextet demonstrate that this component originates from goethite nanoparticles (Cook et al. 1999). The spectral component of lepidocrocite was determined in a similar fashion to that of goethite, essentially by comparing spectra recorded at different temperatures and by comparing the various spectral components with published spectra. One of the major difficulties associated with this analysis is that the low-temperature magnetic behavior of iron oxides is complicated, leading to a considerable variation in the numbers between different reports (Murad 1996).

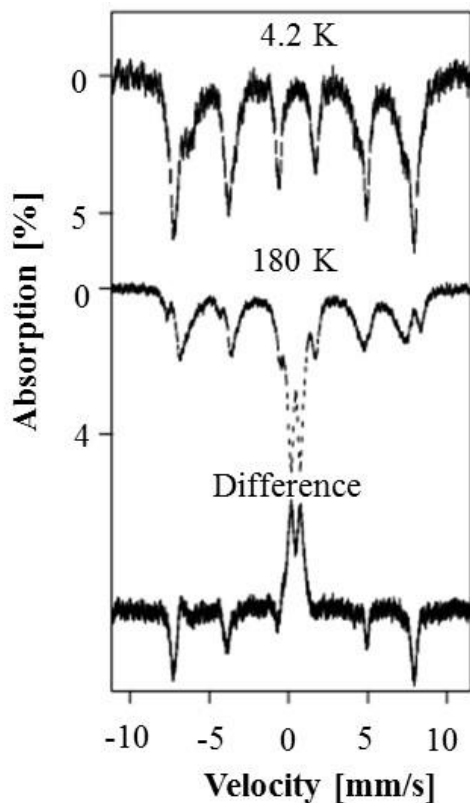


Figure 6.11 ^{57}Fe Mössbauer spectra for pole wall sample from Pole S3B-2L at 4.2 K and 180 K, and difference between spectra at 4.2 K and 180 K.

The analysis of the RT spectra enables one to extract information on the particle size distribution as well as to establish a lower bound for the relative fractions of magnetite and maghemite. These two oxides exhibit ordering temperatures of 850 and 950 K, respectively. These quantities are considerably larger than RT (~ 293 K), and thus nearly all particle sizes and accessible experimental conditions will exhibit hyperfine split spectra. Considering the 4.2 K spectra, approximate amounts of each iron oxide and hydroxide species were determined for the five samples that were investigated by means of MS. These MS-quantified compositions, as well as the associated XRD-quantified compositions for the five samples (Table 6.5), are presented in Table 6.6.

Table 6.6 Mass ratio of iron oxide species determined through MS and XRD analysis.

Pole	Area	Goethite [wt%]	Lepidocrocite [wt%]	Magnetite [wt%]	Maghemite [wt%]
MS					
C1F-20	Reflective tape	42 ± 4	26 ± 4	10 ± 4	14 ± 4
Q3C-2L	Coating line	42 ± 4	26 ± 4	10 ± 4	14 ± 4
S3B-2L	Pole wall	60 ± 4	30 ± 4	10 ± 4	0 ± 4
TL-1	Inner pack out	37 ± 4	20 ± 4	3 ± 4	40 ± 4
8Z-2L	GS fasteners	37 ± 4	20 ± 4	3 ± 4	40 ± 4
XRD					
C1F-20	Reflective tape	37.27 ± 1.00	24.23 ± 1.15	15.20 ± 2.63	23.30 ± 3.29
Q3C-2L	Coating line	14.40 ± 0.00	0.00 ± 0.00	58.40 ± 0.00	27.20 ± 0.00
S3B-2L	Pole wall	33.50 ± 0.00	42.10 ± 0.00	24.40 ± 0.00	0.00 ± 0.00
TL-1	Inner pack out	21.30 ± 0.00	11.50 ± 0.00	34.10 ± 0.00	33.10 ± 0.00
8Z-2L	GS fasteners	27.00 ± 2.69	14.07 ± 0.68	43.83 ± 7.97	15.10 ± 10.8

The following observations are made based on the quantification of iron oxide and hydroxide species via MS analysis, and comparison with the sample compositions estimated via XRD analysis.

- MS analysis yield goethite ratios that are higher for every sample compared to XRD analysis, indicating that MS is better suited to identify superparamagnetic (i.e., nanoscale) variations of goethite. Because goethite enhances the corrosion resistance of WS, the identification of superparamagnetic goethite via MS might aid in defining the quality of WS oxides.
- The patina sample from Pole S3B-2L (Site 3) displays the largest ratio of goethite (60 wt%) among the five samples subject to MS analysis. This mass ratio is significantly larger than that estimated via XRD analysis (33.50 wt%). Because the Pole S3B-2L sample was collected from a relatively adherent

patina (Table 6.2), this sample is likely to contain nanoscale goethite. It is reasonable to expect that higher ratios of goethite for patina samples that were collected from poles with lower corrosion rates than Pole S3B-2L (Table 5.2).

- The samples from Pole TL-1 (Site 4) and Pole 8Z-2L (Site 5), which come from severely damaged areas, exhibit a more limited increase in goethite mass ratio (~10-15 wt%) when using MS instead of XRD estimates. These results are consistent with the expectation that less nanoscale goethite is present in WS samples from more heavily corroded areas.
- It is noted that the samples from Pole Q3C-2L and Pole C1F-20 exhibit the lowest (14.40 wt%) and highest (37.27 wt%) XRD-based ratios of goethite of the five samples in Table 6.6. Conversely, these samples feature a similar ratio of goethite based on MS analysis. Considering the atmospheric corrosivity (Table 4.7) and the mass of each oxide sample (Table 6.2), the sample from Pole C1F-20 likely possesses more goethite than the sample from Pole Q3C-2L, making the XRD-based estimates more plausible.
- Similar to goethite mass ratios, lepidocrocite mass ratios generally increase when considering MS instead of XRD estimates. In fact, the increase in lepidocrocite ratio for the samples from Poles C1F-20, Q3C-2L, TL-1, and 8Z-2R are somewhat proportional to the goethite increases observed for these same specimens. These estimates suggest that nanoscale lepidocrocite phases may also form.
- Magnetite may be underestimated through MS analysis or overestimated through XRD analysis. The average discrepancy between the two methods for

this oxide is calculated to be 28 wt%. More research may be needed to clarify the role of magnetite in WS oxide compositions, which is less discussed in the literature with respect to goethite and akaganeite (Morcillo et al. 2013).

- Both the MS and XRD data indicate that no maghemite is present in the patina sample from Pole S3B-2L. With respect to XRD analysis, MS analysis yields decreased mass ratios of maghemite for the other samples from the sites in Canada (Poles C1F-20 and Q3C-2L), and increased mass ratios for the samples from the sites in Florida (Poles TL-1 and 8Z-2L). This might reflect the different WS compositions for each region (Table 2.1), or an effect of the exposure to consistent humid environments (Table 4.5) resulting in the formation of more maghemite.
- Based on the MS and XRD data, no akaganeite was detected in any of the five oxide samples in Table 6.6. This finding suggests that akaganeite tends to form on outer oxide layers, since the samples from Pole Q3C-2L and Pole TL-1 originate from more interior rust layers. From a practical standpoint, it is important to carefully select the oxide samples for laboratory analysis if the objective is to assess the presence of akaganeite as a result of chloride contamination.
- Based on the MS data, the composition of the rust sample from a GS fastener of Pole 8Z-2L is similar to that of the inner pack-out rust sample from Pole TL-1. Likewise, the mass ratios estimated for the sample from Pole C1F-20 are similar to those of the sample from Pole Q3C-2L. These seemingly unrealistic results indicate that more MS tests are needed to disambiguate the mass ratio

values. Instead, as discussed in Section 6.4.2, XRD analysis consistently yielded reasonable oxide composition estimates, despite the unsuitability to estimate nanoscale fractions. Therefore, XRD data were used to verify a modified “protective ability index” for oxide samples collected in the field, as discussed in Section 6.5.

6.5 Modified Protective Ability Index

From a practical standpoint, an important objective of performing XRD and MS tests was to gain quantitative data to determine a protective ability index (PAI) based on the oxide mass ratios. In particular, this index would serve to describe the quality (protectiveness) of the WS surface patina. As discussed in Section 6.1, Kamimura et al. (2006) first introduced a PAI, denoted as α/γ^* (where α = cumulative mass ratio of protective oxide species, and γ^* = cumulative mass ratio of non-protective oxide species), which is defined as:

$$\alpha/\gamma^* = \frac{P_\alpha}{P_\gamma + P_\beta + P_M} \quad (6-1)$$

where p_α is the mass ratio of goethite, p_γ is the mass ratio of lepidocrocite, p_β is the mass ratio of akaganeite, and p_M is the mass ratio of magnetite. Based on Equation 6-1, protective oxide samples are expected to exhibit $\alpha/\gamma^* > 1$ (Kamimura et al. 2006). Here, goethite alone is credited for the stability and adherence of the protective patina on WS surfaces, reflecting the consideration that the ratio of goethite to lepidocrocite in WS increases with exposure time (Yamashita et al. 1994) under favorable conditions. Because goethite is a stable hydroxide that characterizes protective patinas, lepidocrocite is considered as “detrimental” until it transforms into goethite. However, based on the XRD results

summarized in Table 6.5, a smaller fraction of goethite than of lepidocrocite is not necessarily associated with poor oxide quality, as noted in Section 6.4.2.6. In fact, relatively large mass ratios of lepidocrocite have not been shown to detract from the quality of WS rust layers (Morcillo et al. 2014), and lepidocrocite may transform into goethite over extended periods of time (Wang et al. 1996). Thus, it cannot be excluded that lepidocrocite may contribute to the corrosion resistance of WS. Furthermore, Equation 6-1 neglects the effects of maghemite on oxide quality, reflecting the difficulty in distinguishing maghemite from magnetite posed by XRD analysis (Kamimura et al. 2006), as discussed in Section 6.4.2.6.

6.5.1 Definition

As part of this project, the author defined a modified PAI for use with XRD data, and verified it based on evidence collected from the WS poles inspected. The aim was to offset the shortcomings of Equation 6-1 (Kamimura et al. 2006), and obtain PAI values that are more realistic and thus representative of the findings from visual assessment (Section 3.6, Table 3.2) and atmospheric corrosivity assessment (Section 4.1, Table 4.7). The modified PAI, denoted as $\alpha\gamma/\gamma^+$, is defined as:

$$\alpha\gamma/\gamma^+ = \frac{p_\alpha + p_\gamma}{1 - p_\alpha} = \frac{p_\alpha + p_\gamma}{p_\gamma + p_\beta + p_M + p_m} \quad (6-2)$$

where p_m is the mass ratio of maghemite. The denominator of Equation 6-2 describes the presence of all non-goethite oxide and hydroxide species, including lepidocrocite, akaganeite, magnetite, and maghemite. Two major features distinguish $\alpha\gamma/\gamma^+$ in Equation

6-2 from α/γ^* in Equation 6-1 with respect to role of the oxide compositions (e.g., such as in the data in Table 6.5):

- Lepidocrocite (p_γ) is accounted for as a “neutral” oxide (rather than a detrimental contributor to oxide quality as in α/γ^*) by adding it to the mass ratio of goethite in the numerator of Equation 6-2, and to the mass ratios of “detrimental” oxide species in the denominator of Equation 6-2.
- Maghemite is explicitly considered (through p_m) as a detrimental contributor to oxide quality (Oh et al. 1999), together with magnetite (through p_M) (Morcillo et al. 2014). It is also noted that the inclusion of both p_m and p_M in Equation 6-2 enables one to account for the possible albeit unlikely (De la Fuente et al. 2011) presence of detrimental hematite, which cannot be identified through XRD analysis as discussed in Section 6.4. The phase signals of hematite can be confused with those of magnetite or maghemite because these species share similar microstructures (Yamashita et al. 1998).

6.5.2 Verification of Concept based on Corrosion Assessment from Field Inspections

A comparison of $\alpha\gamma/\gamma^+$ and α/γ^* values for all the oxide samples evaluated through XRD analysis (Table 6.5) is summarized in Table 6.7. Here, the WS poles inspected in Sites 1 through 5 are listed in descending order from most to least protected based on the $\alpha\gamma/\gamma^+$ values. To facilitate comparisons, Table 6.7 also provides the corrosion damage levels resulting from visual assessment (Table 3.2) and the atmospheric corrosivity category (Table 4.7) for each WS pole.

Both PAI models (of $\alpha\gamma/\gamma^+$ and α/γ^*) enable one to identify the two highest-quality oxide samples collected from the walls of Poles C1F-20 (Site 1) and S3B-7L (Site 3),

respectively. In fact, these are the only two samples that would be classified as “protective” according to Equation 6-1 since $\alpha/\gamma^* > 1$ (Kamimura et al. 2006). Instead, according to Equation 6-2, protective oxides appear to be characterized by $\alpha\gamma/\gamma^+$ of approximately 1.5 or greater. Both PAI models also share the three lowest-quality rust samples, which were collected from the coating lines of Poles Q3C-2L and Q3C-2R (Site 2) and the outer pack-out rust of Pole TL-1 (Site 4). The discrepancy between $\alpha\gamma/\gamma^+$ and α/γ^* for these samples is minimal, suggesting that the two PAI models are equally capable of identifying poor-quality oxides.

The key difference between the two models is that Equation 6-2 consistently classifies the patina samples (i.e., the “powder” samples obtained by scraping the pole walls as illustrated in Figure 6.4a) as better than the solid rust samples that were removed from corrosion-damaged areas. In fact, all patina samples are characterized by $\alpha\gamma/\gamma^+$ values that exceed those of the solid rust samples, and of the pack-rust powder sample removed from the reflective tape section on Pole C1F-20 (Site 1). Conversely, the α/γ^* values from Equation 6-1 lend themselves to some improbable interpretations. For example, Equation 6-1 (Kamimura et al. 2006) rates the inner pack-out rust sample from Pole TL-1 ($\alpha/\gamma^* = 0.47$) as higher, albeit marginally, than the patina samples collected from the same pole ($\alpha/\gamma^* = 0.46$) and from the WS poles at Site 2, except Pole Q3C-2L ($\alpha/\gamma^* = 0.48$). This result likely occurs because chlorides did not penetrate deep enough into the pack-out rust on Pole TL-1 to cause the formation of akaganeite where the inner sample was collected. Despite the lack of akaganeite, it is impractical to consider pack-out rust to be more protective than patina.

A similar case is seen in the example of the pack rust sample from Pole C1F-20

($\alpha/\gamma^* = 0.95$, $\alpha\gamma/\gamma^+ = 0.98$). Based on Equation 6-1 (Kamimura et al. 2006), this sample rates better than three of the four pole wall samples from Site 3 and all of the pole wall samples from Site 5 ($\alpha/\gamma^* \leq 0.87$, $\alpha\gamma/\gamma^+ \leq 1.47$), both predominantly rural atmospheres like Site 1. While this sample might be associated with less severe corrosion damage compared to the patina samples collected from Site 2 and 4 ($\alpha/\gamma^* \leq 0.48$, $\alpha\gamma/\gamma^+ \leq 0.91$), it is certainly unrealistic to rank it as the third highest-quality sample. Instead, the proposed Equation 6-2 yields realistic outcomes as it classifies all patina samples from Sites 1, 3, and 5 as more protective than the pack-rust oxide sample collected from Pole C1F-20. It is noted that Equation 6-1 (Kamimura et al. 2006) and Equation 6-2 also disagree on the order of these “intermediately protective” patina samples ($0.50 \leq \alpha/\gamma^* \leq 0.79$, $1.05 \leq \alpha\gamma/\gamma^+ \leq 1.36$). Cases can be made for and against both models by arguing these samples, which shows that Equation 6-1 is not without merit when assessing the protectiveness of WS patinas.

Nonetheless, Equation 6-2 yields realistic and consistent PAI values for oxide samples collected from a given test site. In fact, based on the order of the $\alpha\gamma/\gamma^+$ values in Table 6.7, one can infer which test sites and samples (either from patina or more damaged areas) are associated with more protective oxides. Site 1 is confirmed as the most favorable to the formation of a protective patina on the WS pole walls ($\alpha\gamma/\gamma^+ = 1.51$ for Pole C1F-20). The atmospheres of Sites 3 and 5 are also suitable to form relatively protective patinas. The fact that Site 3 ranks better than Site 5 (with Poles S3B-7L and S3B-3L) is consistent with its lower atmospheric corrosivity (Table 4.7) and the resulting corrosion rates estimated based on thickness measurements (Table 5.2 through Table 5.4). This outcome further supports the need for the proposed remediations for the WS poles at Site 5 (discussed in Section 7.3), which would likely translate in reductions in corrosion rate.

Table 6.7 Values of $\alpha\gamma/\gamma^+$ and α/γ^* based on data from XRD analysis (Table 6 5).

Pole	Area	Site	Visible corrosion damage level (Table 3.2)	Atmospheric corrosivity (Table 4.7)	α/γ^* (Eq. 6-1)	$\alpha\gamma/\gamma^+$ (Eq. 6-2)
C1F-20	Pole wall	1	Negligible	C_3 to C_4	1.08	1.51
S3B-7L	Pole wall	3	Minor	C_3 to C_4	1.05	1.47
S3B-3L	Pole wall	3	Negligible	C_2 to C_3	0.79	1.36
11Z-2R	Pole wall	5	Minor	C_4	0.78	1.32
8Z-2L	Pole wall	5	Moderate	C_4	0.61	1.29
8Z-2R	Pole wall	5	Moderate	C_4	0.52	1.28
11Z-2L	Pole wall	5	Minor	C_4	0.87	1.26
11Z-6R	Pole wall	5	Moderate	C_4	0.60	1.15
S3B-2L	Pole wall	3	Moderate	C_2 to C_3	0.50	1.14
S3B-7R	Pole wall	3	Minor	C_3 to C_4	0.67	1.05
C1F-20	Bottom tape	1	Negligible	C_3 to C_4	0.95	0.98
TL-1	Pole wall	4	Severe	C_4	0.46	0.91
Q3C-2L	Pole wall	2	Severe	C_4	0.48	0.76
Q3C-2R	Pole wall	2	Severe	C_3 to C_4	0.34	0.71
Q3C-1L	Pole wall	2	Severe	C_4	0.33	0.71
Q3C-1R	Pole wall	2	Moderate	C_4	0.29	0.69
8Z-2R	Fasteners	5	Moderate	C_4	0.43	0.61
TL-1	Pit (Figure 3.20b)	4	Severe	C_4	0.53	0.56
8Z-2L	Fasteners	5	Moderate	C_4	0.47	0.56
11Z-6R	Fasteners	5	Moderate	C_4	0.43	0.53
TL-1	Inner pack out	4	Severe	C_4	0.47	0.42
Q3C-1L	Coating line	2	Severe	C_4	0.32	0.37
Q3C-2L	Coating line	2	Severe	C_4	0.25	0.17
TL-1	Outer pack out	4	Severe	C_4	0.15	0.16
Q3C-2R	Coating line	2	Severe	C_3 to C_4	0.10	0.09

The XRD results for the samples collected at Site 2 (industrial atmosphere) and Site 4 (chloride-laden atmosphere) are also consistent with the evidence from visual assessment (Table 3.2) and atmospheric corrosivity assessment (Table 4.7). In fact, the samples from Sites 2 and 4 exhibit much lower $\alpha\gamma/\gamma^+$ values than those from Sites 1, 3 and 5. Interestingly, the lowest (i.e., worst) $\alpha\gamma/\gamma^+$ values are attained at Site 2. This suggests that the industrial

atmosphere near the potash mine and processing plant may be more corrosive than a chloride-laden atmosphere within 300 ft of the ocean. In fact, at Site 2, corrosion damage is reasonably attributed to the exposure to fumes containing sulfur dioxide (Table 4.6), and chlorides as reflected in the presence of akagaenite (Table 6.5). These results are also consistent with the assessment of corrosion potential based on the Pourbaix diagram (Figure 5.8), and thus reinforce the recommendation to re-examine the cathodic protection systems installed at Site 2 (as discussed in Section 5.2.3.2 and Section 7.3).

6.5.3 Definition of Preliminary Rating Criteria

Based on the PAI values from Equation 6-2 listed in Table 6.7, the oxide samples can be sorted into one of four well-recognizable categories, which are presented in Table 6.8. These categories are separated from one another by $\alpha\gamma/\gamma^+$ increments of 0.50, and should be considered as preliminary and approximate categories demonstrating the concrete potential to be refined and eventually used for corrosion rating purpose. Obviously, more field data are needed to further verify and refine these preliminary rating criteria.

Table 6.8 Proposed PAI rating criteria.

PAI rating	Corrosion damage	Recommendations
$\alpha\gamma/\gamma^+ \leq 0.50$	Severe damage (e.g., pack out)	Consider expedited replacement
$0.50 < \alpha\gamma/\gamma^+ \leq 1.00$	Pack rust, moderate pitting	Enact remediation and/or repair measures
$1.00 < \alpha\gamma/\gamma^+ \leq 1.50$	Uniform patina, minor pitting	Prioritize inspection, prevention, control
$\alpha\gamma/\gamma^+ > 1.50$	Negligible to minimal	Inspect and monitor without prioritization

In Table 6.8, for practical purposes, each PAI range is associated with representative visible corrosion damage and recommendations for inspection, prevention and remediation. For all WS poles inspected, these recommendations are discussed in depth and demonstrated in Section 7.3. For the purpose of demonstrating proof of concept, it is encouraging to notice that the proposed PAI ratings (Table 6.7) provide results that consistently mirror those of visual inspection (Table 3.2), for which quantitative parameters are not available besides the pitting categories defined in ASTM G46 (2013c), as illustrated in Figure 2.10. This preliminary evidence shows that the proposed PAI formulation ($\alpha\gamma/\gamma^+$ in Equation 6-2) and criteria (Table 6.8) lend themselves to quantitatively assess corrosion damage based on WS oxide composition as determined by XRD analysis, with no need for more complex MS analysis.

6.6 Concluding Remarks

The following conclusions are drawn from the assessment of the microstructure and chemical composition of oxide samples collected from the WS transmission line poles inspected at Sites 1 through 5.

- SEM and EDX analysis may enable one to document the presence of significant oxide species in rust samples. However, it is difficult to consistently assess oxide composition and related corrosion mechanisms. To this end, a technique that enables one to identify oxide composition (e.g., XRD and MS) instead of elemental composition (EDX) becomes desirable.
- For the poles inspected in Sites 1 through 5, XRD analysis yields quantitative oxide composition data that are consistently in agreement with the evidence

gained from assessment based on visual inspections 4.1, atmospheric corrosivity estimates, corrosion rate estimates, and corrosion potential measurements.

- The results of MS analysis provide further insight into the WS oxide composition by accounting for the contribution of nanoscale phases. This is an important feature since part of the (protective) goethite can be present as a dense nanophase, which may not be identified through XRD analysis (Cook 2005). However, MS analysis is complex and time-consuming. In fact, for some of the oxide samples collected in the field, unrealistic oxide composition estimates were obtained through MS analysis. In addition, few MS facilities are available compared to XRD analysis.
- A modified protective ability index (PAI), $\alpha\gamma/\gamma^+$, is introduced with the purpose of providing a practical tool to quantify the protective ability of WS oxides (e.g., patina) based on oxide composition data (e.g., obtained through XRD analysis). This modified PAI is intended to overcome the limitations of the PAI defined by Kamimura et al. (2006), α/γ^* , by treating lepidocrocite as a “neutral” oxide species rather than a detrimental contributor to oxide quality, and explicitly considering the mass ratio of maghemite.
- When using XRD oxide composition estimates, the modified PAI introduced by the author yields results that are consistently in agreement with the findings of visual assessment and atmospheric corrosivity assessment, different from the original (unmodified) PAI. More research is needed to validate the proposed modified PAI and the associated corrosion rating criteria.

CHAPTER 7.0 CORROSION PREVENTION AND REMEDIATION

This chapter reviews prevention and remediation strategies that can be utilized to minimize corrosion damage in WS overhead transmission line structures, leveraging the direct experience of the authors. Section 7.1 summarizes steps to be taken during the design process to control and prevent corrosion. Section 7.2 presents an overview of specific protective measures that should be considered for corrosion prevention, remediation, and repair. Finally, Section 7.3 offers recommendations for the remediation of WS poles, with an emphasis on the poles inspected as part of the project presented in this report.

7.1 Design and Detailing

WS poles can experience multiple forms of corrosion damage. Pack-rust damage is the most common form of corrosion damage that was encountered during the field inspections reported in Chapter 3.0. This corrosion mechanism tends to occur at crevices and joints, as well as minimal geometric discontinuities (e.g., coating lips), due to water stagnation that prevents the formation of a robust patina on the WS. In these instances, corrosion damage can be exacerbated by the exposure to atmospheric contaminants.

The corrosion resistance of WS poles depends on the steel elemental composition, surface morphology, geometric configuration, and exposure environment. Sensible design and detailing of WS poles are critical for ensuring the intended design life, especially for poles that operate in aggressive environments. A group of utilities previously investigated the impact of excessive corrosion on transmission line structures (Goodwin and Pohlman 1993). Based on their findings and the field observations made in Chapter 3.0, certain steps

are recommended to be taken during the design process of WS transmission line structures.

These steps entail:

- Minimizing moisture accumulation and retention at metal contact surfaces and connections via proper orientation of components, edge and pitch distance, and relevant drainage details.
- Complete sealing of hollow WS members (i.e., poles) to prevent moisture infiltration and stagnation.
- Coating of directly embedded structures or foundation attachments to prevent contact with soils and continuous exposure to moisture.
- Curtailing the encroachment of vegetation at the ground-line.

7.2 Protective Measures

Mainstream corrosion-protection measures for WS poles include the use of coatings, sacrificial sleeves, and cathodic protection, as reviewed in Section 7.2.1 through Section 7.2.3. These measures were also deployed in the WS poles inspected in Sites 1 through 5, although they were not always effective.

7.2.1 Coatings

The overarching objective of corrosion prevention and control measures is to hinder the formation of electrochemical cells that facilitate corrosion. A basic corrosion cell consists of an anode, a cathode, a conductor, and an electrolyte. The anode is the corroding (oxidizing) metal; the cathode is the protected metal; the conductor physically connects the anode and cathode; and the electrolyte is a solution of chemicals that is in contact with both the anode and cathode. A corrosion cell cannot form in the absence of any of these components (Popov 2015). The purpose of a protective coating is to physically isolate

potentially reactive metal surfaces from potential electrolytes provided by the surrounding environment (e.g., humid atmosphere, damp soil). Barrier coatings are widely deployed to separate WS structures from aggressive environment. In the case of WS poles, coating is typically applied below ground and at the ground-line to avoid direct exposure to soil and vegetation, which may hinder the formation of an effective patina on uncoated WS. There are three classes of coatings: organic, inorganic, and metallic coatings:

- Organic coatings include paints, epoxies, resins, lacquers, urethanes and varnishes. They also contain corrosion inhibitors and protect more metal on a weight basis than any other means of corrosion protection.
- Inorganic coatings include enamels, glass linings, and conversion coatings. These are not typically used on WS transmission line structures due to practical and cost considerations.
- Metallic coatings provide an additional barrier between the steel substrate and the environment when an outer organic coating is compromised, while also offering cathodic protection. In the case of WS, thermal spraying, also called metallizing, is the most common application method.

The selection of a suitable coating solution and compatible WS surface preparation warrant careful consideration given the variety of commercially available coating materials and systems (Revie and Uhlig 2008). For example, the amount of time it takes for the coating to cure can influence the selection process. During warmer times of the year, preference should be given to coatings that are appropriate for elevated temperatures and relatively high humidity levels, such as moisture-cured urethanes. Under lower

temperatures, coating chemistry becomes more critical. In these instances, coatings that cure more rapidly are preferable to avoid relatively long waiting times to complete the coating and (if needed) back-filling operations.

Coatings can effectively cover and protect large areas and can be an effective protection method when applied by qualified and experienced personnel. Consideration of the structure design, location, and exposure environment is necessary to select suitable coating systems. It is recommended that the coating extend at least 2 ft above the ground line (e.g., different from the configuration noted on Pole S3B-2L at Site 3, as depicted in Figure 4.15b). To prevent the stagnation of water or accumulation of debris, care should be taken to smooth rough surfaces, eliminate sharp edges, and caulk crevices, if necessary. These actions are especially important for the protection of shaded areas, where it may be more difficult for the WS surface to be exposed to wet/dry cycles, which is critical to form a protective patina. From a practical standpoint, it is noted that WS pole walls lend themselves to coating better than lattice towers because poles have larger undisturbed surface areas that are easier to coat. Therefore, WS pole surfaces may be coated with non-traditional systems that enable one to cover a greater area faster (e.g., petrolatum-wax tapes).

The presence of coating defects and damaged areas (which may also be man-made) may result in the direct exposure of WS surfaces to the surrounding atmosphere or soil, making them susceptible to corrosion attack. The field inspection of in-service coating systems offers some representative evidence to appreciate the type of issues that may arise, such as deterioration and delamination, as illustrated in Figure 3.4, Figure 3.9, Figure 3.14, and Figure 3.20. Possible causes for such failures include:

- Improper application or inadequate preparation of the WS surface.
- Water stagnation at the coating lip, which can be facilitated by thick lip edges.
- Surface contamination introduced during coating application. Water can be introduced into a coating from a faulty compressor, and coatings may have been treated with a blast abrasive that is overly acidic or alkaline, or that contains chlorides.
- Surface contamination introduced during pole operation. Soluble contaminants, such as chlorides and sulfates, can affect the chemistry of a corrosion cell and accentuate attack, for example at the coating lip.
- Moisture absorption into the coatings occurring through water vapor transfer or osmosis. Organic coatings can absorb water in the range 0.1-3% by weight (Roberge 2008). Osmosis occurs when water is drawn at a higher than normal rate through the coating by soluble salt lying beneath the coating.
- Hydrogen or hydroxyl group formation. Highly active molecular hydrogen (H_2) can pry coatings loose. Organic coatings also poorly resist alkaline conditions and may be attacked by hydroxyl ions (OH^-), causing a significant loss of surface adhesion (Greenfield and Scantlebury 2000).
- External cathodic currents provided by cathodic protection. Cathodic currents can force water through a coating, increase the likelihood of hydrogen and hydroxyl group formation, and even strip coatings from a WS surface.

A delay may exist between the exposure of a coated substrate to a corrosive environment and the onset of coating degradation. This behavior reflects the necessary time

lag that is required to attain a steady-state diffusion of oxygen, water, and associated ions through the coating or along the interface between coating and WS surface (Roberge 2008). Degradation typically starts becoming visible in the form of blisters in the coating. These blisters grow larger until they coalesce, thereby facilitating delamination, as noted for example on Pole Q3C-2L at Site 2 (Figure 4.15a).

Metallizing, which consists of thermally spraying metal onto a suitably prepared steel surface to be protected (Figure 7.1), can enhance the corrosion resistance of WS poles. The primary materials that have been used for thermal-spray coatings include aluminum, brass, bronze, copper, iron, lead, molybdenum, monel, nickel, nickel-chrome, steel, tin, and zinc. These materials are used in the form of metallic wires or powders that are fed into a flame and melted. The molten stock is then pulverized by a high-velocity stream of compressed air, and propelled onto the steel substrate. Bonding may occur due to mechanical interlocking with roughened steel surfaces, localized diffusion and alloying, van der Waals forces, and combinations thereof.



Figure 7.1 Metallizing of steel pole.

Metallizing techniques include flame spraying, high-velocity oxy-fuel spraying, electric arc spraying, plasma spraying, ion plating, and use of detonation guns (Roberge 2008). The resulting coating tends to be relatively oxidized and porous, and thus metallized steel surfaces should be top-coated with an organic coating.

Although coatings are an effective control and prevention method, it is important to regularly inspect coatings for deterioration, especially as they near the end of their service life. In fact, deteriorating coatings can cause corrosion activity to concentrate at imperfections, and it is important to note that corrosion at these weak points develops more rapidly than on uniformly uncoated sections (Ibrahim 1999). If allowed to persist, these areas can experience dramatically increased corrosion due to stagnant moisture, and once it has initiated, it continues to worsen until the coating system fails entirely. It is critical to intervene before the structure is severely damaged. To help offset this occurrence, coatings should be periodically replaced. The average service life of a coating system will be one of the key considerations in the selection process. Selecting a coating system with a reasonable expected service life could help ensure continued performance when correctly applied.

7.2.2 Sacrificial Weathering Steel Sleeves

Another way to effectively “coat” a pole is through the application of sacrificial sleeves. An additional sheet of WS can be welded over a structural WS pole wall to inhibit corrosion. The application of WS sleeves is similar to coating in that it is supposed to isolate the surface from the environment. The steel sleeves are added to act as a sacrificial layer and protect the underlying steel surface. Sacrificial sleeves are typically placed where the WS pole intersects the ground line. The size of sacrificial ground line sleeves typically

mirrors the thickness of the underlying pole wall, encompasses the entire circumference of the pole, and is between three and five ft in height. An example of sacrificial WS sleeve is shown in Figure 7.2.



Figure 7.2 Sacrificial WS sleeve installed at base of WS pole.

This control and prevention strategy can be paired with organic coatings to more effectively hinder corrosion effects on the WS pole walls. However, this protection becomes ineffective when poles are set either too low so that the ground line is above the top of the sleeve, or too high, so that the bottom of the sleeve is above the ground line.

7.2.3 Cathodic Protection

The basic principle of cathodic protection (CP) techniques is that undesirable anodic corrosion reactions are suppressed by applying an opposing electric current, thereby forcing local anodes to be polarized to the potential of local cathodes. CP can be applied to WS structures to reduce corrosion activity and is usually deployed in combination with coatings to provide a thorough mitigation solution. CP polarizes the entire surface to the thermodynamic potential of a sacrificial anode. CP has been shown to be an effective method for protecting and reinforcing steel from chloride-induced corrosion. The

effectiveness of CP in protecting steel in soils was demonstrated in the early 1940s for the case of leaking natural-gas pipes. A marked reduction in the number of leaks occurred immediately after CP installation (Beavers 2001). A cathodically protected metal surface can resist in a corrosive environment indefinitely (Ibrahim 1999). For steel transmission line structures, CP systems are designed primarily based on the following considerations:

- Service environment, including soil type and resistivity, and moisture level.
- Exposed steel surface area, and presence of coatings and protective sacrificial components.
- Desired service life of the CP system (normally 20-25 years).

Soil acts as the electrolyte for CP processes, and the structure to be protected acts as the connecting circuit. Electric currents flow from the anodic area of a pole to the soil, through the sacrificial anode, and back up to the cathodic area of the pole to complete the circuit. The degree of current flow is limited by factors such as the resistivity of the environment and the degree of polarization at the anodic and cathodic areas. Corrosion occurs at anodic areas where the current discharges from the pole into the soil. There is no corrosion where currents flow from the environment into the pole at cathodic areas. Thus, the objective of CP is to force the entire pole surface to collect current from the environment, effectively becoming a cathode. As such, corrosion is “transferred” from the structure to the sacrificial anode.

Sacrificial anodes are relatively inexpensive and easy to install. The two most common materials for galvanic (passive) CP systems are magnesium and zinc. Magnesium anodes are usually applied to structures in normal soil conditions whereas zinc anodes are

typically used in saturated soils and water. Soil anodes come in two forms, either bare or bagged. Bare anodes are typically applied in areas with wet conditions but can also be installed in drier areas in combination with engineered backfills. Bagged anodes are typically applied in drier soil conditions and already contain the engineered backfill, which is convenient to expedite and simplify installation. Sacrificial anodes are designed to discharge CP currents for a reasonably long time (typically 10-15 years) and, when consumed, can be easily replaced.

According to Faraday's Law, the amount of electrical energy that can be obtained from a galvanic anode depends on the electrochemical equivalent of the metal used and the efficiency of the anode. The capacity of an anode is typically characterized by the unit Ampere-hour (A-h), which corresponds to 1 A flowing for 1 hour. The efficiency of a galvanic anode is the ratio of its total theoretical capacity divided by the weight sacrificed or consumed as part of a CP system. Galvanic anodes are subject to self-corrosion, lowering their capacity. Efficiency varies with current output density and, indicatively, can be about 50% at a current output density of 0.3 A/m². Working potentials can range from approximately -1.45 V vs. CCSRE for standard magnesium anodes to approximately -1.70 V vs. CCSRE for proprietary alloys or "high-potential" anodes.

In order to achieve adequate levels of protection, it is recommended that one of the following three NACE performance requirements be met (Barlo 2001, Holtsbaum 2003, NACE 2013):

- A negative corrosion potential of at least -0.85 V vs. CCSRE with CP applied.

This criterion is used when the cathodic polarization (i.e., shift in potential) due

to CP cannot be quantified (i.e., for systems in which CP current cannot be interrupted).

- A negative polarized potential (i.e., sum of the corrosion potential and cathodic polarization) of at least -0.85 V vs. CCSRE with CP applied. For example, a steel structure with a corrosion potential of -0.80 V vs. CCSRE and a cathodic polarization of 50 mV or more is considered protected.
- A minimum of 100 mV of cathodic polarization between the surface of a structure and any reference electrode. A potential measurement that satisfies the 100 mV cathodic polarization criterion need not be -0.85 V vs. CCSRE or more negative to reduce corrosion rates. The formation or decay of polarization can be measured to satisfy this criterion.

Consideration was given to these performance indicators in the evaluations presented in Section 5.2.

When designing a CP system or assessing the effectiveness of previously installed CP systems, one must know whether or not stray currents are present. Examples of sources of stray currents include direct current (DC) railway systems, mining operations using DC power, and DC welding operations. Stray currents can severely affect cathodically-protected structures by interfering with the flow of protective current between structure and sacrificial anode. In areas where a stray current is discharging, the anodic potential of a protected structure may not be sufficiently counteracted by means of CP. Such conditions necessitate special stray-current control techniques, for example involving metallic bonds from the affected structure to the source of the damaging current.

7.3 Remediation

Structures that are assessed as providing substandard strength or serviceability performance must be either repaired or replaced. If damage is not excessive, repairing is typically preferable. Several considerations should be made in advance of a repair design to ensure that the finished product meets the necessary requirements to restore the structure to its original (or enhanced) strength, and provide corrosion resistance. This process typically entails the involvement of a utility's engineering staff as well as an outside consulting engineer or specialized contractor.

In many instances, repairs must be done on a structure that is still in service, prompting the use of temporary supports to ensure safety. As with repair methods, temporary support methods can vary widely. They can be in the form of portable support trusses or as pieces of construction equipment such as a crane, excavator or bulldozer. The type and method of support is normally part of the initial repair discussions, as implementation on the project site requires a significant amount of pre-planning and approval of all involved parties.

In the project reported herein, consideration was given to WS transmission line poles operating in diverse environments and displaying different design features. Corrosion assessment demonstrated that certain factors significantly affect the susceptibility to corrosion damage of WS transmission line poles. For each site where field inspections were conducted, the following remediation actions should be considered:

- Site 1: the exposure to a rural-urban environment did allow the formation of an effective protective patina on Pole C1F-20. However, the application of reflective tape onto the pole wall introduced a geometric discontinuity that

facilitated water stagnation, resulting in visible corrosion damage (Figure 3.5).

This tape should be immediately removed, and any pack rust that formed on the underlying WS surface should be removed so that protective oxides can reform.

- Site 2: the industrial environment was such that the WS poles were exposed to atmospheric chlorides. While all WS poles at this site do not raise immediate concerns in regard to thickness losses, they do appear to be affected by the exposure to the local aggressive atmosphere. In fact, despite their relatively young age (14 years), they display the following problems: low-quality surface patina, pack-rust damage at some locations, coating deterioration, and ineffective cathodic protection. Another material, possibly galvanized steel, may be preferable at this site. It should be considered to retrofit the existing WS poles with new coating and cathodic protection.
- Site 3: the WS poles at this site appear to be sufficiently far from the nearby coal mines and power station to be considered as exposed to a rural atmosphere. However, it is likely that stray currents are present, disrupting the cathodic protection of Poles S3B-2L and S3B-3L, and possibly causing localized and accelerated corrosion rates in Pole S3B-2L. Therefore, an in-depth examination of stray current effects should be considered to tailor a more effective CP system. In addition, new coatings should be considered to prevent further damage at the coating lips. For the specific case of Pole S3B-2L, new coating should be immediately installed sufficiently above the ground line.
- Site 4: this chloride-laden site is located at 300 ft from the Atlantic Ocean. Here, the 23-year old Pole TL-1 is part of a test line that the owner set up to study

corrosion performance. This WS pole experienced notable thickness losses. However, critical damage in the form of full-thickness losses occurred in a relatively shaded wall area where effective wet/dry cycles are more difficult to occur, and chlorides are more likely to deposit over time. A comparison between the performance of Pole TL-1 and that of the adjacent Pole TL-2 made with GS clearly shows that the latter material should be preferred to WS in chloride-laden environments. If this structure was in actual service, it would be desirable to deploy cathodic protection to partially mitigate the effects of corrosion.

- Site 5: the corrosivity of this rural environment is influenced by the local humid climate (based on TOW as summarized in Table 4.5). However, the relatively high corrosion rates as well as localized damage experienced by the WS poles of Lines 8Z and 11Z accrue primarily from three ill-conceived design solutions, namely: galvanic coupling of GS fasteners with WS pole structures; use of unfilled GS caisson foundations that inevitably fill with water; use of unsealed poles where the interior WS surfaces are particularly susceptible to corrosion damage. Correct remediation actions had already been taken to correct these issues in two of the six WS poles at this site. Similar measures are recommended for the remaining poles, including: replacing corroding GS fasteners (if similar fasteners are used, CP should be considered to offset galvanic corrosion effects); and draining and filling the GS caisson foundations. One additional action that was not taken for the already remediated structures, and is recommended for all poles on site, is the sealing of all WS pole bases to prevent

further moisture penetration. In addition, further inspection of the WS poles higher above the ground is recommended to understand the extent of corrosion damage as noted at geometric discontinuities (e.g., ladder connection to pole wall, and cracking at cross-bracings), and plan remediation as needed.

Proper prevention and remediation of corrosion damage in transmission line WS poles relies on routine inspection of representative structures. Inspection techniques and schedules inevitably depend on the budget that is made available by the owners. The type of funding, whether capital or Operations and Maintenance, significantly influences the available budget, how frequently and to what extent inspection, assessment and remediation can be performed. Ultimately, related funding will be governed by how owners define and prioritize capital expenditures. For WS poles, experience indicates that most areas require inspection approximately every 10 years. More frequent inspections are necessary in areas characterized by aggressive environments, or in instances where the design and detailing of the poles are of concern and yet impractical to resolve by partial or full replacement (e.g., at Site 5).

CHAPTER 8.0 CONCLUSIONS AND RECOMMENDATIONS

Based on the findings of the research project reported herein, the following conclusions and recommendations are drawn.

8.1 Literature Review of Corrosion Behavior of Weathering Steel Poles

- Electric utilities have used weathering steel (WS) for nearly 50 years, but there is a substantial lack of shared inventory information and empirical data for WS transmission line poles. This current gap prevents life cycle evaluations on a large scale. The limited inventory information and empirical life cycle databases mirrors the lack of standards for adoption by regulatory agencies for the inspection and maintenance of WS transmission line poles.
- Various alloying elements, including copper, chromium, phosphorus, nickel and silicon, contribute to the corrosion resistance of WS.
- The corrosion resistance of WS structures depends on the formation of an adherent and dense surface oxide film. The routine wetting and drying of the steel surface is essential for the build-up of a protective oxide film. The wetness of an environment is significantly heavily influenced by geography, climate, adjacent site features, and structural orientation.
- Corrosion damage in WS transmission line poles is typically due to “pack-rust” phenomena. Pack rust forms as water penetrates the surface oxide film, further oxidizing the underlying steel, and producing significant thickness losses as a result of the build-up of multiple unstable oxide films. Corrosion damage in WS

poles is more likely to occur near the ground line where a damp environment is more likely to form. Pack rust may build up at joints and crevices, exerting significant pressures on the adjoined steel elements, and possibly resulting in “pack-out” damage associated with plastic deformations and thickness losses. Various levels of pitting can be encountered. While pitting is often seen to occur in conjunction with other non-uniform corrosion damage, it is sometimes difficult to ascertain the source of such damage.

8.2 Test Sites and Visual Assessment

- Site 1: an adherent patina forms on WS pole surfaces in this rural-urban environment. The occurrence of localized corrosion damage underneath reflective tape demonstrates the importance of preventing the introduction of (even small) geometric discontinuities where water can stagnate. In fact, water stagnation prevents the formation of a protective patina, and facilitates the occurrence of corrosion damage by acting as an electrolyte.
- Site 2: exposure to an industrial atmosphere (potash mine) can cause moderate to severe corrosion damage to WS pole structures. It is also hypothesized that the presence of atmospheric chlorides contribute to such damage. The selection, installation and detailing of a suitable coating system are critical to ensure that the ground line is protected from corrosion damage.
- Site 3: exposure to a rural/industrial environment (coal mine and coal-fired power station) can result in negligible to moderate corrosion damage. In particular, pitting severity reasonably depends on the distance between the WS structure and industrial facilities, and appears to be exacerbated for WS pole

walls that face directly potential contaminant sources (e.g., smokestacks, coal trucks and storage yards). In addition, stray current effects may be of concern for structures in proximity to power stations. Under these conditions, corrosion damage can be exacerbated by incorrect detailing of the coating at the ground level (e.g., insufficient height above ground).

- Site 4: direct exposure to a marine (chloride-laden) environment inevitably results in severe corrosion on WS transmission line structures. Corrosion forms range from extensive and heavy pitting to pack-out damage, where the latter is facilitated in areas that are more likely to be interested by water stagnation or moisture retention, and formation of chloride deposits. In this environment, WS is not a sound choice for transmission line structures. Instead, GS may be considered.
- Site 5: WS appears to be a viable choice in coastal areas for structures located a few miles from saltwater. However, the formation of a relatively unstable patina may still be attributed to the exposure to atmospheric chlorides. More research is needed to understand practical cut-off distances where the use of WS should be discouraged. While the service environment is a critical factor to consider for corrosion assessment, there are instances where pole design and detailing become more important. For example, at this site, poor design and detailing choices (e.g., unsealed poles, coupling between WS and GS) resulted in severe corrosion damage.

8.3 Assessment of Environmental Corrosivity

- Atmospheric corrosivity is a key measurable indicator of the susceptibility of WS transmission line structures to corrosion damage. The main contributing factors are moisture, which can be conveniently quantified as “time of wetness”, and presence of airborne contaminants, with an emphasis on sulfur dioxide (e.g., sulfates in industrial atmospheres) and chlorides (e.g., near saltwater or due to direct exposure to deicing salts). It appears that exposure to nearby heavily trafficked roads is, per se, not of concern as far as corrosion resistance of WS poles (as noted for Sites 1, 4 and 5).
- Soil corrosivity is an important indicator of susceptibility to corrosion damage for directly embedded WS surfaces when the protective coating does not sufficiently extend above ground, and when a deteriorating coating is present at and below the ground line (e.g., with non-adherent and disrupted areas). This issue is less relevant for well-coated WS surfaces. Soil corrosivity is largely influenced by moisture content and presence of ionic species such as sulfates and chlorides (which also depend on their concentration in the atmosphere).
- For the case studies presented in this report, classification of soil corrosivity using the AWWA (2010) criteria appears less effective than those based on soil resistivity (Roberge 2008) and the DVGW (2011) criteria. In particular, the DVGW (2011) criteria yields classifications that are more consistent with field observations especially in environments with soluble and airborne contaminants, irrespective of the resistivity level (e.g., case of Pole TL-1 exposed to a chloride-laden environment at Site 4).

- Both atmospheric and soil corrosivity should be considered when planning field inspections. In fact, exposure to a corrosive atmosphere may facilitate coating deterioration and disbond on directly embedded WS surfaces, and thus the occurrence of corrosion damage at and below the ground line.
- Both atmospheric and soil corrosivity are highly dependent on moisture contents, which heavily depend on the location and orientation of a given WS structure, and exposure to damp soils that act as low-resistivity electrolytes. Under these circumstances, exposure to a corrosive soil (e.g., a damp soil acting as a low-resistivity electrolyte) may further exacerbate corrosion damage, and excavation may be considered to assess below-ground WS surfaces with respect to unintended direct exposure to stagnant moisture and water penetration.
- Detrimental exposure to excess moisture also depends on structural designs and detailing that facilitate moisture retention (e.g., geometric discontinuities, mechanical connections without seamless transitions) and, in worst-case scenarios, water ponding (e.g., unfilled caisson foundations, especially in conjunction with unsealed poles). These aspects must be considered at the design stage, especially for WS structures that are expected to operate in aggressive environments.
- Site 1 (and, in part, Site 3) offers evidence on the corrosion behavior of a WS transmission line pole operating in a rural environment. This environment tends to exhibit a low-corrosivity atmosphere. Yet, corrosion damage of WS pole surfaces can still occur due to moisture accumulation and stagnation resulting

from seemingly inoffensive details that create geometric discontinuities, such as the reflective tape attached on Pole C1F-20.

- Site 2 and Site 3 offer evidence on the corrosion behavior of WS transmission line poles operating in an industrial environment. Site 2 is characterized by relatively high atmospheric and soil corrosivity, where it is reasonable to expect that the latter be influenced by the exposure to atmospheric contaminants. For example, elevated sulfate deposition levels on WS surfaces appear to be correlated with atmospheric corrosivity as well as soil corrosivity and corrosion damage. Instead, direct exposure to coal may be of concern at Site 3.
- Site 4 offers evidence on the ineffective corrosion resistance of a WS transmission line pole operating in a chloride-laden marine environment, even when cathodic protection is in place. In these instances, galvanized steel is a more sensible choice.
- With regard to atmospheric corrosivity characterization in field inspections, it is noted that it may be impractical to detect of chloride depositions on WS surfaces through swab tests, and Bresle patch tests (ISO 2006) may provide more reliable data. However, chlorides are difficult to detect as they rapidly react with the patina on WS surfaces, possibly resulting in relatively small chloride depositions. Therefore, an elemental analysis of the surface oxide composition based on laboratory tests seems a more rational strategy to understand whether the presence of chlorides in the atmospheres is such that the corrosion resistance of WS is impaired, as demonstrated in Chapter 6.0. This

may reasonably be the case for Pole TL-1 at Site 4 as well as other structures located less close to saltwater.

- Site 5 offers evidence on the corrosion behavior of WS transmission line poles operating in a rural and humid environment, albeit at a relatively small distance from saltwater. Here, atmospheric moisture is the dominant factor affecting atmospheric corrosivity, irrespective of the exposure to airborne contaminants. One additional concern is the possibility of exposure to chlorides carried by winds from the nearby coastline, as remarked in Section 3.7.

8.4 Assessment of Corrosion Rate and Corrosion Potential

- The quantification of corrosion rates allows for a better understanding of the combined impact of the environment, design and detailing on WS poles. The quantification of corrosion potentials allows for the assessment of present and future susceptibility to corrosion damage. This information can be leveraged for diagnosis and prognosis purposes, thereby enabling owners to prioritize and allocate prevention and remediation resources.
- For the different exposure environments covered in Sites 1 through 5, the inspected WS poles exhibit corrosion rates that are typically correlated with low to medium corrosivity classifications per ISO 9223 (ISO 2012b). Comparison of these classifications and those determined based on atmospheric corrosivity (Chapter 4.0), indicates that WS is expected to perform far better than standard carbon steel. In fact, none of the WS poles inspected experienced a uniform corrosion damage of concern. Based on the results of average and maximum thickness loss measurements, it appears that for the representative pole ages and

environments covered in Sites 1 through 5, any relevant corrosion damage accrues from localized corrosion mechanisms, especially due to moisture stagnation.

- Corrosion damage in WS pole walls may be accurately predicted using semi-empirical analytical models that are calibrated based on thickness loss measurements that are collected over an extended period of time. Short-term field inspections are unsuitable to define empirical parameters for such models. More research is needed to define such parameters for WS as a function of exposure environment and pole age.
- Of the 15 poles tested for corrosion potential, 11 failed to satisfy the NACE (2013) protection criterion based on the -0.85 V vs. CCSRE threshold. Five poles did exhibit potential values that are close (within 100 mV) to the -0.85 V vs. CCSRE threshold. Examining corrosion potential (and soil pH) data via the Pourbaix diagram illustrates the importance of adequate cathodic protection for WS poles. It is noted that none of the five WS poles without cathodic protection lies clearly in the passivation domain of the diagram. This outcome highlights the importance of routine checks on the health of cathodic protection systems.
- Site 1: Pole C1F-20 exhibits negligible maximum and average corrosion rates, which are consistent with the presence of a dense and adherent patina, and a low-corrosivity atmosphere. Therefore, the corrosion potential is not of concern although it is slightly greater than the NACE (2013) threshold. However, it is noted that severe corrosion damage can still occur at locations where water can stagnate. The damage observed beneath a seemingly inoffensive reflective tape

is indicative of the susceptibility of WS to corrosion damage at geometric discontinuities.

- Site 2: cathodic protection should be re-examined and corrected on all WS poles (perhaps after assessing the presence of stray currents). In fact, the exposure to an aggressive industrial atmosphere makes it unlikely for a stable and adherent patina to develop, and exacerbates any corrosion damage accruing from moisture stagnation (e.g., at coating lips). It is recommended that routine assessments be prioritized at Site 2.
- Site 3: despite the non-corrosive (rural) atmosphere, Pole S3B-2L experienced significant thickness losses on the surface facing the nearby power station, and exhibited insufficient cathodic protection. These issues likely stem from the combination of: (a) exposure to stray currents emanating from the power station, as highlighted by the difficulties to measure corrosion potentials; and (b) inadequate above-ground extension of the coated area. In fact, Pole S3B-3L, for which the coating area extends well above the ground line, exhibits a similarly inadequate cathodic protection together with negligible corrosion rates. Therefore, for Pole S3B-2L, while cathodic protection may be re-examined and corrected after assessing the presence of stray currents, extending the coating above the ground line may be sufficient. Instead, the 28-year old Poles S3B-7L and S3B-7R are located far away from the power station and exhibited excellent cathodic protection. The resulting low maximum corrosion rate demonstrates that cathodic protection can effectively protect multiple

connected structures and last for decades, provided that suitable ground-line coating is used.

- Site 4: the chloride-laden and humid environment hinders the corrosion resistance of WS wall surfaces of Pole TL-1, as reflected in the corrosion rate estimates. However, far more severe damage may occur at locations where moisture and chlorides can accumulate, as demonstrated by the completely consumed WS substrate behind the junction box. For existing WS poles located near saltwater, installing cathodic protection should be recommended.
- Site 5: a number of questionable design choices are reflected in high corrosion rates. These design issues (hollow GS caisson foundations, unsealed pole bases, galvanic coupling of GS and WS steel elements) should be remediated. Based on the evidence offered by Poles 11Z-2L and 11Z-2R, which were recently remediated, it is reasonable to expect that adding cathodic protection to the other WS poles at Site 5 would be beneficial for corrosion resistance.
- The uncoated WS surface of interest in pole structures lies above ground instead of in direct contact with the soil. Therefore, more research is needed to understand the applicability of the NACE (2013) threshold to above-ground WS surfaces. Based on the results of this study (e.g., for Pole C1F-20 at Site 1), some adjustments are needed to increase the -0.85 V vs. CCSRE (-0.53 V vs. SHE) cathodic protection threshold (NACE 2013), which applies to steel surfaces in direct contact with soil (e.g., buried pipes).
- The use of WS poles connected by steel bracings (e.g., forming H-frames such as in the case of Poles S3B-7R and S3B-7L in Figure 3.12) should be

discouraged. In fact, connecting multiple WS poles may accelerate corrosion damage due to differential potentials, thus forcing some adjoined structures to act as sacrificial anodes. To prevent this event, single poles or non-conductive (e.g., glass fiber-reinforced polymer) connections are recommended.

- Corrosion studies on WS coupons are unlikely to provide comprehensive conclusions with regard to practical worst-case scenarios (e.g., focusing on corrosion-sensitive details). Investigating actual transmission line structures exposed to significant environments is important to generate hard evidence. To this end, extending the scope of the project reported herein from WS poles to WS lattice towers should be considered. In fact, tower structures include numerous corrosion-sensitive details, such as mechanically-fastened joints and other geometric discontinuities that are difficult to protect with coatings.

8.5 Assessment of Oxide Microstructure and Composition

- SEM and EDX analysis may enable one to document the presence of significant oxide species in rust samples. However, it is difficult to consistently assess oxide composition and related corrosion mechanisms. To this end, a technique that enables one to identify oxide composition (e.g., XRD and MS) instead of elemental composition (EDX) becomes desirable.
- For the poles inspected in Sites 1 through 5, XRD analysis yields quantitative oxide composition data that are consistently in agreement with the evidence gained from assessment based on visual inspections^{4.1}, atmospheric corrosivity estimates, corrosion rate estimates, and corrosion potential measurements.

- The results of MS analysis provide further insight into the WS oxide composition by accounting for the contribution of nanoscale phases. This is an important feature since part of the (protective) goethite can be present as a dense nanophase, which may not be identified through XRD analysis (Cook 2005). However, MS analysis is complex and time-consuming. In fact, for some of the oxide samples collected in the field, unrealistic oxide composition estimates were obtained through MS analysis. In addition, few MS facilities are available compared to XRD analysis.
- A modified protective ability index (PAI), $\alpha\gamma/\gamma^+$, is introduced with the purpose of providing a practical tool to quantify the protective ability of WS oxides (e.g., patina) based on oxide composition data (e.g., obtained through XRD analysis). This modified PAI is intended to overcome the limitations of the PAI defined by Kamimura et al. (2006), α/γ^* , by treating lepidocrocite as a “neutral” oxide species rather than a detrimental contributor to oxide quality, and explicitly considering the mass ratio of maghemite.
- When using XRD oxide composition estimates, the modified PAI introduced by the author yields results that are consistently in agreement with the findings of visual assessment and atmospheric corrosivity assessment, different from the original (unmodified) PAI. More research is needed to validate the proposed modified PAI and the associated corrosion rating criteria.

8.6 Corrosion Prevention and Remediation

- Design of corrosion sensitive details is critical for ensuring adequate long-term corrosion protection of WS poles. Such design should minimize moisture

accumulation and retention and take care to ensure the stability ground line regions. The most applicable strategies for the prevention and remediation of corrosion damage in WS poles are coatings, sacrificial WS sleeves, and cathodic protection.

- Site 1: the exposure to a rural-urban environment did allow the formation of an effective protective patina on Pole C1F-20. However, the application of reflective tape onto the pole wall introduced a geometric discontinuity that facilitated water stagnation, resulting in visible corrosion damage. This tape should be immediately removed, and any pack rust that formed on the underlying WS surface should be removed so that protective oxides can reform.
- Site 2: the industrial environment was such that the WS poles were exposed to atmospheric chlorides. While all WS poles at this site do not raise immediate concerns in regard to thickness losses, they do appear to be affected by the exposure to the local aggressive atmosphere. In fact, despite their relatively young age (14 years), they display the following problems: low-quality surface patina, pack-rust damage, coating deterioration, and ineffective cathodic protection. Another material, possibly galvanized steel, may be preferable at this site. New coatings and cathodic protection should be considered for the existing WS poles.
- Site 3: the WS poles at this site appear to be sufficiently far from the nearby coal mines and power station to be considered as exposed to a rural atmosphere. However, it is likely that stray currents are present, disrupting the cathodic protection of Poles S3B-2L and S3B-3L, and possibly causing localized and

accelerated corrosion rates in Pole S3B-2L. Therefore, an in-depth examination of stray current effects should be considered to tailor a more effective CP system. In addition, new coatings should be considered to prevent further damage at the coating lips. For the specific case of Pole S3B-2L, new coating should be immediately installed sufficiently above the ground line.

- Site 4: this chloride-laden site is located at 300 ft from the Atlantic Ocean. Here, the 23-year old Pole TL-1 is part of a test line that the owner set up to study corrosion performance. This WS pole experienced notable thickness losses. However, critical damage in the form of full-thickness losses occurred in a relatively shaded wall area where effective wet/dry cycles are more difficult to occur, and chlorides are more likely to deposit over time. A comparison between the performance of Pole TL-1 and that of the adjacent Pole TL-2 made with GS clearly shows that the latter material should be preferred to WS in chloride-laden environments. If this structure was in actual service, it would be desirable to deploy cathodic protection to mitigate the effects of corrosion.
- Site 5: the corrosivity of this rural environment is influenced by the local humid climate. However, the relatively high corrosion rates as well as localized damage experienced by the WS poles of Lines 8Z and 11Z accrue primarily from three ill-conceived design solutions, namely: galvanic coupling of GS fasteners with WS pole structures; use of unfilled GS caisson foundations that inevitably fill with water; use of unsealed poles where the interior WS surfaces are particularly susceptible to corrosion damage. Correct remediation actions had already been taken to correct these issues in two of the six WS poles at this

site. Similar measures are recommended for the remaining poles, including: replacing corroding GS fasteners (if similar fasteners are used, CP should be considered to offset galvanic corrosion effects); and draining and filling the GS caisson foundations. One additional action that was not taken for the already remediated structures, and is recommended for all poles on site, is the sealing of all WS pole bases to prevent further moisture penetration. In addition, further inspection of the WS poles higher above the ground is recommended to understand the extent of corrosion damage as noted at geometric discontinuities (e.g., ladder connection to pole wall, and cracking at cross-bracings), and plan remediation as needed.

- Proper prevention and remediation of corrosion damage in transmission line WS poles relies on routine inspection of representative structures. Inspection techniques and schedules inevitably depend on the budget that is made available by the owners. For WS poles, most areas require inspection approximately every 10 years. More frequent inspections are necessary in areas characterized by aggressive environments, or in instances where the design and detailing of the poles are of concern and yet impractical to resolve by partial or full replacement.

8.7 Research Needs

- Utilities and contractors likely have pertinent information on corrosion behavior of WS transmission line structures. This information may not have been compiled as part of an industry-wide survey and evaluation. It is recommended that owners and inspectors collaborate to compile a database of

field inspection results. This database should be as accessible as possible at least to owners to maximize contributions as well as benefits for stakeholders.

- Corrosion studies on WS coupons are bound to lead to conclusions that cannot account for corrosion damage mechanisms that are encountered in corrosion-sensitive details of structural systems. Investigating actual transmission line structures exposed to significant environments is necessary to generate hard evidence. To this end, extending the scope of the project reported herein from WS poles to WS lattice towers through a follow-on project should be considered. In fact, tower structures include numerous corrosion-sensitive details, such as mechanically-fastened joints and other geometric discontinuities that are difficult to protect with coatings.
- More research is needed to understand practical cut-off distances where chloride contamination in coastal areas is not of concern for the formation of a protective patina on WS surfaces.
- The uncoated WS surface of interest in pole structures lies above ground instead of in direct contact with the soil. Therefore, more research is needed to understand the applicability of the NACE (2013) threshold to above-ground WS surfaces. Based on the results of this study (e.g., for Pole C1F-20 at Site 1), some adjustments are needed to increase the -0.85 V vs. CCSRE (-0.53 V vs. SHE) cathodic protection threshold (NACE 2013), which applies to steel surfaces in direct contact with soil (e.g., buried pipes).
- More research is needed to understand the applicability and limitations of commercially available coating systems, including metallizing. In addition, a

comparative study of sacrificial magnesium and zinc anodes may offer insight into the possibility of using zinc anodes on WS poles in low-resistivity soils.

- A comparative study of ASTM A588 (ASTM 2015a) and CSA 40.21 (CSA 2013) WS transmission line structures with similar designs and exposure environments may offer insight into the corrosion behavior of these alloys.
- More research, involving XRD and possibly MS analysis of oxide samples collected from operating WS structures, is needed to validate the proposed modified PAI and the associated corrosion rating criteria.
- Empirical data from atmospheric corrosion tests on steel coupons can serve to define a power model relating thickness loss with time, as specified in ASTM G101 (ASTM 2015c). For a given exposure condition, this semi-empirical model can serve to estimate future corrosion damage for exposed WS surfaces. The definition of the empirical parameters (A, n) can be informed by thickness loss measurements that are taken over an extended period of time. More research, largely based on simple field measurements, is needed to define these parameters for WS as a function of operating environment and pole age.

REFERENCES

- [1] Albrecht, P., Hall, T., “Atmospheric Corrosion Resistance of Structural Steels,” *Journal of Materials in Civil Engineering*, Vol. 15, No. 1, pp. 2-24, 2003.
- [2] Amrhein, C., Strong, J., Mosher, P., “Effect of Deicing Salts on Metal and Organic Matter Mobilization in Roadside Soils,” *Environmental Science & Technology*, Vol. 26, No. 4, pp. 703-709, 1992.
- [3] Antony, H., Peulon, S., Legrand, L., Chaussé, A., “Electrochemical synthesis of lepidocrocite thin films on gold substrate—EQCM, IRRAS, SEM and XRD study,” *Electrochimica Acta*, Vol. 50 No. 4, pp. 1015-1021, 2004.
- [4] Asami, K., Kikuchi M., “In-Depth Distribution of Rusts on a Plain Carbon Steel and Weathering Steels Exposed to Coastal–Industrial Atmosphere for 17 Years,” *Corrosion Science*, Vol. 45, No. 11, pp. 2671-2688, 2003.
- [5] ASCE (American Society of Civil Engineers), “ASCE/SEI 48-11 – Design of Steel Transmission Pole Structures,” ASCE, Reston, VA, 2011.
- [6] ASTM (American Society for Testing and Materials), “ASTM A242 – Standard Specification for Low-Alloy Structural Steel,” ASTM International, West Conshohocken, PA, 2013a.
- [7] ASTM (American Society for Testing and Materials), “ASTM A588 – Standard Specification for High-Strength, Low-Alloy Structural Steel, up to 50 ksi [345 MPa] Minimum Yield Point, with Atmospheric Corrosion Resistance,” ASTM International, West Conshohocken, PA, 2015a.
- [8] ASTM (American Society for Testing and Materials), “ASTM G1 – Standard Practice for Preparing, Cleaning, and Evaluating Corrosion Test Specimens,” ASTM International, West Conshohocken, PA, 2011a.
- [9] ASTM (American Society for Testing and Materials), “ASTM G46 – Standard Guide for Examination and Evaluation of Pitting Corrosion Steel,” ASTM International, West Conshohocken, PA, 2013c.
- [10] ASTM (American Society for Testing and Materials), “ASTM G50 – Standard Practice for Conducting Atmospheric Corrosion Tests on Metals,” ASTM International, West Conshohocken, PA, 2015b.

- [11] ASTM (American Society for Testing and Materials), “ASTM G51 – Standard Test Method for Measuring pH of Soil for Use in Corrosion Testing,” ASTM International, West Conshohocken, PA, 2012a.
- [12] ASTM (American Society for Testing and Materials), “ASTM G57 – Standard Test Method for Field Measurement of Soil Resistivity Using the Wenner Four-Electrode Method,” ASTM International, West Conshohocken, PA, 2012b.
- [13] ASTM (American Society for Testing and Materials), “ASTM G84 – Standard Practice for Measurement of Time-of-Wetness on Surfaces Exposed to Wetting Conditions as in Atmospheric Corrosion Testing,” ASTM International, West Conshohocken, PA, 2012c.
- [14] ASTM (American Society for Testing and Materials), “ASTM G91 – Standard Practice for Monitoring Atmospheric SO₂ Deposition Rate for Atmospheric Corrosivity Evaluation,” ASTM International, West Conshohocken, PA, 2011b.
- [15] ASTM (American Society for Testing and Materials), “ASTM G101 – Standard Guide for Estimating the Atmospheric Corrosion Resistance of Low-Alloy Steels,” ASTM International, West Conshohocken, PA, 2015c.
- [16] ASTM (American Society for Testing and Materials), “ASTM G140 – Standard Test Method for Determining Atmospheric Chloride Deposition Rate by Wet Candle Method,” ASTM International, West Conshohocken, PA, 2014a.
- [17] ASTM (American Society for Testing and Materials), “ASTM G187 – Standard Test Method for Measurement of Soil Resistivity Using the Two-Electrode Soil Box Method,” ASTM International, West Conshohocken, PA, 2012d.
- [18] ASTM (American Society for Testing and Materials), “ASTM G200 – Standard Test Method for Measurement of Oxidation-Reduction Potential (ORP) of Soil,” ASTM International, West Conshohocken, PA, 2014b.
- [19] AWWA (American Water Works Association), “AWWA C-105 – Polyethylene Encasement for Ductile-Iron Pipe Systems,” AWWA, Denver, CO, 2010.
- [20] Barlo, T. J., “Origin and Validation of the 100 mV Polarization Criterion,” CORROSION 2001, NACE International, 2001.
- [21] Barth, K., McConnell, J., “An Assessment of Weathering Steel Bridges in West Virginia,” Proc. 8th International Conference on Short and Medium Span Bridges, Niagara Falls, Canada, 2010.
- [22] Buck, D. M., “Recent Progress in Corrosion Resistance,” The Mechanical Engineer, pp. 491-493, 1915.

- [23] Buck, D. M., "Copper in Steel – the Influence on Corrosion," *The Journal of Industrial and Engineering Chemistry*, Vol. 5, No. 6, pp. 447-452, 1913.
- [24] Cano, H., Neff, D., Morcillo, M., Dillmann, P., Diaz, I., de la Fuente, D., "Characterization of Corrosion Products Formed on Ni 2.4 wt.%–Cu 0.5 wt.%–Cr 0.5 wt.% Weathering Steel Exposed in Marine Atmospheres," *Corrosion Science*, Vol. 87, pp. 438-451, 2014.
- [25] Chen, Y. Y., Tzeng, H. J., Wei, L. I., Shih, H. C., "Corrosion Resistance and Mechanical Properties of Low-Alloy Steels Under Atmospheric Conditions," *Corrosion Science*, Vol. 47, pp. 1001-1021, 2005.
- [26] Cook, D. C., "An Active Coating and New Protection Technology for Weathering Steel Structures in Chloride Containing Environments," *Corrosion Conference & Expo*, NACE International, 2007.
- [27] Cook, D. C., "The Corrosion of High Performance Steel in Adverse Environments," *Proc. AIP Conference on Industrial Applications of the Mossbauer Effect: International Symposium on the Industrial Applications of the Mossbauer Effect*, Vol. 765, AIP Publishing, pp. 63-72, 2005.
- [28] Cook, D.C., Oh, S. J., Balasubramanian, R., Yamashita, M., "The role of goethite in the formation of the protective corrosion layer on steels," *Hyperfine Interactions*, Vol. 122, No. 1-2, pp. 59-70, 1999.
- [29] Copson, H. R., "A Theory of the Mechanism of Rusting of Low Alloy Steels in the Atmosphere," *Proc. ASTM*, Vol. 45, pp. 554-590, 1945.
- [30] Copson, H. R., "Long-Time Atmospheric Corrosion Tests on Low-Alloy Steels," *Proc. ASTM*, Vol. 60, pp. 1-16, 1960.
- [31] Cosaboom, B., Mehalchick, G., Zoccola, J. C., "Bridge Construction with Unpainted, High-Strength, Low-Alloy Steel: Eight-Year Progress Report," *New Jersey Department of Transportation, Division of Research and Development*, 1979.
- [32] CSA (Canadian Standards Association), "CSA G40.20/G40.21 – General requirements for rolled or welded structural quality steel / Structural quality steel," CSA, Toronto, ON, 2013.
- [33] De la Fuente, D., Diaz, I., Simancas, J., Chico, B., Morcillo, M., "Long-Term Atmospheric Corrosion of Mild Steel," *Corrosion Science*, Vol. 53, pp. 604-617, 2011.
- [34] Dean, S. W., "Classifying Atmospheric Corrosivity: A Challenge for ISO," *Materials Performance*, Vol. 32, No. 10, pp. 53-58, 1993.

- [35] Diaz, I., Cano, H., Chico, B., De la Fuente, D., Morcillo, M., "Some Clarifications Regarding Literature on Atmospheric Corrosion of Weathering Steels," *International Journal of Corrosion*, 2012.
- [36] Dodson, D., "Winyah-Charity 230kV Line Corrosion Issues on Steel Structures," *Proc. Management of Existing Overhead Lines WG Meeting*, San Diego, CA, 2012.
- [37] DVGW, "Merkblatt für die Beurteilung der Korrosionsgefährdung von Eisen und Stahl im Erdboden (GW9:2011 – Evaluation Of Soils In View Of Their Corrosion Behaviour Towards Buried Pipelines And Vessels Of Non-Alloyed Iron Materials)," German Technical and Scientific Association for Gas and Water, Frankfurt, Germany, 2011.
- [38] EPRI, "Assessment of Treated Wood and Alternate Materials for Utility Poles," *Electric Power Research Institute*, Palo Alto, CA, 2005.
- [39] Epstein, S., Horton, J.B., "Atmospheric Corrosion Tests of Plain Low Carbon and Low Alloy Steels," *Research Department*, Bethlehem Steel, Bethlehem, PA, 1949.
- [40] Fang, S. J., Roy, S., Kramer, J., "Transmission Structures," In: Chen, W. F., Editor, *Structural Engineering Handbook*, CRC Press LLC, Chicago, IL, 1999.
- [41] Ferm, M., Watt, J., O'Hanlon, S., De Santis, F., Varotsos, C., "Deposition Measurement of Particulate Matter in Connection with Corrosion Studies." *Analytical and Bioanalytical Chemistry*, Vol. 384, No. 6, pp. 1320-1330, 2006.
- [42] Flores, S., Simancas, J., Morcillo, M., "Methods for Sampling and Analyzing Soluble Salts on Steel Surfaces: A Comparative Study." *Journal of Protective Coatings and Linings*, Vol. 11, pp. 76-76, 1994.
- [43] Gomez, J. M., Antonissen, J., Palacio, C. A., De Grave, E., "Effects of Si as Alloying Element on Corrosion Resistance of Weathering Steel," *Corrosion Science*, Vol. 59, pp. 198-203, 2012.
- [44] Gomez, J. M., De Resende, V. G., Antonissen, J., De Grave, E., "Characterization of the Effects of Silicon on the Formation of Goethite," *Corrosion Science*, Vol. 53, pp. 1756-1761, 2011.
- [45] Goodwin, E. J., Pohlman, J. C., "Corrosion Resistance of Transmission Line Structures Fabricated from Weathering Steel," *IEEE Transactions on Power Delivery*, Vol. 8, pp. 386-392, 1993.
- [46] Greenfield, D., Scantlebury, D., "The protective action of organic coatings on steel: a review," *Journal of Corrosion Science & Engineering*, Vol. 3, 2000.

- [47] Greenwood, N., Mössbauer spectroscopy. Springer Science & Business Media, 2012.
- [48] Hao, L., Zhang, S., Dong, J., Ke, W., “Atmospheric Corrosion Resistance of MnCuP Weathering Steel in Simulated Environments,” *Corrosion Science*, Vol. 53, pp. 4187-4192, 2011.
- [49] Hoitomt, M. L., “Performance of Weathering Steel Tubular Structures,” In: Townsend, H. E., Editor, ASTM STP 1421 – Outdoor Atmospheric Corrosion, ASTM International, West Conshohocken, PA, pp. 301-315, 2002.
- [50] Holtsbaum, W. B., “Application and Misapplication of the 100-mV Criterion for Cathodic Protection,” *Materials Performance*, Vol. 42, pp. 30-32, 2003.
- [51] Hou, W. T., Liang, C. F., “Effects of Alloying on Atmospheric Corrosion of Steels,” In: Townsend, H. E., Editor, ASTM STP 1421 – Outdoor Atmospheric Corrosion, ASTM International, West Conshohocken, PA, pp. 368-378, 2002.
- [52] Ibrahim, E. S., “Corrosion Control in Electric Power Systems,” *Electric Power Systems Research*, Vol. 52, pp. 9-17, 1999.
- [53] ICDD (International Centre for Diffraction Data), Powder Diffraction File (PDF): PDF-4+, ICDD, Newtown Square, PA, 15 Mar. 2016. <http://www.icdd.com/index.htm>, 2015.
- [54] Ismail, A. I. M., El-Shamy, A. M., “Engineering behaviour of soil materials on the corrosion of mild steel,” *Applied Clay Science*, Vol. 42, No. 3, pp. 356-362, 2009.
- [55] ISO (International Organization for Standardization), “ISO 16831 – Non-destructive testing – Ultrasonic testing – Characterization and verification of ultrasonic thickness measuring equipment,” ISO, Geneva, Switzerland, 2012a.
- [56] ISO (International Organization for Standardization), “ISO 2178 – Non-magnetic coatings on magnetic substrates – Measurement of coating thickness – Magnetic method,” ISO, Geneva, Switzerland, 2016.
- [57] ISO (International Organization for Standardization), “ISO 8502-6 – Preparation of steel substrates before application of paints and related products -- Tests for the assessment of surface cleanliness -- Part 6: Extraction of soluble contaminants for analysis -- The Bresle method,” ISO, Geneva, Switzerland, 2006.
- [58] ISO (International Organization for Standardization), “ISO 9223 – Corrosion of Metals and Alloys – Corrosivity of Atmospheres – Classification, Determination and Estimation,” ISO, Geneva, Switzerland, 2012b.

- [59] ISO (International Organization for Standardization), "ISO 9224 – Corrosion of Metals and Alloys – Corrosivity of Atmospheres – Guiding Values for the Corrosivity Categories," ISO, Geneva, Switzerland, 2012c.
- [60] Johnson, K., "Q3C-QE14 Transmission Line Status Evaluation of Corrosion Levels & Coating," CorrPro Canada, Inc., pp. 12, 2013.
- [61] Kamimura, T., Hara, S., Miyuki, H., Yamashita, M., Uchida, H., "Composition and Protective Ability of Rust Layer Formed on Weathering Steel Exposed to Various Environments," Corrosion Science, Vol. 48, pp. 2799-2812, 2006.
- [62] Kamimura, T., Nasu, S., "Mössbauer Spectroscopic Study of Rust Formed on Weathering Steel Exposed for 15 Years in an Industrial Environment," Materials Transactions, Vol. 41, pp. 1208-1215, 2000.
- [63] Kamimura, T., Nasu, S., Tazaki, T., Kuzushita, K., Morimoto, S., "Mössbauer Spectroscopic Study of Rust Formed on a Weathering Steel and a Mild Steel Exposed for a Long Term in an Industrial Environment," Materials Transactions, Vol. 43, pp. 694-703, 2002.
- [64] Kamimura, T., Stratmann, M., "The Influence of Chromium on the Atmospheric Corrosion of Steel," Corrosion Science, Vol. 43, pp. 429-447, 2001.
- [65] Knotkova-Cermakova, D., Vlckova, J., Honzak, J., "Atmospheric Corrosion of Weathering Steels," In: ASTM STP 767 – Atmospheric Corrosion of Metals, ASTM International, West Conshohocken, PA, pp. 7-44, 1982.
- [66] Kucera, V., Mattsson, E., "Atmospheric Corrosion," In: Mansfeld, F., Editor, Corrosion Mechanisms, Vol. 28, Marcel Dekker, Inc., New York, NY, pp. 211-284, 1987.
- [67] Larrabee, C. P., "Corrosion Resistance of High-Strength Low-Alloy Steels as Influenced by Composition and Environment," Corrosion, Vol. 9, No. 8, pp. 259-271, 1953.
- [68] Larrabee, C. P., Coburn, S. K., "The Atmospheric Corrosion of Steels as Influenced by Changes in Chemical Composition," Proc. First International Congress on Metallic Corrosion, London, 1961, pp. 279-285, 1961.
- [69] Leidheiser, H., Czako-Nagy, I., "A Mössbauer Spectroscopic Study of Rust Formed During Simulated Atmospheric Corrosion," Corrosion Science, Vol. 24, No. 7, pp. 569-577, 1984.
- [70] Li, Q.X., Wang, Z.Y., Han W., Han, E.H., "Characterization of the Rust Formed on Weathering Steel Exposed to Qinghai Salt Lake Atmosphere," Corrosion Science, Vol. 50, pp. 365-371, 2008.

- [71] Matsushima, I., Ishizu, Y., Ueno, T., Kanasashi, M., Horikawa, K., "Effect of Structural and Environmental Factors on the Practical Use of Low-Alloy Weathering Steel," *Corrosion Engineering*, Vol. 23, pp. 177-182, 1974.
- [72] Matta, F., Pierce, C.E., Rizzo, P., "New Structural Materials for Transmission Lines," Final Report T103700-3370, Centre for Energy Advancement through Technological Innovation (CEATI), 2012.
- [73] Matta, F., Vélez, W., Rizzo, P., "Corrosion Assessment of Tubular Steel Poles," Final Report T123700-3386, Centre for Energy Advancement through Technological Innovation (CEATI), 2014.
- [74] McCuen, R. H., Albrecht, P., "Reanalysis of Thickness Loss Data for Weathering Steel," *Journal of Materials in Civil Engineering*, Vol. 16, No. 3, pp. 237-246, 2004.
- [75] Mendoza, A.R., Corvo, F., "Outdoor and Indoor Atmospheric Corrosion of Carbon Steel," *Corrosion Science*, Vol. 41, No. 1, pp. 75-86, 1999.
- [76] Misawa, T., "Corrosion Science in Rusting of Iron and Weathering Steel," *Boshoku Gijutsu (Corrosion Engineering)*, Vol. 37, No. 8, pp. 501-506, 1988.
- [77] Misawa, T., Asami, K., Hashimoto, K., Shimodaira, S., "The Mechanism of Atmospheric Rusting and the Protective Amorphous Rust on Low Alloy Steel," *Corrosion Science*, Vol. 14, pp. 279-289, 1974.
- [78] Morcillo, M., Chico, B., Diaz, I., Cano, H., de la Fuente, D., "Atmospheric Corrosion Data of Weathering Steels. A Review," *Corrosion Science*, Vol. 77, pp. 6-24, 2013.
- [79] Morcillo, M., Chico, B., Diaz, I., Cano, H., de la Fuente, D., "Weathering Steels: From Empirical Development to Scientific Design. A Review," *Corrosion Science*, Vol. 83, pp. 6-31, 2014.
- [80] Moroishi, T., Satake, J., "Effect of Alloying Elements on Atmospheric Corrosion of High-Tensile-Strength Steels," *Tetsu-to-Hagane*, Vol. 59, No. 2, pp. 293-300, 1973.
- [81] Mozaffari, M., Shatooti, S., Jafarzadeh, M., Niyafar, M., Aftabi, A., Mohammadpour, H., Amiri, S., "Synthesis of Zn ²⁺ substituted maghemite nanoparticles and investigation of their structural and magnetic properties," *Journal of Magnetism and Magnetic Materials* Vol. 382, pp. 366-375, 2015.
- [82] Murad, E., "Magnetic properties of microcrystalline iron (III) oxides and related materials as reflected in their Mössbauer spectra," *Physics and chemistry of minerals*, Vol. 23, No. 4-5, pp. 248-262, 1996.

- [83] Murata, T., "Weathering Steel," In: Revie, R. W., Editor, Uhlig's Corrosion Handbook, John Wiley & Sons, New York, NY, 2000.
- [84] NACE (National Association of Corrosion Engineers), "Control of External Corrosion on Underground or Submerged Metallic Piping Systems," NACE SP0169-2013 (formerly RP0169), NACE International, Houston, TX, 2013.
- [85] NFPA (National Fire Protection Association), "NFPA 70 – National Electrical Code," NFPA, Quincy, MA, pp. 94-104, 2014.
- [86] Nishikata, A., Yamashita, Y., Katayama, H., Tsuru, T., Tanabe, K., Mabuchi, H., "An Electrochemical Impedance Study on Atmospheric Corrosion of Steels in a Cyclic Wet-Dry Condition," Corrosion Science, Vol. 37, No. 12, pp. 2059-2069, 1995.
- [87] Oesch, S., "The effect of SO₂, NO₂, NO and O₃ on the Corrosion of Unalloyed Carbon Steel and Weathering Steel—The Results of Laboratory Exposures," Corrosion Science, Vol. 38, No. 8, pp. 1357-1368, 1996.
- [88] Oh, S. J., Cook, D. C., Townsend, H. E., "Atmospheric Corrosion of Different Steels in Marine, Rural and Industrial Environments," Corrosion Science, Vol. 41, No. 9, pp. 1687-1702, 1999.
- [89] Popov, B. N., Corrosion Engineering, 1st Edition, Elsevier, 2015.
- [90] PotashCorp, "2015 Annual Integrated Report," PotashCorp, Saskatoon, SK, 2015.
- [91] Pourbaix, M., "The Linear Bilogarithmic Law for Atmospheric Corrosion," Proc. Atmospheric Corrosion Conference, Hollywood, FL, John Wiley & Sons, pp. 107-121, 1980.
- [92] Pourbaix, M., Pourbaix, A., "Recent Progress in Atmospheric Corrosion Testing," Corrosion, Vol. 45, No. 1, pp. 71-83, 1989.
- [93] Poursaee, A., Hansson, C. M., "Potential Pitfalls in Assessing Chloride-Induced Corrosion of Steel in Concrete," Cement and Concrete Research, Vol. 39, pp. 391-400, 2009.
- [94] Qian, Y., Ma, C., Niu, D., Xu, J., Li, M., "Influence of Alloyed Chromium on the Atmospheric Corrosion Resistance of Weathering Steels," Corrosion Science, Vol. 74, pp. 424-429, 2013.
- [95] Rancourt, D.G., Ping, J.Y., "Voigt-based methods for arbitrary-shape static hyperfine parameter distributions in Mössbauer spectroscopy," Nuclear Instruments and Methods in Physics Research Section B: Beam Interactions with Materials and Atoms, Vol. 58, No. 1, pp. 85-97, 1991.

- [96] Revie, R. W., Uhlig, H. H., Corrosion and Corrosion Control, John Wiley & Sons, pp. 191-316, 2008.
- [97] Roberge, P. R., Corrosion Engineering: Principles and Practice, McGraw-Hill, New York, NY, 2008.
- [98] Roberge, P. R., Klassen, R. D., Haberecht, P. W., "Atmospheric Corrosivity Modeling—A Review," *Materials & Design*, Vol. 23, No. 3, pp. 321-330, 2001.
- [99] Roque-Malherbe, R., Lugo, F., Rivera-Maldonado, C., "Synthesis, Characterization and Thermodynamic Study of Carbon Dioxide Adsorption on Akaganeite," *Current Applied Physics* Vol. 15, No. 4, pp. 571-579, 2015.
- [100] Schmitt, R. J., Gallagher, W.P., "Unpainted High Strength Low Alloy Steel," *Materials Protection*, 1969.
- [101] Sereda, P. J., "Atmospheric Factors Affecting the Corrosion of Steel," *Industrial & Engineering Chemistry*, Vol. 52, No. 2, pp. 157-160, 1960.
- [102] Tallavo, F., Pandey, M. D., Cascante, G., "Experimental and Numerical Methods for Detection of Voids in Wood Poles Using Ultrasonic Testing." *Journal of Materials in Civil Engineering*, Vol. 25, No. 6, pp. 772-780, 2013.
- [103] Tanner, R. L., Leaderer, B. P., Spengler, J. D., "Acidity of Atmospheric Aerosols," *Environmental Science & Technology*, Vol. 15, No. 10, pp. 1150-1153, 1981.
- [104] Topal, U., Aksan, M., "Phase stabilization of magnetite (Fe₃O₄) nanoparticles with B₂O₃ addition: A significant enhancement on the phase transition temperature," *Journal of Magnetism and Magnetic Materials*, Vol. 406, pp. 123-128, 2016.
- [105] Townsend, H. E., Zoccola, J. C., "Eight-Year Atmospheric Corrosion Performance of Weathering Steel in Industrial, Rural, and Marine Environments," In: *ASTM STP 767 – Atmospheric Corrosion of Metals*, ASTM International, West Conshohocken, PA, pp. 45-59, 1982.
- [106] Townsend, H. E., "Estimating the Atmospheric Corrosion Resistance of Weathering Steel," In: Townsend, H. E., Editor, *ASTM STP 1421 – Outdoor Atmospheric Corrosion*, ASTM International, West Conshohocken, PA, pp. 292-300, 2002.
- [107] Wang, J. H., Wei F. I., Shin H. C., "Modeling of Atmospheric Corrosion Behavior of Weathering Steel in Sulfur Dioxide-Polluted Atmospheres," *Corrosion*, Vol. 52, No. 12, pp. 900-909, 1996.

- [108] Wang, J. H., Wei, F. I., Chang, Y. S., Shih, H. C., “The Corrosion Mechanisms of Carbon Steel and Weathering Steel in SO₂ Polluted Atmospheres,” *Materials Chemistry and Physics*, Vol. 47, No. 1, pp. 1-8, 1997.
- [109] Wang, J., Wang, Z. Y., Ke, W., “A Study of the Evolution of Rust on Weathering Steel Submitted to the Qinghai Salt Lake Atmospheric Corrosion,” *Materials Chemistry and Physics*, Vol. 139, pp. 225-232, 2013.
- [110] Wang, J., Wang, Z. Y., Ke, W., “Corrosion Behavior of Weathering Steel in Diluted Qinghai Salt Water in a Laboratory Accelerated Test that Involved Cyclic Wet/Dry Conditions,” *Materials Chemistry and Physics*, Vol. 124, pp. 952-958, 2010.
- [111] WeatherSpark, “Average Weather for Cocoa Beach, Florida, USA,” *WeatherSpark*, Patrick Air Force Base weather station, 17 Nov. 2015. <https://weatherspark.com/averages/29944/Cocoa-Beach-Florida-United-States>, 2015a.
- [112] WeatherSpark, “Average Weather for Estevan, Saskatchewan, Canada,” *WeatherSpark*, Estevan Regional Aerodrome weather station, 17 Nov. 2015. <https://weatherspark.com/averages/28238/Estevan-Saskatchewan-Canada>, 2015b.
- [113] WeatherSpark, “Average Weather for Melbourne, Florida, USA,” *WeatherSpark*, Melbourne International Airport weather station, 17 Nov. 2015. <https://weatherspark.com/averages/30903/Melbourne-Florida-United-States>, 2015c.
- [114] WeatherSpark, “Average Weather for Regina, Saskatchewan, Canada,” *WeatherSpark*, Regina International Airport weather station, 17 Nov. 2015. <https://weatherspark.com/averages/27675/Regina-Saskatchewan-Canada>, 2015d.
- [115] WeatherSpark, “Average Weather for Saskatoon, Saskatchewan, Canada,” *WeatherSpark*, John G. Diefenbaker International Airport weather station, 17 Nov. 2015. <https://weatherspark.com/averages/28418/Saskatoon-Saskatchewan-Canada>, 2015e.
- [116] Wong, C. J., “Fact or Fiction—Weathering Steel Can Provide Effective Corrosion Protection to Steel Structures,” *Electrical Transmission and Substation Structures*, ASCE, pp. 1-8, 2009.
- [117] Yamashita, M., Miyuki, H., Matsuda, Y., Nagano, H., Misawa, T., “The Long Term Growth of the Protective Rust Layer formed on Weathering Steel by Atmospheric Corrosion during a Quarter of a Century,” *Corrosion Science*, Vol. 36, No.2, pp. 283-299, 1994.
- [118] Yamashita, M., Nagano, H., Misawa, T., Townsend, H. E., “Structure of Protective Rust Layers Formed on Weathering Steels by Long-Term Exposure in the Industrial

- Atmospheres of Japan and North America,” ISIJ international, Vol. 38, No. 3, pp. 285-290, 1998.
- [119] Yang, F., Han, J., Yang, J., Li, Z., “Some Advances in the Application of Weathering and Cold-Formed Steel in Transmission Tower,” Journal of Electromagnetic Analysis and Applications, Vol. 1, pp. 24-30, 2009.
- [120] Zamanzadeh, M., Kempkes, C., Aichinger, D., Riley, D., “Laboratory and Field Corrosion Investigation of Galvanized Utility Poles,” Electrical Transmission Line and Substation Structures, pp. 235-249, 2006.
- [121] Zeng, Z., Natesan, K., Cai, Z., Rink, D. L., “Effect of Coal Ash on the Performance of Alloys in Simulated Oxy-Fuel Environments,” Fuel, Vol. 117, pp. 133-145, 2014.
- [122] Zic, M., Ristić, M., Musić, S., “⁵⁷Fe Mössbauer, FT-IR and FE SEM Investigation of the Formation of Hematite and Goethite at High pH Values,” Journal of Molecular Structure, Vol. 834-836, pp. 141-149, 2007.

APPENDIX A: SUPPLEMENTARY RESULTS FROM LABORATORY ANALYSIS

This appendix presents supplementary results from laboratory testing and analysis performed on oxide samples collected from WS transmission line poles. Section A.1 offers looks at solid rust specimens that were evaluated by SEM, as well as micrographs displaying various magnifications of these specimens. Section A.2 reports XRD spectra obtained for powder oxide specimens collected. Section A.3 presents ^{57}Fe Mössbauer spectra and parameters obtained from simulations of these spectra.

A.1 Scanning Electron Microscopy (SEM)

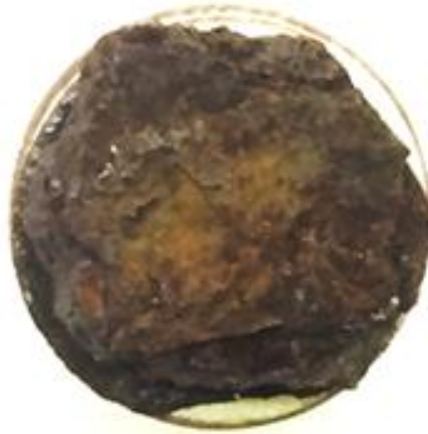


Figure A.1 Pack-rust sample from coating line region of Pole Q3C-1L at Site 2.

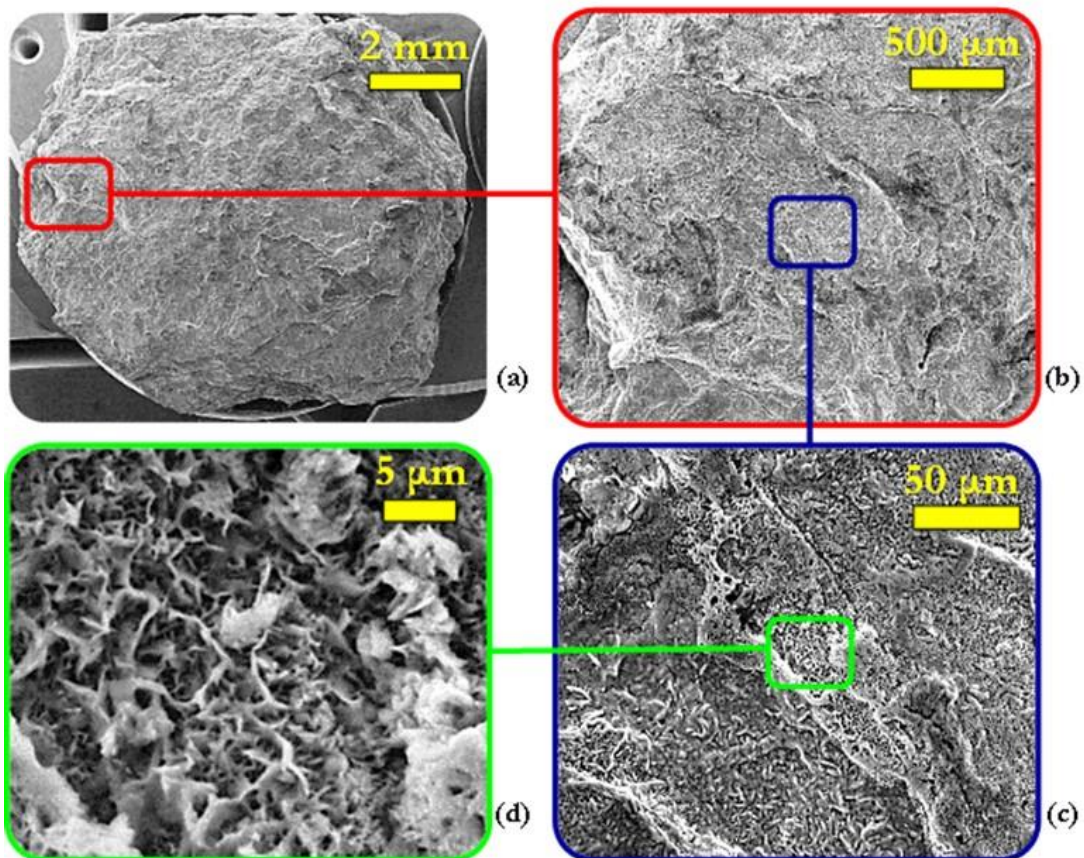


Figure A.2 SEM micrographs for pack-rust sample from coating line region of Pole Q3C-1L at Site 2: (a) full view; (b) magnified 100x; (c) magnified 1000x; and (d) magnified 5000x.



Figure A.3 Pack-rust sample from coating line region of Pole Q3C-2L at Site 2.

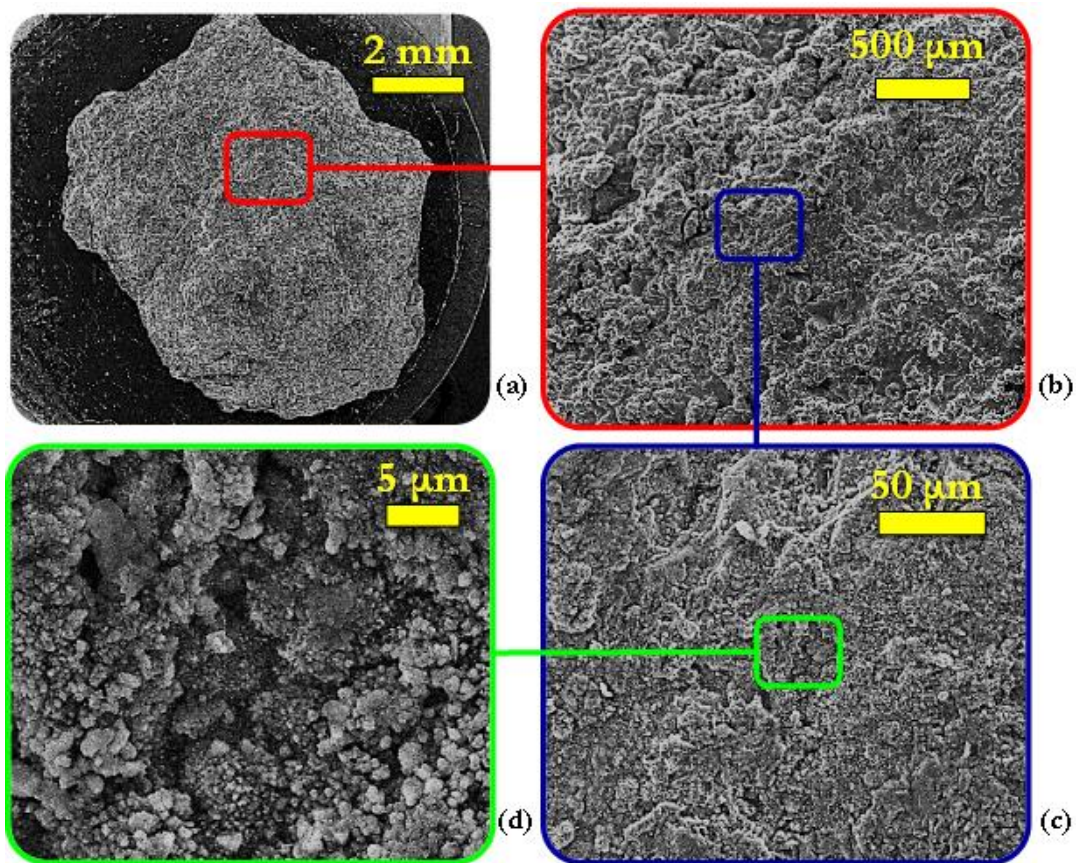


Figure A.4 SEM micrographs for pack-rust sample from coating line region of Pole Q3C-2L at Site 2: (a) full view; (b) magnified 100x; (c) magnified 1000x; and (d) magnified 5000x.



Figure A.5 Pack-rust sample from coating line region of Pole Q3C-2R at Site 2.

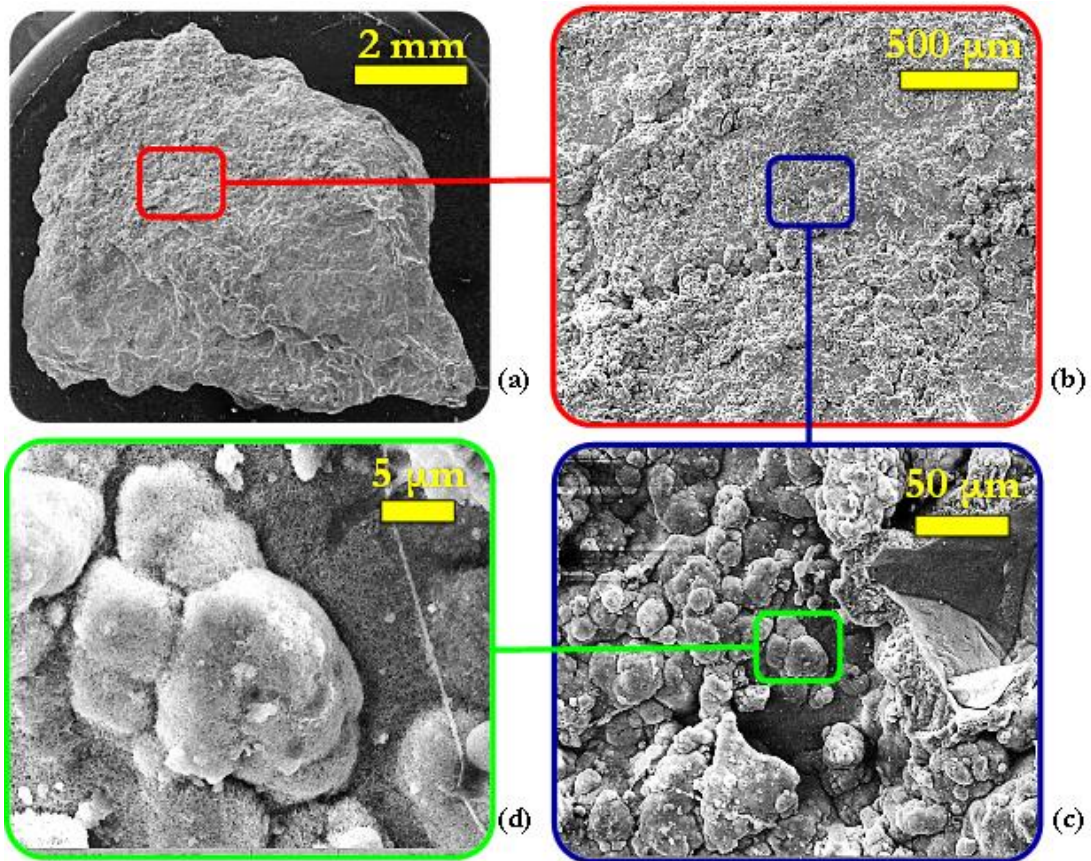


Figure A.6 SEM micrographs for pack-rust sample from coating line region of Pole Q3C-2R at Site 2: (a) full view; (b) magnified 100x; (c) magnified 1000x; and (d) magnified 5000x.



Figure A.7 Outer pack-out sample from Pole TL-1 at Site 4.

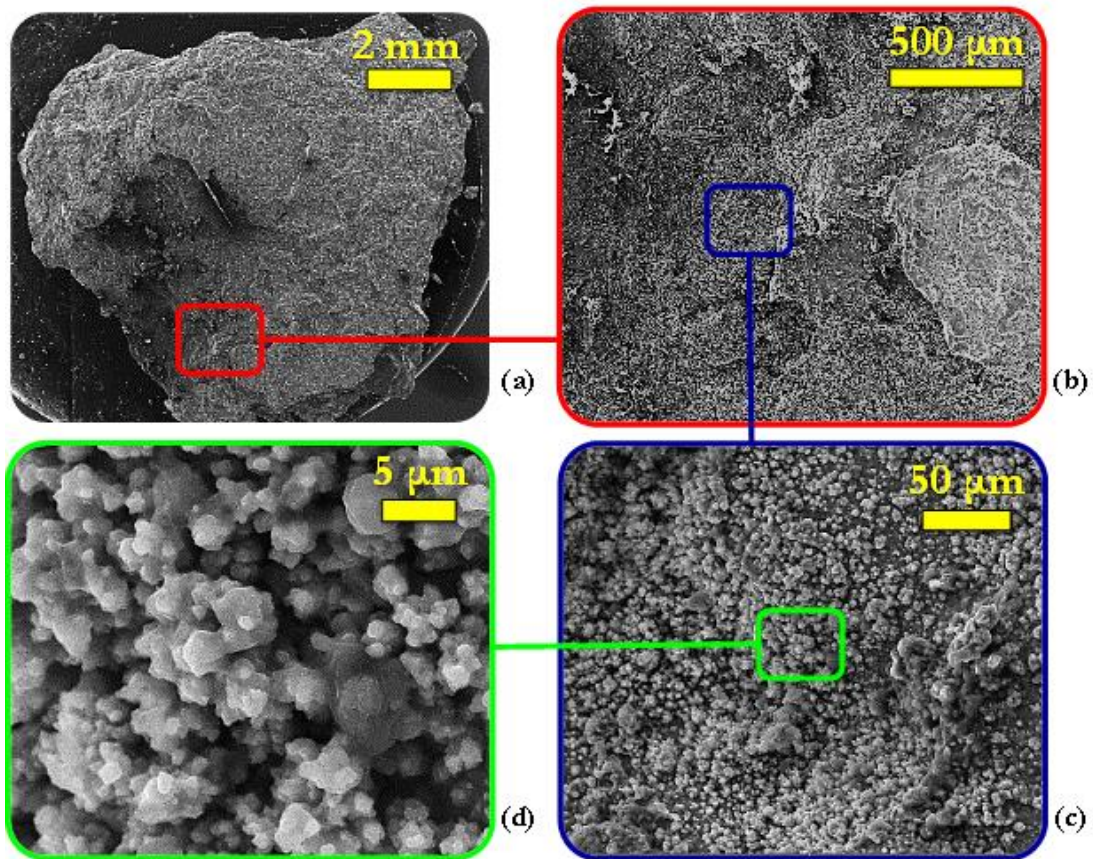


Figure A.8 SEM micrographs for outer pack-out sample from Pole TL-1 at Site 4: (a) full view; (b) magnified 100x; (c) magnified 1000x; and (d) magnified 5000x.



Figure A.9 Inner pack-out sample from Pole TL-1 at Site 4.

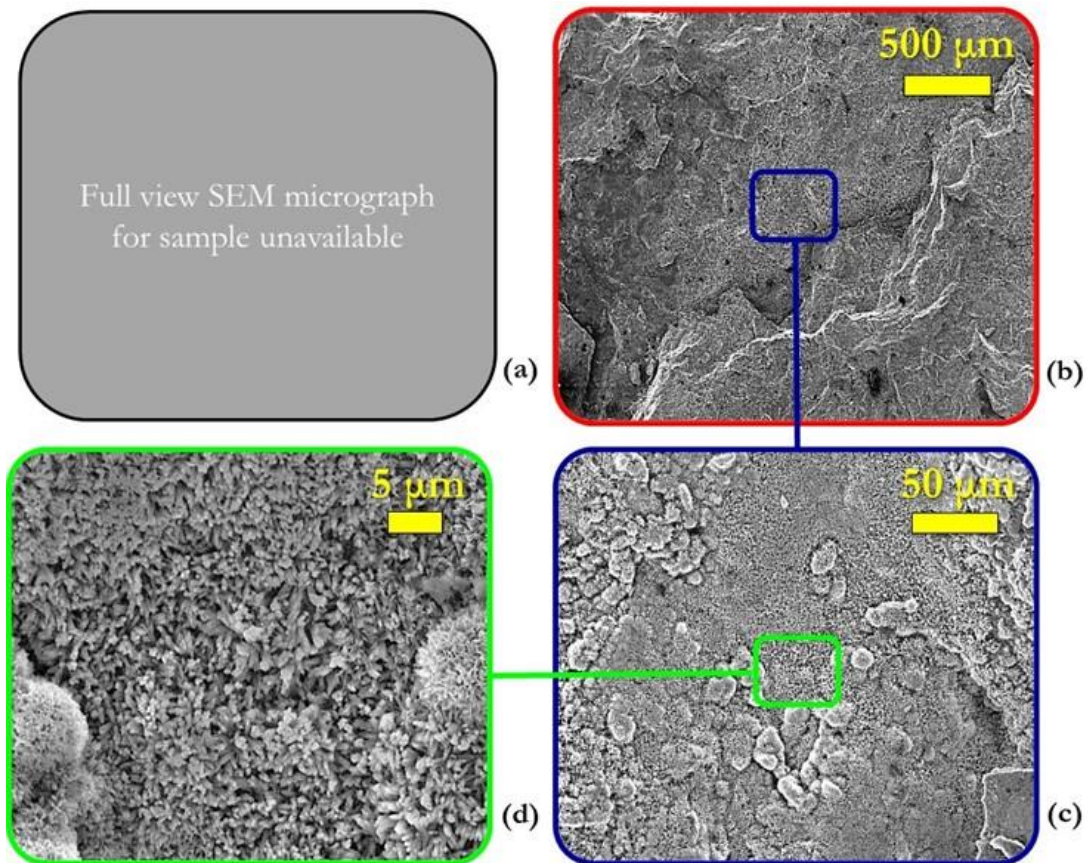


Figure A.10 SEM micrographs for inner pack-out sample from Pole TL-1 at Site 4:
(a) full view; (b) magnified 100x; (c) magnified 1000x; and (d) magnified 5000x.

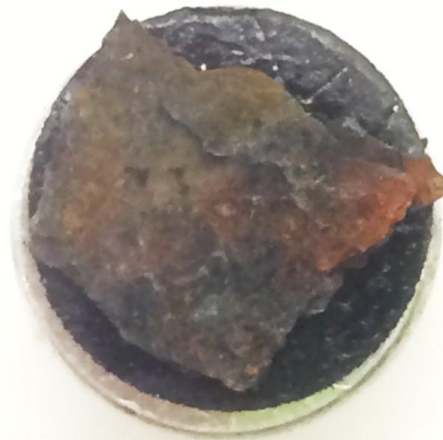


Figure A.11 Loose rust sample from GS fastener region of Pole 8Z-2L at Site 5.

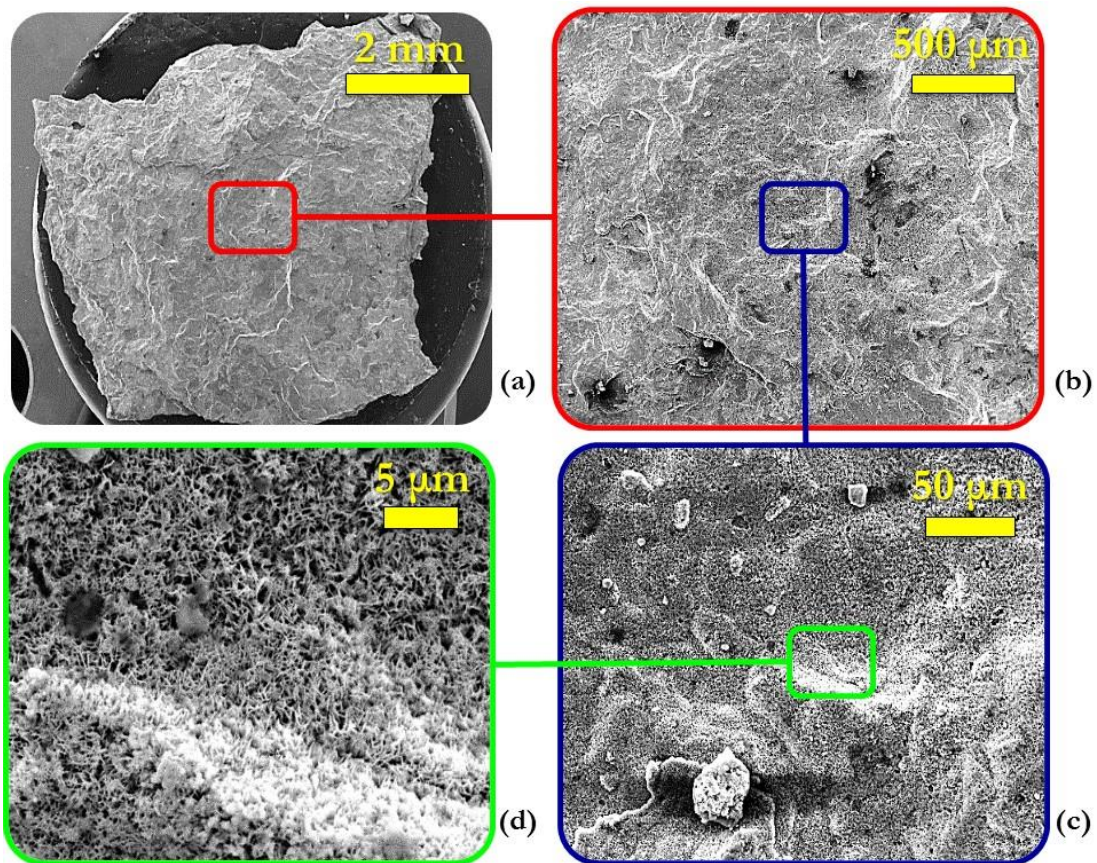


Figure A.12 SEM micrographs for loose rust sample from GS fastener region of Pole 8Z-2L at Site 5: (a) full view; (b) magnified 100x; (c) magnified 1000x; and (d) magnified 5000x.



Figure A.13 Loose rust sample from GS fastener region of Pole 8Z-2R at Site 5.

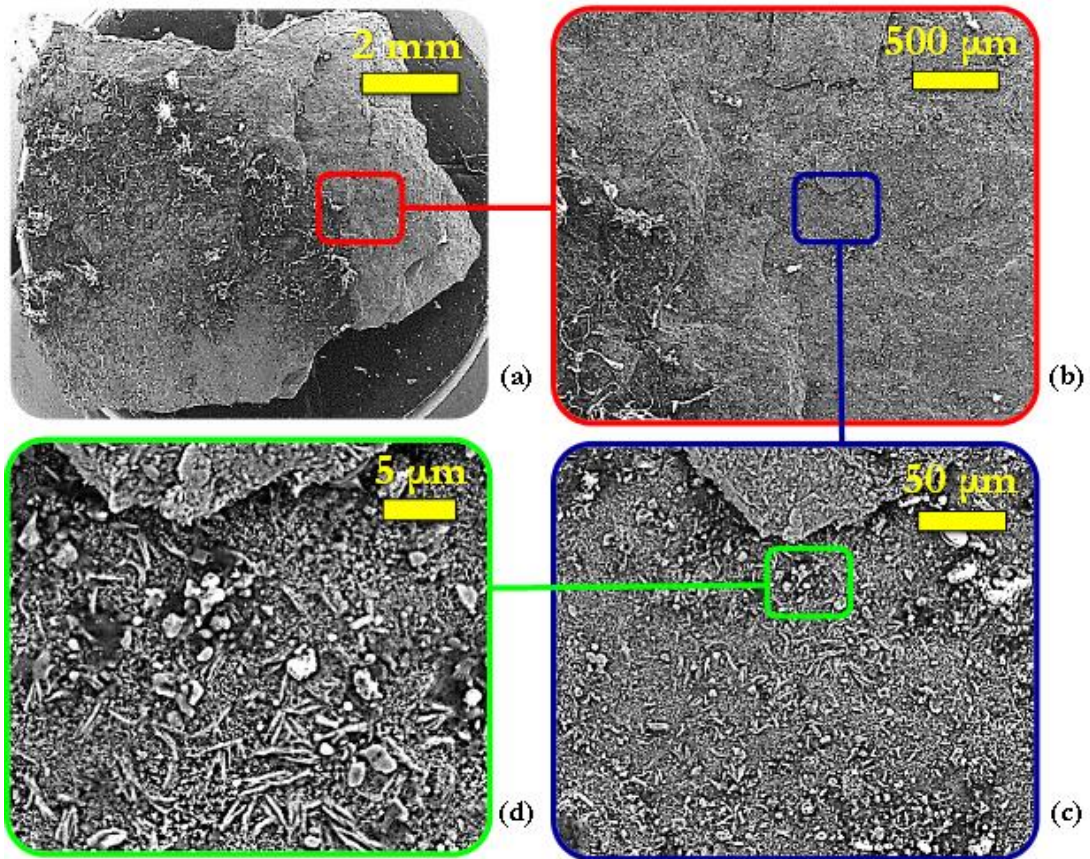


Figure A.14 SEM micrographs for loose rust sample from GS fastener region of Pole 8Z-2R at Site 5: (a) full view; (b) magnified 100x; (c) magnified 1000x; and (d) magnified 5000x.



Figure A.15 Loose rust sample from GS fastener region of Pole 11Z-6R at Site 5.

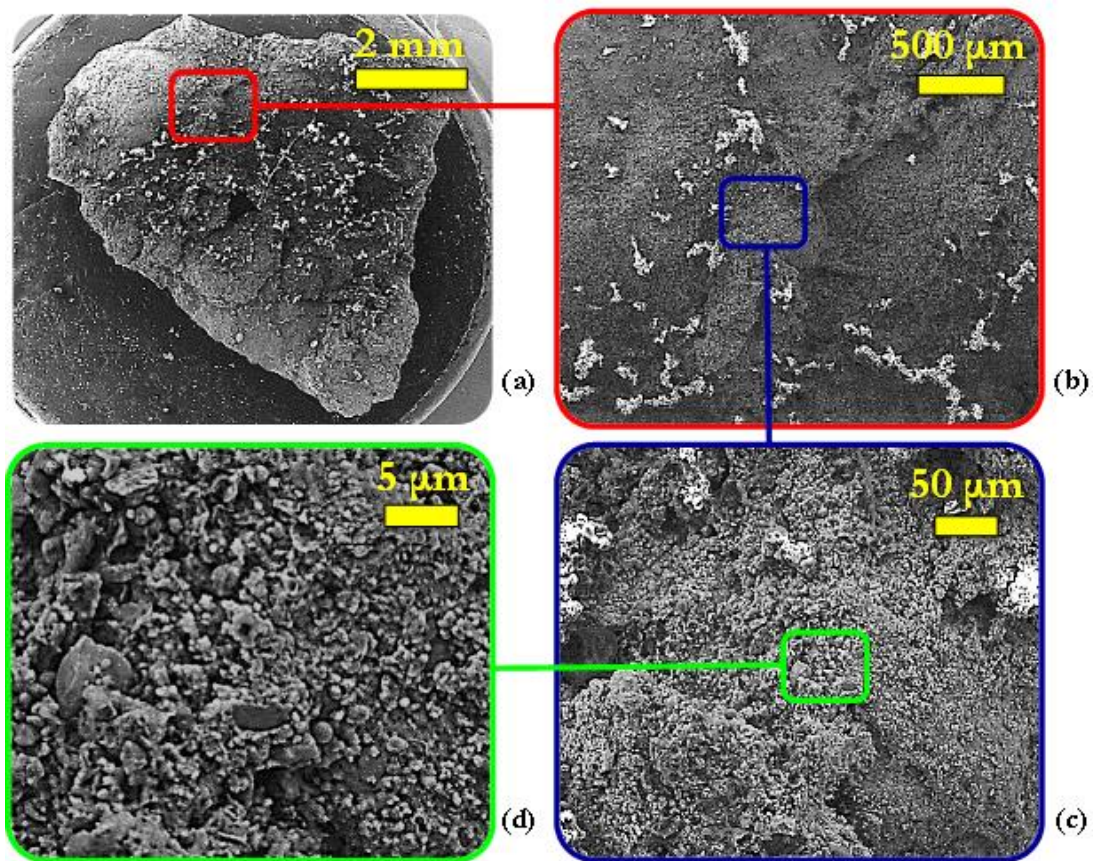


Figure A.16 SEM micrographs for loose rust sample from GS fastener region of Pole 11Z-6R at Site 5: (a) full view; (b) magnified 100x; (c) magnified 1000x; and (d) magnified 5000x.

A.2 X-Ray Diffraction (XRD)

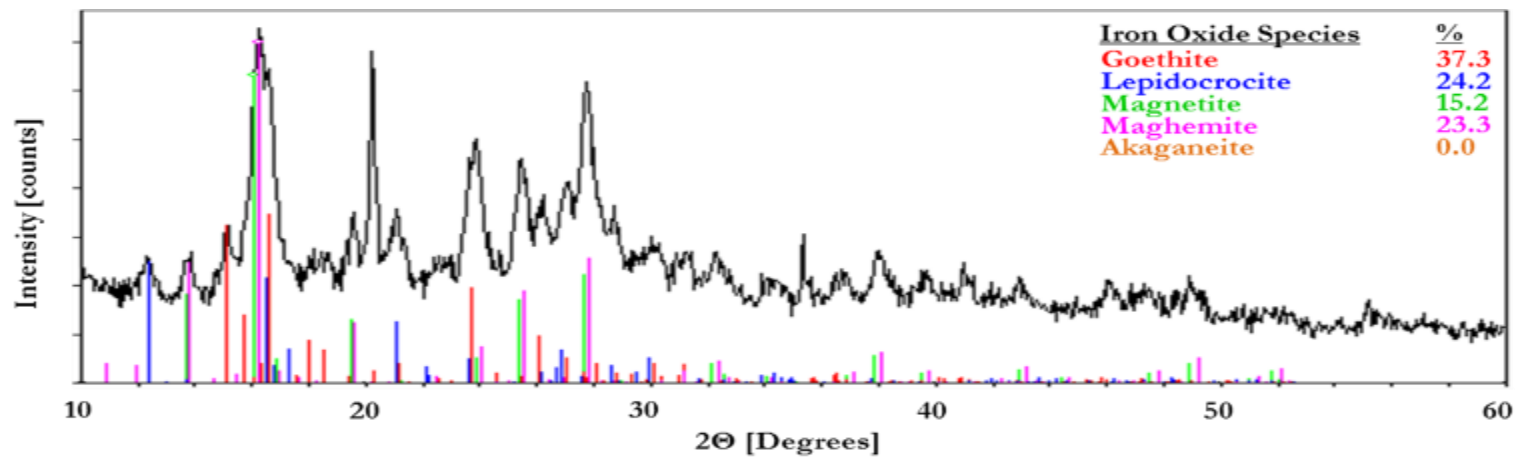


Figure A.17 XRD spectrum for pack-rust sample from reflective tape region of Pole C1F-20 at Site 1.

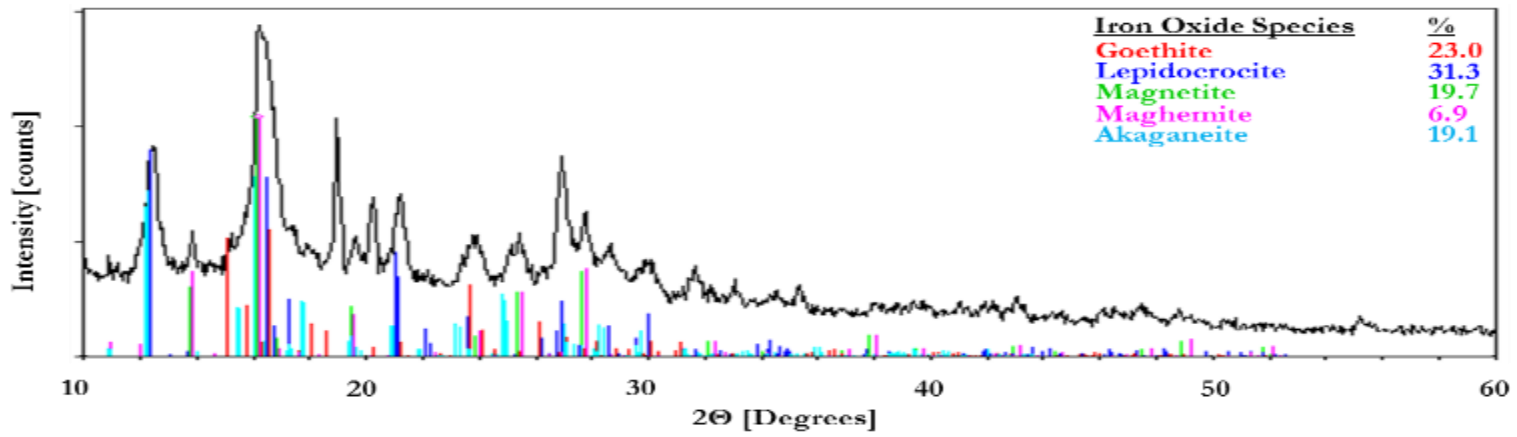


Figure A.18 XRD spectrum for pole wall sample from Pole Q3C-1L at Site 2.

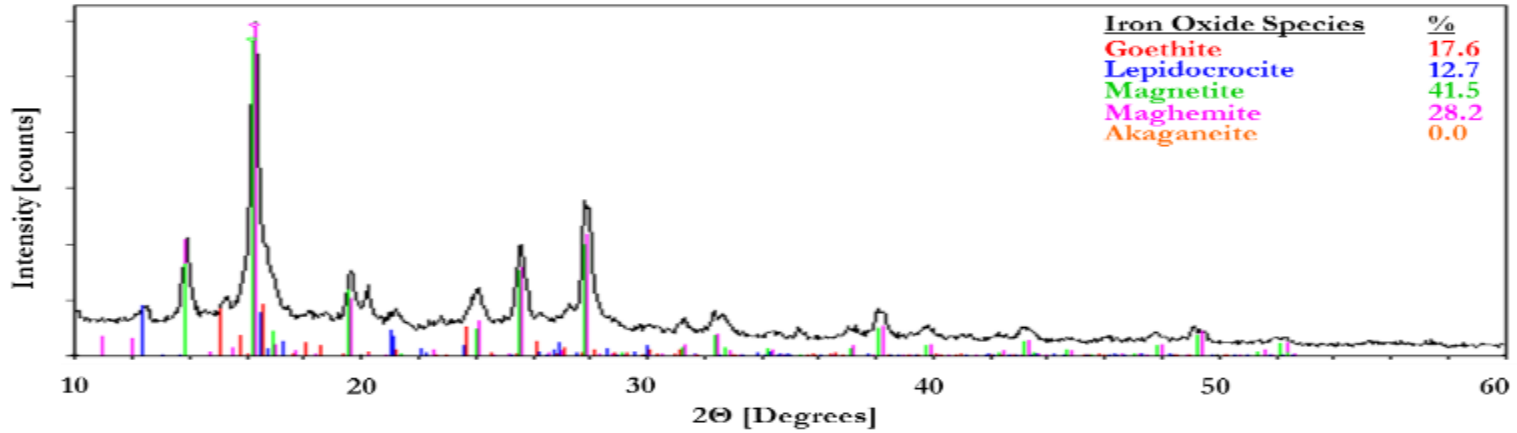


Figure A.19 XRD spectrum for pack-rust sample from coating line region of Pole Q3C-1L at Site 2.

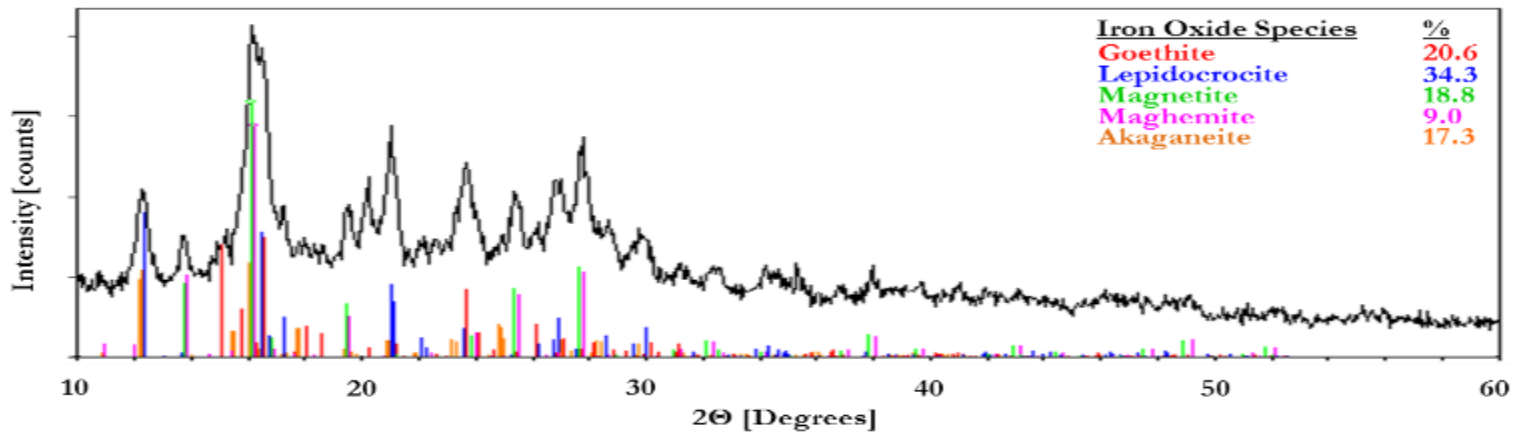


Figure A.20 XRD spectrum for pole wall sample from Pole Q3C-1R at Site 2.

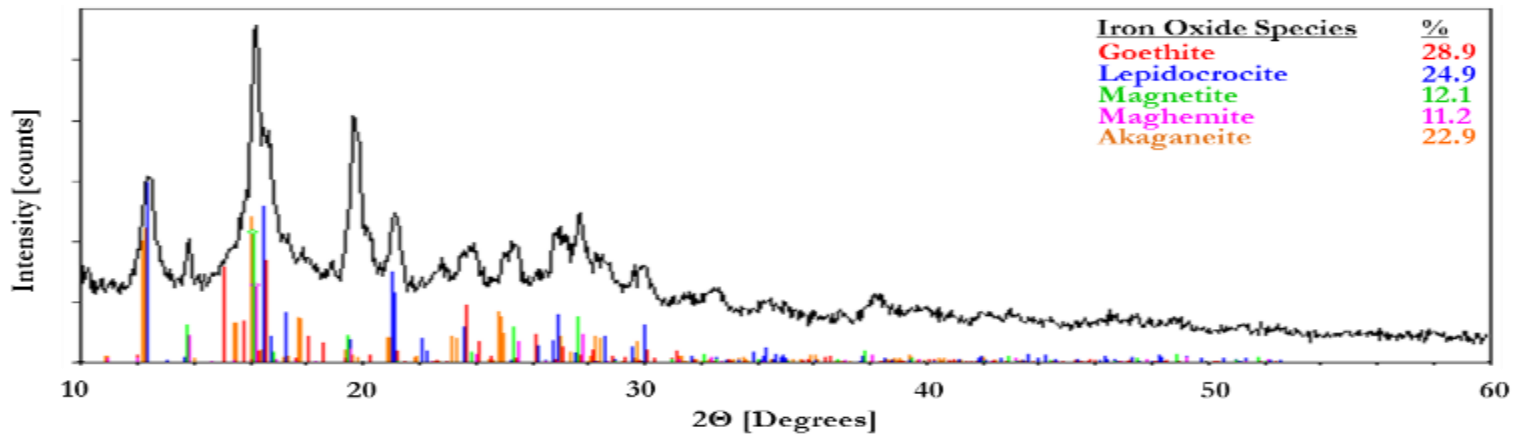


Figure A.21 XRD spectrum for pole wall sample from Pole Q3C-2L at Site 2.

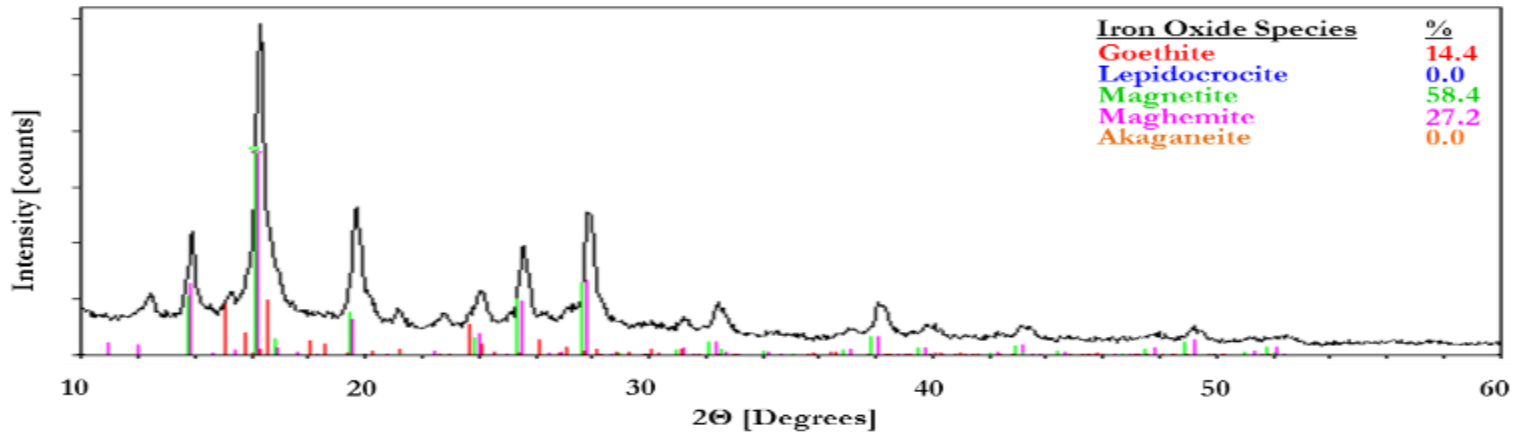


Figure A.22 XRD spectrum for pack-rust sample from coating line region of Pole Q3C-2L at Site 2.

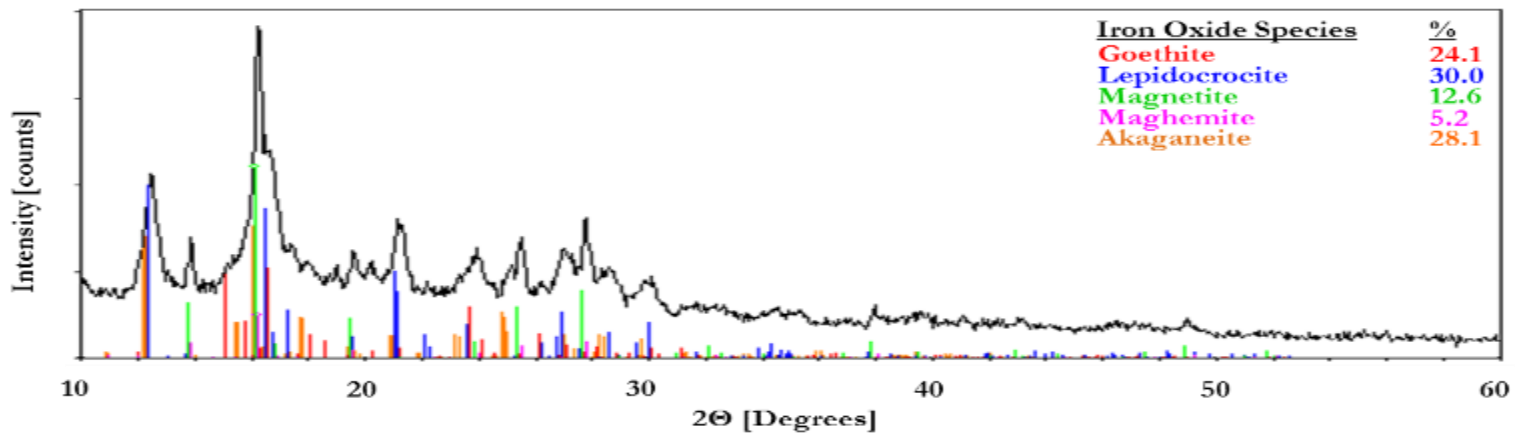


Figure A.23 XRD spectrum for pole wall sample from Pole Q3C-2R at Site 2.

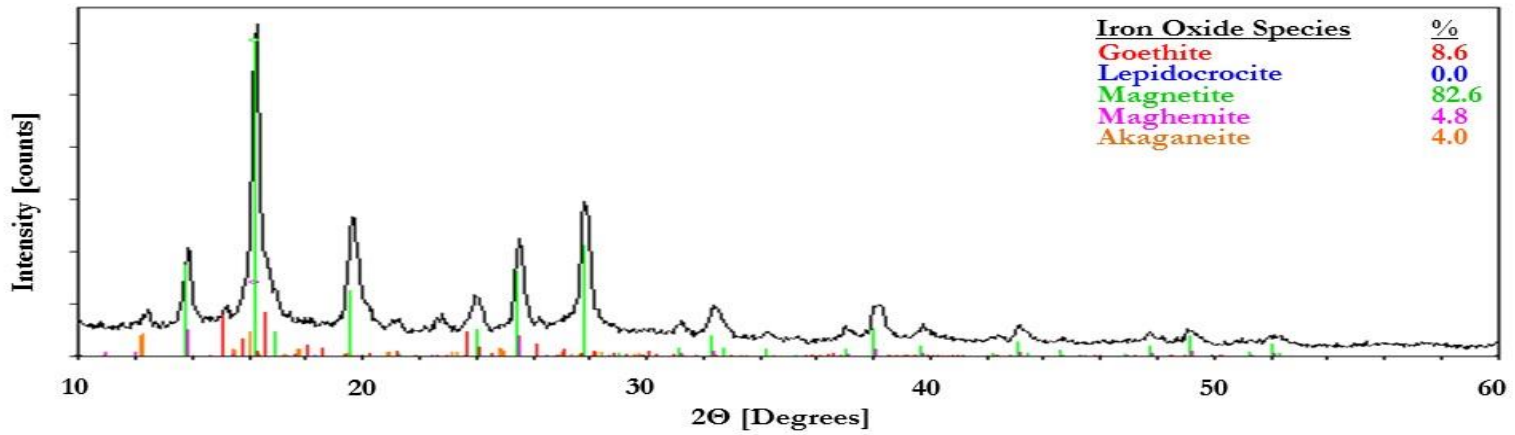


Figure A.24 XRD spectrum for pack-rust sample from coating line region of Pole Q3C-2R at Site 2.

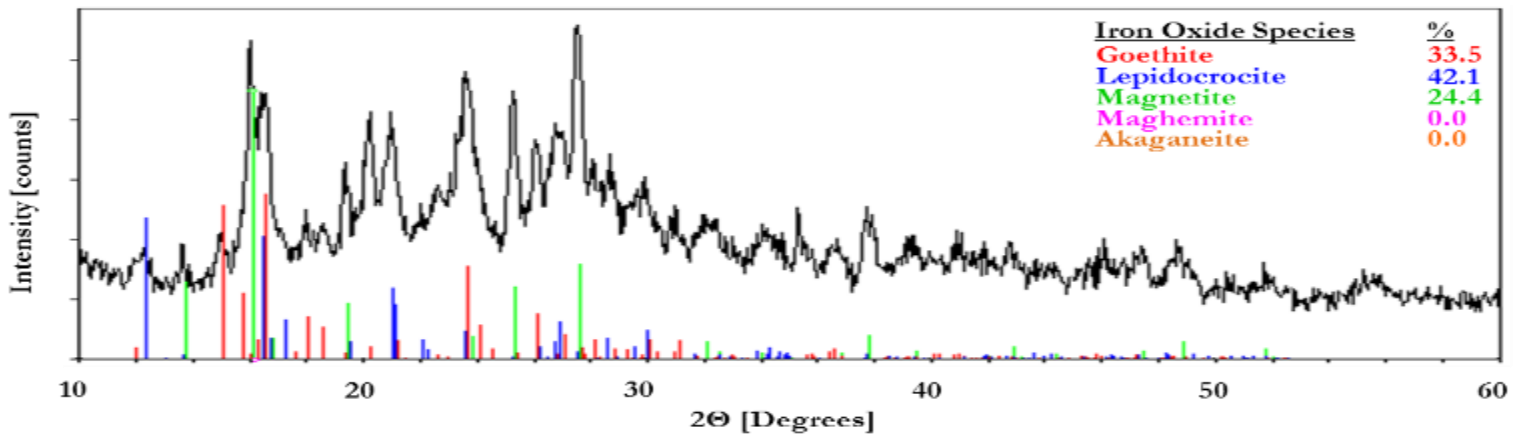


Figure A.25 XRD spectrum for pole wall sample from Pole S3B-2L at Site 3.

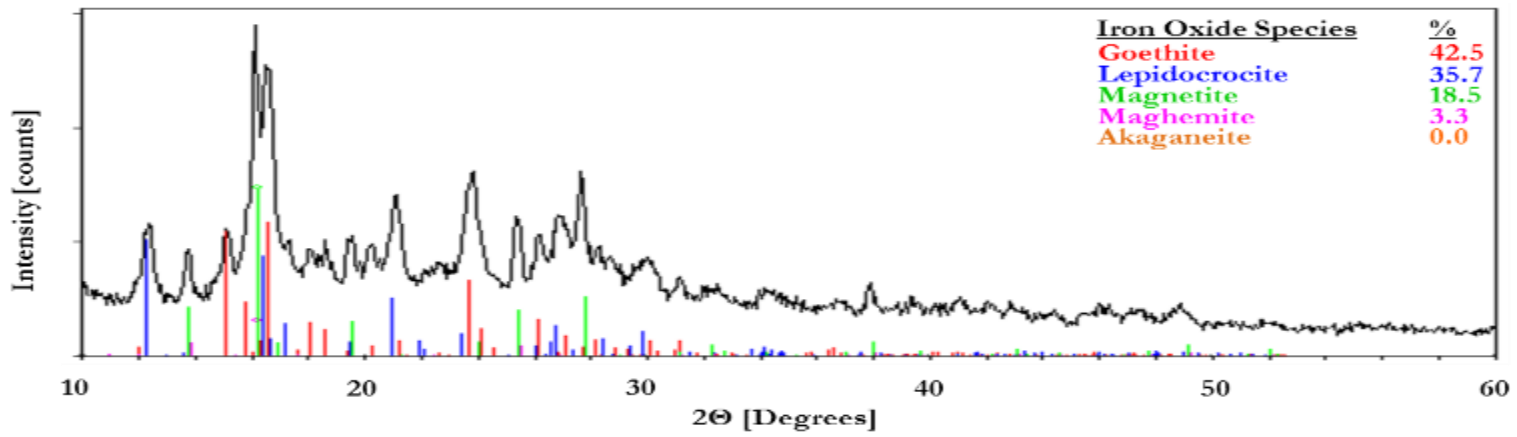


Figure A.26 XRD spectrum for pole wall sample from Pole S3B-3L at Site 3.

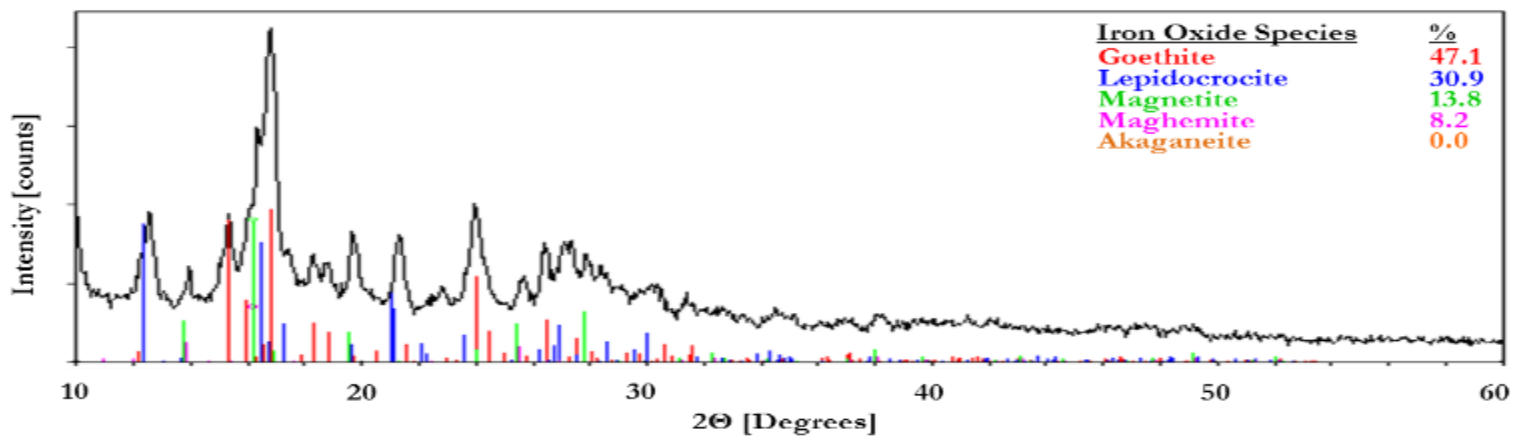


Figure A.27 XRD spectrum for pole wall sample from Pole S3B-7L at Site 3.

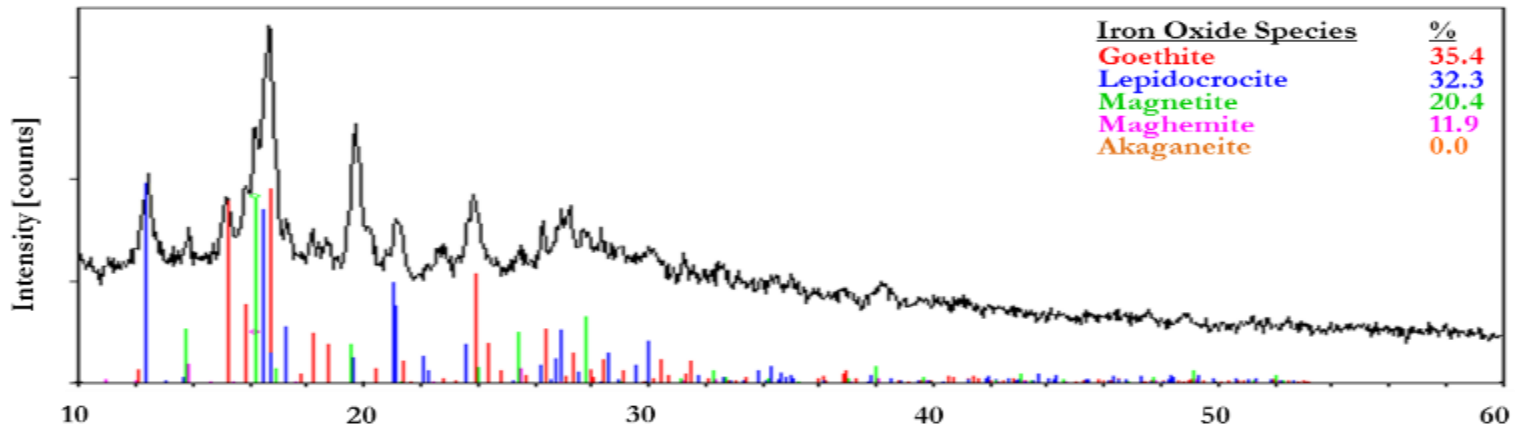


Figure A.28 XRD spectrum for pole wall sample from Pole S3B-7R at Site 3.

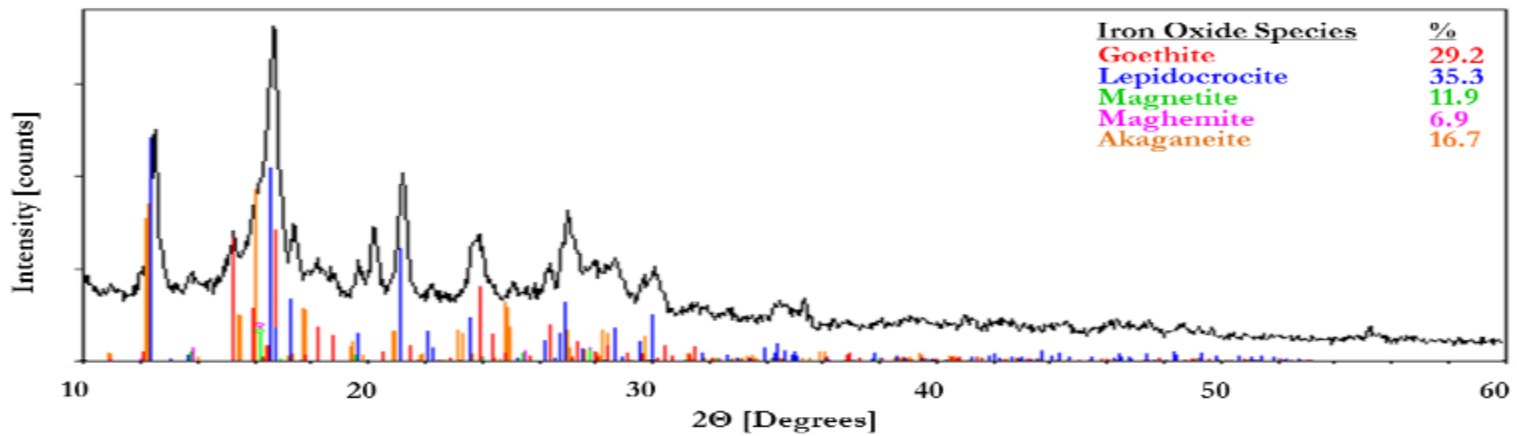


Figure A.29 XRD spectrum for pole wall sample from Pole TL-1 at Site 4.

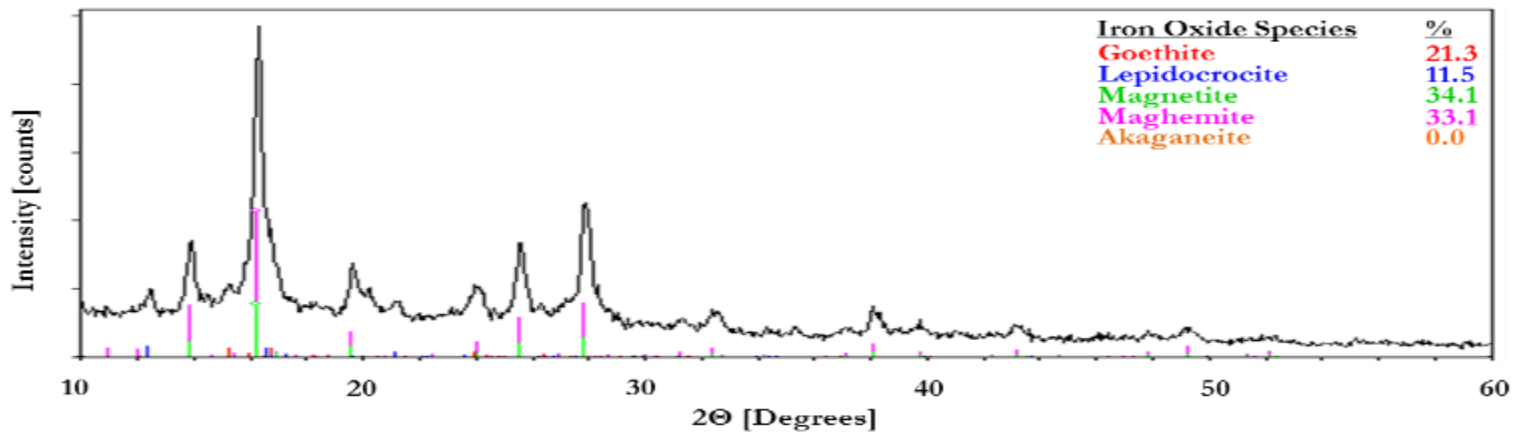


Figure A.30 XRD spectrum for inner pack-out sample from Pole TL-1 at Site 4.

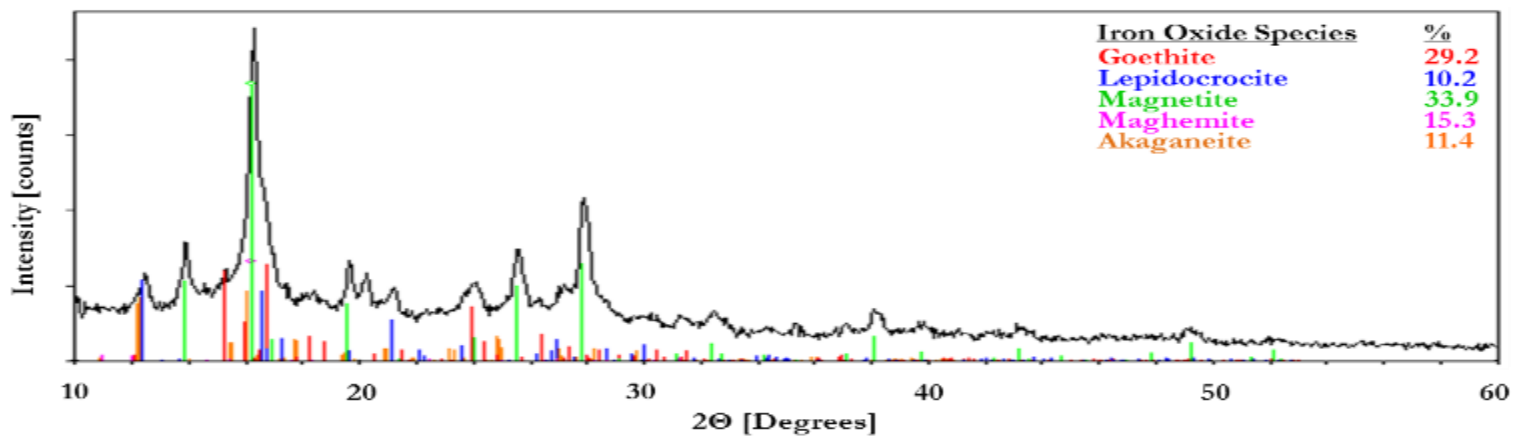


Figure A.31 XRD spectrum for pack-rust sample from deepest pit on Pole TL-1 at Site 4.

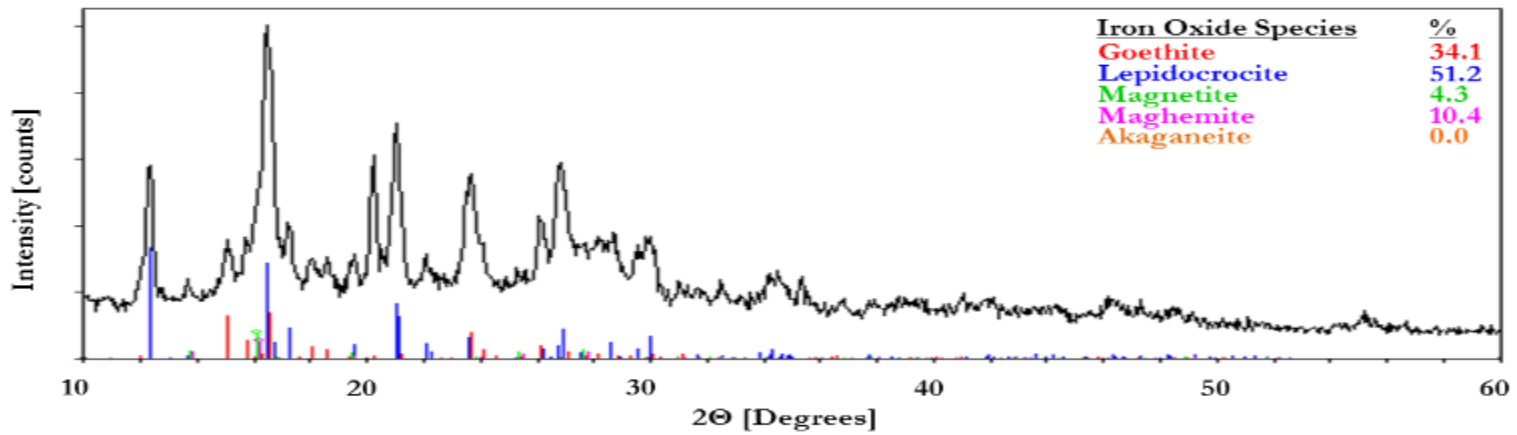


Figure A.32 XRD spectrum for pole wall sample from Pole 8Z-2L at Site 5.

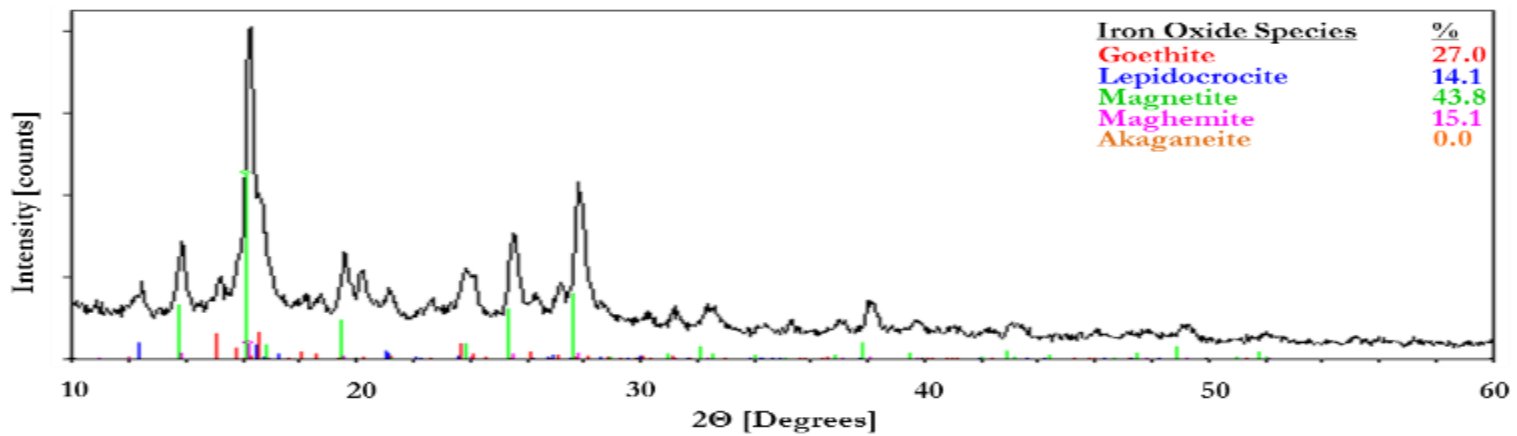


Figure A.33 XRD spectrum for loose rust sample from GS fastener region of Pole 8Z-2L at Site 5.

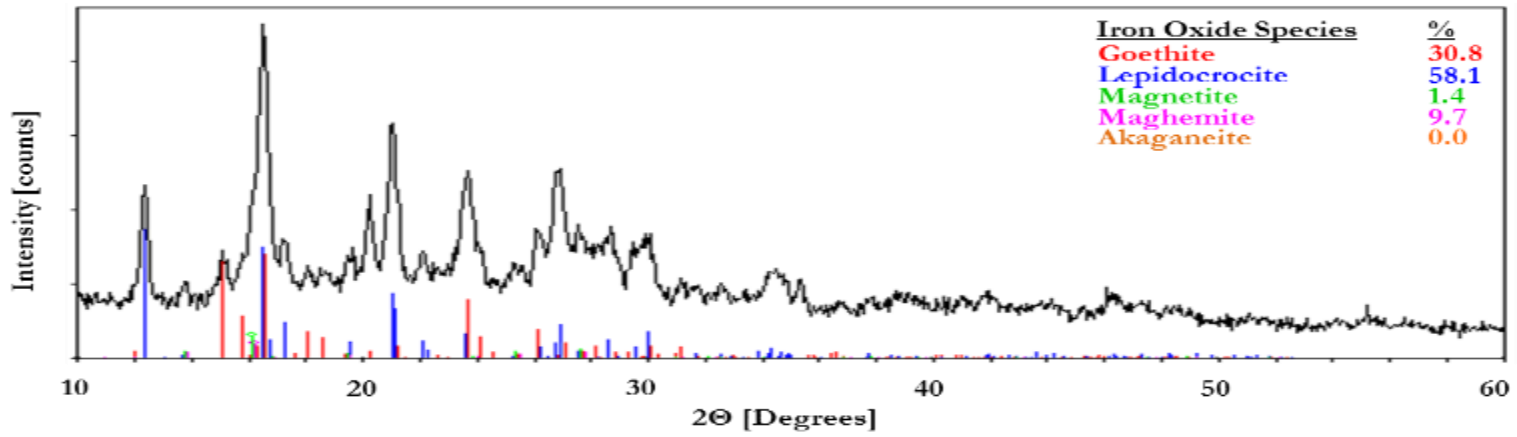


Figure A.34 XRD spectrum for pole wall sample from Pole 8Z-2R at Site 5.

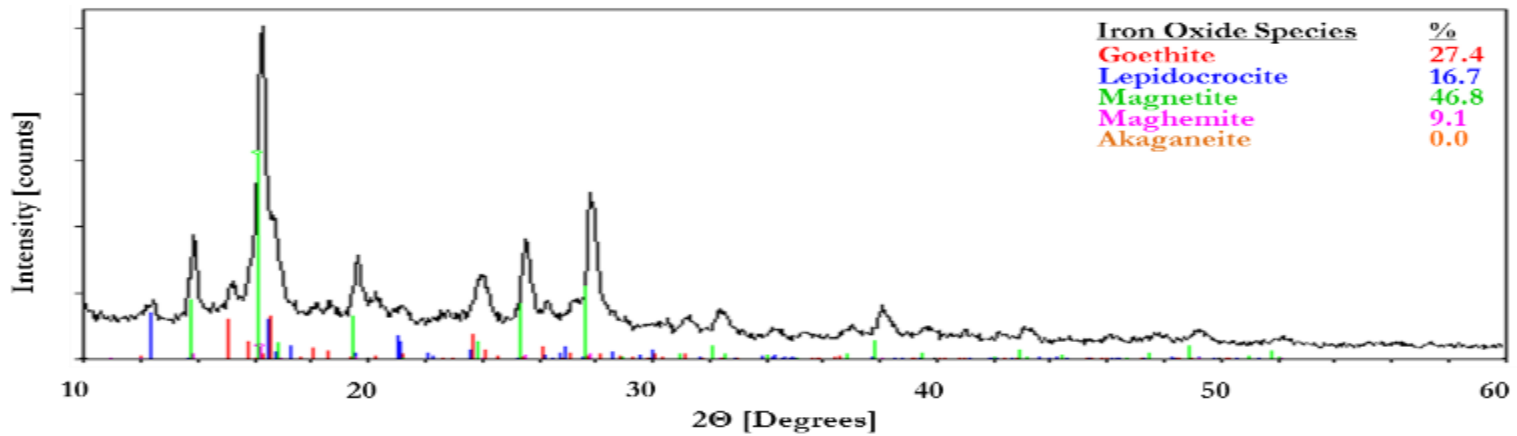


Figure A.35 XRD spectrum for loose rust sample from GS fastener region of Pole 8Z-2R at Site 5.

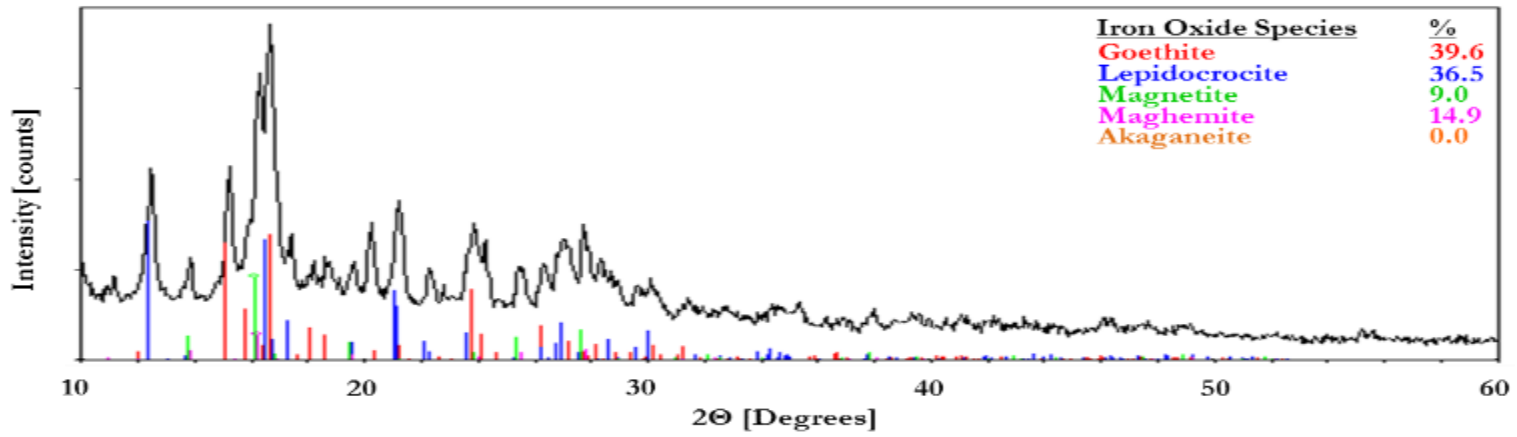


Figure A.36 XRD spectrum for pole wall sample from Pole 11Z-2L at Site 5.

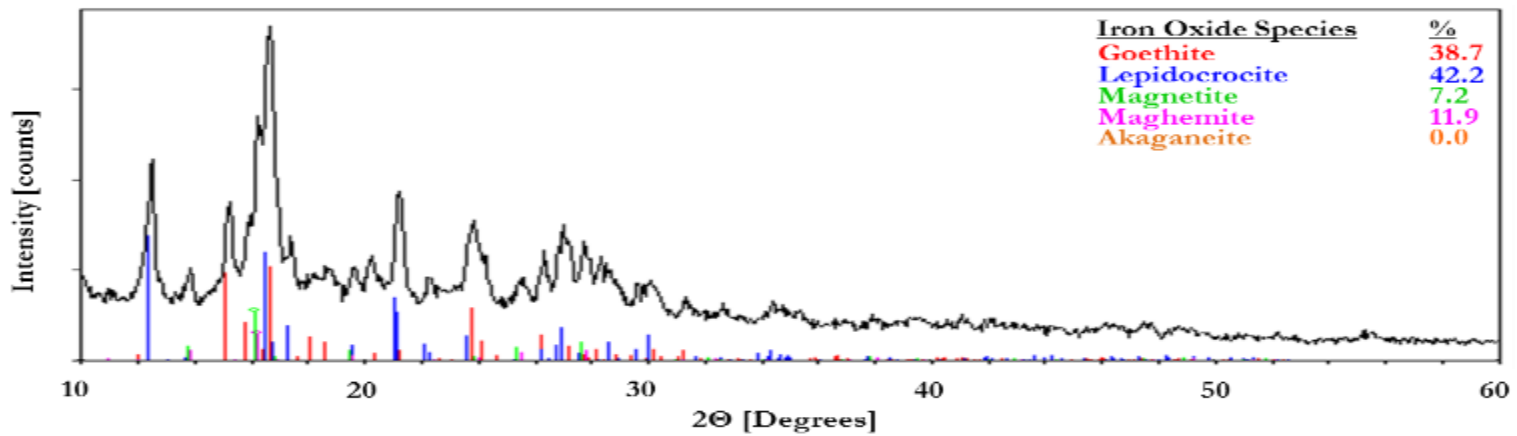


Figure A.37 XRD spectrum for pole wall sample from Pole 11Z-2R at Site 5.

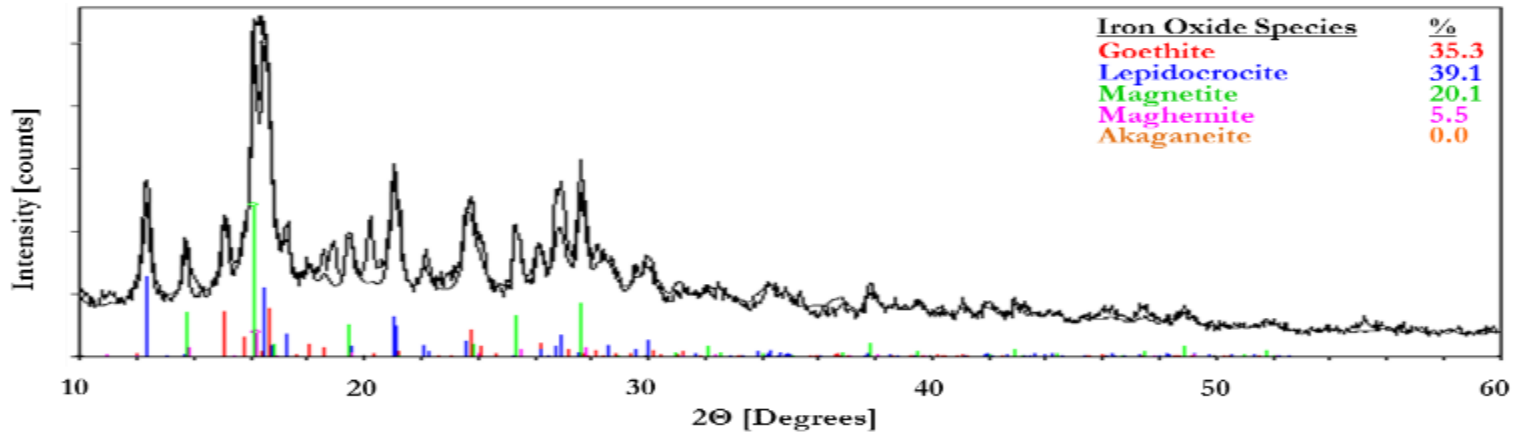


Figure A.38 XRD spectrum for pole wall sample from Pole 11Z-6R at Site 5.

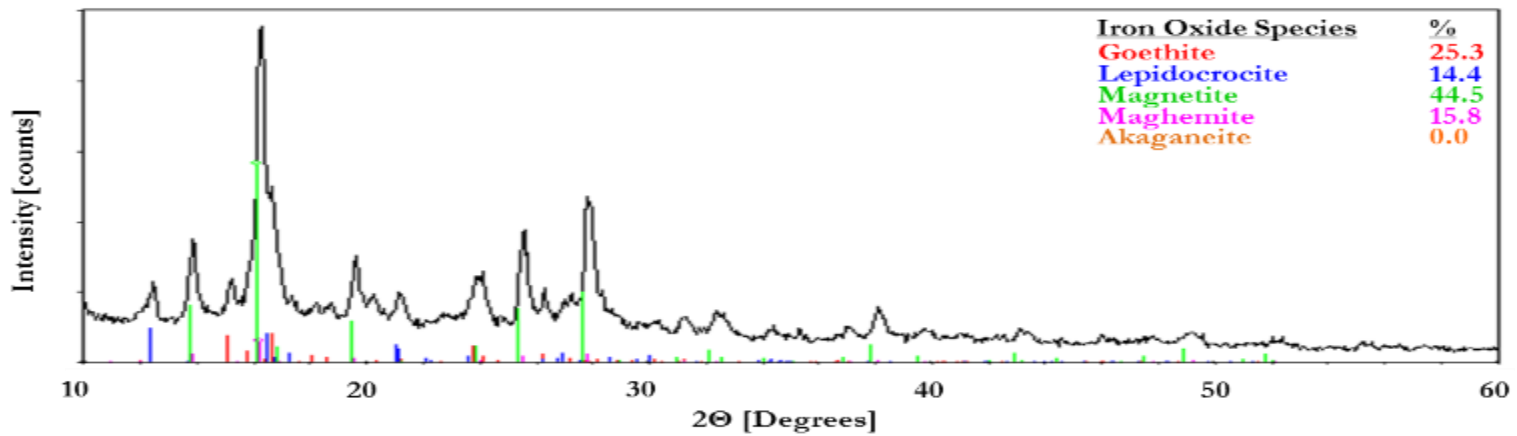


Figure A.39 XRD spectrum for loose rust sample from GS fastener region of Pole 11Z-6R at Site 5.

A.3 Mössbauer Spectroscopy (MS)

Table A.1 Parameters obtained from simulations of spectra for pack-rust sample from reflective tape region of Pole C1F-20 at Site 1.

Temperature [K]	Comp. #	Γ [mm/s]	z_0 [kG]	dz [kG]	δ [mm/s]	Δ [mm/s]	%
4.2	1	n.a.					0.00
	2	0.35	42.92	349.13	0.31	2.08	11.10
	3	0.35	476.87	115.54	0.47	0.00	56.00
	4	0.35	503.62	21.32	0.48	-0.25	37.00
100	1	0.41	n.a.		0.49	-0.60	24.20
	2	0.35	460.11	413.51	0.45	-0.38	29.40
	3	0.35	476.28	42.48	0.47	-0.22	52.60
	4	0.35	512.59	22.64	0.43	0.14	9.00
150	1	0.41	n.a.		0.46	-0.60	25.30
	2	0.35	422.92	411.01	0.57	0.18	29.60
	3	0.35	454.67	50.86	0.45	-0.24	45.10
	4	0.35	50.79	0.00	0.37	0.03	11.00
200	1	0.00	n.a.		0.44	0.60	28.90
	2	0.35	384.41	263.28	0.53	0.00	34.00
	3	0.35	422.18	53.07	0.42	-0.29	31.40
	4	0.35	497.74	51.45	0.00	0.00	15.00
RT	1	0.45	n.a.		0.38	0.60	38.00
	2	0.35	292.82	276.21	0.34	-0.22	50.60
	3	0.35	0.00	0.00	0.00	0.00	0.00
	4	0.35	480.69	34.55	0.29	0.00	17.10

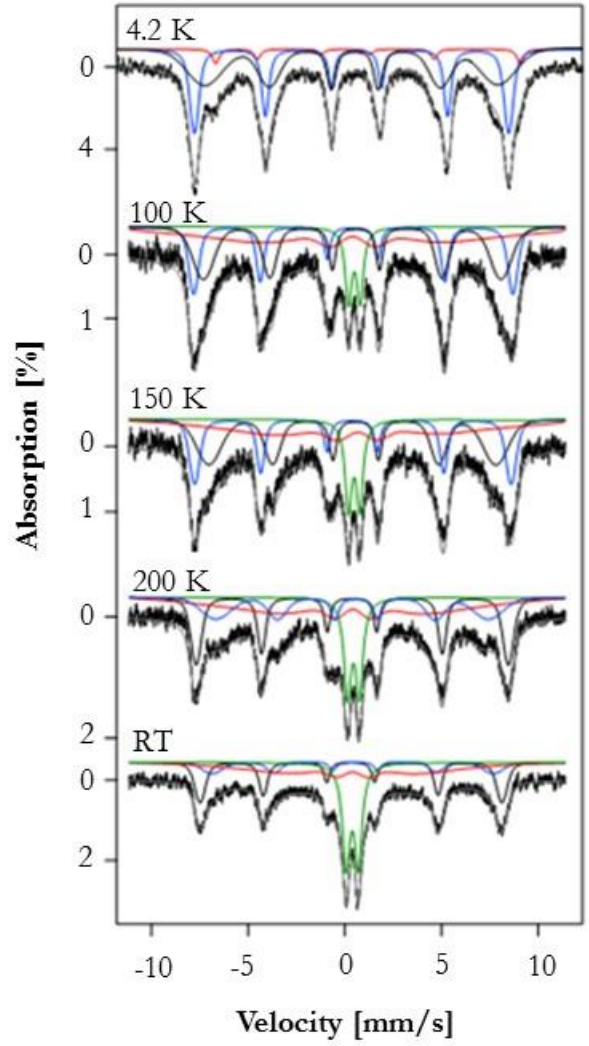


Figure A.40 ^{57}Fe Mössbauer spectra recorded for pack-rust sample from coating line region of Pole Q3C-2L at Site 2.

Table A.2 Parameters obtained from simulations of spectra for pack-rust sample from coating line region of Pole Q3C-2L at Site 2.

Temperature [K]	Comp. #	Γ [mm/s]	z_0 [kG]	dz [kG]	δ [mm/s]	Δ [mm/s]	%
4.2	1	n.a.					0.00
	2	0.35	486.57	0.00	0.62	1.14	5.00
	3	0.35	502.59	21.76	0.47	-0.26	39.30
	4	0.35	472.16	122.16	0.45	-0.13	53.00
100	1	0.39	n.a.		0.48	0.60	12.20
	2	0.35	437.91	480.10	0.44	0.00	35.70
	3	0.35	510.53	24.55	0.41	0.00	29.40
	4	0.35	476.13	68.36	0.47	-0.19	42.90
150	1	0.41	n.a.		0.47	0.58	15.10
	2	0.35	385.14	469.37	0.88	0.46	36.50
	3	0.35	506.12	26.90	0.39	0.00	32.50
	4	0.35	459.08	80.85	0.47	-0.17	37.00
200	1	0.44	n.a.		0.44	0.61	18.90
	2	0.35	348.39	395.28	0.33	-0.17	35.40
	3	0.35	436.15	100.99	0.49	-0.22	26.20
	4	0.35	499.21	28.81	0.37	0.00	34.00
RT	1	0.45	n.a.		0.37	0.63	30.30
	2	0.35	302.53	360.15	0.31	-0.17	32.00
	3	0.35	449.67	65.71	0.68	-0.13	14.20
	4	0.35	482.90	27.78	0.31	0.00	29.80

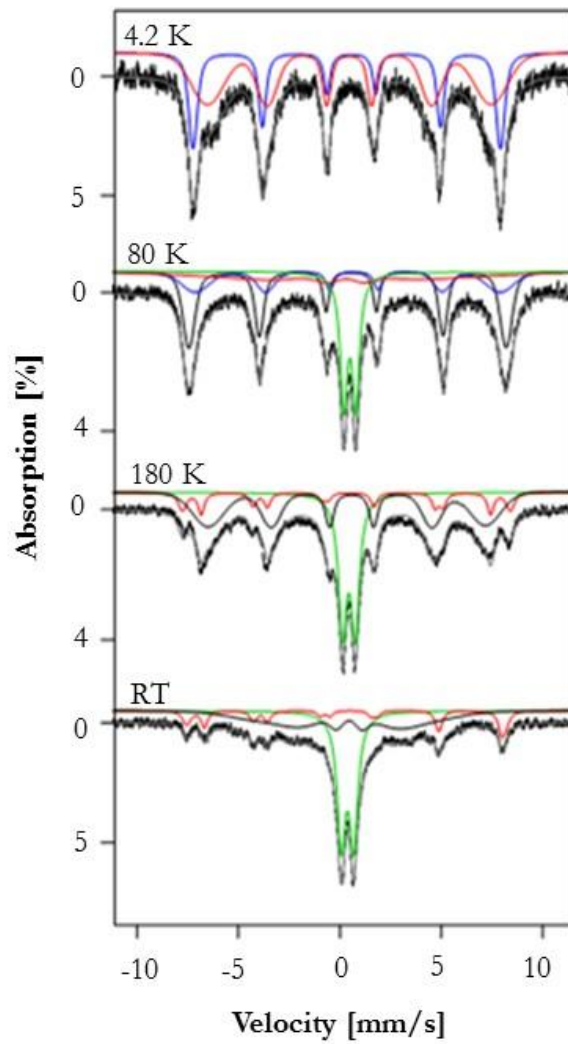


Figure A.41 ^{57}Fe Mössbauer spectra recorded for pole wall sample from Pole S3B-2L at Site 3.

Table A.3 Parameters obtained from simulations of spectra for pole wall sample from Pole S3B-2L at Site 3.

Temperature [K]	Comp. #	Γ [mm/s]	z_0 [kG]	dz [kG]	δ [mm/s]	Δ [mm/s]	%
4.2	1	n.a.					0
	2	0.35	432.47	105.98	0.47	0.00	59.7
	3	0.35	468.63	18.08	0.45	-0.23	37
	4	n.a.					0
80	1	0.42	n.a.		0.49	0.6	25.7
	2	0.35	349.419	441	0.288	0	19.7
	3	0.35	464.814	86.73	0.543	-0.307	22
	4	0.35	483.483	31.017	0.47	-0.181	41.4
180	1	0.454	n.a.		0.446	0.63	33.6
	2	0.35	443.94	0	0.429	-0.262	0.08
	3	0.35	499.653	14.7	0.36	-0.08	0.08
	4	0.35	423.213	101.136	0.464	-0.232	47
RT	1	0.488	n.a.		0.377	0.614	47
	2	0.35	452.76	0	0.66	0	9
	3	0.35	485.541	14.7	0.29	0	9
	4	0.35	241.08	230.79	0.34	-0.24	40

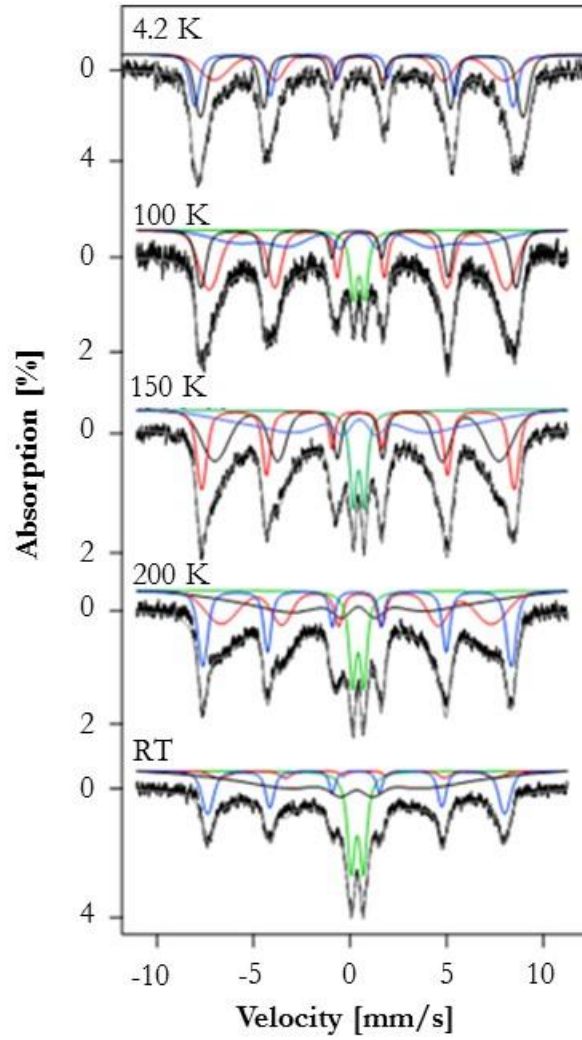


Figure A.42 ^{57}Fe Mössbauer spectra recorded for inner pack-out sample from Pole TL-1 at Site 4.

Table A.4 Parameters obtained from simulations of spectra for inner pack-out sample from Pole TL-1 at Site 4.

Temperature [K]	Comp. #	Γ [mm/s]	z_0 [kG]	dz [kG]	δ [mm/s]	Δ [mm/s]	%
4.2	1	n.a.					0.00
	2	0.35	464.81	97.17	0.48	-0.02	32.50
	3	0.35	509.65	23.96	0.43	-0.45	0.26
	4	0.35	516.12	32.34	0.49	0.24	0.37
100	1	0.43	n.a.		0.47	0.58	11.90
	2	0.35	475.40	65.42	0.48	-0.17	48.80
	3	0.35	379.41	196.54	0.43	-0.03	26.50
	4	0.35	504.50	25.58	0.39	0.09	26.70
150	1	0.40	n.a.		0.45	0.57	12.00
	2	0.35	455.26	91.14	0.44	-0.15	41.70
	3	0.35	500.39	24.84	0.39	0.04	27.80
	4	0.35	329.28	294.00	0.47	-0.02	29.30
200	1	0.42	n.a.		0.42	0.58	13.70
	2	0.35	432.47	110.25	0.42	-0.19	34.40
	3	0.35	493.92	23.52	0.36	0.02	28.30
	4	0.35	319.58	367.50	0.49	0.14	34.30
RT	1	0.45	n.a.		0.37	0.63	24.50
	2	0.35	440.12	54.83	0.58	-0.38	4.00
	3	0.35	476.28	31.02	0.31	0.01	28.90
	4	0.35	315.17	427.62	0.31	0.05	51.20

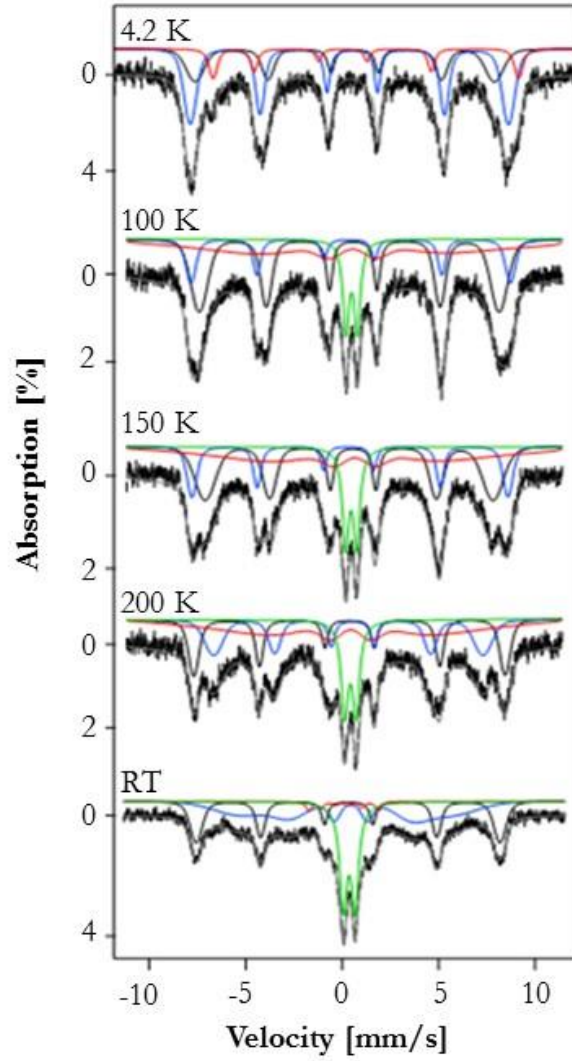


Figure A.43 ^{57}Fe Mössbauer spectra recorded for loose rust sample from GS fastener region of Pole 8Z-2L at Site 5.

Table A.5 Parameters obtained from simulations of spectra for loose rust sample from GS fastener region of Pole 8Z-2L at Site 5.

Temperature [K]	Comp. #	Γ [mm/s]	z_0 [kG]	dz [kG]	δ [mm/s]	Δ [mm/s]	%
4.2	1	n.a.					0
	2	0.35	489.51	17.64	0.63	1.2	13.6
	3	0.35	509.796	36.015	0.45	-0.153	48.4
	4	0.35	479.514	56.595	0.392	-0.52	28
100	1	0.376	n.a.		0.489	0.588	14.1
	2	0.35	460.11	521.85	0.768	0.465	34.8
	3	0.35	512.442	24.843	0.406	0	19.4
	4	0.35	481.131	51.891	0.469	-0.2	47.6
150	1	0.41	n.a.		0.463	0.572	17
	2	0.35	407.043	473.781	0.796	0.284	34.9
	3	0.35	507.003	24.108	0.372	0	23
	4	0.35	461.58	66.885	0.462	-0.2	45.3
200	1	0.41	n.a.		0.423	0.6	18.2
	2	0.35	392.931	443.352	0.387	-0.112	40.4
	3	0.35	432.033	57.771	0.433	-0.22	28.5
	4	0.35	499.359	26.901	0.382	0	28.4
RT	1	0.45	n.a.		0.368	0.61	28.8
	2	0.35	111.72	0	0.02	0.124	0.05
	3	0.35	332.514	194.628	0.312	-0.277	41.4
	4	0.35	486.717	34.104	0.324	0	32